IN SITU REMEDIATION OF PB/ZN CONTAMINATED MATERIALS: FIELD- AND
MOLECULAR-SCALE INVESTIGATIONS

by

LUCAS R. BAKER

B.S., Wilmington College, 2003
M.S., Kansas State University, 2005

AN ABSTRACT OF A DISSERTATION

submitted in partial fulfillment of the requirements for the degree

DOCTOR OF PHILOSOPHY

Department of Agronomy
College of Agriculture

KANSAS STATE UNIVERSITY
Manhattan, Kansas

2008

Abstract

The bioavailability of Pb and Zn is linked to the solubility of solid phases and other soil chemical characteristics, which is associated with their environmental risk, suggesting that *in situ* stabilization of these elements can be accomplished by influencing their chemistry. However, more research is needed to investigate the effectiveness of different soil amendments on reduing Pb and Zn bioavailability. A lab study was conducted to evaluate the effects of five different P amendments and time on Pb/Zn speciation in a contaminated soil using synchrotron-based techniques, while a field investigation studied the effects of composted beef manure on plant biomass production and the influence on microbial function, size, and community shifts. In the lab study, the Pb-phosphate mineral plumbogummite was found as an intermediate phase of pyromorphite formation, which has not been documented until now. Additionally, all fluid and granular P sources were able to induce Pb-phosphate formation, but fluid phosphoric acid (PA) was the most effective with time and distance from the treatment. However, acidity from PA increased the prescence of soluble Zn species, which can have negative environmental consequences. Granular phosphate rock (PR) and triple super phosphate (TSP) reacted to generate both Pb- and Zn-phosphates, with TSP being more effective at greater distances than PR. In the field study, compost additions of 269 Mg ha^{-1} significantly decreased bioavailable Zn, while increasing estimated available water, plant nutrients, and plant biomass as compared to a contaminated control and low addition of compost (45 Mg ha^{-1}) over three years. Additionally, compost additions of 269 Mg ha^{-1} significantly increased microbial enzyme activities, nitrification, and microbial biomass over the contaminated control through the duration of the study. Increases in microbial activity and biomass are related to increases in total C, available water, and extractable P, while negative relationships were found with electrical conductivity and with bioavailable Zn. The addition of lime or lime plus bentonite with compost did not further reduce metal availability, increase plant biomass, or improve the size or function of microbial communities. High compost additions caused a slight shift in microbial community structure according to phospholipids fatty acid analysis. Increases in the mole percents of both Gram-positive (Gm^{+}) and Gram negative (Gm^{-}) bacteria were found depending on site. Microbial biomass of Gm^{+}, Gm^{-}, and fungi were also increased by high compost additions. Results indicate that large additions of compost are needed to increase microbial biomass, improve

microbial activity, and re-establish a healthy vegetative community. This study proposes that organic matter and P amendents can be used to stabilize and reduce the bioavailability of heavy metals in soils and mine waste materials, but must be managed carefully and intelligently.

IN SITU REMEDIATION OF PB/ZN CONTAMINATED MATERIALS: FIELD- AND
MOLECULAR-SCALE INVESTIGATIONS

by

LUCAS R. BAKER

B.S., Wilmington College, 2003
M.S., Kansas State University, 2005

A DISSERTATION

submitted in partial fulfillment of the requirements for the degree

DOCTOR OF PHILOSOPHY

Department of Agronomy
College of Agriculture

KANSAS STATE UNIVERSITY
Manhattan, Kansas

2008

Approved by:

Major Professor
Gary M. Pierzynski

Abstract

The bioavailability of Pb and Zn is linked to the solubility of solid phases and other soil chemical characteristics, which is associated with their environmental risk, suggesting that *in situ* stabilization of these elements can be accomplished by influencing their chemistry. However, more research is needed to investigate the effectiveness of different soil amendments on reducing Pb and Zn bioavailability. A lab study was conducted to evaluate the effects of five different P amendments and time on Pb/Zn speciation in a contaminated soil using synchrotron-based techniques, while a field investigation studied the effects of composted beef manure on plant biomass production and the influence on microbial function, size, and community shifts. In the lab study, the Pb-phosphate mineral plumbogummite was found as an intermediate phase of pyromorphite formation, which has not been documented until now. Additionally, all fluid and granular P sources were able to induce Pb-phosphate formation, but fluid phosphoric acid (PA) was the most effective with time and distance from the treatment. However, acidity from PA increased the prescence of soluble Zn species, which can have negative environmental consequences. Granular phosphate rock (PR) and triple super phosphate (TSP) reacted to generate both Pb- and Zn-phosphates, with TSP being more effective at greater distances than PR. In the field study, compost additions of 269 Mg ha^{-1} significantly decreased bioavailable Zn, while increasing estimated available water, plant nutrients, and plant biomass as compared to a contaminated control and low addition of compost (45 Mg ha^{-1}) over three years. Additionally, compost additions of 269 Mg ha^{-1} significantly increased microbial enzyme activities, nitrification, and microbial biomass over the contaminated control through the duration of the study. Increases in microbial activity and biomass are related to increases in total C, available water, and extractable P, while negative relationships were found with electrical conductivity and

with bioavailable Zn. The addition of lime or lime plus bentonite with compost did not further reduce metal availability, increase plant biomass, or improve the size or function of microbial communities. High compost additions caused a slight shift in microbial community structure according to phospholipids fatty acid analysis. Increases in the mole percents of both Gram-positive (Gm^+) and Gram negative (Gm^-) bacteria were found depending on site. Microbial biomass of Gm^+, Gm^-, and fungi were also increased by high compost additions. Results indicate that large additions of compost are needed to increase microbial biomass, improve microbial activity, and re-establish a healthy vegetative community. This study proposes that organic matter and P amendents can be used to stabilize and reduce the bioavailability of heavy metals in soils and mine waste materials, but must be managed carefully and intelligently.

Table of Contents

List of Figures

List of Tables

Acknowledgements

There are so many people that I need to acknowledge and thank for helping me along this journey. I first would like to thank my major professor, Dr. Gary Pierzynski, for all of his help, guidance, and support. I have enjoyed working, traveling, and conversing over the last 3.5 years. I appreciate all the time that you have spent editing and providing comments for our work. Your efforts have not gone unnoticed and I honestly would have never continued on through graduate school if I didn't have the opportunity to work with you. I also would like to thank departmental committee members Dr. Charles Rice and Dr. Michel Ransom. I enjoyed taking classes from both of you, am grateful for the opportunity to work with you, and appreciate the fact that anytime I had a question you always made yourselves available. I would like to thank outside committee member Dr. Larry Erickson. I appreciate the effort put forth to be on my committee and the thought provoking questions you have always asked. Lastly, I want to thank the outside committee chair Dr. Stacey Hutchinson. I know that it takes time and effort to be part of a Ph.D committee, but your effort has not gone unnoticed. I would like to extend a special thanks to all of the office staff for making my life much easier over the years. Additionally, I would like to thank Alexis, Brad, and Kathy from the KSU soil testing lab for their efforts and being so easy to work with. I would like to thank Dr. Paul White Jr. for his hard work in helping me with microbial data analysis and being a great friend over the years. We have had so much fun and were always good at being mischievous together. In addition, I want to thank Dr. Kirk Scheckel of the US EPA and Dr. Matt Newville of the University of Chicago for assisting with the use of synchrotron-based techniques and data analysis. I would like to extend a special thanks to Dr. Ganga Hettiarachchi for her help with data analysis, thought stimulating talks, and just for always being someone to talk over the last year. You have become a real good friend and I can't begin to tell you how much I appreciate everything that you have done for me. There are so many graduate and former graduate students that I would like to thank too. This list includes Kent Martin, Meghan Buckley, Peg Althoff, DeAnn Presley, Chad Godsey, Ron Gehl, Tom Desutter, Jaime Loecker, Priscilla Mfombep, and so many more. I need to give a special thanks to Ellen Burke, who has been an undergradute student worker for me. Without her hard work and help, I seriously doubt that I would have been able to get everything done. Plus, it has been fun getting to know you and I wish you best of luck in the bright future that you have ahead of

you. There are so many other friends that I need to thank that have kept me going over the years and they are Ben, Stephanie, Chad, Becky, Amy, Danny, Kenneth, Jason, Ryan, and Julie. Finally, I would like to thank the group of people who really has made this all happen and that is my family. I thank you guys so much for being patient with me and giving me the opportunity and support to fulfill my dreams. None of this would be possible without you. I can honestly say that I have been truly blessed. I would just like to thank everyone once again for all that they have done.

Dedication

I would like to dedicate this dissertation in the memory of my grandmothers LaDonna Baker and Clair Schilling. In addition, I would like to dedicate this in honor of my grandfathers, Richard Schilling and Roy Baker Jr., and my parents Jerry and Brenda Baker. Thanks for all of the love and support.

CHAPTER 1 - Introduction

Lead and Zn are natural constituents of all soils and are ubiquitous throughout the environment (Adriano, 2001). The concentrations of Pb and Zn in the soil continue to increase due to anthropogenic activities such as mining, smelting, burning of fossil fuels, tire wear, paints, and other industrial activities (Adriano, 2001; Basta et al., 2005). There is significant concern regarding Pb in the environment because of the wide variety of negative impacts on human health that have been recognized (ATSDR, 2005). The primary risk with Zn is phytotoxicity (Brown et al., 2003a; Chaney, 1993), which can leave soils devoid of vegetation. Lack of vegetation has the potential to increase the exposure of Zn and other contaminants commonly associated with Zn, most notably Cd and Pb. As a result, areas that have been contaminated with these metals must be cleaned up to reduce the risk to the environment.

Lead and Zn are inorganic contaminants and therefore, can not be broken down in soils by microorganisms like most organic contaminants. Commonly used remediation methods for Pb and Zn have involved the excavation and disposal of contaminated materials in landfills. However, this approach is expensive and time consuming it can create large amounts of dust and clean back-fill material is needed. As a result, considerable effort has been put forth to develop cost-effective, *in situ* remediation strategies to reduce metal mobility and bioavailability in the environment (Iskandar and Adriano, 1997). Precipitation of sparingly soluble minerals, the formation of relatively stable organic complexes, and the adsorption to both inorganic and organic constituents are the major controls on the bioavailablity of Pb and Zn in the environment. Therefore, the movement and bioavailability of these metals primarily depends on the solubility of the original Pb/Zn bearing minerals and the primary weathering products produced from the

1

minerals, which have the potential to be altered in a controlled manner through soil amendment additions.

Chemical immobilization is an *in situ* remediation method where inexpensive materials, such as fertilizers and waste products, are added to contaminated soils to reduce the solubility of heavy metals. Since contaminant solubility is related to its mobility and bioavailability in the environment, chemical immobilization has the potential to reduce the environmental risk associated with metals such as Pb and Zn. Recent research has focused on the ability to change the bioavailability of soil Cd, Pb, and Zn *in situ* by altering the mineral forms of these elements or providing excess adsorptive capacity (Mench et al., 1994). The success of chemical immobilization can then be evaluated by its ability to reduce contaminant bioavailability and human exposure to these heavy metals (Basta et al., 2001). However, long-term effectiveness and permanence are important criteria that need to be taken into consideration when assessing these alternative remediation technologies.

Lead phosphates, in particular pyromorphites, are one of the most stable forms of Pb in soils under a wide range of environmental conditions (Lindsay, 1979; Nriagu, 1984). Numerous studies have found that when P is added to a Pb contaminated soil the bioavailability of Pb is reduced (Cao et al., 2003; Hettiarachchi and Pierzynski, 2004; Hettiarachchi et al., 2000; Yoon et al., 2007). This reduction in Pb bioavailability has been proposed to be due to the formation of pyromorphite or other Pb phosphate minerals. Hettiarachchi et al. (2000) were able to detect changes in Pb mineralogy in P treated soils using X-ray diffraction (XRD). They found that pyromrophite peaks increased in intensity after P amendment addition. However, XRD can only detect crystalline species and the diffraction patterns can often be muddled due the prescence of other minerals that commonly occur in the bulk soil. Therefore, complex matrices, such as soil,

make it difficult to ascertain changes in soil mineralogy/metal speciation upon P amendment additions. However, advances in spectroscopic techniques, namely synchrotron-based techniques, have allowed scientists to determine the speciation of multiple elements *in situ* at the molecular level in complex environmental samples (Brown et al., 2005a). Additionally, this approach is more definitive than bulk techniques and can speciate elements that occur in all phases, including those that are crystalline or non-crystalline in nature. Knowledge of the molecular-level speciation of pollutants is fundamental for predicting their environmental properties such as their stability, mobility, toxicity, and potential bioavailability to humans, plants, and other organisms as well as designing effective remediation strategies. Studies using synchrotron-based techniques have confirmed the formation of pyromorphite when P amendments were added to a Pb contaminated soil (Chappell and Scheckel, 2007; Scheckel and Ryan, 2004).

Other research has focused on the use of different P amendments (phosphate rock, triple super phosphate, disodium phosphate, phosphoric acid, and diammonium phosphate) to reduce Pb bioavailability in soils, sediments, and water (Cao et al., 2003; Hettiarachchi et al., 2000; Ma et al., 1993; Ma et al., 1995; McGowen et al., 2001; Yoon et al., 2007). All P amendments were able to reduce the bioavailability or mobility of Pb as indicated by some sort of assessment procedure (i.e. physiologically-based extraction test, seqential extraction procedure, toxicity characteristic leaching procedure, etc…). However, no information exists on the efficacy of different P amendments reacted over various periods of time, which would have impacts on the type (highly soluble vs. sparingly soluble) and amount of P needed to immobilize Pb in contaminated environments. In addition, the influence of P on Zn speciation has not been well documented, which is problematic because Pb and Zn often occur as co-contaminants. While Zn

is not a human health concern, it is phytotoxic and could increase the exposure to other contaminants occurring in the same environment. Additionally, little information exists on metal phosphate formation at the molecular level. Therefore, research is needed to address the impact of P on Pb and Zn speciation in Pb/Zn co-contaminated soils.

Organic amendments have also been used to reduce the bioavailability of heavy metal contaminants through the process of sorption. Furthermore, the addition of organic materials provides soil organic matter and nutrients, while increasing biological activity, which contribute to ecosystem-level processes and are important for productivity, community structure, and fertility in all ecosystems (Stevenson, 1994). Mine waste materials are most commonly characterized by the absence of organic matter, nitrogen, phosphorus, and by their neutral to low pH, high acid-producing potential, and poor soil structure (Wong et al., 1998; Krzaklewski and Pietrzykowski, 2002). As a result, organic amendments would provide the necessary qualities needed for healthy ecosystem function in mine waste materials. Benefits directly associated with improved organic matter content include: enhanced water infiltration and moisture holding, improved aggregation, aeration, and nutrient supply for plant growth, and increases in microbial population size and activity.

The impacts of elevated heavy metal levels on the size and activity of natural soil microbial communities have been well documented. Heavy metals affect the growth, morphology, and metabolism of microorganisms in soils, through functional disturbance, protein denaturization, and/or the destruction of the integrity of cell membranes (Leita et al., 1995). It is generally accepted that accumulated heavy metals reduce the amount of soil microbial biomass (Brookes and McGrath, 1994; Chander et al., 1995) and the presence of metals can alter the microbial community structure (Šmejkalová et al., 2003), which can be extremely damaging to

4

ecosystem function. A diverse microbial community is important because of the key role that microorganisms play in the biogeochemical cycling of nutrients, transformation of soil organic matter, plant pathogen protection, and production of growth promoting substances for plants (Bolton et al., 1992). Therefore, the success of natural ecosystems depends appreciably on the rate of turnover of the soil organic matter, which is directly mediated by the soil microbial biomass (Brookes, 1995).

Several studies have used organic materials in an attempt to re-vegetate and help support microbial activity in heavy metal contaminated soils/mine wastes (Brown et al., 2003b; Brown et al., 2005b; Clemente et al., 2006; DeVolder et al., 2003; Kelly et al., 2003; Pérez de Mora et al., 2005; Pierzynski et al., 2002a). Pierzynski et al. (2002a) discovered that additions of beef manure applied at 90 Mg ha^{-1} resulted in an increase in growth of tall fescue (*Festuca arundinacea* Shreb) in the first year after amendment addition. However, by year 3 plant growth began to decline and plant tissue analysis suggested Zn phytotoxicity. Brown et al. (2003b) found that a combination of wood ash and high N biosolids (66 Mg ha^{-1} biosolids), which were surface applied to Cd, Pb, and Zn contaminated mine tailing, resulted in the establishment of a vegetative plant cover for at least two growing seasons. However, with time they observed a decrease in plant Ca, K, and Mg concentrations over the study period, which led them to conclude that higher amendment loadings may be needed to supply essential plant nutrients required to produce a self-sustaining plant cover.

A few studies have been conducted to examine the effects of organic amendments on microbial communities when applied to heavy metal contaminated soils. Tejada et al. (2007) applied two forms of beet vinasse to a semi-arid metal contaminated soil and monitored microbial parameters as an indicator of restoration. They found that beet vinasse alone

decreased microbial biomass, microbial respiration, and a suite of microbial enzymes as compared to the non-amended control. When the beet vinasse was composted with cotton gin, all of these parameters increased over the non-amended control and the beet vinasse alone, which was attributed to an increase in readily available C. Clemente et al. (2007) used microbial biomass measurements and established that the addition of organic amendments to heavy metal contaminated soils can improve soil fertility, but the response of the microbial population depends on the amendment used. Manure helped to reduce the metal stress symptoms quickly, which resulted in rapid microbial growth, while a waste material of olive hush resulted in substantially slower microbial population increases. This was attributed to differences in C availability in the amendments. Classens et al. (2005) used several different enzyme activities to monitor coal mine tailings under rehabilitation. They determined that sites that had more vegetation and an increased organic C content had a greater positive association with soil enzyme activities, which they determined was an indication of increased nutrient cycling and soil quality. To evaluate microbial community shifts upon sewage sludge additions to a Zn smelter contaminated soil, Kelly et al. (2003) examined changes in phosphoplipid fatty acid profiles (PLFA) over time. They found that the remediation program had changed soil microbial communities. PLFA profiles for recently remediated sites were similar to the less contaminated sites, and there were significant increases in key indicator fatty acids for fungi, actinomycetes, and Gr +ve (gram-positive) bacteria, which they concluded is an indication of recovery. Although PLFA data presented by Kelly et al. (2003) suggested that the remediation program was having a positive effect on soil microbial communities, their results also indicate a loss of effectiveness over time.

Remediation studies involving plants and microbial communities have both indicated a

decrease in amendment effectiveness over time when using organic amendments (applied at 90 Mg ha^{-1} or less). This is expected since C is used by microbes for energy and maintenance; therefore, the benefits of the organic amendments disappear gradually with time. However, studies have not been conducted to determine if a single large application (> 200 Mg ha^{-1}) of organic material can sustain plant growth and improve microbial community size and function over time, which is important for the recovery of heavy metal contaminated areas. Success of this type of remediation technology will likely depend on the ability of a healthy plant community to supply C back into the system to support microbial growth and activity. In addition, a healthy and diverse microbial population is needed to maintain the biogeochemical nutrient cycles that provide nutrients to plants and turnover the organic pool. As a result, research is needed to investigate if a single large application of compost can establish and sustain both plant and microbial communities over time.

Objectives

1. The objective for the first study, <u>Changes in Microbial Enzymes, Biomass, and Phospholipid Fatty Acid Profiles upon Addition of Amendments to a Heavy Metal Contaminated Mine Waste</u> (Chapter 3), was to evaluate the effects of beef manure compost with and with out lime and bentonite on the size, activity, and shift in microbial community when applied to a heavy metal contaminated mine waste.

2. The objective for the second study, <u>Revegetation of Pb/Zn Mine Wastes with *Panicum virgatum* using Beef Manure Compost and Other Inorganic Amendments</u> (Chapter 4), was to determine if a single high treatment of compost (269 Mg ha^{-1}) with and without lime and bentonite could support and sustain a vegetative community over time.

3. The objective of the third study, <u>Spectroscopic Speciation of Pb after Addition of Different P Amendments to a Smelter-Contaminated Soil</u> (Chapter 5), was to determine the efficacy of different P amendments at forming Pb phosphates in a Pb/Zn smelter-contaminated soil.

4. The objective of the fourth study, <u>Speciation of Zn as Influenced by P Addition in a Pb/Zn Smelter-Contaminated Soil</u> (Chapter 6), was to evaluate the effects that different P amendments have on Zn speciation when applied to immobilize Pb in a Pb/Zn smelter-contaminated soil.

CHAPTER 2 - Literature Review

2.1 Chemistry of Pb and Zn

Lead is a main group element in the periodic table (group 14) that has an atomic number of 82, and is classified as a trace element because of its low natural abundance in soils (Essington, 2004). Naturally occurring Pb compounds occur in a mixture of isotopes. Common mass numbers for Pb are 204 (1.4%), 206 (24.1%), 207 (22.1%), and 208 (52.4%), with 208 being the most common; thus giving an atomic weight of 207.21 g mol^{-1}. Pure Pb is a bluish white metal of bright luster, is soft, very malleable, ductile, and a poor conductor of electricity (Callendar, 2005). Because of these properties, its low melting point (327 ^{o}C), and resistance to corrosion, Pb has been used in the manufacture of metal products for thousands of years. Lead has a density of 11.34 g cm^{-3}; hence it finds extensive use as a shield for radiation. Lead's valence shell electrons ($6s^2\ 6p^2$) allow it to have three possible oxidation states, +2, +3, and +4. The tetravalent state is a powerful oxidizer and is therefore not common at the Earth's surface. The divalent state, on the other hand, is the most stable oxidation state, which makes it important over the wide range of environmental conditions that exist in soils. Representative background concentrations of Pb found in surface agricultural soils are approximately 11 mg kg^{-1}, while contaminated soils significantly exceed this level (Holmgren et al., 1993). Lead is considered to be a chalcophile (associated with sulfur) element that mainly occurs as sulfides in mineral deposits. Lead can also occur in other mineral deposits by being substituted in minerals during the crystallization process for potassium, strontium, barium, and calcium (lithophiles: associated with silicates) due to their similar ionic radii (Nesse, 2000).

Zinc is a transition metal element with an atomic number of 30, belongs to group 12, and is known as a trace element due to its low natural concentration in soils. Zinc, like Pb, is found

to have a number of natural occurring isotopes. Mass numbers for Zn include: 64 (48.6%), 66 (27.9%), 67 (4.1%), 68 (18.8%), and 70 (0.6%) with 64 being the most prevalent, providing an average atomic mass of 65.39 g mol^{-1}. Pure Zn is bluish-white in color, is a relatively soft metal, and has a density of 7.14 g cm^{-3}. Its melting point is 419.6 ^{o}C, and it boils at 907 ^{o}C.   Zinc is a chalcophile element that occurs in mineral deposits mainly as sulfides, but can substitute into other minerals by replacing cations of similar size. Zinc's valence shell electrons ($3d^{10}$ $4s^{2}$) allow it to possess two oxidation states in natural environments. They are Zn^{o} and Zn^{+2}, but only the Zn^{2+} ion is significant in soil environments. The average background concentration of Zn found in most uncontaminated agricultural soils whose parent material does not contain elevated levels of Zn is roughly 43 mg kg^{-1} (Holmgren et al., 1993).

2.2 Uses of Pb and Zn

Lead has a wide range of industrial applications, which can be largely attributed to its unique physical properties (low melting point, high density, and malleability). For example, due to its high corrosion resistance and ability to attenuate gamma- and X-rays efficiently without becoming radioactive itself, Pb is commonly used in the shielding of radiation (Hoffman, 1970).

A persistent problem associated with high compression engines is known as "knocking", which occurs because of nonuniform power surges generated from spontaneous combustion of the fuel mixture in the cylinders of an engine. There are a couple of ways to fix this problem. One is to increase the octane level of the fuel mixture, which is expensive. The other, which was discovered in the 1920's, is a more inexpensive way and involves adding tetramethyl ($PbMe_4$) or tetraethyl lead (PbE_4) compounds to the fuel mixtures. As a result, large quantities of these compounds were made as anti-knock additives for gasoline.   A significant amount of anthropogenic Pb in the environment is due to these additives. Lead gasoline additives have

10

helped to cause widespread increases in background levels of Pb, even in Antarctica and Greenland where Boutron et al. (1994) reported that the concentrations of Pb in snow had increased by factors of 10 and more than 200, respectively, from 1750 to 1989. In 1989, leaded gasoline was banned in the U.S., but Pb additives are still used in racing fuels, boat fuels, farm tractors, and personal watercraft fuels (Mielke, 1999). Use of leaded gasoline has also been widely discontinued in Canada and most European nations, but it is still regularly used in many developing countries.

Some additional uses of Pb include lead-acid batteries (elemental Pb-Pb^0 and Pb sulfate-$PbSO_4$) used in cars, trucks, motorcycles, and boats; lead solder (tin-Pb alloy); lead based paint (lead chromate- $PbCrO_4$); and hair coloring cosmetic products (lead acetate). Lead is also the base of a large number of important industrial alloys with tin, antimony, copper, and silver. In addition, Pb can be introduced to the environment through the mining and processing of Pb ore minerals.

Lead from acid batteries should not be an environmental problem if battery casings are kept properly sealed and recycled. However, there have been cases where batteries have not been disposed of properly resulting in localized contamination. Hair coloring products and cosmetics are not significant sources of environmental Pb, because concentrations of Pb are very low in these products. Lead based paints have been a significant source of Pb to the environment. Used on both interior and exterior surfaces, Pb is released to the soil, dust, or can be directly ingested as the paint produces flakes with age. Lead-based paint was officially banned from household use in 1978, although Pb can still be found in some specialty paints to this day. In the residential environment, Pb based paints and leaded gasoline are the major sources of this element.

Zinc is the fourth most common metal in use, trailing only iron, aluminum, and copper in annual production (Wikipedia, 2001). Zinc has a wide range of industrial applications, but also is important in plant, animal, and human nutrition. Zinc is used to galvanize steel to prevent rust and corrosion, form alloys such as brass, die casting in the automobile industry, pigments in paints, vulcanization of rubber, soldering formulas, lotions, deodorants, fungicides, wood treatments, and in Zn-air batteries (National Research Council, 1979).

Zinc has been most popularized for its usage in the galvanization of iron and steel. Dipping steel or iron in a bath of molten Zn results in a coating of approximately 300 to 600 g m^{-2} of Zn on the surface (National Research Council, 1979). This coating galvanically protects the underlying iron and steel from corrosion because of the higher electromotive potential of Zn over the Fe in the materials. As a result, the Zn coating must be entirely corroded away before the iron substrate begins to rust. Thus, the structural strength of the material is preserved by sacrificial corrosion of the Zn.

Zinc in the environment has both natural and anthropogenic sources. The largest anthropogenic sources of Zn to the atmosphere are activities related to metal production (mining and processing of Zn ore minerals), while second-tier sources to the atmosphere include waste incineration, fossil fuel consumption, phosphate fertilizer, and cement production (Nriagu and Pacyna, 1988). It has been found that a substantial release of Zn in residential areas is due to tire wear. It has been found that Zn concentrations in soils are orders of magnitude higher in suburban areas when compared with rural areas due to this phenomenon (Councell et al., 2004).

2.3 History of the Tri-State Mining Region

The Tri-State Mining District, which is located in southeastern Kansas, northeastern Oklahoma, and southwestern Missouri, covers an area of about 6475 square km and has a history

12

of mining that predates the Civil War (Pope, 2005). During this time, Pb was mined by trappers and explorers. It was then smelted and made into bullets. However, commercial mining of this region did not begin until about 1850. During the first 20 years, commercial mining activity took place in shallow pits and was limited to small mining operations because of the lack of adequate transportation and heavy machinery. After the Civil War, around 1870, railroads began to extend their lines into the Tri-State District. With this came a reliable means of transportation and steam powered equipment to operate drills, hoists, and pumps that were necessary for rapid expansion of mining operations (Pope, 2005).

The period from 1880 to 1900 was one of great technological advances for Pb and Zn mining in Kansas (Pope, 2005). There were immense improvements in drills, hoists, pumps, blasting equipment, and transportation that allowed for deeper mines and reduced labor. Furthermore, local ore-processing and smelting facilities were established so that the raw ore did not have to be transported before processing, which reduced shipping costs. This also was the period of consolidation. Small, individually owned surface mines slowly began to decline and were bought out by larger mining companies who had the capital to exploit the deeper reserve ores (Gibson, 1972).

Each milling operation produced smelter slag and tailings or waste rock (chat) that was typically stored on site. Since Pb and Zn minerals only averaged about 4 percent of the total ore processed in this region, large volumes of tailings were generated during milling and range in size from <1mm to about 10 mm in diameter (Ritchie, 1986). Unfortunately, the milling processes were not 100 percent efficient and residual concentrations of Pb and Zn minerals remain in all waste materials that have now become a source of environmental contamination. Chat has some distinct characteristics, such as low organic matter and nutrient contents and poor

water holding capacity, both of which can severely limit plant growth. In addition to these physical and chemical properties, elevated concentrations of metals in the mine wastes have the potential to cause phytotoxicity. Average concentrations of Pb and Zn in chat have been found to range from about 360 to 1,500 mg kg^{-1} and 6,000 to 13,000 mg kg^{-1}, respectively (USEPA, 1997). Smelter slag wastes are present in much lower quantities than chat, but are highly enriched in metals (Pierzynski and Gehl, 2004). In a smelter slag material from Dearing, KS, it was reported that Pb and Zn concentrations ranged from 9,111 to 25,313 and 42,592 to 67,654, respectively (Hettiarachchi et al, 2001; Sonmez and Pierzynski, 2005). At these levels, there is significant concern that Pb and Zn could negatively impact human health and cause harm to native ecosystems.

2.4 Effects of Pb and Zn on Human, Plant, and Microbial Health

Lead is not needed to sustain life, in fact it has been found to cause chronic to acute poisoning in wildlife (Beyer et al., 1985; Conder et al., 2001) and can negatively impact the health of humans (ATSDR, 2005). In addition to the human health concern of elevated soil Pb, there are studies that suggest that elevated Pb, Zn, and Cd levels, which naturally occur in geologic deposits together, can endanger native ecosystems (Beyer, 2000; Brown et al., 2005b).

2.4.1 Human Health

Lead is a naturally occurring element that has been used since the beginning of civilization. Today Pb is ubiquitous in the environment, mainly due to the increase in anthropogenic activities (Adriano, 2001). As a result, all humans have Pb in their bodies, but in most cases Pb concentrations are low enough to not impact human health.

There are two key exposure pathways for humans: inhalation of dusts or ingestion of soils/paint chips. In adults, inhalation of dust is most important; however, in children hand to

mouth activity is of great significance especially for children in areas containing soil or dust with elevated cocnetrations of Pb (Pierzynski and Gehl, 2004). Children therefore, receive most of their Pb through ingestion of soil, dust, or paint chips. Acute toxicity can occur in both adults and children. Some symptoms include weakness to extremities, abdominal cramping, slowed reaction time, and anemia. In the reproductive system of adults, Pb can cause low sperm counts in men and diminished fertility in women. Young children are most commonly associated with chronic toxicity due to more hand to mouth activity. Symptoms of chronic toxicity include kidney disease, heart disease, breakdown in both sensory and motor communication, anemia, testicular atrophy, abnormalities in the offspring of women, and severe neurological impairment. Death is probable in children whose blood Pb levels approach or exceed 150 μg dL^{-1} (ATSDR, 2005). Current health guidelines in the United States suggest that children's blood Pb concentrations should not exceed 10 μg dL^{-1} and Pb in drinking water must not exceed 15 μg dL^{-1}. Table 2-1 provides a list of blood Pb concentrations and the effects that one would expect to see in adults and children.

Table 2-1. Blood Pb levels and the effects they have on adults and children (ATSDR, 2005).

	Adult Blood Pb	Children Blood Pb
	$\mu g\ dL^{-1}$	$\mu g\ dL^{-1}$
Nervous System: Encepholapathy	100-120	80-100
Kidney: Atrophy, Interstitial Nephritis	40-100	80-120
Gastrointestinal: Colic	40-60	60-100
Formation of blood Cells: Anemia	50	20-40
Reproductive System: Hypospermia, Testicular Atrophy	40-50	-
Nervous System: IQ, Sensory System Deficits	40	<10
Heart and Blood Vessels: Hypertension	<7	-
Formation of Blood Cells: Enzyme Changes	3-30	<10

Unlike Pb, Zn is one of the essential trace elements. In addition, Zn is a member of one of the major subgroups of micronutrients that have attained prominence in human nutrition and health (Hambidge, 2000). Zinc's ability to participate in strong ligand binding, but yet be readily exchangeable and its ability to have flexible coordination geometry have proved to be extremely useful in biological systems. Furthermore, the incorporation of Zn into the biological systems of mammals has been facilitated by its lack of redox properties, which, in contrast to Fe and Cu, allows it to be utilized without the risk of oxidation damage.

Zinc is ever-present in subcellular metabolism. For example, it is an essential component of the catalytic sites for at least one enzyme in each enzyme classification category (Fierke, 2000). Altogether, there have been hundreds of metalloenzymes identified in both the plant and animal kingdoms; however, it is still unknown whether Zn acts as a functional, structural, or regulatory cofactor (National Research Council, 1979; Havlin et al., 1999). Typcially, Zn does have specific structural roles in enzyme molecules or in other proteins. On occasion, it has been

found that some cells actually secrete Zn^{2+} ions. The roles of these secreted signals remain unidentified, but are currently being pursued in medicinal research. Zinc stands out in human biology due to its versatility, ubiquity, and its important role in cellular growth. As a result, Zn deficiency may result in a generalized impairment of many important metabolic functions (Fierke, 2000).

Although, the consequences of Zn deficiency have been recognized for years, recent attention has been directed to the potential for excessive Zn intake. Zinc is considered to be relatively non-toxic to both humans and animals. However, at exceptionally high intakes, that are in excess of the Recommended Daily Allowance (RDA) for Zn (100 to 300 mg Zn d^{-1} versus an RDA of 15 mg Zn d^{-1}) can cause nausea, vomiting, lethargy, and fatigue (Fosmire, 1990). Additionally, there is overwhelming evidence that excess Zn can induce Cu deficiency in mammals, which can lead to anemia, adverse affects on cholesterol, and an impaired immune system (Sanstead, 1995). However, this is highly unlikely, even in metal contaminated areas, because Zn toxicity is generally limited to cases of accidental overdose. Accidental ingestion of ZnO or cold pills is not overly toxic and recovery is likely, but medical assistance should be immediately sought.

The primary risks associated with excess Zn is predominantly to plant and aquatic ecosystems (Chaney, 1993). Environments having elevated concentrations of Zn will regularly be phytotoxic to most species (Brown et al., 2003b), resulting in poor or no plant growth. Poorly vegetated contaminated areas are prone to erosion, which further enhances the dispersal of the Zn into aquatic systems and increases exposure of co-contaminants in the soil to a variety of organisms through a number of pathways.

2.4.2 Plants

Metal toxicity limits plant growth around many industrial areas in the United States and other countries (Chaney et al., 1988). In many areas where metal concentrations are elevated, primarily caused by anthropogenic activities, the land is completely devoid of vegetation due to interference with biochemical functions. The elements most often responsible are Zn, Cu, and Ni. Zinc is an essential element that is needed by all plants to fulfill certain biochemical functions, although it can be quite toxic to plants at high concentrations. Lead, on the other hand, is considered to be a nonessential element.

Unlike the major nutrients typically supplied in mixed fertilizers (N, P, and K), Zn is only required in relatively small amounts. Yet without this small fraction, no plant could complete its life cycle. Zinc is extremely important in plant nutrition because it is involved in a number of metallo-enzymes (Adriano, 2001), which include dehydrogenase, proteinases, peptidases, and phosphohydrolases (Kabata-Pendias, 2001). Zinc is essential in the stability of cytoplasmic ribosomes, the cell membranes of roots, and also catalyzes oxidation processes (Romheld and Marschner, 1991). Despite being an essential element, excessive soil Zn can be quite harmful to many plant species.

The deficiency of Zn in plants is perhaps more common worldwide, but due to anthropogenic activities such as mining, smelting, and excess fertilization, Zn phytotoxicity problems are becoming an increasing problem. The potential for Zn to become phytotoxic to plants exists because Zn is relatively immobile in soil. As a result, it is easy to build Zn cocentrations to excessive levels in soils. Furthermore, reversion to less plant available forms occurs slowly under nearly all soil conditions and is highly dependent on soil pH (Lindsay, 1979), thus allowing Zn to be available for uptake by plants in soil environments.

Zinc phytotoxicity is undesirable because of decreased crop yield, loss of crop quality,

difficulty in correcting Zn toxicity problems, and the likelihood of Zn transfer through the food chain. The general toxicity symptoms associated with Zn are stunting of the shoot, curling and rolling of young leaves, death of leaf tips, and chlorosis. Chaney et al. (1989) have reported that Zn phytoxicity to grasses is so severe in Palmerton, PA that many homeowners have covered their lawns with stones or other mulch materials to provide a more aesthetic appearance. Plant Zn concentrations that are above 500 mg kg^{-1} are normally considered to be in the toxic range for plant growth (Chaney, 1993). However, in many plant species, Zn leaf concentrations in excess of 100 mg kg^{-1} often result in yield reduction or phytotoxcity symptoms similar to Fe chlorosis (Adriano, 2001).

As previously mentioned, Zn is rarely a human health concern; however, phytotoxic levels of Zn can result in little to no vegetation. Thus, increases in soil erosion by wind and water is expected, which could potentially increase the exposure of other elements that naturally occur with Zn, namely Cd and Pb, to mankind. For this reason, studies have focused on using soil amendments to alter metal bioavailabilities and less sensitive plant species to stabilize mine waste materials (Li et al., 2000; Basta et al., 2001; Hettiarachchi and Pierzynski, 2002; Pierzynski et al., 2002a; Pierzynski et al., 2002b; Brown et al., 2003b; Zwonitzer et al., 2003; Brown et al., 2004). Today work continues in this area because many of these revegetation/stabilization strategies have not been successful, which is related to poor chemical and physical properties of the contaminated soil/waste material materials.

Although Pb occurs naturally in all plants, it has not been shown to play any essential role in their metabolism (Kabata-Pendias, 2001). Recently, Pb has received much attention as a major chemical pollutant of the environment, but is rarely toxic to plants. The phytotoxicity of Pb is relatively low as compared with other trace elements. In rice plants, Kitagishi and Yamane

(1981) found that the order of phytotoxicity for metal contaminants is Cd > Cu > Co ≈ Ni > As ≈ Cr > Zn > Mn ≈ Fe ≥ Pb. Because of the high affinity of Pb for soil organic matter, Pb may not be a significant problem to most agricultural vegetation worldwide. Aside from agricultural settings, plants may be subjected to unusually high levels of Pb in old mining and smelting sites. In this situation, potential phytotoxicity could increase due to acidification by SO_x emissions or acid mine drainage, which could increase Pb bioavailability (Dudka and Adriano, 1997).

Lead is available for plant uptake through both soil and airborne sources. Roots have shown the ability to take up large quantities of Pb from soil; however, the bulk of this Pb stays in the roots and is not translocated throughout the plant (Kumar et al., 1995). Like Zn, Pb accumulates in the surface layers of soils and is quite immobile. Its availability to plants for uptake largely depends on soil conditions; Pb binds strongly to organic matter and its bioavailability depends on the size of soil particles, adsorption capacity, and is influenced by plant factors that control uptake and translocation (Davies, 1995). Lead adsorption in soil increases as pH increases from 3 to 8.5, but between pH values of 5.5 and 7.5. Blaylock et al. (1997) has shown that Pb solubility is controlled by carbonate or phosphate precipitates. Therefore, Pb found in most soil environments will have reduced uptake potential.

The visual non-specific symptoms of Pb toxicity in plants are inhibition of root growth, stunted size, and chlorosis. When Pb enters inside the cells of plants even in small amounts it can have a wide range of adverse effects on physiological processes. Lead phytotoxicity leads to inhibition of enzyme activities, interferes with proper nutrition, causes water imbalances, may cause cell death, and can alter the cell membranes (Sharma and Dubey, 2005). Furthermore, Pb toxicity can inhibit germination of seeds and retard the growth of young seedlings. These disorders upset and interfere with the normal plant growth.

Unlike Zn, some plants are able to tolerate excess of Pb^{+2} by involving processes like exclusion, compartmentalization, or by synthesizing metal detoxifying organic compounds, which essentially bind Pb inside the plant (Singh et al., 1997). Due to these exclusion mechanisms, Pb toxicity is typically further reduced. However, there is great concern of plant uptake and transport into the food chain, especially in plants where roots or tubers are consumed as food. Ingestion of soil particles adhering to the plants can play a more significant role in the dose recieved of Pb received by humans and animals.

2.4.3 Microbes

The soil microbes and soil fauna mineralize organic inputs and soil organic matter to release large quantities of nutrients. Therefore, fertility of natural ecosystems largely depends on the rate of soil organic matter turnover, which is mediated by the soil microbial biomass (Brookes, 1995). Microbes encounter metals and metalloids of various kinds in the environment, which is not surprising. Microbes interact with metals and metalloids, which can either be beneficial or detrimental (Ehrlich, 1997). Of the inorganic pollutants, the heavy metals are by far some of the most damaging to microbial communities. Once heavy metals enter the soil they remain for long periods due to their large half lives, which can be on the order of several thousand years. An increasing body of evidence suggests that heavy metals will have a strong influence on the structure of microbial communities (Frostegård et al., 1993; Frostegård et al., 1996; Sandaa et al., 1999, Kelly et al., 1999), although bacteria have been found to develop tolerances against heavy metal contamination (Diaz-Ravina and Bååth, 1996; Kelly et al., 1999).

The fertility of the soil greatly depends on the activity of the soil microbial biomass, which is generally a small fraction of the organic matter (1-3%). Soil microbial biomass is of fundamental importance in the biogeochemic cycles of all major plant nutrients. In fact, soil

microbes control the major processes involved in nutrient transformation, soil organic matter cycling, and helps to form aggregates, which is essential for plant nutrition, water storage and movement, and proper soil aeration (Robert and Chenu, 1992). Abiotic stress caused by the addition of heavy metals can affect growth, morphology, and metabolism of microorganisms, through functional disturbance, destruction of cell membranes, and interruption of enzymes. Therefore, heavy metal pollution can reduce the size and activity of microbial community and could potentially change its structure (Chander and Brookes, 1993; Kandeler et al., 1996; Barajas-Aceves et al., 1999; Šmejkalová et al., 2003). A diverse microbial community is important because of its role in supporting plant growth by cycling nutrients, performing maintanence on soil organic matter, and production of growth promoting compounds (Bolton et al., 1992). The microbial community is particularly important in heavy metal mine waste systems because microbes are the primary driving force in acid mine drainage, which is related to solubilization, transport, and bioavailabililty of heavy metals (Lovely, 1991).

To have any physiological or toxic effect, most heavy metal ions have to penetrate into the cell. Lead and Zn occur in soils in their ionic forms (Pb^{2+} and Zn^{2+}). This is unfortunate because these metals then get mistaken by microbial cells for other ions with similar charge and size that are needed for proper growth and function. As a result, it is theoretically possible for them to be taken up and transported within a cell's internal system.

Just as in humans and plants, Zn is needed by microbes in small amounts for proper function. Zinc is important to microorganisms because it is not redox sensitive under normal biological conditions and is perfect to complex polypeptide chains when redox changes are undesirable (Nies, 1999). However, elevated concentrations of Zn may be inhibitory or toxic to cellular activities and growth. Zinc is thought to inhibit many microbial processes, including

22

respiration and growth of fungi, germination of fungal spores, growth of algae and protozoa, bacterial conjugation, and nitrification in soil; all of which may lead to changes in the structure and activity of the microbial community. Several researchers have confirmed shifts in microbial populations in contaminated soils by conducting phospholipid-linked fatty acid (PLFA) analysis (Frostegård et al., 1993; Pennanen et al., 1996; Kelly et al., 2003; Hinojosa et al., 2005). Results from Kelly et al. (2003) indicate the soils from the most contaminated Zn sites tend to have lower levels of indicator fatty acids for mycorrhizal fungi and Gram-positive (Gm +ve) bacteria when compared to soils with less Zn contamination. Similarly, Hinojosa et al. (2005) found that Cu, Cd, and Zn were the most important in affecting microbial community structure, along with pH, which would directly affect the availability of these metals. It has been proposed that the toxicity of metals towards PLFA patterns decreases in the order of $Cd = Ni > Zn = Cu > Pb$ (Frostegård et al., 1993).

Unfortunately, most studies on the toxicology of Pb have focused on mankind and plants, and very few studies have been conducted on the direct effects of Pb on microbes. Due to its low solubility in soils, Pb may not be toxic to most microbial species. In fact, there have actually been reports of Pb tolerant bacteria that precipitate Pb-phosphates inside their cell walls (Levison and Mahler, 1998). However, Konopka et al. (1999) found using PLFA analysis that there was a microbial community shift present in a soil containing high concentrations of Pb (approximately 10,000 mg kg^{-1}). Marzadori et al. (1996) concluded that when soil Pb content was 5,000 mg kg^{-1} there was a significant reduction in both dehydrogenase and phosphatase enzymes activities, but in general the decrease was not proportional to the increase in Pb additions. This variation is likely due to differences in physiochemical characteristics of the soils (pH, organic matter content, and moisture) that were studied.

23

2.5 Lead mineral types and stability

Equilibrium reactions of different Pb containing minerals and complexes are given in Table 2-2. It is unlikely that elemental Pb (Pb^o) will persist in natural soil environments, as can be illustrated by the following half-cell reaction.

$$Pb^{2+} + 2e^- \leftrightarrow Pb\,(c) \qquad \log K^o = -4.33$$

Assuming the maintenance of an aqueous Pb concentration of $10^{-8.5}$ M, an electron activity (pe) of -6.41 would be required for elemental Pb to form. In natural environments worldwide, it has been determined that pe normally ranges from -6.0 to approximately 13.0 (Sposito, 1989). Given these values it is highly unlikely for elemental Pb to form in soil environments.

The most common and precious Pb ore mineral is galena (PbS) because it contains roughly 87% Pb by weight. As a result, galena is the only Pb mineral that contains adequate Pb amounts for use an economic source. In oxidized environments (oxygen rich), galena is readily transformed into other common Pb minerals such as anglesite (PbSO$_4$), cerussite (PbCO$_3$), and pyromorphites (Pb$_5$(PO$_4$)$_3$X ; where X = Cl$^-$, F$^-$, or OH$^-$) upon the oxidation of sulfide. In reduced environments, when sulfur is present, the most stable form of Pb is galena.

Table 2-2. Equilibrium reactions of various Pb minerals at 25°C (adapted from Lindsay, 1979).

Reaction No.	Equilibrium Reaction	log K^o
1	PbO (yellow) + $2H^+$ ↔ Pb^{2+} + H_2O	12.89
2	PbO (red) + 2H+ ↔ Pb2+ + H2O	12.72
3	$Pb(OH)_2$ (c) + $2H^+$ ↔ Pb^{2+} + $2H_2O$	8.16
4	Pb_3O_4 (c)+ $8H^+$ +$2e^-$ ↔ $3Pb^{2+}$ + $4H_2O$	73.79
5	PbO_2 (c) + $4H^+$ + $2e^-$ ↔ Pb^{2+} + $2H_2O$	49.68
6	$PbCO_3$ (cerussite) + $2H^+$ ↔ Pb^{2+} + CO_2 (g) + H_2O	4.65
7	$Pb_2CO_3Cl_2$ (phosgenite) + $2H^+$ ↔ $2Pb^{2+}$ + CO_2 (g) + H_2O + $2Cl^-$	-1.80
8	$Pb_3(CO_3)_2(OH)_2$ (c) + $6H^+$ ↔ $3Pb^{2+}$ + $2CO_2$ (g) + 4H2O	17.51
9	$PbCO_3*PbO$ (c) + $4H^+$ ↔ $2Pb^{2+}$ + CO_2 (g) + $2H_2O$	17.39
10	$PbSO_4$ (anglesite) ↔ Pb^{2+} + SO_4^{2-}	-7.79
11	$PbSO_4*PbO$ (c) + $2H^+$ ↔ $2Pb^{2+}$ + SO_4^{2-} + H_2O	-0.19
12	$PbSO_4*2PbO$ (c) + $4H^+$ ↔ $3Pb^{2+}$ + SO_4^{2-} + $2H_2O$	11.01
13	$PbSO_4*3PbO$ (c) + $6H^+$ ↔ $4Pb^{2+}$ + SO_4^{2-} + $3H_2O$	22.30
14	$PbSiO_3$ (c) + $2H^+$ + H_2O ↔ Pb^{2+} + $H_4SiO_4^o$	5.94
15	Pb_2SiO_4 (c) + $4H^+$ ↔ $2Pb^{2+}$ + $H_4SiO_4^o$	18.45
16	$Pb(H_2PO_4)_2$ (c) ↔ Pb^{2+} + $2H_2PO_4^-$	-9.85
17	$PbHPO_4$ (c) ↔ Pb^{2+} + $H_2PO_4^-$	-4.25
18	$Pb_3(PO_4)_2$ (c) + $4H^+$ ↔ $3Pb^{2+}$ + $2H_2PO_4^-$	-5.26
19	$Pb_4O(PO_4)_2$ (c) + $6H^+$ ↔ $4Pb^{2+}$ + $2H_2PO_4^-$ + H_2O	2.24
20	$Pb_5(PO_4)_3OH$ (c) (hydroxypyromorphite) + $7H^+$ ↔ $5Pb^{2+}$ + $3H_2PO_4^-$ + H_2O	-4.14
21	$Pb_5(PO_4)_3Br$ (c) (bromopyromorphite) + $6H^+$ ↔ $5Pb^{2+}$ + $3H_2PO_4^-$ + Br^-	-19.49
22	$Pb_5(PO_4)_3Cl$ (c) (chloropyromorphite) + $6H^+$ ↔ $5Pb^{2+}$ + $3H_2PO_4^-$ + Cl^-	-25.05
23	$Pb_5(PO_4)_3F$ (c) (fluoropyromorphite) + $6H^+$ ↔ $5Pb^{2+}$ + $3H_2PO_4^-$ + F^-	-12.98
24	$PbAl_3(PO_4)_2(OH)_5*H_2O$ (c) (plumbogummite) + $9H^+$ ↔ $Pb2+$ + $2H_2PO_4^-$ + $3Al^{3+}$ + $6H_2O$	9.80†
25	Soil-Pb ↔ Pb^{2+}	-8.50‡
26	$PbMoO_4$ (wulfenite) ↔ Pb^{2+} + MoO_4^{2-}	-16.04
27	PbS (galena) ↔ Pb^{2+} + S^{2-}	-27.51

† Calculated using data from Nriagu (1984) and Lindsay (1979).
‡ Developed using reference level for Pb^{2+} in soils not containing cerussite.

2.5.1 Lead carbonates, oxides, and sulfates

In oxidized systems that have elevated pH values the most stable Pb minerals are the Pb

carbonates (cerussite: $PbCO_3$), basic Pb carbonates ($Pb_3(CO_3)_2OH$), and Pb hydroxides

(Pb(OH)$_2$). Under low pH conditions, the mineral anglesite (PbSO$_4$) would be predicted to have lower solubility as compared to oxide, hydroxide, and carbonates of Pb depending on SO$_4^{2-}$ activity (Figure 2-1). Figure 2-1 was constructed assuming that sulfate activity is 10^{-3} M, because sulfate levels typically range from 10^{-2} to 10^{-4} M for the majority of soils world-wide (Lindsay, 1979). Therefore, given this sulfate activity it is predicted that the solubility of Pb in equilibrium with anglesite is such that the Pb activity would be well above the United States Environmental Protection Agencies (USEPA) action level for drinking water (15 μg L^{-1}). This would suggest that anglesite is much too soluble to persist in soil environments given standard levels of sulfate activity. Thus, Pb is expected to be in a highly bioavailable form when pH is low.

2.5.2 Lead Phosphates

Out of the numerous Pb minerals and complexes listed in Table 2-2, the Pb phosphates and in particular pyromorphites, are some of the most stable forms of Pb under a wide range of environmental and equilibrium conditions (Nriagu, 1972; 1973; 1974; 1978; Lindsay, 1979). Figure 2-2 shows the relative stability and solubility of several Pb phosphates as compared to other common Pb mineral phases. The exact position of the lines depends on the chemical reactions considered and the assumed ion activities of the relevant chemical species. However, the diagram does demonstrate that the pyromorphite species are much more stable over a wider range of pH values than other Pb mineral phases. In general Pb phosphates decrease in solubility in the order:

Pb(H$_2$PO$_4$)$_2$ (c) > PbHPO$_4$ (c) > Pb$_4$O(PO$_4$)$_2$ (c) > Pb$_5$(PO$_4$)$_3$F (c) > Pb$_5$(PO$_4$)$_3$OH > Pb$_3$(PO$_4$)$_2$ (c) > Pb$_5$(PO$_4$)$_3$Br (c) > Pb$_5$(PO$_4$)$_3$Cl (c).
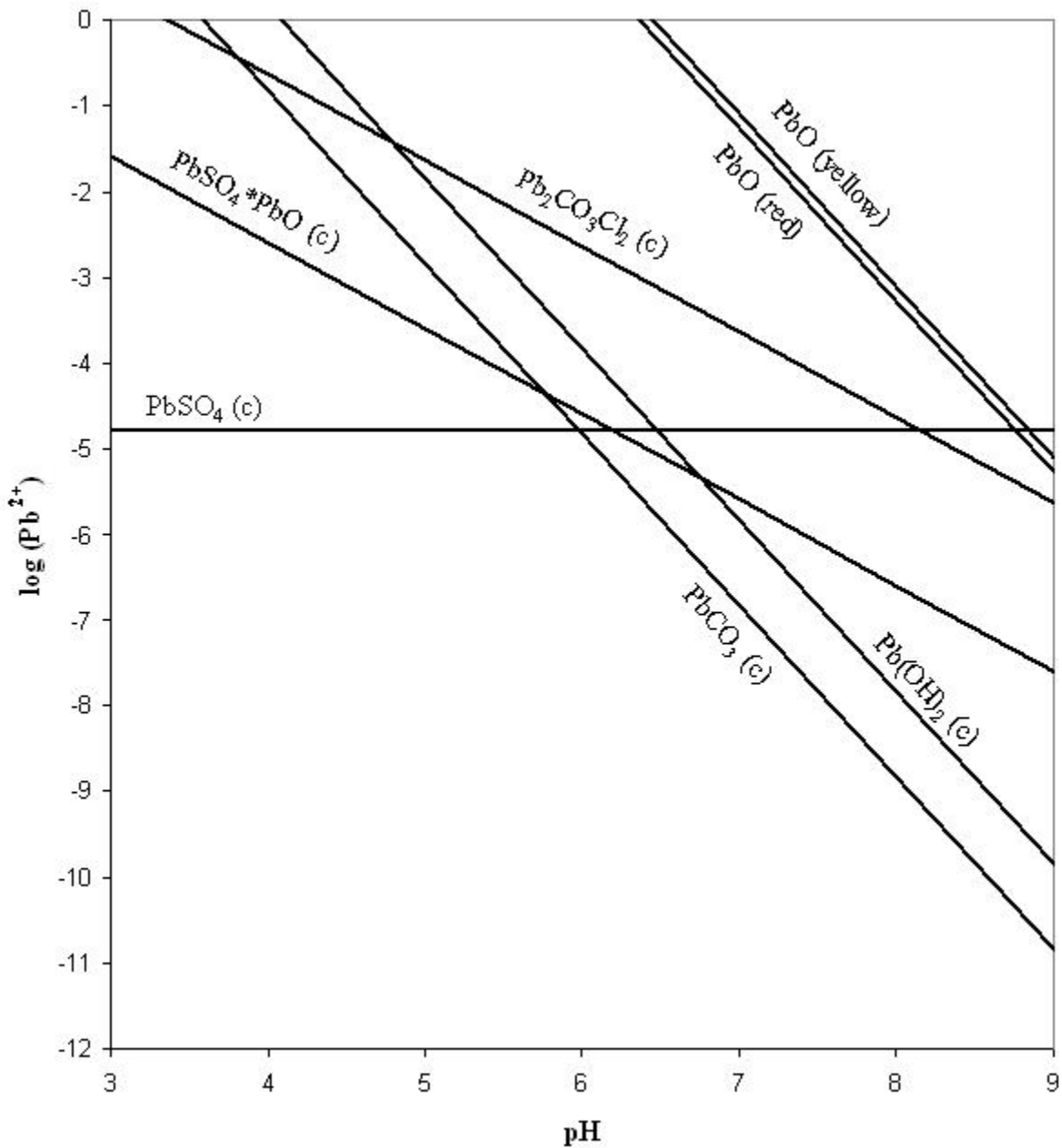
Figure 2-1. The solubility of Pb oxides, hydroxides, carbonates, and sulfates. Developed using the reactions given in Table 2 with $SO_4^{2-} = Cl^- = 10^{-4}$ M and $CO_2 = 0.003$ atm (adapted from Lindsay, 1979).
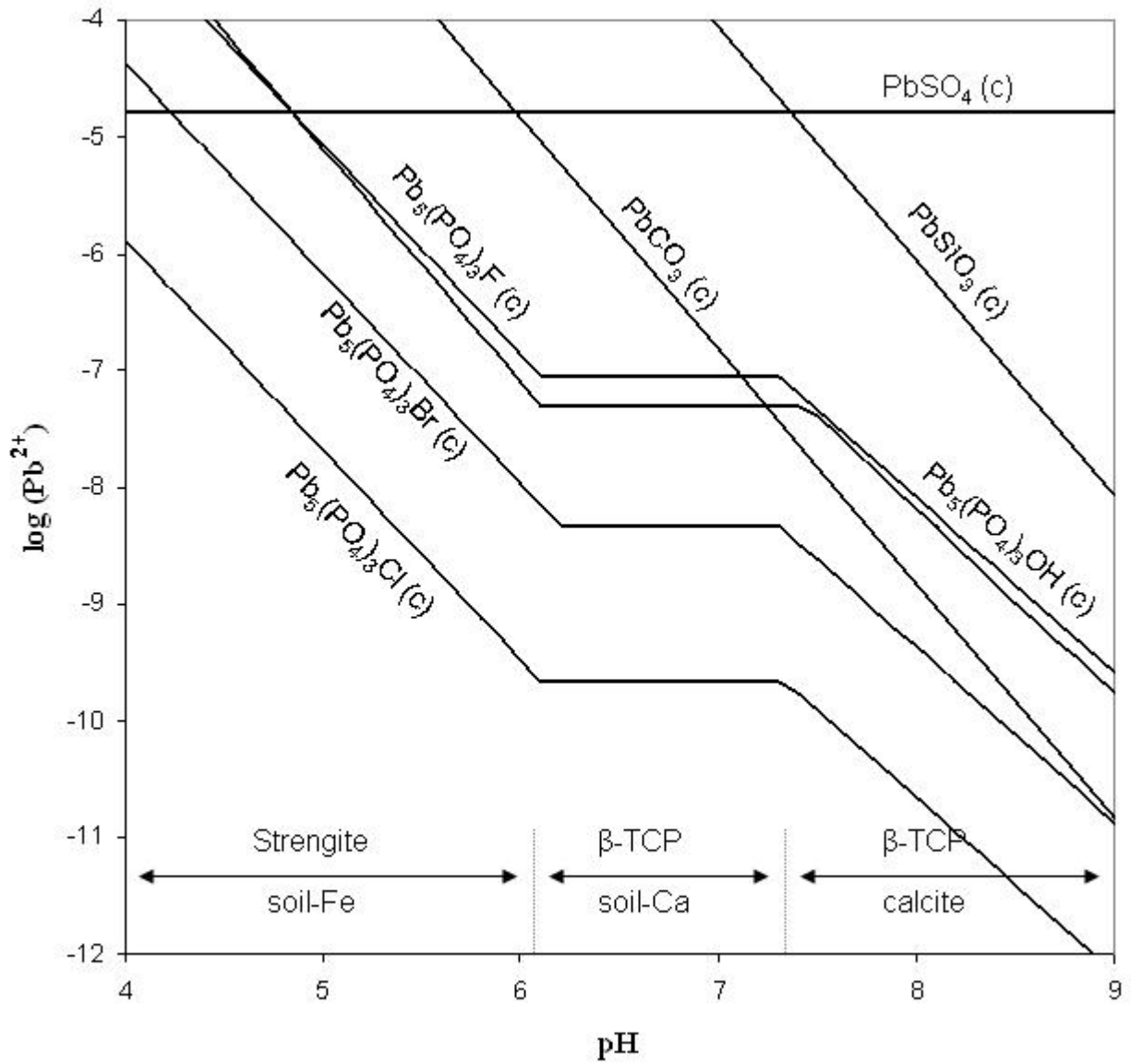
Figure 2-2. The solubility of Pb phosphates as compared to other common Pb minerals. Developed using the reactions in Table 2 with $SO_4^{2-} = Cl^- = 10^{-3}$ M, $F^- = 10^{-4}$ M, $Br^- = 10^{-5}$ M, $H_4SiO_4 = 10^{-4}$ M, and $CO_2 = 0.003$ atm. Adapted from Lindsay (1979).

This comparison is based on 10^{-3} M Cl⁻, 10^{-4} M F⁻, and 10^{-5} M Br⁻ (Lindsay, 1979). Nriagu (1974) presented the stability relations of several lead minerals at 25 °C and 1 atm of pressure in which he demonstrated the principal field of chloropyromorphite stability under aerobic conditions. Additionally, he confirmed that the chloropyromorphites are stable not only in aerobic conditions, but also in moderately reducing environments for the conditions used to derive the limits. For instance, when soil pH is approximately 9.0, the conversion of chloropyromorphite to galena occurs at an Eh of roughly -270 mV.

2.6 Zinc mineral types and stability

Equilibrium reactions of several Zn containing minerals and complexes are given in Table 1-3. It is highly unlikely that elemental Zn (Zn^0) will exist in natural soil environments, as can be observed in reaction 1 of Table 2-3.

$$Zn^{2+} + 2e^- \leftrightarrow Zn \text{ (c)} \qquad \log K^o = -25.80$$

Therefore, if we assumed a maintenance Zn^{2+} concentration of 1 M, an electron activity (pe) of -12.90 would be required for Zn (c) to form. However, as stated earlier, the pe of natural soil environments typically ranges from -6.0 to 13.0 (Sposito, 1989) and therefore, it is unlikely that Zn concentrations would approach 1 M in solution.

Most of the Zn produced globally comes from ores containing the Zn sulfide minerals sphalerite and wurtzite because these minerals contain approximately 64% and 61% Zn by weight, respectively. Other important Zn ores are smithsonite ($ZnCO_3$) and hemimorphite [$Zn_4Si_2O_7(OH)_2 * H_2O$] (52% and 54% Zn by weight, respectively). However, these ores are not as important because they do not contain as much concentrated Zn as compared to the sulfide forms. In oxidized environments, Zn sulfides are readily transformed into Zn silicate, hydroxide, oxide, sulfate, carbonate, and phosphate minerals.

Table 2-3. Equilibrium reactions of various Zn minerals at 25°C (adapted from Lindsay, 1979).

Reaction No.	Equilibrium Reaction	log K^o
1	$Zn^{2+} + 2e^- \leftrightarrow Zn$ (c)	-25.80
2	$Zn(OH)_2$ (amorphous) $+ 2H^+ \leftrightarrow Zn^{2+} + 2H_2O$	12.48
3	$\alpha\text{-}Zn(OH)_2$ (c) $+2H^+ \leftrightarrow Zn^{2+} + 2H_2O$	12.19
4	$\beta\text{-}Zn(OH)_2$ (c) $+2H^+ \leftrightarrow Zn^{2+} + 2H_2O$	11.78
5	$\gamma\text{-}Zn(OH)_2$ (c) $+2H^+ \leftrightarrow Zn^{2+} + 2H_2O$	11.74
6	$\varepsilon\text{-}Zn(OH)_2$ (c) $+2H^+ \leftrightarrow Zn^{2+} + 2H_2O$	11.53
7	ZnO (zincite) $+ 2H^+ \leftrightarrow Zn^{2+} + H_2O$	11.16
8	$ZnCO_3$ (smithsonite) $+ 2H^+ \leftrightarrow Zn^{2+} + CO_2$ (g) $+ H_2O$	7.91
9	Soil-Zn $+ 2H^+ \leftrightarrow Zn^{2+}$	5.80
10	$ZnFe_2O_4$ (franklinite) $+ 8H^+ \leftrightarrow Zn^{2+} + 2Fe^{3+} + 4H_2O$	9.85
11	Zn_2SiO_4 (willemite) $+ 4H^+ \leftrightarrow 2Zn^{2+} + H_4SiO_4^o$	13.15
12	$ZnCl_2$ (c) $\leftrightarrow Zn^{2+} + 2Cl^-$	7.07
13	$ZnSO_4$ (zinkosite) $\leftrightarrow Zn^{2+} + SO_4^{2-}$	3.41
14	$ZnO*2ZnSO_4$ (c) $+ 2H^+ \leftrightarrow 3Zn^{2+} + 2SO_4^{2-} + H_2O$	19.12
15	$Zn(OH)_2*ZnSO_4$ (c) $+ 2H^+ \leftrightarrow 3Zn^{2+} + SO_4^{2-} + 2H_2O$	7.50
16	$Zn_3(PO_4)_2*4H_2O$ (hopeite) $+ 4H^+ \leftrightarrow 3Zn^{2+} + 2H_2PO_4^- + 4H_2O$	3.80

The solubilities of a number of Zn minerals are plotted in Figure 2-3. Franklinite is generally considered the most insoluble of these Zn minerals, but this is highly dependent upon the Fe(III) oxides that control Fe^{3+} activity. Zn carbonates, oxides, sulfates (not shown), and hydroxides (not shown) are far more soluble than franklinite, willemite (a Zn-silicate), and the Zn-phosphate mineral hopeite. Willemite solubility is highly dependent on the activity of H_4SiO_4 in soils, which is considered to be controlled by quartz (SiO_2) (Lindsay, 1979). It is interesting to note that all Zn concentrations are highly influenced by pH. In fact, the solubilities of all Zn minerals in Table 2-3 decrease 100-fold for every unit increase in pH.

Hopeite is an interesting Zn mineral because its existence is believed to be highly dependent upon the concentration of PO_4^{3-} in soils. Lindsay (1979) has considered the activity of
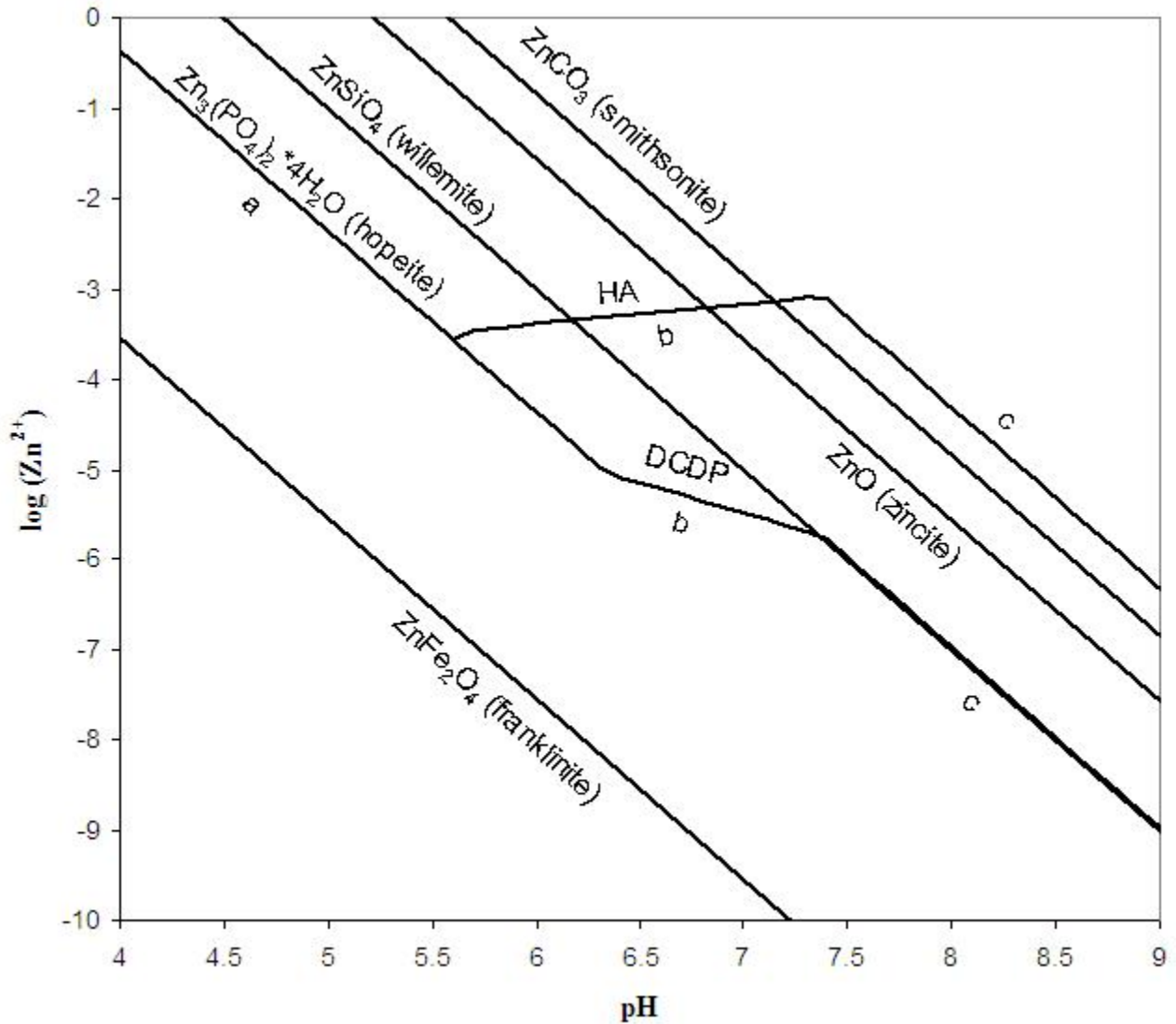
Figure 2-3. The solubility of several Zn minerals. Developed using the reactions in Table 3 with H_4SiO_4 controlled by quartz, Fe controlled by soil-Fe, PO_4^{3-} controlled by hydroxyapatite (HA) or dicalcium phosphate dihydrate (DCDP), Ca = $10^{-2.5}$ M, and CO_2 = 0.003 atm. Adapted from Lindsay (1979).

PO_4^{3-} to be controlled by fixation to strengite-soil-Fe at low pH and by highly insoluble Ca-phosphates at high pH values, which is why the hopeite solubility lines shift upward as pH increases in Figure 2-3. In fact, hopeite becomes quite soluble if hydroxyapatite is controlling PO_4^{3-}. The conclusion that can be drawn from Figure 2-3 is that most Zn containing minerals are typically much more soluble than "soil" Zn in natural systems and therefore, can be expected to supply Zn to plants. Since soils can contain substantial amounts of P and Zn, it is more realistic to consider how P may control the solubility of Zn in most uncontaminated environments.

2.7 Factors Influencing Pb and Zn Solubility

2.7.1 pH

In general, the solubility and phytoavailability of most metals are inversely related to soil pH. Soil pH directly or indirectly controls both Pb and Zn dissolution/precipitation, reduction/oxidation, and sorption/desorption reactions. Thus, pH is one of the primary chemical properties that determine the mobility of Pb and Zn in the soil environment. It is very clear from Figures 2-1, 2-2, and 2-3 that the solubility of Pb and Zn containing minerals is significantly affected by pH. High pH favors precipitation of Pb as hydroxides, carbonates, or phosphates, as well as promotes the formation of Pb-organic complexes, which are considered to be rather stable. As a result, under oxidizing conditions, Pb becomes less soluble as soil pH increases. As previously mentioned, Zn is highly influenced by pH. In fact, for every unit of pH increase the solubility of Zn decreases by 100-fold (Lindsay, 1979). Zinc deficiencies are quite common in calcareous soils because any added Zn rapidly precipitates in soil (Adriano, 2001). The adsorption of Pb and Zn onto organic and inorganic compounds is also affected by the pH of the surrounding environment. This can be attributed to the pH dependency of the surface charges of clays, metal (hydr)oxides, and organic matter. As the pH of the soil environment increases,

adsorption of cationic metals generally increases due to the enhanced dissociation of protons from the surface functional groups of the variably charged organic and inorganic soil components.

2.7.2 Dissolved ions and complexes

Dissolved concentrations of both organic and inorganic species can be quite important in determining the solubility of Pb and Zn in soils and natural waters. The bioavailability of Pb and Zn in natural waters that move through materials that contain carbonate, phosphate, or silica rocks, as well as the rhizosphere (containing high concentrations of organic acids) may perhaps change significantly. Precipitation or adsorption of these metals is quite possible under ideal conditions, which would remove dissolved ions from solution making them less bioavailable. Both Pb and Zn can be associated with numerous phases in soils, all of which are extremely pH dependent. Dissolved ions of Pb^{2+} and Zn^{2+} are particularly important species when pH values fall below 7. Above pH of 7, the Pb and Zn hydrolysis species [$PbOH^+$, $Pb(OH)_2$, $Pb(OH)_3^-$, $ZnOH^+$, $Zn(OH)_2$, and $Zn(OH)_3^-$] become increasingly more significant, which reduces the activity of the free ions, and thus decreases the bioavailability of these metals to all organisms.

2.7.3 Effects of redox

Lead ($6s^2\ 6p^6$) can exist in three oxidation states naturally. They are Pb (0), Pb (II), and Pb (IV). However, only the Pb^{2+} oxidation state is important over the wide range of environmental conditions that exist in soils. Zinc ($3d^{10}\ 4s^2$), however, can exist in only two oxidation states naturally. They are Zn (0) and Zn (II) and just like Pb, only the Zn^{2+} oxidation state is important in soil environments. Pb and Zn redox reactions are more important in an indirect way. In fact, the major sources of Pb and Zn contamination to surface and ground water is through mining activities that expose unstable sulfide minerals to the oxygen-rich waters

33

(Carroll et al., 1998). In addition, the redox status of a soil or system can induce the formation/dissolution of Fe and Mn oxides, cause reformation of sulfide minerals, and affect the interactions of Pb and Zn with P.

2.8 Adsorption of Pb and Zn

In addition to the solid phases that control Pb^{2+} and Zn^{2+} activities in the soil solution, adsorption processes can also have considerable control over both Pb and Zn bioavailability. The adsorption of heavy metals has been studied and reported in the literature for silicate minerals (Swift and McLaren, 1991); for Fe-, Al-, and Mn-oxides (Schwertmann and Taylor, 1989); and for humic substances (Stevenson and Fitch, 1986). This adsorption has been described in terms of two molecular mechanisms: (i) nonospecific adsorption where the metallic cations behave as counter-ions in the diffuse layer; and (ii) specific adsorption resulting from surface complexation (Msaky and Calvet, 1990). Several models have been proposed in an attempt to explain the specific adsorption of metal cations. Sposito (1989) defined the tendency of the metals to form covalent bonds on the basis of ionic radius and the ionization potential quantified by the Misono softness parameter. This parameter measures the ability of the metal cations to form strong complexes according to their ability to form covalent bonds, in the following order: Pb > Cd > Cu > Co > Ni > Zn. According to McBride (1994), electronegativity is an important factor in determining which of the trace metals chemisorb with the highest preference and, on this basis, the predicted order would be Cu > Ni > Co > Pb > Cd > Zn > Mg > Sr. On the other hand, if the ability of the metals to sorb were based only on electrostatics, the strongest bond should be formed by the metal with the greatest charge-to-radius ratio, which again changes the metal preference [Ni > Mg > Cu > Co > Zn > Cd > Sr > Pb] (McBride, 1994). Soil pH is probably the most influential parameter that controls the metal-solution and soil-

surface chemistry. The number of negatively charged surface sites increases with pH. Therefore, heavy metal sorption in low pH soils is expected to be minimal.

Research investigating Zn sorption in simplified oxide and clay mineral systems and in soils displays its variable reactivity and speciation. Macroscopic sorption studies have shown that Zn can effectively adsorb onto Mn oxides (Stahl and James, 1991), Fe (hydr)oxides, Al (hydr)oxides (Kinniburgh and Jackson, 1982), and aluminosilicates (Sparks et al., 1995), with the extent of adsorption increasing with pH. However, at high pH values and high initial Zn concentrations the precipitation of $Zn(OH)_2$, $ZnCO_3$, and $ZnFe_2O_4$ are likely to control Zn solubility (Lindsay, 1979). By employing X-ray absorption fine structure (XAFS) spectroscopy to investigate Zn sorption to oxides in neutral to basic pH environments, researchers have demonstrated that Zn can form both inner-sphere surface complexes and Zn hydrotalcite-like phases upon adsorption to Al bearing minerals (Ford and Sparks, 2000), inner-sphere complexes on goethite (Schlegel et al., 1997), and both inner-sphere and multinuclear hydroxo-complexes on manganite (Bochatay and Persson, 2000). Manceau et al. (2000) used a variety of techniques, including XAFS and microfocused XAFS to demonstrate that upon weathering of Zn mineral phases, Zn was removed from solution by the formation of Zn-containing phyllosilicates and to a lesser extent by adsorption to Fe and Mn (oxyhdry)oxides. Zinc can also adsorb to humic substances. However, when compared to other trace metals (Cu, Pb, Ni, and Co) the selectivity for Zn sorption to humic materials is minimal when competing cations are present (Schnitzer, 1969).

Like Zn, Pb has been found to adsorb to metal oxides, clay minerals, and humic substances. Sorption mechanisms of Pb onto these materials are extremely complex and difficult to investigate (Matocha et al., 2001). Gomes et al. (2001) found that the cation exchange

capacity was the variable that most strongly correlated to Pb adsorption in Brazilian soils. This research also demonstrated that pH may play an important role in the sorption of Pb, which could be related to Pb hydrolysis. Increasing soil pH reduces the solubility of most Pb-bearing minerals, while increasing the adsorption affinity of Fe (hydr)oxides, Al (hydr)oxides, Mn (hydr)oxides, organic matter, and other adsorptive surfaces. Strawn et al. (1998), employing X-ray absorption spectroscopy (XAS), noted that Pb sorbed as an inner-sphere bidentate surface complex on γ-Al_2O_3, while Bargar et al. (1996) showed that both outer- and inner-sphere surface complexes occur between Pb and surface functional groups of α-Al_2O_3 depending on the specific site exposed. Weesner and Bleam (1998) determined that Pb can bind as an inner sphere complex on pristine goethite and often groups into oxy-clusters on the surface of pristine boehmite. Furthermore, they found that boehmite is a much poorer adsorbent for Pb per unit surface than goethite. Other studies using 2:1 phyllosilicates minerals with fixed structural charge have reported metal exchange on basal planes and inner-sphere surface complexation at edge sites for Pb depending on ionic strength and pH (Strawn and Sparks, 1999). Matocha et al. (2001) concluded that Pb was adsorbed as an inner-sphere complex by both birnessite (δ-$MnO_{1.7}$) and manganite (γ-MnOOH), but was much more strongly sorbed by birnessite under all experimental conditions. Beak et al. (2008) concluded that birnessite has a very high affinity for Pb and as a result, Pb sorbed to birnessite would have very little bioaccessibility. Additionally, by using XAFS they proposed that the surface speciation of birnessite Pb was due to a triple corner sharing complex in the birnessite interlayer. Under certain conditions, Pb adsorption may be enhanced or reduced in the presence of certain anions. Bargar et al. (1998) showed that the uptake of Pb by goethite was enhanced in the presence of Cl^- due to the Pb-Cl^--Fe(s) ternary complex formation found using XAFS derived atomic distances. Weesner and Bleam (1998)

concluded that the presence of either phosphate or sulfate anions generally increased the ability of goethite and boehmite to retain Pb in solution. In addition, they found that when P was added to the goethite system that Pb-phosphate phases precipitated on the surface, suggesting that a FeOOH/P/Pb relationship may exist.

Organic matter is an important component of the soil since it has a high surface area and has functional groups that can chemically react with metals (Sparks, 2003). It has been observed that Pb forms strong complexes with soil organic matter, and Pb can preferentially bind to adsorption sites on soil organic matter better than most other metals (Kendorff and Schnitzer, 1980; Jin et al., 1996; Suave et al., 1998). Strawn and Sparks (2000) discovered that there is a strong correlation between soil organic matter and the percent of Pb desorbed in soils. Their study suggests that soil organic matter plays a significant role in the slow desorption reactions of Pb from most soil materials.

2.9 Remediation of Pb and Zn contaminated soils

As previously discussed, a primary source of Pb and Zn contamination in soils is due to the mining and smelting of ores containing these metals. Mining-related wastes, such as waste rock and tailings, represent potential sources of metals that can be redistributed to the surrounding environment by both aerial and fluvial transport. Adverse environmental impacts from exposure to Pb and Zn from contaminated mining sites include risks to human health, phytotoxicity, contamination of soil and water, and ecotoxicity (Adriano et al., 1997; Pierzynski, 1997). Contaminated soil often presents an unacceptable risk to human and ecological health and must be cleaned up. Commonly used methods have involved excavation and landfilling of smelter/mine contaminated soil/waste materials, but more recently less invasive and expensive *in situ* solutions have been favored to reduce metal bioavailability (Iskandar and Adriano, 1997).

Chemical immobilization is an *in situ* remediation method where inexpensive materials, such as fertilizers and waste products, are added to contaminated soils to reduce the solubility of heavy metal contaminants. Since contaminant solubility is related to its mobility and bioavailability in the environment, chemical immobilization may reduce the environmental risk. Recent research has focused on the potential to change the bioavailability of soil Pb, Zn, and Cd *in situ* by altering the mineral forms of these elements or by providing reactive surfaces to increase adsorption (Mench et al., 1994). In the fixation processes of amendments, the general mechanisms behind the immobilization of heavy metals are cation exchange, adsorption, surface complexation, and precipitation. Numerous studies have been conducted using chemical amendments (including organic matter, alkaline material, phosphate fertilizer, and metal oxide adsorbents for remediation of Cd, Pb, and Zn). The success of chemical immobilization can then be evaluated by a given amendments ability to reduce contaminant bioavailability in a contaminated soil or waste material (Basta et al., 2001). Long-term effectiveness and permanence are important criteria that need to be taken into consideration when assessing alternative remediation technologies.

2.9.1 Organic Amendments

Soil organic matter, nutrients, and biological activity contribute to ecosystem-level processes, which are important for sustaining terrestrial ecosystems (Stevenson, 1994). In recent years, successful application of biosolids or composted materials has been used in an attempt to remediate heavy metal contaminated soils (Vangronsveld et al., 1995; Li et al., 2000; Brown et al., 2003b; Clemente et al., 2005). Such treatments provide large amounts of organic matter, which significantly increase the sorption capacity for metals in a given soil (Adriano, 2001). Furthermore, organic materials favor plant growth through the improvement of soil fertility,

physical properties, and nutrient cycling in areas that are devoid of vegeatation caused by the presence of heavy metals.

Mine tailings are most often characterized by the absence of organic matter, nitrogen, phosphorus, and by their neutral to low pH, high acid-producing potential, and poor soil structure (Wong et al., 1998; Krzaklewski and Pietrzykowski, 2002). As a result, organic amendments provide many of the necessary traits needed for healthy ecosystem function. Benefits directly associated with improved organic matter content include: enhanced water infiltration and moisture holding, improved aggregation, proper aeration, increased nutrient supply, and greater microbial activity. However, a concern with using organic materials alone to remediate contaminated areas is the permanence of the materials. Unfortunately, the C contained in organic materials is used by microbial communities as an energy source and, unless replenished by C additions from vegetation, the benefits of the organic amendment additions will be lost as the C content decreases. Thus, for an organic amendment to be successful over time, one may have to add large quantities of an organic material to a contaminated soil in hopes of establishing a new equilibrium of organic matter in the system that would retain the toxic metals and support healthy ecosystem function.

Berti and Cunningham (1997) performed a study involving the use of various types of organic amendments such as ground alfalfa (*Medicago sativa* L.), sphagnum peat moss, and composted leaves. They concluded that organic materials reduced bioavailability of Pb as measured by the physiologically based extraction test (PBET), but not to the same extent as inorganic soil P amendments. Pearson et al. (2000) found that composted leaves did not reduce the bioavailability of Pb to earthworms (*Eisenia fetida*), while Basta et al. (2001) reported that lime stabilized biosolids did not reduce the GI-available Pb in both gastric and intestinal

39

solutions. However, it was found that alkaline organic treatments can reduce human exposure to both Cd and Pb by reducing Zn phytotoxcity thus promoting the revegetation of contaminated sites (Basta et al., 2001).

In several studies, composts and biosolids have been mixed with other inorganic additives to either help raise soil pH or provide more permanent adsorptive capacity. In a study conducted by Brown et al. (2004), municipal biosolids compost (called Compro) high in both lime equivalent and Fe was added to a Pb, Zn, and Cd contaminated soil. They found that Compro was able to reduce the phyto- and bioavailability of all three heavy metals. Li et al. (2000) used biosolids compost with a high pH, organic matter, Fe, and P content to find that it was able to improve the overall success of vegetation establishment on highly Zn-contaminated soils. Similarly, DeVolder et al. (2003) reported that biosolids compost mixed with wood ash allowed for vigorous plant growth in metal contaminated tailings, thus indicating a reduction in phytotoxicity. In addition to these studies, others have found that the combination of biosolids with other residuals have the ability to increase soil fertility, restore a vegetative cover, and improve ecosystem function in areas that are contaminated by heavy metals (Brown et al., 2003b; Brown et al., 2005b). As a result, the mobility and exposure pathways of heavy metals to humans would be reduced, while reestablishing a self sufficient, fully functioning ecosystem.

Biosolids isn't the only organic waste material that has been studied. Composted organic household wastes were also found to be successful at remediation of a soil polluted by a Cu/Ni smelter as shown by the restoration of microbial communities (Kiikkilä et al., 2001). Ruttens et al. (2006) reported that using composted organic household wastes in combination with cyclonic ashes and steel shots was an efficient treatment for phytostabilization of a contaminated soil. In a greenhouse study, composted manure along with lime increased the germination and dry

weight yields of *Cynodon dactylon* (Bermuda grass) and *Agropyron elongatum* (tall wheatgrass) in Pb/Zn mine tailings from China (Ye et al., 2000). Furthermore, the addition of high pH spent mushroom compost to a sandy soil contaminated with Zn-containing flue dust was able to ameliorate the toxic effects of Zn (Shuman and Li, 1997). The above studies suggest that a wide assortment of available organic soil amendments exists, with varying levels of processing and characteristics in most regions of the U.S. and the world that can be used for the successful remediation of heavy metal contaminated soils.

The intent of using organic materials to help phytostabilize metal contaminated soils/wastes is to create a self-sustaining system where nutrients are cycled internally by healthy microbial and plant populations with no further inputs needed. Pierzynski et al. (2002a) discovered that additions of beef manure applied at a rate of 90 Mg ha^{-1} resulted in an increase in tall fescue (*Festuca arundinacea* Shreb) growth in the first year after the amendment addition. However, by year three plant growth started to decline and plant tissue analysis suggested Zn phytotoxicity. In another study, Brown et al. (2003b) concluded that surface applications of high N biosolids (66 Mg ha^{-1} biosolids) with wood ash is effective at establishing a vegetative cover on Cd, Pb, and Zn mine tailings for at least two growing seasons, but with time they observed a decrease in plant Ca, K, and Mg concentrations. This led them to conclude that higher amendment loadings may be needed to supply essential plant nutrients that are required to support proper plant growth. Therefore, more research is needed to investigate the effectiveness of increased additions of organic amendments on permanence of the amendments, plant growth, and the effects on microbial populations over time.

2.9.2 Phosphate Amendments

In situ stabilization using P has the potential to decrease metal solubility through the

formation of metal-phosphate precipitates, thus increase long-term stability by forming these less soluble, more stable metal-phosphate minerals (Mench et al., 1998). Decreasing metal solubility is critical for reducing metal transport and bioavailability to plants, animals, and humans. The formation of insoluble complexes with phosphates in soils has been considered as an important self-purifying process, which can regulate the Pb levels in soils for a period of time (Nriagu, 1973; 1974; 1978; 1984; Lindsay, 1979). Additionally, researchers have proposed that the formation of metal phosphates may control the solubility of Zn and Cd as shown in soil suspensions when a soluble P source was introduced (Santillian-Medrano and Jurinak, 1975; Xie and MacKenzie, 1990). Cotter-Howells and Caporn (1996) reported that the addition of soluble phosphates does indeed induce the formation of heavy metal phosphate precipitates. These findings are extremely important because it is well known that phosphate materials or the inherent presence of sufficient soil P levels has proven extremely effective as a chemical immobilization treatment for Pb, but not much information exists on the effects of phosphates on other metals (Cd and Zn) that geochemically exist with Pb in the environment.

Research involving the use of phosphate materials as a way to immobilize heavy metals in soils has utilized a number of phosphate containing materials. Currently the materials that have been studied include the mineral apatite (commonly called phosphate rock, PR), synthetic apatites, diammonium phosphate (DAP), monopotassium phosphate (KH_2PO_4), disodium phosphate (Na_2HPO_4), triple superphosphate (TSP), pyrophosphates, and phosphoric acid (PA) (Basta et al., 2001; Basta and McGowen, 2004; Brown et al., 2004; Cao et al., 2002; Cao et al., 2003; Cao et al., 2004; Cao et al., 2008; Chen et al., 1997; Cotter-Howells and Caporn, 1996; Hettiarachchi et al., 2000; Hettiarachchi et al., 2001; Hettiarachchi and Pierzynsksi, 2002; Ma et al., 1993; Ma et al., 1995; Ma and Rao, 1997; McGowen et al., 2001; Stanforth and Qiu, 2001;

Xie and MacKenzie, 1990; Yang et al., 2001; Zwonitzer et al., 2003). The majority of these studies focus on the formation of Pb-phosphates or more specifically the precipitation of the highly insoluble Pb mineral pyromorphite [$Pb_5(PO_4)_3(OH, Cl)$] upon the addition of P amendments. Studies have mainly focused on Pb because of its known negative impacts on human health and it is estimated to affect greater than a billion people worldwide (Nriagu, 1988).

Phosphates of Pb and Zn have low solubilities (Nriagu, 1973; 1984) and are generally several orders of magnitude less soluble than the analogous carbonates and sulfates (Lindsay, 1979). Thus, formation of Pb and Zn phosphates in contaminated soils is ideal to reduce bioavailability of these metals. Ruby et al. (1994) has indicated that adequate levels of soil P were responsible for the formation of insoluble complexes and the reduction in potentially bioavailable Pb. Several studies have been conducted to confirm that P additions do indeed decrease Pb bioavailability. In a few studies, the PBET procedure was used to mimic the human digestive system. It was concluded in these studies that PR, TSP, and PA were all able to reduce bioavailable Pb to humans (Hettiarachchi et al., 2000; Hettiarachachi et al., 2001; Hettiarachchi and Pierzynski, 2002). They found that reductions in bioavailability ranged from 15 to 41% for P treatments alone. When cryptomelane, a manganese oxide, was added in addition to P, the bioavailable Pb was reduced by 23 to 67% over the control. Similarly, Yang et al. (2001) reported a reduction up to 60% in bioavailable Pb, using the PBET procedure, when treating contaminated soils with PA, while Stanforth and Qiu (2001) found that TSP and a sodium phosphate solution significantly reduced bioavailable Pb as determined by the PBET.

A few researchers have reported less soluble Pb minerals after contaminated soils had been treated with PR or TSP, as determined by the toxicity characteristic leaching procedure (Cao et al., 2004; Chen et al., 1997; Hettiarachchi et al., 2000). Chen et al. (1997) determined

that PR was also effective at removing dissolved Cd and Zn leached from contaminated soil using solutions of differing pH (3 to 12) by 20 to 97.9% and 28.6 to 98.7%, respectively. This disappearance of Cd and Zn has been credited to surface complexation, ion exchange, and the formation of amorphous solids on phosphate rock, with the possibility of metal phosphate mineral formation. Hettiarachchi et al. (2000) used X-ray diffraction (XRD) analysis to detect changes in Pb mineralogy in P treated soils. Pyromorphite peaks increased in intensity after addition of P amendments, which confirmed their toxicity characteristic leaching procedure findings that Pb was becoming less bioavailable. Additionally, they found that while PR did decrease Pb bioavailability, the use of more soluble P source, such as TSP, was far superior at reducing Pb concentrations. Cao et al. (2002) studied the use of PA, PA + TSP, and PA + PR as potential P treatments. They concluded that the PA + PR treatment was the best overall because it was able to reduce Pb bioavailability and was able to reduce the possible negative impacts of PA when applied alone. Cotter-Howells and Caporn (1996) used XRD and scanning electron microscopy/energy dispersive X-ray analysis to confirm the formation of Pb- and Zn-phosphates after contaminated soils were treated with Na_2HPO_4 or planted with *Agricostis capillaries*. The uniqueness of this study is that they were able to detect the formation of metal phosphates in the rhizosphere of *Agricostis capillaries* without the addition of soluble P, suggesting a biochemical transformation that is root induced. Other studies have looked at the influence on plant growth by adding soluble forms of P to contaminated soils. Brown et al. (2004) concluded that a 3.2% P-TSP and 1% P-H_3PO_4 treatments were able to significantly reduce Cd, Pb, and Zn uptake by plants. Similarly, Hettiarachchi and Pierzynski (2002) found that TSP was able to reduce concentrations of Cd, Pb, and Zn in shoot tissues of sudax [*Sorghum vulgare* (L.) Moench] and swiss chard [*Beta vulgaris* (L.) Koch], but the addition of PR was unsuccessful. By using a

combination of PA and PR together, Cao et al. (2002) were able to determine that the uptake of Pb in St. Augustine grass (*Stenotaphrum secundatum*) used to induce the formation of metal phosphates in soils. Zwonitzer et al. (2003) used KH_2PO_4 as a source of P to reduce Cd, Pb, and Zn. While they found that KH_2PO_4 was able to reduce bioavailability of Pb, it had variable effects on the availability of Cd and Zn. McGowen et al. (2001) employed the use of DAP and found it effective at reducing the elution of Cd, Pb, and Zn from a smelter-contaminated soil. However, they concluded that the co-application of liming materials with DAP may be necessary to offset potential soil acidification from ammonium fertilizer application in non-alkaline soils. Acidity can increase the solubility of Zn, which can negatively impact plant production. Pierzynski and Schwab (1993) found that DAP increased both Cd and Zn bioavailability to soybean [*Glycine max* (L.) Merr.]. Levi-Minzi and Petruzzelli (1984) showed that monammonium phosphate (MAP) decreased and DAP increased the amount of Cd sorbed by the soil. It appears that different soil types and conditions may provide conflicting results; thus there is a need for understanding the reactions of different P amendments at the molecular level. Furthermore, P amendments may have to be applied on a location/amendment specific basis to maximize its potential.

It is unrealistic to assume that once a metal is complexed or precipitated in a crystalline phase that it is forever removed from the system (Scheckel and Ryan, 2002). As a result, it is necessary to examine the stability of immobilized contaminants. The literature previously discussed demonstrates that metal phosphate formation can be easily accomplished by the reaction of metal contaminated soils with available P. However, it is inevitable that one of these components will be rate limiting under normal environmental conditions and should be considered before adopting this remediation strategy to metal contaminated soils/waste materials

(Scheckel and Ryan, 2002). The potential impact of using P sources to safely sequester metal contaminants in the natural environment holds great promise, but must be managed carefully and intelligently. Additional research is still needed to evaluate the reduction of heavy metal solubility, mobility, transport, and speciation in the immediate area of a treatment in multiple soil chemical environements with different P amendments.

2.9.3 Alkaline Materials

Research on chemical immobilization of heavy metals has included the use of alkaline amendments. Alkaline amendments reduce heavy metal solubility in soil by increasing pH, which subsequently increases metal sorption to soil particles (Filius et al., 1998; McBride et al., 1997). Additionally, increased soil pH and carbonate buffering can lead to the formation of metal-carbonate precipitates, complexes, and secondary minerals that decrease metal solubility and reduce metal transport (Chlopeka and Adriano, 1996; Lindsay, 1979; McBride, 1989; Mench et al., 1994). Alkaline materials are anticipated to be effective only for a relatively short period of time before the pH-buffering capacity of the amendment is depleted. This effect is typically even more pronounced in mine wastes due to the potential acidity that exists. For example, the most common ore minerals for Pb and Zn are their sulfide forms galena and sphalerite, respectively. When sulfide minerals are introduced to oxidized conditions they immediately begin to form sulfate, which releases large quantities of H^+. As a result, large or repeated applications of alkaline materials are regularly needed to combat acidity (Vangronsveld and Cunningham, 1998). However, an increase in pH has the potential to increase the dissolved organic matter concentration, which may cause organically bound metals to be further dispersed throughout the environment. Additions of alkaline materials may also impact microbial activity (Haynes and Naidu, 1998) and change the ecosystem in terms of vegetation (Roem and

Berendse, 2000) and other soil organisms (Korthals et al., 1996). Nevertheless, a pH increase is often effective in reducing metal leaching and plant uptake.

Alkaline materials used as chemical immobilization treatments include calcium oxides, and calcium and/or magnesium carbonates (Derome, 2000; Derome and Saarsalmi, 1999; Filius et al., 1998; Friesl et al., 2006; Gray et al., 2006; Hooda and Alloway, 1996; Krebs et al., 1998; Li et al., 2000; Palazzo et al., 2003; Pierzynski and Schwab, 1993). Lime materials have been shown to be effective at reducing plant uptake of Zn, but mixed results have been reported for plant uptake of Cd (Krebs et al., 1998; Pierzynski and Schwab, 1993). Li and Chaney (1998) found that lime was fairly ineffective for treatment of highly Zn contaminated soils at the Palmerton, PA Superfund site. However, when the lime was combined with high iron biosolids the combination reduced Zn uptake, thus phytostabilizing the area.

While alkaline materials may not always be highly successful as an individual treatment, when paired with other inorganic or organic amendments, alkaline materials can aid in the sequestration of metals. The organic or inorganic amendments provide binding sites that can immobilize heavy metals and an increase in soil pH further contributes to the immobilization of heavy metals by making the surface adsorption sites more reactive toward metal binding due to decreased proton competition. Recent work suggests that application of limestone or other high calcium carbonate material in combination with biosolids effectively restores ecological function to metal-contaminated soils (Brown et al., 2003a; 2003b; Conder et al, 2001; Li et al., 2000).

Beef cattle feedlot manure/compost could serve as a possible dual purpose amendment. Not only would the material supply organic matter to adsorb metals, but feed rations routinely contain calcium carbonate that is expelled in animal waste, thus giving the manure/compost some liming potential (Eghball, 1999). Ye et al. (2000) found that lime and composted manure

applied simultaneously reduced extractable concentrations of both Pb and Zn and improved seed germination of *C. dactylon* and *A. elongatum*. Gravel sludge has also been proposed as a potential immobilizing agent to sequester heavy metals in soils (Krebs et al., 1999; Lothenbach et al., 1998). Gravel sludge is a waste product of the gravel industry that contains approximately 42% clay minerals, 31% calcium carbonate, 18% quartz, 2% organic matter, and 7% dolomite/plagioclase. Consequently, it provides both adsorptive and alkaline amendments in one treatment. Lothenbach et al. (1998) discovered that a gravel sludge amendment was able to decrease both Cd and Zn concentrations in red clover (*Trifolium pretense*). Similarly, Krebs et al. (1999) found reductions in Cd and Zn in ryegrass (*Lolium perenne* L.) and lettuce (*Lactuca sativa* L.) when using the same gravel sludge as a soil amendment. In both studies, $NaNO_3$ extractable metals were decreased upon the additions of the amendment. Part of the immobilization effect can be credited to the increase in pH, but an increase in adsorptive capacity is likely just as significant.

2.9.4 Adsorption of metals by oxides, clay minerals, and zeolites

Surface adsorption is a potentially important process for reducing heavy metal bioavailabilities in contaminated soils. Metal oxides (such as Fe, Mn, Al, and Ti (hydr)oxides) and clay minerals can occur naturally as discrete particles and as coatings on the surfaces of other minerals in soil environments. Due to their high surface reactivity, essentially irreversible adsorption reactions toward dissolved metal ion species may occur. As a result, additions of natural or synthetic metal oxides and/or clay minerals to heavy metal contaminated soil have the potential to reduce bioavailable metal concentrations. A large number of different inorganic adsorption amendments have been proposed and evaluated for *in situ* immobilization of heavy metals in soils. Amendments have included manganese, aluminum, and iron oxides (Beak et al.,

2008; Cheng and Hseu, 2002; Ciccu et al., 2001; Crawford et al., 1993; Gray et al., 2006; Hettiarachchi and Pierzynski, 2002; Hettiarachchi et al., 2000; Kinniburgh et al., 1976; Matocha et al., 2001; Mckenzie, 1980; Suave et al., 2000; Weesner and Bleam, 1998), gravel sludge (Krebs et al., 1999; Lothenbach et al., 1998), zeolites (Cheng and Hseu, 2002; Oste et al., 2002), and clay minerals (Aubooiroux et al., 1996; Lothenbach et al., 1998; Cheng and Hseu, 2002; Strawn and Sparks, 1999; Vangronsveld et al., 1995).

2.9.4.1 Metal Oxides

Additions of hydrous metal oxides have been found to be effective at reducing the leachability, bioaccessibility, and phytoavailability of several heavy metals (Beak et al., 2008; Berti and Cunningham, 1997; Cheng and Hseu, 2002; Chlopecka and Adriano, 1996; Crawford et al., 1993; Garcia-Sanchez et al., 1999; Hettiarachchi and Pierzynski, 2002; Hettiarachchi et al., 2000; Hettiarachchi et al., 2003; Kinniburgh et al., 1976; Matocha et al., 2001; Mckenzie, 1980; Sauve et al., 2000). The hydrous metal oxides, which are commonly referred to as accessory minerals, are weathering products that are hydrous and anhydrous oxides, hydroxides, and oxyhydroxides of metals, such as Fe, Al, and Mn (Table 2-4).

Table 2-4. Hydrous metal oxides that commonly occur in soils and have the potential to adsorb heavy metals (adapted from Essington, 2002; Lindsay, 1979).

Mineral Name	Chemical Formula
Gibbsite	γ-$Al(OH)_3$
Boehmite	γ-$AlOOH$
Hematite	α-Fe_2O_3
Goethite	α-$FeOOH$
Maghematite	γ-Fe_2O_3
Lepidocrocite	γ-$FeOOH$
Birnessite	δ-$MnO_{1.8}$
Pyrolusite	β-MnO_2
Manganite	γ-$MnOOH$
Hausmannite	Mn_3O_4

As their name implies, accessory minerals are accessory to and often intimately associated with primary and secondary aluminosilicates, from which they are principally derived (Essington, 2004). Due to this association, accessory minerals can mask the surface properties of layer silicates by blocking the access of solutes to interlayer adsorption sites. However, many hydrous metal oxides, particularly those that are poorly crystalline or amorphous in nature, have highly reactive surfaces, thus forming strong surface complexes with a multitude of metal species. Unlike aluminosilicates, hydrous metal oxides are commonly amphoteric, and can develop either positive or negative surface charge depending on the chemical characteristics of the soil solution. As a result, these minerals may exert a pronounced influence over the chemical characteristics of a soil solution and significantly impact the fate and behavior of substances in the soil environment.

Aluminum, Fe and Mn oxides are ubiquitous throughout the environment. Surfaces of freshly precipitated Al and Fe (hydr)oxides are known to be highly active sites for sorption of most dissolved metal ion species. Until more recently, Mn oxides have received less attention in

spite of their lower point of zero charge (PZC) and, therefore, high negative surface charge in the pH range that commonly occurs in soils (Hettiarachchi et al., 2003). However, poorly crystalline or amorphous Mn oxides do have large surface areas, which give them significant surface reactivity, allowing them to possibly be important in controlling metal availabilities in soils (Birnie and Paterson, 1991; Matocha et al., 2001). It has been accepted that trace metals sorb onto metal oxides through chemisorption and have poor reversibility (McBride, 1994; Sposito, 1989). One explanation for this irreversible nature of metal sorption by metal oxides is that the activation energies for desorption may be much larger than that for sorption; thus, rates of desorption at standard temperature and pressure are likely to be much slower (McBride, 1994). Another explanation involves the incorporation of metals into the oxides, making them unavailable for desorption or truly irreversible (Sposito, 1989). As a result, trace metal adsorption to Fe, Al, and Mn oxides has been extensively studied (Beak et al., 2008; Chlopecka and Adriano, 1996; Hettiarachchi and Pierzynski, 2002; Hettiarachchi et al., 2000; Hettiarachchi et al., 2003; Kinniburgh et al., 1976; Matocha et al., 2001; McKenzie, 1980; Mench et al., 1994; Suave et al., 2000).

Iron oxides occur in soils in varying concentrations, depending on pedogenic processes. The high affinity of Fe oxides for certain trace elements, Pb in particular, makes them a likely long-term sink for cationic polyvalent metals. Kinniburgh et al. (1976) demonstrated that Pb, Zn, and Cd could all be adsorbed on synthetic Fe hydrous oxide gels, with Pb being most preferentially adsorbed. In a study using iron-rich materials as an amendment in Pb contaminated soils, the physiologically-based extraction test (PBET), which is a test that is performed to mimic the human digestive system, showed a significant reduction in Pb bioavailability (Berti and Cunningham, 1997). Chlopecka and Adriano (1996) discovered that an

iron oxide waste byproduct was able to reduce Zn uptake by over 80% in maize (*Zea mays*), barley (*Hordeum vulgare*), and radish (*Raphanus sativus*). These findings were also consistent with the reductions that were found in soil-exchangeable Zn upon Fe oxide additions. Hettiarachchi et al. (2003) discovered that the presence of Fe and Mn oxides in biosolids increased the retention of Cd in biosolids-amended soils, thus providing more evidence of heavy metal retention by Fe oxides.

Like Fe oxides, Mn oxides could play an important role in the retention of heavy metals in contaminated soils. McKenzie (1980) demonstrated that adsorption of Pb to Mn oxides was 40 times greater than adsorption to Fe oxides and was more or less irreversible, suggesting that that Mn oxides can be used as strong adsorbents for Pb in soils. Hettiarachchi et al. (2000) established that the combination of P and Mn oxide reduced Pb bioavailability more than either amendment alone suggesting a synergistic effect between the two amendments. McKenzie (1980) reported that the affinity of Mn oxide for different metals follows the order of: Pb >> Cu > Mn > Co > Zn > Ni. This observation was supported when Hettiarachchi and Pierzynski (2002) did not observe significant changes in plant uptake of Zn when a Pb and Zn contaminated soil was amended with both phosphate rock and Mn oxide.

Many studies that have investigated the possible retention of Pb, Zn, and Cd by oxide species have used pure, laboratory synthesized oxide materials instead of naturally-occurring minerals. Suave et al. (2000) conducted a study to compare the adsorption of Pb by two pedogenic Fe oxides to a synthetic ferrihydrite. They found that the synthetic Fe oxide had higher Pb adsorption than the pedogenic oxides. This could indicate that metal adsorption when using synthesized, well-characterized materials may actually be overestimating the adsorption by pedogenic oxides that are naturally occurring in soil environments. As a result, one must be

careful when using pure, synthetic materials as a comparison to real soil environments.

2.9.4.2 Clay Minerals

Clay minerals such as montmorillonite seem suitable as binding additives because they have large specific surface areas and high cation exchange capacities. Adsorption of heavy metals onto clay minerals can occur via two mechanisms: outer-sphere adsorption, which occurs primarily on the basal planes existing in the interlayer of the clay minerals, and inner-sphere adsorption, which occurs at the amphoteric ligand sites existing on the edges of clay minerals (Sparks, 2003; Sparks et al., 1998). Montmorillonite is a dioctahedral smectite mineral having an ideal half cell formula $M_{0.33}H_2OSi_4(Al_{1.67}(Fe^{2+}, Mg)_{0.33}O_{10}(OH)_2$, where M is a monovalent interlayer cation (Sparks, 2003). Substitution of Fe and Mg atoms for Al in the octahedral layer creates a positive charge deficit that is delocalized throughout the crystal structure, while pH dependent charge can form on the broken edges. Therefore, based on this information, cations can adsorb by either electrostatic attraction on the basal plane or form covalent bonds with the functional groups at the broken edges (Sparks et al., 1998).

Studies have shown that additions of clay minerals, in particular montmorillonite, are effective additives at immobilizing heavy metal cations. Lothenbach et al. (1998) concluded that Al-montmorillonite was more effective at adsorbing Zn and Cd than montmorillonite alone. This result confirmed the findings in an earlier study in which the addition of Al to montmorillonite actually improved the adsorption of heavy metals to the clay mineral (Lothenbach et al., 1997). The proposed reason for this is that the Al-hydroxy polymers actually take away part of the permanent negative charge of the clay mineral, thus the adsorption of heavy metals by cation exchange is less than on the untreated montmorillonite. However, the loss of cation exchange sites is more than offset by the formation of surface hydroxyl functional groups at the surface of

the interlayer hydroxyl-Al polymer. For this reason, the adsorption of heavy metals actually increases. Cheng and Hseu (2002) studied the additions of 1% bentonite (consists mainly of Na saturated montmorillonite), 5% Penghu soil (a highly weathered, high pH, high CEC kaolinite containing soil), and 5% Penghu soil + 1% Mn oxide to two Cd and Pb contaminated soils. None of these additions increased the dry matter weight of Chinese cabbage (*Brassica chinensis* L.), but they were able to decrease uptake of both Pb and Cd by the plants. Extractions of Pb and Cd from the contaminated soils were only reduced by the 5% Penghu soil and 5% Penghu soil + 1% Mn oxide. Vangronsveld et al. (1995) concluded that use of montmorillite was successful at restoring vegetation at an industrial site contaminated by non-ferrous metals. Even 30 months after the amendment addition, plant growth and propagation was abundant. Gravel sludge was discussed in a previous section due to its high alkalinity, but this amendment also fits into the clay mineral section. Gravel sludge composition is approximately 42% clay minerals (Krebs et al., 1999; Lothenbach et al., 1998). It really serves as a "dual" amendment, in that; it provides both liming potential and adsorptive materials. Both Lothenbach et al. (1998) and Krebs et al. (1999) found gravel sludge to be suitable at immobilizing Cd, Cu, and Zn in contaminated soils.

2.9.4.3 Zeolites

Zeolites are crystalline alumino silicate minerals that are generally formed in nature when water of high pH and high salt content interacts with volcanic ash causing rapid crystal formation. Zeolites can be synthetically produced by industry too. Generally, the process starts by crystallizing a non-homogeneous gel that is created from silica and alumina sources which are combined with water at elevated pH conditions (Oste et al., 2002). The final product can be altered by SiO_2 to Al_2O_3 ratios, solution pH, temperature, mixing, drying speed, and any impurities that may exist (Dyer, 1988). The framework of zeolite minerals consists of $[SiO_4]^{4-}$

and $[AlO_4]^{5-}$ tetrahedra that are linked at all corners. The framework is open and contains channels and cavities in which metal cations and water molecules can be adsorbed. The channel structure of zeolites makes them rather ion selective because of size constraints. Therefore, the selectivity for different ions is determined by the size and state of the ions, the Si and Al ratio (charge), the number of sites available within the framework, and the temperature (Dyer, 1988).

Natural zeolites have been used for some time as a way to improve soil pH and increase ammonium retention, but not until more recently have they been studied for use in metal immobilization. Synthetic zeolites typically are better at adsorbing metals than natural zeolites because they can be manufactured to fit a specific cation size. In a greenhouse study, 1% synthetic zeolites A and X were added to a Cd contaminated loamy soil where lettuce (*Lactuca sativa* L.) and ryegrass (*Lolium perenne* L.) were grown (Gworek, 1992). The Cd uptake for both plants was significantly reduced in the zeolite treated soils. According to Oste et al. (2002), zeolites may need special management if applied to a contaminated site. It is well known that zeolites increase pH and bind Ca, which may lead to dispersion of organic matter. In a column experiment, the amount of dissolved organic matter (DOM) and metal-DOM complexes were increased after zeolite addition in the beginning of the experiment (Oste et al., 2002). However, over time the free ionic concentration of Cd and Zn significantly decreased and metal uptake was reduced to plants. This is clear evidence that zeolites can be useful adsorbents, but care must be taken so large amounts of DOM do not rapidly carry the potential contaminants out of the reaction zone.

2.10 Techniques to Assess Bioavailability

In situ remediation of contaminated sites using soil amendments, which modify the physiochemical properties of the contaminating heavy metals, is a valuable alternative to more

expensive and complicated civil engineering techniques such as excavation and landfilling of contaminated wastes (Vangronsveld et al., 1996). Many additives, as discussed in the previous section, have been screened for their potential to immobilize heavy metal contaminants in soils. Each of the additives that were discussed in the previous section have a different effect on the bioavailability of the metals, nutrient availability, soil solution pH, and soil microstructure (Lombi et al., 2003; Mench et al., 1994; Oste et al., 2002). Regulatory acceptance of *in situ* immobilization as an effective reclamation method will most likely depend on the ability to predict the long-term fate/stability of the heavy metal contaminants and the restoration of ecosystem function. In order to realistically address long term stability of metals, one needs to probe metal speciation changes as a result of the soil reclamation activities and determine if these changes in metal speciation have lead to a reduction in bioavailability of the metal(s) over the course of its residence time. Techniques and/or devices that may be used to garner such information include: chemical extractions (Ruby et al., 1996; Tessier et al., 1979; USEPA, 1986), diffusive gradients in thin films (DGT) (Zhang et al., 2001), microbiological indicators (Brookes, 1995), vegetative indicators (Brown et al., 2003b; Brown et al., 2004; Hettiarachchi et al., 2002; Palazzo et al., 2003; Pierzynski et al., 2002a; Pierzynski et al., 2002b; Ye et al., 2000), and solid phase speciation (D'Amore et al., 2005). Solid phase speciation techniques include scanning electron microscopy (SEM), transmission electron microscopy (TEM), X-ray diffraction (XRD), nuclear magnetic resonance spectroscopy (NMR), infrared spectroscopy (IR), synchrotron radiation, and many more. For the sake of this review, only synchrotron radiation and its techniques will be further discussed.

2.10.1 Microbial Indicators

Microbial properties, such as community function and structure, have been reported to be

useful indicators of soil quality and; therefore, could serve as assessment criteria for successful stabilization of ecologically disturbed areas (Claassens et al., 2005). While microbial indicators do not elicit any information directly on metal speciation, they provide us with information about metal bioavailability and the health of a contaminated system. Soil microorganisms (collectively the soil microbial biomass) mineralize organic inputs and the soil organic matter pool. As a result, the fertility of natural soil ecosystems will largely depend on the rate of soil organic matter turnover, which is controlled by the microbial biomass (Brookes, 1995).

Inorganic contaminants that may change the quality or quantity of organic matter can damage the soil-plant ecosystem, either in the short-term or over much longer periods. The impacts of elevated heavy metal levels on the size and activity of natural soil microbial communities have been well documented. Of the inorganic pollutants, heavy metals are by far some of the most important (Cu, Ni, Cd, Zn, Cr, Pb). Heavy metals affect the growth, morphology, and metabolism of microorganisms in soils (Leita et al., 1995). Once the heavy metals enter the soil they remain for extremely long periods of time and can be removed only by removal of the contaminated material itself. Since removal is not a valid remedial option in most cases, due to cost and labor, *in situ* techniques have been employed in an attempt to re-establish self-sustainable ecosystems. One way of doing this is through the addition of single or multiple soil amendments. However, a monitoring system needs to be in place to determine the effectiveness of the amendments at reducing bioavailability of heavy metals to microbes and the viability of the treatment(s) over a period of time.

Soil microorganisms are often considered to be quite sensitive to environmental change (Turco et al., 1994), and significant changes of the microbial community can occur following disturbance, both in terms of total biomass and community composition (Harris et al., 1991,

57

1993). Therefore, measures of the microbial community following the initiation of reclamation efforts could be used as an indicator of restoration progress (Harris et al., 1991).

Methods to assess microbial ecosystem function can be complicated due to the natural fluctuations in microbial populations and activity, which can make results difficult to interpret. However, Brookes (1995) has proposed a number of basic criteria that a microbiological property might be expected to fulfill as an indicator in monitoring pollution or the recovery of a heavy metal polluted system. These include: (1) Easy to measure and adaptable across soils and environments; (2) Quickly and economically measured; (3) Needs to have a control so amendment effects can be determined; (4) Measurements need to be both sensitive and robust; (5) Measurements need to be scientifically valid; and (6) Multiple properties need to be measured to monitor pollution or recovery. Measurement of only one property to monitor pollution or assess recovery after treatment is risky. Due to the diversity of microbial communities the measurement of a single property could provide false information. Therefore, multiple properties should always be used to assess microbial function and community structure.

Microbial activity measurements such as respiration, C and N mineralization, biological N_2 fixation, nitrification, and soil enzyme activities, along with total soil microbial biomass have been proposed and used to assess the pollution levels or the recovery of a contaminated soil. Microbial biomass parameters have been widely used for testing soil quality and the degree of restoration in degraded and/or contaminated soils (Clemente et al., 2006; Pérez de Mora et al., 2005). It is generally accepted that accumulated heavy metals reduce the amount of soil microbial biomass (Brookes and McGrath, 1994; Chander et al., 1995). However, metal exposure may also lead to the development of metal-tolerant populations (Ellis et al., 2003). Soil microbial parameters have great potential as indicators of stresses or perturbations in soils

affected heavy by metal pollutants. Therefore, the study of soil microbial function can provide important information when evaluating soil remediation techniques (Pérez de Mora et al., 2005).

The biggest challenge of using microbial indicators is to identify the best choice or choices among the many techniques available to assess soil quality. Several studies have been conducted to determine the effects on microbial community activity upon additions of amendments to metal contaminated soils (Barajas-Aceves et al., 1999; Clemente et al., 2007; Kandeler et al., 1996; Killham, 1985; Lee et al., 2002; Pérez de Mora et al., 2005; Tejada et al., 2007). Tejada et al. (2007) applied two forms of beet vinasse to a semi-arid metal contaminated soil and monitored microbial parameters as an indicator of restoration. They found that beet vinasse alone decreased microbial biomass, microbial respiration, and a suite of microbial enzymes, which all indicate a decrease in activity when compared to a non-amended control. When the beet vinasse was composted with cotton gin, all of these parameters increased over the non-amended control, which they concluded was an indication of restoration. Four different organic amendments (municipal waste compost, biosolid compost, leonardite, and a litter material) were used to remediate a heavy metal contaminated soil in Spain (Pérez de Mora et al., 2005). In general, these amendments improved soil chemical properties and increased microbial biomass carbon and enzyme activities. However, plant cover was just as important in restoring soil chemical and biological properties in all of the contaminated soils evaluated, illustrating the importance of plants to microbial communities. Clemente et al. (2007) used microbial biomass measurements and found that the addition of organic amendments to heavy metal contaminated calcareous soils can improve soil fertility, but the response of the microbial population depends on the amendment used. Manure helped to reduce the metal stress symptoms quickly, which resulted in rapid microbial growth, while an olive husk waste material resulted in much slower

microbial recovery. It has been hypothesized that this is most likely due to the differences in the forms of C in each source.

In soils that had Pb contents that ranged from 0.00039 to 48 mmol Pb kg^{-1}, microbial biomass was found to be significantly reduced at the highest Pb concentration (Konopka et al., 1999). However, it was concluded that this may not necessarily be a direct effect of Pb because the soils did not have plant communities and, therefore, the lack of a rhizosphere and organic matter input could have reduced microbial populations over time. Kandeler et al. (1996) studied the influence that heavy metals have on the functional diversity of soil microbial communities. They discovered that as heavy metal pollution increased, microbial biomass and enzyme activities decreased. However, enzymes that involved C-cycling were less affected by heavy metal pollution, whereas enzyme activities related to N, P, and S showed considerable decrease. In particular, this study demonstrated that arylsulfatase and phosphatase activities were dramatically affected. Similarly, Lee et al. (2002) concluded that as heavy metal concentrations increase, enzyme activities begin to significantly decrease, which one would expect.

The use of soil enzymes can be controversial because the total enzymatic activity of soil is made up of various fractions of growing microbes, dead cells, and extracellular enzymes that can associate with soil particles and soil organic matter (Brookes, 1995). However, their quick assessment and relationship to certain microbial functions justify their use. Claassens et al. (2005) used several soil enzyme activities to monitor coal mine tailings under rehabilitation. They found that sites that had more vegetation cover and organic C content had positive association with soil enzyme activities, which likely indicates an increase in nutrient cycling and soil quality. Stuczynski et al. (2003) studied the response of several enzyme activities upon the addition of Cd, Pb, and Zn salt amendments. They found that Zn had a substantial inhibitory

effect on soil dehydrogenase, acid and alkaline phosphatase, arylsulfatase, and urease activities. However, Cd and Pb either had limited or stimulatory affects on majority of these enzymes. This indicates that Zn may play a larger role in inhibiting microbial community function and growth than certain other heavy metals. Respiration has been proposed as tool to measure the effects of heavy metal pollution in soils, mainly because only at large metal loadings is CO_2 evolution decreased (Brookes, 1995). However, Barajas-Aceves et al. (1999) show that as the concentration of Zn increases so does microbial respiration. Interestingly enough, soils in their study that had the highest Zn concentrations had the highest respiration rates, but the lowest microbial biomass, which indicates a fast rate of organic matter mineralization. This agrees with Killham (1985) who suggested that microorganisms in heavily polluted soils are under stress and have a lower efficiency of C utilization, which results in more CO_2 evolved per unit of substrate. Nitrification potential has also been proposed to be a sensitive measure to monitor microbial community function. Stuczynski et al. (2003) showed that nitrification was inhibited when Zn and Pb salt amendments were added to both metal polluted and non-polluted soils, while Cd appeared to have no effect. There are a number of different methods available to possibly evaluate the function of a microbial community upon the addition of a substrate to soil.

The recent development of molecular and biochemical techniques has enabled scientists to gain a better understanding of microbial community structures in soil ecosystems (Kennedy and Gerwin, 1997). Most microbial species are still unknown or are unculturable (Torvisk et al., 1998). One widely used approach is the analysis of microbial phospholipids-linked fatty acid (PLFA) composition. In this method, microbial lipids are extracted from environmental samples in a mixture of chloroform, methanol, and water (Bligh and Dyer, 1959). Lipids associated with the organic phase are then fractionated into neutral, glycol-, and phospholipids on silicic acid

columns (Vestal and White, 1989). Finally, the phospholipids are subjected to alkaline methanolysis to produce fatty acid methyl esters (FAMEs) for gas chromatography analysis.

Phospholipid-linked fatty acids are major cell membrane constituents, and their various compositions differ between several microbial groups (Hinojosa et al., 2005). These compounds rapidly degrade on cell death; as a result, the variation in types of PLFAs provides a picture of the living microbial community and has been used to study microbial shifts in soils for a given period (Pinkart et al., 2002). Therefore, changes in community structure in response to an environmental stressor (positive or negative) can then be monitored by the comparison of PLFAs that differ among specific groups of microorganisms between treatments and over time.

Phospholipid-linked fatty acid methods have been used to characterize microbial communities from heavy metal contaminated soils (Bååth et al., 1998; Frostegård et al., 1993; Konopka et al., 1999; Pennanen et al., 1996; Rajapaksha et al., 2004; Shi et al., 2002). However, the only recent studies that use PLFA's to assess microbial community structures on remediated metal-polluted soils are Kelly et al. (2003) and Hinojosa et al. (2005), in which either municipal sewage sludge, power plant fly ash, or a combination of calcium carbonate and iron oxy-hydroxides were used to remediate the metal contaminated soils. Hinojosa et al. (2005) used calcium carbonate and iron oxy-hydroxides to remediate a Cd, Cu, and Zn contaminated soil. They found that reclaimed soils had higher fungal to bacterial ratios than the contaminated control as indicated by PLFA analysis, which is considered an important indicator of soil microbial community stability (Bardgett and McAlister, 1999). It was also determined that there were higher amounts of Gram negative (Gm$^-$) bacteria PLFA's than Gram positive (Gm$^+$) bacteria PLFA's in polluted soils (Hinojosa et al., 2005). This was attributed to the fact that Gm$^-$ bacteria are considered to be fast growing microorganisms that utilize a variety of C sources and

can adapt quickly to a variety of environmental stressors, which can be attributed to their thin cell membranes and inability to go produce spores to protect themselves (Ponder and Tadros, 2002). In other words, they either adapt or die. Kelly et al. (2003) added a 2:1 combination of sewage sludge and fly ash to a Zn smelter contaminated soil. Upon examination of the PLFA profiles from remediated areas, they found that the remediation program had a positive effect on the composition of the soil microbial communities. PLFA profiles for recently remediated sites were similar to the less contaminated sites, and there were significant increases in indicator fatty acids of fungi, actinomycetes, and Gm^+ bacteria. These results suggest that the remediation program that was employed was resulting in the recovery of the microbial community. Although PLFA data presented by Kelly et al. (2003) suggested that the remediation program was having a positive effect on soil microbial communities, their results also indicate a loss of this effect over time. These studies signify that PLFA profiles are indicative of changes in the overall structure of microbial communities and could be an excellent method to use to assess remediation efforts.

2.10.2 Chemical Extractions

Several procedures have been developed to measure the bioavailable, rather than the total, fraction of contaminants in soils and sediments (Brown et al., 2005a). Most of these procedures are based on the most sensitive ecological receptor where toxicity is the defined endpoint. For example, soil extracts are routinely used to determine the phytoavailable fraction of total nutrient concentrations in soils (McLaughlin et al., 2000; Sparks, 1996). In most cases, for contaminated soils, extracts have been modified to better mimic the behavior of plants in these environments. However, extracts have also been correlated with reductions in microbial activity, as measured by microbial biosensors (Shaw et al., 2000; Vulkan et al., 2000).

Partial or sequential extraction methods are among the oldest and most commonly used

methods of chemical partitioning of solid environmental samples. These techniques are easy to apply, inexpensive, and require little data analysis. However, original research done on many of these extractants was not performed on soils and most likely not on soils with high metal concentrations. An example is the sequential extraction procedure. Tessier et al. (1979) developed this methodology to quantitatively predict the various chemical forms of metals in sediments. However, many researchers have attempted to adapt this research to better predict or estimate metal bioavailability in various other materials, such as soils. Therefore, one must be careful at interpreting the results when dealing with complex environmental systems like soils.

The idea behind the extraction methodology is based on the assumption that a particular extractant will be phase or retention mode specific in its chemical attack on a mixture of soil media (D'Amore et al., 2005). For example, it is assumed that water will only remove readily soluble mineral forms of an element, buffered acetic acid will attack and dissolve only carbonates, and that ammonium acetate (NH_4OAc) at pH 7 will release only adsorbates. Sequential application of a series of specific reagents coupled with elemental determination for each yields a fractionation pattern or a relative partitioning of metal forms into operationally defined species. In sequential extraction schemes, reagents used are increasingly more reactive or specifically target different phases, thus providing clear distinctions among sources of the extracts obtained. In practice, selectivity for a single phase does not really occur. As a result, it has been suggested that operational species that have been extracted should be defined in terms of the reagent used rather than the phase or retention mode that is assumed to be attacked (Nirel and Morel, 1990). Several reviews are available that report on the most important criticisms of sequential extraction methods (Nirel and Morel, 1990; Scheckel et al., 2003; Scheckel et al., 2005). Given the arguments in these reviews, more independent and precise methods for species

determination are needed. Such methods, of the spectroscopic nature, are now becoming more commonplace and will be discussed in more detail in the synchrotron-based techniques review.

While chemical extraction methods often fail at determining speciation of a given metal in soils, they can be quite valuable in the assessment of metal bioavailability to plants and other organisms, especially to predict the success of a remediation technique used on a contaminated material. Nolan et al. (2005) concluded that soil extraction with $CaCl_2$ appears to be highly effective, inexpensive, and a simple technique to predict Cd uptake by plants. Similarly, Sonmez and Pierzynski (2005) found that $CaCl_2$ did a fair job at predicting Zn uptake by sorghum-sudan (*Sorghum vulgare* var. Sudanese). Extracts can also be used to estimate phytotoxic metal levels in a contaminated soil after an amendment addition. Basta et al. (2001) concluded that phytotoxic Zn levels (1188 mg Zn kg^{-1} extracted by a $Ca(NO_3)_2$ solution) in a disturbed soil was reduced by lime-stabilized biosolids, N-Viro soil, and rock phosphate amendments to 166, 25, and 784 mg Zn kg^{-1}, respectively. Surface applications of biosolids amendments were able to reduce $Ca(NO_3)_2$ extractable Zn in a contaminated subsoil from 50 mg kg^{-1} to 4 mg kg^{-1}, which enabled a vegetative cover to be established within two years of amendment addition (Brown et al., 2003b). Conder et al. (2001) used a $Ca(NO_3)_2$ extractant to assess metal bioavailability to earthworms in a smelter contaminated soil. They concluded that $Ca(NO_3)_2$ extractable metals appear to be a promising surrogate measure of metal bioavailability for earthworms in soils. Results from another study produced a reduction in NH_4NO_3 extractable Cd (< 41%) and Pb (<49%) compared to a contaminated control, with a subsequent reduction of Cd uptake by barley grain upon addition of ferrihydrite-bearing/gravel sludge amendments (Friesl et al., 2006). Krebs et al. (1999) found that applications of gravel sludge to a contaminated soil reduced the $NaNO_3$ extractable Zn concentrations by more than 65%, which was related to a reduction of Zn

uptake in ryegrass (*Lolilum perenne* L.). Similarly, Lothenbach et al. (1998) showed a decrease in NaNO$_3$ extractable Zn and Cd when montmorillinte and gravel sludge were added to a contaminated soil. The binding agents were also able to reduce Zn concentration in red clover (*Trifolium pretense*). Other common soil extractants can also be used to assess metal availability. Ye et al. (2000) showed that a combination of lime and manure was able to reduce both EDTA extractable Pb and Zn in acidic mine tailings. All of the above studies illustrate the usefulness of chemical extractions in predicting and/or estimating the amount of a metal that may be potentially bioavailable.

2.10.3 Diffusive Gradients in Thin Films (DGT)

As previously discussed, assessment of metal phytotoxicities can be predicted with routine soil extractants. However, these methods generally do not perform well across a wide range of soils. Metal toxicity is thought to be related to bioavailability rather than the total concentration of a given metal in soil, but metal bioavailability is difficult to determine because it is influenced by multiple soil properties (Rieuwerts et al., 1998). Soil properties that are directly related to bioavailability include, but are not limited to pH, redox potential, soil texture, clay content, organic matter content, Al, Fe and Mn oxides, differencese in mineral surface area, and the presence of cations and anions in the soil solution. Any procedure that separates solution and solid phase inevitably disrupts the physical-chemical equilibrium, which may affect the distribution of species in solution. Furthermore, soil solution obtained by separation cannot represent the "true" unaltered solution because separation will hide the spatial variability of soil-solution properties that can occur at multiple scales (Sposito, 1989). Ideally chemical speciation measurements in soil solution should be made *in situ* by procedures which either minimize disturbance or interact with the solution in a controlled way.

To predict the bioavailability of metals to plants, it is necessary to understand both solution- and solid-phase supply processes in soils. Processes that affect the supply of solutes to plants include diffusional transport to the root, the root encountering fresh surfaces as it grows through the soil, and the influence of the rhizosphere (Barber, 1995; McLaughlin et al., 1998). Therefore, unless one process is dominant, it is unlikely that any single chemical measurement could adequately assess plant uptake. As a result, an *in situ* procedure able to measure labile solution species and the flux of available species from solid phase to solution has been developed and measures the effective concentration (Zhang et al., 2001). This new procedure provides *in situ* quantification of metal supply from the solid and solution phases by using an ion sink with a well-defined geometry, and the technique is called diffusive gradients in thin films (DGT) (Davison and Zhang, 1994). The DGT technique will locally lower soil solution concentrations, which induces metal resupply from the solid phase, just as a root would.

A few studies have been conducted to assess how this method relates to plant uptake of certain ions. Zhang et al. (2001) grew pepperwort (*Lepidium heterophyllum* Benth.) plants in 29 soil samples covering a wide range of total Cu concentrations and found that plant Cu concentrations were linearly related and highly correlated with effective concentrations, but were more scattered and nonlinear with respect to other Cu measurements such as free Cu^{2+} activity, soil solution Cu, and EDTA extractable Cu. The results of this study suggest that the overall dominant supply of Cu to pepperwort in those soils were the solution pools, coupled with diffusion and metal release from the solid phase that is induced by the mimicked biological uptake of the DGT technique. A study by Nolan et al. (2005) compared uptake of Zn, Cu, Cd, and Pb by wheat (*Triticum aestivum* L.) in a range of well equilibrated soils using several techniques as a basis for uptake (total soil metal concentrations, total soluble metal

67

concentrations, free metal activities in pore waters, 0.01 M $CaCl_2$ extractable metal concentrations, isotope dilution, and effective metal concentrations as determined by DGT). They concluded that plant Zn and Cd concentrations were highly related to effective concentration as determined by DGT, while relationships with other measures of Zn and Cd were generally lower. This indicates that in these soils the available solid phase played an important role in Zn and Cd uptake by wheat. Plant Pb concentrations were highly related to both DGT and soil pore water concentrations, signifying that supply from the solid phase may not be that important for Pb uptake. Predictions of Cu uptake by wheat from the selected soils were poor for all measurements employed.

Sonmez and Pierzynski (2005) used a greenhouse pot study to evaluate phytotoxicity of Zn in relation to sorghum-sudan (*Sorghum vulgare* var. Sudanese) uptake. They concluded that in general, increasing Zn concentrations in a contaminated sand matrix as determined by DGT led to a decrease in plant biomass yield. However, the performance of DGT and $CaCl_2$ extraction for assessing Zn phytoavailabililty was similar. Their study also suggested that Zn phytotoxicity was induced by mine waste materials, but further evaluation is needed to establish a link between mine waste and Zn phytotoxicity. For Pb and Zn, assessment of soils using DGT appears to provide a convenient and relatively simple technique (compared to soil solution extraction/speciation) to predict metal concentrations in plants. Therefore, it may be useful in predicting phytotoxicity thresholds (Nolan et al., 2005).

2.10.4 Synchrotron Radiation Based Techniques for Speciation

Being able to determine the behavior of potentially hazardous substances in complex systems like soils is becoming increasingly important due to concerns over the deterioration of our environment. However, this can be quite difficult due to complicated matrices and low

concentrations of a given contaminant. During the past decade, applications of synchrotron-based techniques to environmental science have grown significantly, which has resulted in a new interdisciplinary field that Brown et al. (2005a) has coined molecular environmental science. This scientific field focuses on the molecular-level speciation of environmental pollutants and the fundamental processes that determine their fate, behaviour, and transport in natural systems. Knowledge of the molecular-level speciation of inorganic pollutants is essential for predicting stablilty, mobility, toxicity, and bioavailability of a given element to plants, microbes, and humans in the environment and can be used to help design effective remediation strategies.

There are several synchrotron-based techniques that can assist in the molecular level speciation of inorganic contaminants. These include but are not limited to: X-ray fluorescence (XRF), X-ray absorption spectroscopy (XAS) and X-ray diffraction (XRD). X-ray fluorescence was the first technique to take advantage of the increased brightness that synchrotron-based techniques offer. This allowed researchers to probe substances at the micron level and capture the fluorescence of multiple elements using a multi-element detector at one time (Newville et al., 1999). A real limitation of XRF is that it is difficult to quantify the exact matrix effects, which can prevent the determination of elemental concentrations (Manceau et al., 2002). As a result, it is quite difficult to determine the structural formula of a mineral phase. However, XRF can be used to produce elemental maps to locate trace metals within a complex matrix and to correlate trace and major elements. In complex environmental samples, this is the first step before any speciation (XAS or XRD) work is performed.

X-ray absorption spectroscopy is one of the most widely used synchrotron-based techniques (D'Amore et al., 2005). It can be used to study most elements in crystalline or non-crystalline forms over a wide range of concentrations and environmental conditions (D'Amore et

al., 2005; Sparks, 2003).   This spectroscopy includes X-ray absorption near edge structure (XANES) and extended X-ray absorption fine structure (EXAFS) techniques. The ability of a given element(s) to fluoresce strongly influences its ability to sorb photons of a given energy for that element (D'Amore et al., 2005). Any shift or change in the spectrum near the absorption edge for that element is due to the changes in the local chemical environment around the element (Sparks, 2003). These shifts are what are referred to as the fine structure (EXAFS) and can provide information on oxidation state, coordination number, nearest neighbor atoms, and bond distances.   The XANES region of the spectrum does not provide as much quantitative information as the EXAFS region, but it is more intense than the fine structure portion and can provide qualitative or semi-quantitative information on the oxidation state for the element of interest (Brown et al., 1995). To obtain chemical information the unknown XANES and/or EXAFS regions for an element must be compared to the XANES/EXAFS spectra for well-characterized reference compounds that have known composition and contain the element of interest (Sparks, 2003).

X-ray absorption techniques can provide wealth of information, including mineral speciation. However, XAS alone can have problems distinguishing mineral species present in multicomponent mixtures of the same element, which can make quantification difficult. However, innovative application of linear combination fitting (LCF), principle component analysis (PCA), or the combination of the two have provided researchers a way to statistically confirm species quantification (Beauchemin et al., 2002; Isaure et al., 2002; Nachtegaal et al., 2005; Roberts et al., 2002; Scheckel and Ryan, 2004; Scheinost et al., 2002). Even with the difficulty of identifying mineral species in complex environmental samples, XAS techniques have at least an order of magnitude advantage as an indicator of species and structure over other

lab-based techniques (i.e. laboratory based XRD, NMR, IR, etc.) (D'Amore et al., 2005). To help further enhance speciation in complex matrices, Manceau et al. (2004) has proposed the combined use of different synchrotron-based techniques. This can be accomplished by employing synchrotron-based XRF, XANES/EXAFS, and XRD analyses on the same samples. However, these techniques cannot be measured simultaneously, due to differences in energy requirements for an element of interest, but XRF maps can be collected and used to locate points of interest (POI's). Then XANES/EXAFS and XRD spectra can be collected at each POI for a given element to speciate that element at the POI. For this approach to be successful, all data has to be collected at the same beamline without removing the sample between the analyses.

X-ray diffraction is one of the most commonly used techniques to solve the atomic structure of crystalline minerals. The arrangement of atoms in a crystal can be determined using either single crystal diffraction or powder diffraction techniques. Singe crystal diffraction is the most straightforward and precise technique and is preferred to powder diffraction for structure identification. However, it is often difficult to find a single crystal that is large enough and of good quality to obtain diagnostic diffraction patterns. X-rays produced by synchrotron radiation are several orders of magnitude brighter than those produced by X-ray tubes and anodes in laboratory equipment (Manceau et al., 2002). Thus, the brightness of synchrotron radiation allows scientists to view micrometer sized crystals, which makes single crystal diffraction more achievable. However, environmental materials are heterogeneous in nature and generally have poor crystallinity, which makes single crystal diffraction unrealistic. For such heterogeneous samples, the powder diffraction technique has to be used. The advantage of using synchrotron radiation for diffraction is related to the small size of the X-ray beam, which reduces the heterogeneity of a sample by providing the ability to focus on a single point of interest.

Additionally, the high intensity of the X-ray beam allows the collection of diffraction patterns with exceptional counting statistics. Furthermore, the energy can be easily changed, which allows one to avoid fluorescence of certain atoms in complex matices (Manceau et al., 2002). As a result, μ-XRD is a unique tool that can be used synergistically with other synchrotron-based techniques (μ-XRF, μ-XANES, and μ-EXAFS), which can be used to improve mineral species identification (Manceau et al., 2004).

X-ray absorption fine structure spectroscopy (XAFS) has been used to identify chemical species *in situ* with minor or no pretreatments and the use of multishell fitting techniques can be used to determine major elemental species in a sample (Scheinost et al., 2002). However, in the presence of minerals that produce strong fluorescence (i.e. Fe), some secondary species can go unidentified. Alternatively, statistical analysis by linear combination fitting (LCF) can be applied to XAFS spectra of Pb/Zn contaminated soil samples. Unknown spectra can then be fit to known Pb/Zn reference material, which would be able to identify dominate Pb/Zn species in complex environmental samples without chemical or physical disruption to the Pb/Zn species (Manceau et al., 2002). This technique would also provide weighted quantification so samples/treatments can be compared. Even when a larger database of reference spectra is available and a good fit is achieved (commonly estimated by χ^2), there is still some uncertainty in whether all elemental species have been properly identified (Roberts et al., 2002). Therefore, LCF is often teamed with principal components analysis (PCA) to limit the amount of components that are used to provide a fit for a given dataset (Nachtegaal et al., 2005; Roberts et al., 2002).

The literature provides a large number of examples on low temperature geochemical and environmental science applications of XAS techniques. Several of which study the speciation of

Pb and Zn will now be briefly discussed. Numerous studies have been conducted on Pb due to its negative impacts on humans and the environment. Lead was actually the first heavy metal whose speciation in a contaminated soil was studied by EXAFS (Cotter-Howells et al., 1994) and it has received considerable attention since that study (Beak et al., 2008; Chappell and Scheckel, 2007; Elzinga and Sparks, 2002; Jackson et al., 2005; Matocha et al., 2001; Morin et al., 1999; O'Day et al., 1998; Ostergren et al., 1999; Scheckel et al., 2003; Scheckel and Ryan, 2002; Scheckel and Ryan, 2004; Strawn and Sparks, 1999; Weesner and Bleam, 1998). X-ray absorption spectroscopic techniques were used to quantitatively speciate Pb in three different mine tailings from Leadville, CO (Ostergren et al., 1999). They discovered that Pb speciation varies dramatically among different environments in the Leadville area. Other techniques such as sequential extraction and electron microprobe analysis were also used to characterize the mine waste material, but EXAFS analysis conducted on the material following sequential extraction procedures showed significant redistribution of Pb during its extraction and removal, while electron microprobe analysis was inconclusive. Thus, Ostergren et al. (1999) concluded that characterization of Pb minerals in complex matrices is not definitive when using chemical extraction and more conventional microanalytical techniques conducted in the laboratory. Similarly, it was found using XAS techniques that sequential extraction procedures failed to identify the proper Pb species when Pb contaminated soils were treated with calcium phosphate amendments (Scheckel et al., 2003). They stated that speciation techniques involving extractions may not be suitable in amended soils unless results are supported by methods such as XAS.

Chappell and Scheckel (2007) employed synchrotron-based XAFS to study pyromorphite formation and stability after quick lime neutralization in the presence of soil and clay sorbents. They were able to demonstrate that pyromorphite was the major Pb species formed after addition

of phosphoric acid. In addition, their XAFS data shows that quick lime enhances pyromorphite content in the systems that were studied. Scheckel and Ryan (2004) evaluated the spectroscopic speciation and quantification of Pb in phosphate amended soils. They determined that the addition of P promoted pyromorphite formation and the rate of formation increased with increasing P concentration. In this study, a supplemental addition of an iron amendment as an iron-byproduct was made with TSP for some treatments. It was found that iron enhanced the formation of pyromorphite relative to independent TSP amendment additions of similar concentrations. On the other hand, the amendment of biosolids or biosolids plus TSP resulted in a significant decrease in pyromorphite as indicated by XAS studies.

Synchrotron-based techniques can also be used to study Pb in other matrices. Jackson et al. (2005) used synchrotron X-ray techniques and found biogenic pyromorphite formation by the nematode *Caenorhabditis elegans*, which can be quite common in soil invertebrates. A synchrotron-based μ-XRD pattern of the phosphate granule revealed the formation of pyromorphite and it is thought to be the first report of crystalline pyromorphite formed internally by an organism. All of the above information that has been gained on Pb speciation helps to demonstrate how a better understanding of molecular scale mechanisms of trace element immobilization can help to provide more confident responses to environmental concerns.

Zinc has also been well studied using XAS techniques. The bulk of this work has involved speciating Zn in contaminated soils and evaluating the changes in speciation when *in situ* remediation techniques are employed (Ford and Sparks, 2000; Manceau et al. 2000; Nachtegaal et al., 2005; Roberts et al., 2002; Sheinost et al., 2002; Voegelin et al., 2005). Voegelin et al. (2005) studied the changes in zinc speciation in field soil after contamination by zinc oxide using XAS techniques. It was found that after just nine months the zinc oxide had

dissolved and over half of the total Zn reprecipitated in other forms. The precipitate was determined to be mostly a Zn double layer hydroxide with minor amounts of Zn phyllosilicate minerals present. Similarly, Scheinost et al. (2002) using synchrotron-based techniques established Zn to be incorporated by hydroxyl-Al interlayer phyllosilicates in contaminated subsoils. However, in the surface soil they predominantly found franklinite and sphalerite, which are common smelter emitted minerals. In two separate studies of smelter-contaminated soils, XAS revealed that Zn was most often bound to Al-groups and to a lesser extent Fe and Mn (hydr)oxides (Manceau et al., 2000; Roberts et al., 2002). Roberts et al. (2002) also reported that minor amounts of Zn were associated with organic matter or formed outer-sphere complexes with other constituents. In a cultivated soil taken from a high terrace of the Ohio River, Manceau et al. (2004) found Zn to be precipitated as sphalerite, zincochromite, Zn-containing phyllosilicates, Zn-containing lithiophorite, Zn-sorbed ferrihydrite, and Zn-phosphates. This study is an example of Zn speciation under more natural, non-contaminated conditions.

In situ remediation techniques are commonly employed to change the speciation of Zn in contaminated soils to make it less bioavailable. In 1990, a study began to access the effect of cyclonic ash additions when they were applied with organic compost amendment in an attempt to remediate a smelter-contaminated soil. In 1998, it was observed that there was increasing colonization of the non-treated area by metal-tolerant plants from the treated areas. As a result, samples were collected from both non-treated and treated areas to determine Zn speciation via XAS. It was found that there were no major differences in Zn speciation between the treated and non-treated areas (Nachtegaal et al., 2005). However, in both areas over half of the Zn was incorporated into newly formed precipitates. It was concluded that the incorporation of Zn into the newly formed species in both the treated and non-treated soils lead to a significant natural

attenuation of exchangeable/bioavailable Zn fraction at or near neutral pH conditions. At lower pH values, conditions are not favorable for this formation and Zn would likely be much more bioavailable.

2.11 Conclusions

Lead and Zn are ubiquitous in the environment (Adriano, 2001). They have many industrial uses, which is why their concentrations continue to increase in soils worldwide. Both Pb and Zn exist in the environment in numerous mineral species and their presence, whether natural or anthropogenic, can have negative impacts on human health and the environment. As a result, areas that have been contaminated by these elements need to be contained and/or remediated. *In situ* remediation techniques are being extensively studied because they reduce cost, clean-up time, and labor needed. In addition, these techniques do not require landfills and the help to minimize further transport of Pb and Zn throughout the environment. The additions of organic and phosphate amendments have shown to be effective at reducing the bioavailability of Pb and Zn. However, work is still needed to determine the efficacy of different P amendments reacted at different times on metal phosphate formation in multi-element contaminated soils.

2.12 References

Adriano, D.C. 2001. Trace elements in terrestrial environments: Biogeochemistry, bioavailability, and risks of metals. 2nd ed. Springer-Verlag, New York, NY.

Adriano, D.C., J. Albright, F.W. Whicker, I.K. Iskandar, and C. Sherony. 1997. Remediation of metal- and radionuclide-contaminated soils. p. 27-46. *In* I.K. Iskandar and D.C. Adriano (eds.) Remediation of soils contaminated with metals. Advances in Environmental Science. Science Reviews, Middlesex, UK.

Agency for Toxic Substances and Disease Registry. 2005. ToxFAQS for lead [Online]. Available at www.atsdr.cdc.gov/tfacts13.html (accessed 10 Oct. 2006). ATSDR, Atlanta, GA.

Auboiroux, M., P. Baillif, J.C. Touray, and F. Bergaya. 1996. Fixation of Zn^{2+} and Pb^{2+} by a Ca-montmorillinite in brines and dilute solutions: Preliminary results. Appl. Clay Sci. 11:117-126.

Bååth, E., Å. Díaz-Raviňa Frostegård, and C.D. Cambell. 1998. Effect of metal-rich sludge amendments on the soil microbial community. Appl. Environ. Microbiol. 64:238-245.

Barajas-Aceves, M., C. Grace, J. Ansorena, L. Dendooven, and P.C. Brookes. 1999. Soil microbial biomass and organic C in a gradient of zinc concentrations in soils around a mine spoil tip. Soil Biol. Biochem. 31:867-876.

Barber, S.A. 1995. Soil nutrient bioavailability. A mechanistic approach. John Wiley & Sons, New York.

Bardgett, R.D., and E. McAlister. 1999. The measurement of soil fungal: bacterial-biomass ratios as an indicator of ecosystem self-regulation in temperate meadow grasslands. Biol. Fertil. Soils 29:282-290.

Bargar J.R., G.E. Brown, and G.A. Parks. 1998. Surface complexation of Pb(II) at oxide-water interfaces: III. XAFS determination of Pb(II) and Pb(II)-chloro adsorption complexes on goethite and alumina-Implications for adsorption of metal ions in natural waters. Geoch. Cosmochim. Acta 62:193-207.

Bargar, J.R., S.N. Towle, G.E. Brown Jr., and G.E. Parks. 1996. Outer-sphere Pb(II) adsorbed at specific surface sites on single crystal α-alumina. Geoch. Comsochim. Acta 60:3541-3546.

Basta, N.T., R. Gradwohl, K.L. Snethen, and J.L. Shroder. 2001. Chemical immobilization of lead, zinc, and cadmium in smelter-contaminated soils using biosolids and

rock phosphate. J. Environ. Qual. 30:1222-1230.

Basta, N.T., and S.L. McGowen. 2004. Evaluation of chemical immobilization treatments for reducing heavy metal transport in a smelter-contaminated soil. Environ. Pollut. 127:73-82.

Basta, N.T., J.A. Ryan, and R.L. Chaney. 2005. Trace element chemistry in residual treated soil: Key concepts and metal bioavailability. J. Environ. Qual. 34:49-63.

Beak, D.G., N.T. Basta, K.G. Scheckel, and S.J. Traina. 2008. Linking solid phase speciation of Pb sequestered to birnessite to oral Pb bioaccessibility: Implications for soil remediation. Environ. Sci. Technol. 42:779-785.

Beauchemin, S., D. Hesterberg, and M. Beauchemin. 2002. Principal component analysis approach for modeling sulfur K-XANES spectra of humic acids. Soil Sci. Soc. Am. J. 66:83-91.

Beckett, P.H.T., R.T. Davis, and P. Brindley. 1979. The disposal of sewage sludge onto farmland: The scope of the problems of toxic elements. Water, Pollut. Control (Maidstone, England) 78:419-445.

Berti, W.R., and S.D. Cunningham. 1997. In-place inactivation of Pb in Pb-contaminated soils. Environ. Sci. Technol. 31:1359-1364.

Beyer, W.N. 2000. Hazards to wildlife from soil-borne cadmium recognition. J. Envriron. Qual. 29:1380-1384.

Beyer, W.N., O.H. Pattee, L. Sileo, D.J. Hoffman, and B.M. Mulhern. 1985. Metal contamination in wildlife living near two zinc smelters. Environ. Poll. Ser. A 38:63-86.

Birnie, A.C., and E. Paterson. 1991. The mineralogy and morphology of iron and manganese oxides in an imperfectly-drained Scottish soil. Geoderma 50:219-237.

Blaylock, M.J., D.E. Salt, S. Dushenkov, O. Zakarova, C. Gussman, Y. Kapulnik, B.D. Ensley, and I. Raskin. 1997. Enhanced accumulation of Pb in Indian mustard by soil-applied chelating agents. Environ. Sci. Tech. 31:860-865.

Bligh, E.G., and W.J. Dyer. 1959. A rapid method of total lipid extraction and purification. Can. J. Biochem. Physiol. 37:911-917.

Bochatay, L., and P. Persson. 2000. Metal ion coordination at the water-manganite (γ-MnOOH) interface II: An EXAFS study of zinc (II). J. Colloid Interface Sci. 229:593-599.

Bolton, H. Jr., J.K. Frederickson, and L.F. Elliot. 1992. Microbial ecology of the

rhizosphere. *In* F.B. Metting (ed.) Soil microbial ecology. p. 27-63. Marcel Dekker, Inc., New York.

Boutron, C.F., J.P. Candelone, and S. Hong. 1994. Past and recent changes in the large-scale tropospheric cycles of lead and other heavy metals as documented in Antartic and Greenland snow and ice: a review. Geochim. Cosmochim. Acta. 58:3217-3225.

Brookes, P.C. 1995. The use of microbial parameters in monitoring soil pollution by heavy metals. Biol. Fertil. Soils 19:269-279.

Brookes, P.C., and S.P. McGrath. 1994. Effect of metal toxicity on the size of the soil microbial biomass. J. Soil Sci. 35:341-346.

Brown, G.E., Jr., J.G. Catalano, A.S. Templeton, T.P. Trainor, F. Farges, B.C. Bostick, T. Kendelewicz, C.S. Doyle, A.M. Spormann, K. Revill, G. Morin, F. Juillot, and G. Calas. 2005a. Environmental interfaces, heavy metals, microbes, and plants: Applications of XAFS spectroscopy and related synchrotron radiation methods to environmental science. Physcia Scripta 115:80-87.

Brown, G.E., Jr., G.A. Parks, and P.A. O'Day. 1995. Sorption at the mineral-water interfaces: Macroscopic and microscopic perspectives. p. 129-183. *In* D.J. Vaughan and R.A.D. Pattrick (ed.) Mineral Surfaces. Chapman and Hall, London.

Brown, S.L., R. Chaney, J. Hallfrisch, J.A. Ryan, and W.R. Berti. 2004. In situ soil treatments to reduce the phyto- and bioavailability of lead, zinc, and cadmium. J. Environ. Qual. 33:522-531.

Brown, S.L., R. Chaney, J. Halfrisch, and Q. Xue. 2003a. Effect of biosolids processing on lead bioavailability in an urban soil. J. Environ. Qual. 32:100-108.

Brown, S.L., C.L. Henry, R.L. Chaney, H. Compton, and P. DeVolder. 2003b. Using municipal biosolids in combination with other residuals to restore metal-contaminated mining areas. Plant Soil 249:203-215.

Brown, S., M. Sprenger, A. Maxemchuk, and H. Compton. 2005b. Ecosystem function in alluvial tailings after biosolids and lime addition. J. Environ. Qual. 34:139-148.

Callendar, E. 2005. Heavy metals in the environment-Historical trends. p. 67-105. *In* B.S. Sherwood (ed.) Environmental Geochemistry. Vol. 9. Treatise on geochemistry. Elsevier, New York, NY.

Cao, X., L.Q. Ma, M. Chen, S.P. Singh, and W.G. Harris. 2002. Impacts of phosphate

amendments on lead biogeochemistry at a contaminated site. Environ. Sci. Technol. 36:5296-5304.

Cao, R.X., L.Q. Ma, M. Chen, S.P. Singh, and W.G. Harris. 2003. Phosphate-induced metal immobilization in a contaminated site. Environ. Pollut. 122:19-28.

Cao, X., L.Q. Ma, D.R. Rhue, and C.S. Appel. 2004. Mechanisms of lead, copper, and zinc retention by phosphate rock. Environ. Pollut. 131:434-444.

Cao, X., L.Q. Ma, S.P. Singh, and Q Zhou. 2008. Phosphate-induced lead immobilization from different lead minerals in soils under varying pH conditions. Environ. Pollut. 152:184-192.

Carroll, S.A., P.A. O'Day, and M. Piechowski. 1998. Rock-water interactions controlling zinc, cadmium, and lead concentrations in surface waters and sediments, U.S. Tri-State Mining District. 2. Geochemical interpretation. Environ. Sci. Technol. 32:956-965.

Chander, K., and P.C. Brookes. 1993. Residual effects of zinc, copper, and nickel in sewage sludge on microbial biomass in a sandy loam. Soil Biol. Biochem. 25:1231-1239.

Chander, K., P.C. Brookes, and S.A. Harding. 1995. Microbial biomass dynamics following addition of metal-enriched sewage sludges to a sandy loam. Sil Biol. Biochem. 27:1409-1421.

Chaney, R.L. 1993. Zinc phytotoxicity. p. 135-150. *In* A.D. Robson (ed.) Zinc in soils and plants. Kluwer Academic Publ., Dordrecht, The Netherlands.

Chaney, R.L., W.N. Beyer, C.H. Gifford, and L.Sileo. 1988. Effects of zinc smelter emissions on farms and gardens at Palmerton, PA. Trace Subst. Environ. Health 22:263-280.

Chaney, R.L., M.H. Lee, and J.J. Murray. 1989. Response of yellow nutsedge, barley, lettuce, soybean, little bluestem, Canada bluegrass, and perennial ryegrass to excessive sewage-sewage sludge applied soil zinc in an acidic soil. Final report. U.S. Army Corps of Eng., Environ. Lab., Waterways Exp. Stn., Vicksburg, MS.

Chappell, M.A., and K.G. Scheckel. 2007. Pyromorphite formation and stability after quick lime neutralization in the prescence of soil and clay sorbents. Environ. Chem. 4:109-113.

Chen, X., J.V. Wright, J.L. Conca, and L.M. Peurrung. 1997. Evaluation of heavy metal remediation using mineral apatite. Water Air Soil Pollut. 98:57-78.

Cheng, S., and Z. Hseu. 2002. In-situ immobilization of cadmium and lead by different amendments in two contaminated soils. Water Air Soil Pollut. 140:73-84.

Chlopeka, A, and D.C. Adriano. 1996. Mimicked in-situ stabilization of metals in a cropped soil: Bioavailability and chemical form of zinc. Environ. Sci. Technol. 30:3294-3303.

Ciccu, R., M. Ghiani, R. Peretti, A. Serci, and A. Zucca. 2001. Heavy metal immobilization by fly ash in soils contaminated by mine activity. Intl. Ash Utilization Symp. Center for Applied Energy Research, Univ. Kentucky, Paper No. 6.

Claassens, S., K.J. Riedel, L. Van Rensburg, T.L. Morgenthal, and P.J. Jansen Van Rensburg. 2005. Soil microbial properties in coal mine tailings under rehabilitation. Appl. Ecology Environ. Res. 4:75-83.

Clemente, R., D.J. Walker, and M. Pilar Bernal. 2005. Uptake of heavy metals and As by Brassica juncea grown in a contaminated soil in Aznalcollar (Spain): The effect of soil amendments. Environmental Pollution 138:46-58.

Clemente, R., C. Almela, and M.P. Bernal. 2006. A remediation strategy based on active phytoremediation followed by natural attenuation in a soil contaminated by pyrite waste. Environ. Pollut. 143:397-406.

Clemente, R., C. de la Fuente, R. Moral, and M.P. Bernal. 2007. Changes in microbial biomass parameters of a heavy metal-contaminated calcareous soil during a field remediation study. J. Environ. Qual. 36:1137-1144.

Conder, J.M, R.P. Lanno, and N.T. Basta. 2001. Assessment of metal bioavailability in a chemically remediated smelter-contaminated soil by *Eisenai fetida* and chemical extraction surrogate methods. J. Environ. Qual. 30:1231-1237.

Cotter-Howells, J.D., P.E. Champnes, J.M. Charnock, and R.A.D. Pattrick. 1994. Identification of pyromorphite in mine-waste contaminated soils by ATEM and EXAFS. Eur. J. Soil Sci. 45:393-402.

Cotter-Howells, J., and S. Caporn. 1996. Remediation of contaminated land by formation of heavy metal phosphates. Appl. Geochem. 11:335-342.

Councell, T.B., K.U. Duckenfield, E.R. Landa, and E. Callender. 2004. Tire-wear particles as a source of zinc to the environment. Environ. Sci. Technol. 38:4206-4214.

Crawford, R.J., I.H. Harding, and D.E. Mainwaring. 1993. Adsorption and coprecipitation of single heavy metal ions onto the hydrated oxides of iron and chromium. Langmuir 9:3050-3056.

D'Amore, J.J., S.R. Al-Abed, K.G. Scheckel, and J.A. Ryan. 2005. Methods for

speciation of metals in soils: A review. J. Environ. Qual. 34:1707-1745.

Davies, B.E. 1995. Lead and other heavy metals in urban areas and consequences for the health of their inhabitants. *In* S.K. Majumdar, E.W. Miller, and F.J. Brenner (eds.) Environmental Contaminants, Ecosystems, and Human Health, p. 287-307. The Pennsylvania Academy of Science, Easton PA, USA.

Davison, W., and H. Zhang. 1994. In situ speciation of trace components in natural waters using thin-film gels. Nature 367:545-548.

Derome, J. 2000. Detoxificaiton and amelioration of heavy-metal contaminated forest soils by means of liming and ferilisation. Environ. Pollut. 104:79-88.

Derome, J., and A. Saarsalmi. 1999. The effect of liming and correction fertilization on heavy metal and macronutrient concentrations in soil solution in heavy-metal polluted Scots pine stands. Environ. Pollut. 104:249-259.

Devolder, P.S., S.L. Brown, D. Hesterberg, K. Pandya. 2003. Metal bioavailability and speciation in a wetland tailings repository amended with biosolids compost, wood ash, and sulfate. J. Environ. Qual. 32:851-864.

Diaz-Ravina M., and E. Bååth. 1996. Development of metal tolerance in soil bacterial communities exposed to experimentally increased metal levels. Applied and Environ. Microbiol. 62:2970-2977.

Dudka, S. and D.C. Adriano. 1997. Environmental impacts of metal ore mining and processing : A review. J. Envrion. Qual. 26: 590-602.

Dyer, A. 1988. An introduction to zeolite molecular sieves. 1st ed. John Wiley & Sons, Bath, UK.

Eghball, B. 1999. Liming effects of beef cattle feedlot manure or compost. Commun. Soil Sci. Plant Anal. 30:2563-2570.

Ehrlich, H.L. 1997. Microbes and metals. Appl. Microbiol. Biotechnol. 48:687-692.

Ellis, R.J., P. Morgan, A.J. Weightman, and J.C. Fry. 2003. Cultivation dependent and independent approaches for determining bacterial diversity in heavy metal-contaminated soil. App. Environ. Microbiol. 69:3223-3230.

Elzinga, E.J., and D.L. Sparks. 2002. X-ray absorption spectroscopy study of the effects of pH and ionic strength on Pb(II) sorption to amorphous silica. Environ. Sci. Tech. 36:4352-4357.

Essington, M.E. 2004. Soil and water chemistry. CRC Press, Boca Raton, FL.

Fierke, C. 2000. Function and mechanism of zinc. J. Nutrition 130:1437S-1446S.

Filius, A.,T. Streck, and J. Richter. 1998. Cadmium sorption and desorption in limed topsoils as influenced by pH: Isotherms and simulated leaching. J. Environ. Qual. 27:12-18.

Ford, R.G., and D.L. Sparks. 2000. The nature of Zn precipitates formed in the presence of pyrophyllite. Environ. Sci. Tech. 34:2479-2483.

Fosmire, G.J. 1990. Zinc toxicity. Am. J. Clin. Nutrition 51:225-227.

Friesl, W., J. Friedl, K. Platzer, O. Horak, and M.H. Gerzabeck. 2006. Remediation of contaminated agricultural soils near a former Pb/Zn smelter in Austria: Batch, pot and field experiments. Environ. Pollut. 144:40-50.

Frostegård, A., A. Tunlid, and E. Bååth. 1993. Phospholipid fatty acid compostion, biomass, and activity of microbial communities from two soil types experimentally exposed to different heavy metals. Applied and Environ. Microbiol. 59:3605-3617.

Frostegård, A., A. Tunlid, and E. Bååth. 1996. Changes in microbial community structure during long-term incubation in two soils experimentally contaminated with metals. Soil Biol. Biochem. 28:55-63.

Garcia-Sanchez, A., A. Alastuey, and X. Querol. 1999. Heavy metal adsorption by different minerals: Application to the remediation of polluted soils. Sci. Total Environ. 242:179-188.

Gibson, A.M. 1972. Wilderness bonanza-the Tri-State District of Missouri, Kansas, and Oklahoma. p. 362. University of Oklahoma Press, Norman, Oklahoma.

Gomes, P.C., M.P.F. Fontes, A.G. da Silva, E. de S. Mendonca, and A.R. Netto. 2001. Selectivity sequence and competitive adsorption of heavy metals by Brazilian soils. Soil Sci. Soc. Am. J. 65:1115-1121.

Gray, C.W., S.J. Dunham, P.G. Dennis, F.J. Zhao, and S.P. McGrath. 2006. Field evaluation of in situ remediation of a heavy metal contaminated soil using lime and red-mud. Environ. Pollut. 142:530-539.

Gworek, B. 1992. Inactivation of cadmium in contaminated soils using synthetic zeolites. Environ. Pollut. 75:269-271.

Hambidge, M. 2000. Zinc and health: Current status and future directions. J. Nutrition 130:1344S-1349S.

Harris, J.A., H. Bentham, and P. Birch. 1991. Soil microbial community provides index to progress, direction of restoration. Restoration Manage. Notes 9:133-135.

Harris, J.A., P. Birch, and K.C. Short. 1993. The impact of storage of soils during opencast mining on the microbial community: A strategist theory interpretation. Restor. Ecol. 1:88-100.

Havlin, J.L., J.D. Beaton, S.L. Tisdale, and W.L. Nelson. 1999. Soil fertility and fertilizers: An introduction to nutrient management. 6th ed. Prentice Hall, Upper Saddle River, NJ.

Haynes, R.J., and R. Naidu. 1998. Influence of lime, fertilizer, and manure applications on soil organic matter content and soil physical conditions: A review. Nutr. Cycling Agroecosyst. 51:123-137.

Hettiarachchi, G.M., and G.M. Pierzynski. 2002. In situ stabilization of soil lead using phosphorus and manganese oxide: Influence on plant growth. J. Environ. Qual. 31:564-572.

Hettiarachchi, G.M., and G.M. Pierzynski. 2004. Soil lead bioavailability and in situ remediation of lead contaminatd soils: A review. Environ. Prog. 23:78-93.

Hettiarachchi, G.M., G.M. Pierzynski, and M.D. Ransom. 2000. In situ stabilization of soil lead using phosphorus and manganese oxide. Environ. Sci. Technol. 34:4614-4619.

Hettiarachchi, G.M., G.M. Pierzynski, and M.D. Ransom. 2001. In situ stabilization of soil lead using phosphorus. J. Environ. Qual. 30:1214-1221.

Hettiarachchi, G.M., J.A. Ryan, R.L. Chaney, and C.M. La Fleur. 2003. Sorption and desorption of cadmium by different fractions of biosolids-amended soils. J. Environ. Qual. 32:1684-1693.

Hinojosa, M.B., J.A. Carreira, R. García-Ruíz, and R.P. Dick. 2005. Microbial response to heavy metal-polluted soils: Community analysis from phospholipid-linked fatty acids and ester-linked fatty acids extracts. J. Environ. Qual. 34:1789-1800.

Hoffman, W. 1970. Lead and lead alloys. New York, Springer-Verlag.

Holmgren, G.G.S., M.W. Meyer, R.L. Chaney, and R.B. Daniels. 1993. Cadmium, lead, zinc, copper, and nickel in agricultural soils of the United States of America. J. Environ. Qual. 22:335-348.

Hooda, P.S., and B.J. Alloway. 1996. The effect of liming on heavy metal concentrations in wheat, carrots, and spinach grown on previously sludged-applied soils. J.

Agric. Sci. 127:289-294.

Isaure, M.P., A. Laboudigue, A. Manceau, G. Sarret, C. Tiffreau, P. TRocellier, G. Lamble, J.L. Hazemann, and D. Chateigner. 2002. Quantitative Zn speciation in a contaminated dredged sediment by μ-PIXE, μ-SXRF, and EXAFS spectroscopy and principal components analysis. Geochim. Cosmochim. Acta 66:1549-1567.

Iskandar, I.K., and D.C. Adriano. 1997. Remediation of soils contaminated with metals: A review of current practices in the USA. p. 1-26. *In* I.K. Iskandar and D.C. Adriano (eds.) Remediation of soils contaminated with metals. Advances in Environmental Science. Science Reviews, Middlesex, UK.

Jackson, B.P., P.L. Williams, A. Lanzirotti, and P.M. Bertsch. 2005. Evidence for biogenic pyromorphite formation by the nematode *Caenorhabditis elegans*. Environ. Sci. Tech. 39:5620-5625.

Jin, X., G.W. Bailey, Y.S. Yu, and A.T. Lynch. 1996. Kinetics of single and multiple metal ion sorption processes on humic substances. Soil Sci. 8:509-520.

Kabata-Pendias, A. 2001. Trace elements in soils and plants. 3rd ed. CRC Press, Boca Raton, FL.

Kandeler, E., C. Kampichler, and O. Horak. 1996. Influence of heavy metals on the functional diversity of soil microbial communities. Biol. Fertil. Soils 23:299-306.

Kelly, J.J., M. Håggblom, and R.L. Tate. 1999. Changes in soil microbial communities over time resulting from one time application of zinc: A laboratory microcosm study. Soil Biol. Biochem. 31:1455-1465.

Kelly, J.J., M. Håggblom, and R.L. Tate. 2003. Effects of heavy metal contamination and remediation on soil microbial communities in the vicinity of a zinc smelter as indicated by analysis of microbial community phospholipid fatty acid profiles. Biol. Ferti. Soils 38:65-71.

Kendorff, H., and M. Schnitzer. 1980. Sorption of metals on humic acid. Geoch. Cosmochim. Acta 44:1701-1708.

Kennedy, A.C., and V.L. Gerwin. 1997. Soil microbial diversity: Present and future considerations. Soil Sci. 162:607-617.

Kiikkilä, O, J. Perkiömäki, M. Barnette, J. Derome, T. pennanen, E. Tulisalo, and H. Fritze. 2001. In situ bioremediation through mulching of soil polluted by a copper-nickel smelter. J. Environ. Qual. 30:1134-1143.

Killham, K. 1985. A physiological determination of the impact of environmental stress on the activity of microbial biomass. Environ. Pollut. 38:283-294.

Kinniburgh, D.G., and M.L. Jackson. 1982. Concentration and pH dependence of calcium and zinc adsorption iron hydrous oxide gel. Soil Sci. Soc. Am. J. 46:56-61.

Kinniburgh, D.G., M.L. Jackson, and J.K. Syers. 1976. Adsorption of alkaline earth, transition, and heavy metal cations by hydrous oxide gels of iron and aluminum. Soil Sci. Soc. Am. J. 40:796-799.

Kitagishi, K., and I. Yamane. 1981. *Heavy metal pollution in soils of Japan.* Tokyo: Japan Scientific Societies Press.

Konopka, A., T. Zakharova, M. Bischoff, L. Oliver, C. Nakatsu, and R.F. Turco. 1999. Microbial biomass and activity of lead-contaminated soil. App. Environ. Microbiol. 65:2256-2259.

Korthals, G.W., A.D. Alexiev, T.M. Lexmond, J.E. Kammenga, and T. Bongers. 1996. Long-term effects of copper and pH on the nematode community in an agroecosystem. Environ. Toxicol. Chem. 15:979-985.

Krebs, R., K.S. Gupta, G. Furrer, and R. Schulin. 1998. Solubility and plant uptake of metals with and without liming of sludge-amended soils. J. Environ. Qual. 27:18-23.

Krebs, R., K.S. Gupta, G. Furrer, and R. Schulin. 1999. Gravel sludge as an immobilizing agent in soils contaminated by heavy metals: A field study. Water Air Soil Pollut. 115:465-479.

Krzaklewski, W. and M. Pietrzykowski. 2002. Selected physio-chemical properties of zinc and lead ore tailings and the biological stabilization. Water, Air, Soil Pollut. 141:125-142.

Kumar, N.P.B.A., V. Dushenkov, H. Motto, and I. Raskin. 1995. Phytoextraction: The use of plants to remove heavy metals from soils. Environ. Sci. Tech. 29:1232-1238.

Lee, I., O.K. Kim, Y. Chang, B. Bae, H.H. Kim, and K.H. Baek. 2002. Heavy metal concentrations and enzyme activities in soil from a contaminated Korean shooting range. J. Biosci. Bioeng. 5:406-411.

Leita, L., M. De Nobili, G. Muhlbachova, C. Mondini, L. Marchiol, and G. Zerbi. 1995. Bioavailability and effects of heavy metals on soil microbial biomass survival during laboratory incubation. Biol. Fertil. Soils 19:103-108.

Levi-Minzi, R., and G. Petruzzelli. 1984. The influence of phosphate fertilizers on Cd

solubility in soil. Water Air Soil Pollut. 23:423-429.

Levison, H.S. and I. Mahler. 1998. Phosphate activity and lead resistance and sensitivity in *Citrobacter freundii* and *Staphylococcus aures*. FEMS Microbiol. Lett. 161:135-138.

Li, Y., and R.L. Chaney. 1998. Case studies in the field-Industrial sites: Phytostabilization of zinc smelter-contaminated sites: The Palmerton case. *In* J. Vangronsveld and S.D. Cunningham (eds.) Metal contaminated soils: In situ inactivation and phytorestoration. p. 197-210. Georgetown, TX: Spring-Verlag and R.G. Landes Company.

Li, Y., R.L. Chaney, G. Siebielec, and B.A. Kerschner. 2000. Response of four turfgrass cultivars to limestone and biosolids-compost amendment of a zinc and cadmium contaminated soil at Palmerton, Pennsylvania. J. Environ. Qual. 29:1440-1447.

Lindsay, W.L. 1979. Chemical equilibria in soils. Wiley, New York, NY.

Lombi, E., R.E. Hamond, S.P. McGrath, and M.J. McLaughlin. 2003. Lability of Cd, Cu, and Zn in polluted soils treated with lime, beringite, and red mud and identification of a non-labile colloidal fraction of metals using isotopic techniques. Environ. Sci. Tech. 37:979-984.

Lothenbach, B., G. Furrer, and R. Schulin. 1997. Adsorption of heavy metals by polynuclear aluminum and modified montmorillonite. Environ. Sci. Technol. 31:1452-1462.

Lothenbach, B., R. Krebs, G. Furrer, S.K. Gupta, and R. Schulin. 1998. Immobilization of cadmium and zinc by Al-montmorillinite and gravel sludge. Eurpean J. Soil Sci. 49:141-148.

Lovely, D.R. 1991. Dissimilatory Fe(III) and Mn(IV) reduction. Microbiological Reviews 55:259-287.

Ma, L.Q., and G.N. Rao. 1997. Effects of phosphate rock on sequential chemical extraction of lead in contaminated soils. J. Environ. Qual. 26:788-794.

Ma, Q.Y., T.J. Logan, and S.J. Traina. 1995. Lead immobilization from aqueous solutions and contaminated soils using phosphate rocks. Environ. Sci. Techol. 29:1118-1126.

Ma, Q.Y., S.J. Traina, and T.J. Logan. 1993. In situ lead immobilization by apatite. Environ. Sci. Technol. 27:1803-1810.

Manceau, A., B. Lanson, M.L. Schlegel, J.C. Hargé, M. Musso, L. Eybert-Bérard, J.L. Hazemann, D. Chateigner, and G.M. Lamble. 2000. Quantitative Zn speciation in smelter-contaminated soils by EXAFS spectroscopy. Am. J. Sci. 300:289-343.

Manceau, A., M.A. Marcus, and N. Tamura. 2002. Quantitative speciation of heavy metals in soils and sediments by synchrotron X-ray techniques. *In* P.A. Fenter, M.L. Rivers,

N.C. Sturchio, and S.R. Sutton (ed.) Applicatons of synchrotron radiation in low-temperature geochemistry and environmental science. Vol. 49. Reviews in Mineralogy and Geochemistry, The Mineralogical Society of America, Washington D.C.

Manceau, A., M.A. Marcus, N. Tamura, O. Proux, N. Geoffroy, and B. Lanson. 2004. Natural speciation of Zn at the micrometer scale in a clayey soil using X-ray fluorescence, absorption, and diffraction. Geochim. Cosmochim. Acta 68:2467-2483.

Marzadori, C., C. Ciavatta, D. Montecchio, and C. Gessa. 1996. Effects of lead pollution on different soil enzyme activities. Biol. Fertil. Soils. 22:53-58.

Matocha, C.J., E.J. Elzinga, and D.L. Sparks. 2001. Reactivity of Pb(II) at the Mn(III, IV) (oxyhydr)oxide-water interface. Environ. Sci. Tech. 35:2967-2972.

McBride, M.B. 1989. Reactions controlling heavy metal solubility in soils. Adv. Soil Sci. 10:1-56.

McBride, M.B. 1994. Environmental chemistry of soils. Oxford University Press, New York.

McBride, M.B., S. Suave, and W. Hendershot. 1997. Solubility control of Cu, Zn, Cd, and Pb in contaminated soils. European J. Soil Sci. 48:337-346.

McGowen, S.L., N.T. Basta, and G.O. Brown. 2001. Use of diammonium phosphate to reduce heavy metal solubility and transport in smelter-contaminated soil. J. Environ. Qual. 30:493-500.

McKenzie, R.M. 1980. The adsorption of lead and other heavy metals on oxides of manganese and iron. Aust. J. Soil Res. 18:61-73.

McLaughlin, M., E. Smolders, and R. Merckx. 1998. Soil-root interface: Physiochemical processes. p. 233-277. *In* P.M. Huang (ed.) Soil chemistry and ecosystem health. SSSA, Madison, WI.

McLaughlin, M., B.A. Zarcinas, D.P. Stevens, and N. Cook. 2000. Soil testing for heavy metals. Commun. Soil Sci. Plant Anal. 31:1661-1700.

Mench, J., V. Didier, M. Loffler, A. Gomez, and P. Masson. 1994. A mimicked in-situ remediation study of metal-contaminated soils with emphasis on Cd and Pb. J. Environ. Qual. 23:58-63.

Mielke, H.W. 1999. Lead in the inner cities: Policies to reduce children's exposure to lead may be overlooking a major source of lead in the environments. American Scientist. Vol.

87:62-73.

Morin, G., J.D. Ostergren, F. Julliot, P. Ildefonse, G. Calas, and G.E. Brown. 1999. XAFS determination of the chemical form of lead in smelter-contaminated soils and mine tailings: Importance of adsorption processes. Am. Mineral. 84:420-434.

Msaky, J.J., and R. Calvet. 1990. Adsorption behaviour of copper and zinc in soils: Influence of pH on adsorption characteristics. Soil Sci. 164:513-522.

Nachtegaal, M., M.A. Marcus, J.E. Sonke, J. Vangronsveld, K.J.T. Livi, D. Van Der Lelie, and D.L. Sparks. 2005. Effects of in situ remediation on the speciation and bioavailability of zinc in a smelter contaminated soil. Geochim. Cosmochim. Acta 69:4649-4664.

National Research Council: Subcommittee on Zinc. 1979. Zinc. University Park Press, Baltimore, MD.

Nesse, W.D. 2000. Introduction to Mineralogy. Oxford University Press, NewYork.

Newville, M., S. Sutton, M. Rivers, and P. Eng. 1999. Micro-beam X-ray absorption and fluorescence spectroscopies at GSECARS: APS beamline 13-ID. J. Synch. Rad. 6:353-355.

Nies, D.H. 1999. Microbial heavy-metal resistance. Appl. Microbiol. Biotechnol. 51:730-750.

Nirel, P.V., and F.M. Morel. 1990. Pitfalls of sequential extractions. Water Res. 24:1055-1056.

Nolan, A.L., H. Zhang, and M.J. McLaughlin. 2005. Prediction of zinc, cadmium, lead, and copper availability to wheat n contaminated soils using chemical speciation, diffusive gradients in thin films, extraction, and isotopic dilution techniques. J. Environ. Qual. 34:496-507.

Nriagu, J.O. 1972. Lead orthophosphates-I. Solubility and hydrolysis of secondary lead orthophosphate. Inorg. Chem. 11:2499-2503.

Nriagu, J.O. 1973. Lead orthophosphates-II. Solubility of chloropyromorphite at 25° C. Geochim. Cosmochim. Acta 37:367-377.

Nriagu, J.O. 1974. Lead orthophosphates-IV. Formation and stability in the environment. Geochim. Cosmochim. Acta 38:887-898.

Nriagu, J.O. 1978. The Biogeochmistry of Lead in the Environment. Part A. Elsevier/North-Holland Biomedical Press, NY.

Nriagu, J.O. 1984. Formation and stability of base metal phosphates in soils and

sediments. *In* J.O. Nriagu and P.B. Moore (eds.) Phosphate Minerals. Springer-Verlag, Berlin, Germany.

Nriagu, J.O. 1988. A silent epidemic of environmental metal poisoning. Environ. Pollut. 50:139-161.

Nriagu, J.O. and J.M. Pacyna. 1988. Quantitative assessment of worldwide contamination of air, water and soils by trace metals. Nature. 333:134-139.

O'Day, P.A., S.A. Carroll, and G.A. Waychunas. 1998. Rock-water interactions controlling zinc, cadmium, and lead concentrations in surface waters and sediments, U.S. Tri-State Mining District. I. Molecular identification using X-ray absorption spectroscopy. Environ. Sci. Technol. 32:943-955.

Oste, L.A., T.M. Lexmond, and W.H. Van Riemsdijk. 2002. Metal immobilization in soils using synthetic zeolites. J. Environ. Qual. 31:813-821.

Ostergren, J.D., G.E. Brown Jr., G.A. Parks, and T.N. Tingle. 1999. Quantitative speciation of lead in selected mine tailings from Leadville, CO. Environ. Sci. Tech. 33:1627-1636.

Palazzo, A.J, T.J. Cary, S.E. Hardy, and C. Richard Lee. 2003. Root growth and metal uptake in four grasses grown on zinc-contaminated soils. J. Environ. Qual. 32:834-840.

Pearson, M.S., K. Maenpaa, G.M. Pierzynski, and M.J. Lydy. 2000. Effects of soil amendments on bioavailability of lead, zinc, and cadmium to earthworms. J. Environ. Qual. 29:1611-1617.

Pennanen, T., Á. Frostegård, H. Fritze, and E. Bååth. 1996. Phospholipid fatty acid composition and heavy metal tolerance of soil microbial communities along two heavy metal-polluted gradients in coniferous forests. Appl. Environ. Microbiol. 62:420-428.

Pérez de Mora, A., J.J. Ortega-Calvo, F. Cabrera, and E. Madejón. 2005. Changes in enzyme activities and microbial biomass after "in situ" remediation of a heavy metal-contaminated soil. Appl. Soil Ecol. 28:125-137.

Pierzynski, G.M. 1997. Strategies for remediating trace-element contaminated sites. p. 67-84. *In* I.K. Iskandar and D.C. Adriano (eds.) Remediation of soils contaminated with metals. Advances in Environmental Science. Science Reviews, Middlesex, UK.

Pierzynski, G.M. and K.A. Gehl. 2004. An alternative method for remediating lead-contaminated soils in residential areas: A decision case study. J. Nat. Resour. Life Sci. Educ.

33:63-69.

Pierzynski, G.M., M. Lambert, B.A.D. Hetrick, D.W. Sweeney, and L.E. Erickson. 2002a. Phytostabilization of metal mine tailings using tall fescue. Practice Periodical of Hazardous, Toxic, and Radioactive Waste Management 6:212-217.

Pierzynski, G.M., J.L. Schnoor, A. Youngman, L. Licht, and L.E. Erickson. 2002b. Popular trees for phytostabilization of abandoned zinc-lead smelter. Practice Periodical of Hazardous, Toxic, and Radioactive Waste Management 6:177-183.

Pierzynski, G.M., and A.P. Schwab. 1993. Bioavailability of zinc, cadmium, and lead in a metal-contaminated alluvial soil. J. Environ. Qual. 22:247-254.

Pinkhart, H.C., D.B. Ringelberg, Y.M. Piceno, S.J. Macnaughton, and D.C. White. 2002. Biochemical approaches to biomass measurements and community structure analysis. p. 101-113. *In* C.J. Hurst, R.L. Crawford, G.R. Knudsen, M.J. McInerney, and L.D. Stentzenbach (ed.) Manual of environmental microbiology. ASM Press, Washington, D.C.

Ponder, F.P., and M. Tadros. 2002. Phospholipid fatty acids in forest soil four years after organic matter removal and soil compaction. Appl. Soil Ecol. 19:173-182.

Pope, L.M. 2005. Assessment of contaminated streambed sediment in the Kansas part of the historic Tri-State lead and zinc mining district, Cherokee County, 2004. USGS Scientific Investigations Report 2005-5251.

Rajapaksha, R.M.C.P., M.A. Tobor-Kaplon, and E. Bååth. 2004. Metal toxicity affects fungal and bacterial activities in soil differently. Appl. Environ. Microbiol. 70:2966-2973.

Rieuwerts, J.S., I. Thorton, M.E. Farago, and M.R. Ashmore. 1998. Factors influencing metal bioavailability in soils. Chem. Speciation Bioavailabilty 10:61-76.

Ritchie, E. 1986. Guide book to the Tri-State Mineral Museum. p. 83. A&J Printing, Nixa, MO.

Robert, M., and C. Chenu. 1992. Interactions between soil minerals and microorganisms. Soil Biochem. 7:307-379.

Roberts, D.R., A.C. Scheinost, and D.L. Sparks. 2002. Zinc speciation in a smelter-contaminated soil profile using bulk and microspectroscopic techniques. Environ. Sci. Tech. 36:1742-1750.

Roem, W.J., and F. Berendse. 2000. Soil acidity and nutrient supply ratio as possible factors determining changes in plants species and diversity in grassland and heathland

communities. Biol. Conserv. 92:151-161.

Romheld, V., and H. Marschner. 1991. Function of micronutrients in plants. *In* J.J. Mortvedt et al., eds. Micronutrients in agriculture. 2nd ed. SSSA 4. Soil Sci. Soc. Am., Madision, WI.

Ruby, M.V., A. Davis, and A. Nicholson. 1994. In situ formation of lead phosphates as a method to immobilize lead. Environ. Sci. Technol. 28:646-654.

Ruby, M.V., A. Davis, R. Schoof, S. Eberle, and C.M. Sellstone. 1996. Estimation of bioavailability using a physiologically based extraction test. Environ. Sci. Technol. 30:420-430.

Ruttens, A., M. Mench, J.V. Colpaert, J.Boisson, R. Carleer, and J. Vangronsveld. 2006. Phytostabilization of a metal contaminated sandy soil. I: Influence of compost and/or inorganic metal immobilizing soil amendments on phytotoxicity and plant availability of metals. Environ. Pollut. 144:524-532.

Sandaa, R.A., V. Torsvik, O. Enger, F.L. Daae, T. Castberg, and D. Hahn. 1999. Analysis of bacterial communities in heavy-metal contaminated soils at different level of resolution. Microbiol. Ecol. 30:237-251.

Sanstead, H.H. 1995. Requirements and toxicity of essential trace elements, illustrated by zinc and copper. Am. J. Clin. Nutrition 61:621S-624S.

Santillian-Medrano, J., and J.J. Jurinak. 1975. The chemistry of lead and cadmium in soil: Solid phase formation. Soil Sci. Soc. Am. Proc. 39:851-856.

Scheckel, K.G., and J.A. Ryan. 2002. Effects of aging and pH on dissolution kinetics and stability of chloropyromorphite. Environ. Sci. Technol. 36:2198-2204.

Scheckel, K.G., and J.A. Ryan. 2004. Spectroscopic speciation and quantification of Pb in phosphate amended soils. J. Environ. Qual. 33:1288-1295.

Scheckel, K.G., C.A. Impellitteri, J.A. Ryan, and T. McEvoy. 2003. Assessment of a sequential extraction procedure for perturbed lead contaminated samples with and without phosphorus amendments. Environ. Sci. Technol. 37:1892-1898.

Scheckel, K.G., J.A. Ryan, D. Allen, and N.V. Lescano. 2005. Determining speciation of Pb in phosphate-amended soils: Method limitations. Sci. Total Eviron. 350:261-272.

Scheinost, A.C., R. Kretzschmar, and S. Pfister. 2002. Combining selective sequential extractions, X-ray absorption spectroscopy, and principal components analysis for quantitative zinc speciation in soil. Environ. Sci. Tech. 36:5021-5028.

Schlegel, M.L., A. Manceau, and L. Charlet. 1997. EXAFS study of Zn and ZnEDTA sorption at the goethite (α-FeOOH)/water interface. J. Phys. IV. 7:823-824.

Schnitzer, M. 1969. Reactions between fulvic acid, a soil humic compound and inorganic constituents. Soil Sci. Soc. Am. Proc. 33:75-81.

Schwertmann, U., and R.M. Taylor. 1989. Iron oxides. p. 379-438. *In* J.B. Dixon and S.B. Weed (ed.) Minerals in soil environments. ASA and SSSA, Madison, WI

Sharma, P., and R.S. Dubey. 2005. Lead toxicity in plants. Braz. J. Plant Physiol. 17:35-52.

Shaw, L.J., Y. Beaton, L.A. Glover, K. Killham, and A.A. Meharg. 2000. Interactions between soil, toxicant, and a lux-marked bacterium during solid phase-contact toxicity testing. Environ. Toxicol. Chem. 19:1247-1252.

Shi, W., J. Becker, M. Bischoff, R.F. Turco, an dA.E. Konopka. 2002. Association of microbial community composition and activity with lead, chromium, and hydrocarbon contamination. Appl. Environ. Microbiol. 68:3859-3866.

Shuman, L.M., and Z. Li. 1997. Amelioration of zinc toxicity in cotton using lime and mushroom compost. J. Soil Contam. 6:425-438.

Singh, R.P., R.D. Tripathi, S.K. Sinha, R. Maheshwari, and H.S. Srivastava. 1997. Response of higher plants to lead contaminated environment. Chemosphere 34:2467-2493.

Šmejkalová, M., O. Mikanová, and L. Borůvka. 2003. Effects of heavy metal concentrations on biological activity of soil micro-organisms. Plant Soil Environ. 49:321-326.

Sonmez, O., and G.M. Pierzynski. 2005. Assessment of zinc phytoavailability by diffusive gradients in thin films. Environ. Toxicol. Chem. 24:934-941.

Spark, K.M., B.B. Johnson, and J.D. Wells. 1995. Characterizing heavy-metal adsorption on oxides and oxyhydroxides. Eur. J. Soil Sci. 46:621–631.

Sparks, D.L. 2003. Environmental soil chemistry. 2nd ed. Academic Press, San Diego, CA.

Sparks, D.L. (ed.) 1996. Methods of soil analysis. Part 3. SSSA Book Ser. 5. Soil Sci. Soc. Am. Madison, WI.

Sparks, D.L., A.M. Scheidegger, D.G. Strawn, and K.G. Scheckel. 1998. Kinetics and mechanisms of reactions at the mineral/water interface. *In* D.L. Sparks and T.J. Grundl (eds.) Mineral-water interfacial reactions. Am. Chem. Soc. Symp. Ser., Washington D.C.

Sposito, G. 1989. The chemistry of soils. Oxford University Press, New York.

Sposito, G. 1981. The thermodynamics of soil solutions. Oxford University Press, New York.

Stahl, R.S., and B.R. James. 1991. Zinc sorption by manganese-coated sand as a function of pH. Soil Sci. Soc. Am. J. 55:1291-1294.

Stanforth, R., and J. Qiu. 2001. Effect of phosphate treatment on the solubility of lead in contaminated soil. Environ. Geol. 41:1-10.

Stevenson, F.J. 1994. Humus chemistry: Genesis, composition, reactions. Wiley-Interscience, New York.

Stevenson, F.J., and A. Fitch. 1986. Chemistry and complexation of metal ions with soil solution organics. p. 29-58. *In* P.M. Huang et al. (ed.) Interactions of soil minerals with natural organics and microbes. ASA and SSSA, Madison, WI.

Strawn, D.G., A.M. Schiedegger, and D.L. Sparks. 1998. Kinetics and mechanisms of Pb(II) sorption and desorption at the aluminum oxide-water interface. Environ. Sci. Tech. 32:2596-2601.

Strawn, D.G., and D.L. Sparks. 1999. The use of XAFS to distinguish between inner- and outer-sphere lead adsorption complexes on montmorillinte. J. Coll. Inter. Sci. 216:257-269.

Strawn, D.G., and D.L. Sparks. 2000. Effects of soil organic matter on the kinetics and mechanisms of Pb(II) sorption and desorption in soil. Soil Sci. Soc. Am. J. 64:144-156.

Stucynski, T.I., G.W. McCary, and G. Siebielec. 2003. Response of soil microbiological activities to cadmium, lead, and zinc salt amendments. J. Environ. Qual. 32:1346-1355.

Suave, S., C.E. Martinez, M. McBride, and W. Hendershot. 2000. Adsorption of free lead (Pb^{2+}) by pedogenic oxides, ferrihydrite, and leaf compost. Soil Sci. Soc. Am. J. 64:595-599.

Suave, S., M. McBride, and W. Hendershot. 1998. Soil solution speciation of lead(II): Effects of organic matter and pH. Soil Sci. Soc. Am. J. 62:618-621.

Swift, R.S., and R.G. McLaren. 1991. Micronutrient adsorption by soil and soil colloids. p. 257-292. *In* F.H. Bolt et al. (ed.) Interactions at the soil colloid-soil solution interface. Part 2. Kluwer Academic Publishers. Dordrecht, The Netherlands.

Tejada, M., J.L. Moreno, M.T. Hernandez, and C. Garcia. 2007. Application of two beet vinasse forms in soil restoration: Effects on soil properties in an arid environment in southern

Spain. Agriculture, Ecosystems, and Environment 119:289-298.

Tessier, A., P.G.C. Cambell, and M. Bisson. 1979. Sequential extraction procedure for the speciation of particulate trace metals. Anal. Chem. 51:844-851.

Torvisk, V., F.L. Daae, R.A., Sandaa, and L. Ovreas. 1998. Novel techniques for analyzing microbial diversity in natural and perturbed environments. J. Biotechnol. 64:53-62.

Turco, R.F., A.C. Kennedy, and M.D. Jawson. 1994. Microbial indicators of soil quality. p. 73-99. *In* J.W. Doran, D.C. Coleman, D.F. Bezdicek, and B.A. Stewart (ed.) Defining soil quality for a sustainable environment. SSSA Spec. Publ. 35. SSSA, Madison, WI.

United Nations Environment Programme (UNEP). 2006. Interim review of scientific informationon lead. Available at http://www.chem.unep.ch/Pb_and_Cd/SR/Files/Interim_reviews/UNEP_Lead_review_Interim-Oct2006.pdf.

U.S. Environmental Protection Agency. 1986. Test methods for evaluating solid wastes. SW-846. 3rd ed. U.S. Gov. Print Office, Washington D.C.

U.S. Environmental Protection Agency. 1997. EPA Superfund Record of Decision: Cherokee County, Kansas. U.S. Environmental Protection Agency Report EPA/ROD/R0797/073.

Vangronsveld, J., and S. Cunningham (eds.). 1998. Metal-contaminated soils: In situ inactivation and phytorestoration. Georgetown, TX: Spring-Verlag and R.G. Landes Company.

Vangronsveld, J., F.V. Assche, and H. Clijsters. 1995. Reclamation of a bare industrial area contaminated by non-ferrous metals: In situ metal immobilization and revegetation. Environmental Pollution 87:51-59.

Vansgronsveld, J., J.V. Colpaert, and K.K. Van Tichelen. 1996. Reclamation of a bare industrial area contaminated by non-ferrous metals: Physio-chemical and biological evaluation of the durability of soil treatment and revegetation. Environ. Pollut. 94:131-140.

Vestal, J.R., and D.C. White. 1989. Lipid analysis in microbial ecology. Bioscience 39:535-541.

Voegelin, A., S. Pfister, M.A. Marcus, and R. Kretzschmar. 2005. Changes in zinc speciation in field soil after contamination with zinc oxide. Environ. Sci. Technol. 39:6616-6623.

Vulkan, R., F.J. Zhao, V. Barbosa-Jefferson, S. Preston, G.J. Paton, E. Tipping, and S.P.

McGrath. 2000. Copper speciation and impacts on bacterial biosensors in the pore water of copper-contaminated soils. Environ. Sci. Technol. 34:5115-5121.

Weesner, F.J., and W.F. Bleam. 1998. Binding characteristics of Pb^{2+} on anion-modified and pristine hydrous oxide surfaces studied by electrophoretic mobility and X-ray absorption spectroscopy. J. Colloid Interface Sci. 205:380-389.

Wikipedia: The Free Encyclopedia. 2001. Zinc [Online]. Available at http://en.wikipedia.org/wiki/Zinc (verified 20 Sept. 2006).

Wong, J.W.C., C.M. Ip, and M.H. Wong. 1998. Acid-forming capacity of lead-zinc mine tailings and its implications for mine rehabilitation. Env. Geochem. Hlth. 20:149-155.

Xie, R.J., and A.F. MacKenzie. 1990. Zinc sorption, desorption, and fractions in three autoclaved soils treated with pyrophosphate. Soil Sci. Soc. Am. J. 54:71-77.

Yang, J., D.E. Mosby, S.W. Casteel, and R.W. Blanchar. 2001. Lead immobilizatioin using phosphoric acid in a smelter-contaminated urban soil. Environ. Sci. Technol. 35:3553-3559.

Ye, Z.H., J.W.C. Wong, and M.H. Wong. 2000. Vegetation response to lime and manure compost amendments on acid lead/zinc mine tailings: A greenhouse study. Restoration Ecol. 8:289-295.

Yoon, J.K., X.D. Cao, and L.Q. Ma. 2007. Application methods affect phosphorus-induced lead immobilization from a contaminated soil. J. Environ. Qual. 36:373-378.

Zhang, H., F.J. Zao, B. Sun, W. Davison, and S.P. McGrath. 2001. A new method to measure effective soil solution concentration predicts copper availability to plants. Environ. Sci. Technol. 32:704-710.

Zwonitzer, J.C., G.M. Pierzynski, and G.M. Hettiarachchi. 2003. Effects of phosphorus additions on lead, cadmium, and zinc bioavailabilites in a metal-contaminated soil. Water Air Soil Pollut. 143:193-209.

CHAPTER 3 - Changes in Microbial Enzymes, Biomass, and Phospholipid Fatty Acid Profiles upon the Addition of Amendments to a Heavy Metal Contaminated Mine Waste

3.1 Abstract

One proposed method for stabilizing a Pb/Zn contaminated mine wastes is to apply large quantities of organic matter in order to improve physical, chemical, and biological characteristics, which enhances biogeochemical nutrient cycles. Our hypothesis is that large applications of compost (> 200 Mg ha^{-1}) will support increased microbial activity over time. We used beef manure compost applied at two different levels (45 and 269 Mg ha^{-1}) with and without lime and bentonite to investigate the changes in microbial community structure and function. Switchgrass (*Panicum virgatum*) was seeded into plots to establish a vegetative cover. Compost additions significantly changed C, N, P, and K contents along with pH values. Enzyme activities and microbial biomass measurements were used to monitor nutrient cycles upon amendment addition. After five months the high compost, high compost + lime, and high compost + lime + bentonite treatments had significantly higher arylsulfatase and phosphatase activities compared to all other treatments. The high compost treatment had a significantly increased β-glucosidase activity and also more microbial biomass C, while other measurements were more variable. Increases in microbial activities were significantly related to increases in total C, P, and estimated available water, while negative relationships existed with electrical conductivity and bioavailable Zn. Phospholipid fatty acid analysis (PLFA) was used to assess changes in microbial community structure. Principal components analysis (PCA) of PLFA profiles shows that the high compost treatments caused a significant shift in microbial community composition.

Gram-positive bacteria, Gram-negative bacteria, and fungal biomass as determined by PLFA were significantly higher in the 269 Mg ha^{-1} treatment than in the control and 45 Mg ha^{-1} treatments. Results suggest that an organic matter addition ranging between 45 and 269 Mg ha^{-1} is needed to support and sustain microbial activity and biomass in contaminated mine waste materials.

3.2 Introduction

The Tri-State Mining Region, located in southwest Missouri, southeast Kansas, and northeast Oklahoma, has a long legacy of Pb and Zn mining. Mine waste materials are often characterized by very low concentrations of organic matter, nitrogen (N), phosphorus (P), and by their neutral to low pH, high acid-producing potential, and poor soil physcial structure (Wong et al., 1998; Krzaklewski and Pietrzykowski, 2002), which harms native ecosystems (Pierzynski, 1997). The lack of vegetative cover leaves the mine wastes exposed to erosion processes, direct-contact exposures, and inhibits the development of a functional ecosystem (Martin and Ruby, 2004). Agents that may suppress, poison, or change the quality or quantity of organic matter can damage the functioning of the soil-plant ecosystem. Of the inorganic pollutants, a number of the most important are the heavy metals (Cu, Ni, Cd, Zn, Cr, Pb). Heavy metals negatively affect microbial activity and growth through functional disturbances, by damaging proteins, and/or by disrupting cell membranes (Leita et al., 1995). Since removal is not a valid remedial option, due to cost and labor, *in situ* techniques have been developed in an attempt to establish self-sustainable ecosystems and stabilize mine waste materials. One way of accomplishing this is through the addition of organic materials or composts. These materials improve physical and chemical properties and also reduce the bioavailability of heavy metals through sorption (Clemente et al., 2006). As a result, metal mobility is limited through establishment of a

vegetative cover.

Soil organic matter, nutrients, and biological activity contribute to ecosystem-level process and are important for productivity, community structure, and fertility in terrestrial ecosystems (Stevenson, 1994). The intent of using organic materials to help phytostabilize metal contaminated soils/wastes is to create a self-sustaining system where nutrients are cycled internally by healthy microbial and plant populations with no further inputs needed. Pierzynski et al. (2002) discovered that additions of beef manure applied at a rate of 90 Mg ha^{-1} resulted in an increase in tall fescue (*Festuca arundinacea* Shreb) growth in the first year after amendment addition. However, by year 3 plant growth began to decline and plant tissue analysis suggested Zn phytotoxicity as one causative factor. In another study, Brown et al. (2003) found that surface applications of high N biosolids (66 Mg ha^{-1} biosolids) with wood ash was effective at establishing a vegetative plant cover on Cd, Pb, and Zn mine tailings for at least 2 growing seasons through the reduction of metal bioavailability. Over time they observed a decrease in plant/soil Ca, K, and Mg concentrations, which led them to conclude that higher amendment loadings may be needed to supply essential plant nutrients required to produce a self-sustaining plant cover. As a result, more research is needed to investigate the effectiveness of increased additions of organic amendments on the permanence of vegetative covers over time.

Microbial properties, such as community function and diversity, are reported to be useful indicators of soil quality and could serve as criteria of successful rehabilitation of ecologically disturbed areas (Claassens et al., 2005). While microbial indicators don't elicit any information directly on metal speciation, they provide us with information about metal bioavailability and ecosystem function. Soil microorganisms and soil fauna mineralize both fresh organic inputs and the larger pool of soil organic matter (SOM), which cycles C, N, P, and S. As a result, the

fertility of natural soil ecosystems depends on SOM turnover, which is mediated by the microbial biomass and can be influenced by heavy metal pollution (Brookes, 1995). Therefore, simple microbial-based measurement methods could be utilized to determine the degree of effectiveness that *in situ* remediation techniques have on heavy metal contaminated soils and mine wastes.

Other amendments, such as lime, are often applied with compost to further enhance reclamation. It is recognized that as pH increases the availability of most metal species, especially Zn, decreases (Lindsay, 1979). Additionally, in the pelletization process, bentonite is added to provide rigidity to the pellets; therefore, the effects of bentonite on microbial populations when added to contaminated mine wastes needs to be explored.

Microbial activity measurements such as nitrification and soil enzyme activities, along with total soil microbial biomass have been proposed to assess ecosystem recovery (Brookes, 1995). Microbial biomass parameters have been widely used for testing soil quality and the degree of restoration in degraded and/or contaminated soils (Clemente et al., 2006; Pérez de Mora et al., 2005). It is generally accepted that accumulated heavy metals reduce the amount of soil microbial biomass (Brookes and McGrath, 1994; Chander et al., 1995), but no single measurement should be used to monitor restoration (Brookes, 1995). Therefore, Harris (2003) has proposed the use of multiple measurements to estimate community size, functional composition, and activity to identify the effects of restoration in heavy metal contaminated mine wastes and soils.

Microbial phospholipid-linked fatty acid (PLFA) composition is a method used to evaluate microbial community structure and biomass. These lipids are major cell membrane constituents, and the fatty acids themselves vary, thus the variation and relative abundance of

PLFA provides a "fingerprint" of the microbial community (Hinojosa et al., 2005). The variability can then be used to study community shifts (Turco et al., 1994). This method has been utilized to characterize microbial communities in heavy metal contaminated soils (Bååth et al., 1998; Frostegård et al., 1993b; Konopka et al., 1999; Pennanen et al., 1996; Rajapaksha et al., 2004; Shi et al., 2002). Studies that have investigated microbial community structures upon remediation include Kelly et al. (2003) and Hinojosa et al. (2005). Hinojosa et al. (2005) discovered that reclaimed soils had higher fungal to bacterial ratios than the contaminated control as indicated by PLFA analysis, which is proposed as an important indicator of successful remediation (Bardgett and McAlister, 1999). It was also established that there were higher amounts of Gm$^-$ (gram-negative) bacteria than Gm$^+$ (gram-positive) bacteria in polluted soils (Hinojosa et al., 2005), which they attributed to the fact that Gm$^-$ bacteria are considered to be fast growing microorganisms that easily adapt to changing environments (Ponder and Tadros, 2002). Whereas Gm$^+$ bacteria have thicker cell membranes and can undergo dormancy during periods of high stress (Doelman, 1985). Kelly et al. (2003) discovered that PLFA profiles for recently remediated sites were similar to the less contaminated sites, and there were significant increases in indicator fatty acids of fungi, actinomycetes, and Gm$^+$ bacteria, but their results indicate a loss of amendment effectiveness over time.

Our hypothesis is that large additions of composted beef manure can increase and maintain microbial activity and biomass in heavy metal contaminated mine wastes. The specific objectives of this research are to 1) to monitor changes in microbial activity over time upon addition of composted beef manure, 2) investigate the effects of composted beef manure when applied to mine wastes on microbial community structure and composition by PLFA profiling, and 3) determine if the addition of lime and/or bentonite with the compost further improves or

deters microbial function and community composition as compared to compost alone.

3.3 Materials and Methods

Site and Treatments. Two field sites were selected from the Tri-State Mining Region near Galena, KS. Mean annual precipitation for the area is 117 cm, ranging from 4.7 cm mo^{-1} in January to 13.8 cm mo^{-1} in June. Average monthly minimum and maximum temperatures range from -4.4^{o} C in January to 32.2^{o} C in July, respectively, while the average frost-free period is 210 d, extending from 5 April to 1 November or approximately 4,000 growing degree days (GDD). Both sites are located in the vicinity of an old mining area in which mine waste materials have been collected and deposited on the surface over a 100 y period. This gravel-like material is commonly referred to as chat and was a by-product in the initial processing of Zn/Pb ores at the now abandoned mine sites. No vegetation was present at either site prior to establishment of the field studies.

A tractor equipped with a front-end loader was used to loosen up the selected study areas so treatments that could be applied. Each site was then raked to smooth the terrain and the plots were installed with a border around each to reduce the potential for inter-plot contamination. A representative sample of chat was then taken from each site to determine particle size distribution as described by Gee and Bauder (1986). Soil samples were then taken from each plot to establish an initial baseline Cd, Pb, Zn, and nutrient content before amendment addition (Table 3-1). The amendments that were applied in the study consisted of composted beef manure, lime as Ca(OH)$_2$, and Enviroplug Grout (Wyo-Ben, Inc., Billings, MT), which is a Wyoming bentonite.

The experimental plots were 1 m by 2 m in size with 3 replications of each treatment. The treatments were the following: (1) CO, non-amended control plot; (2) LC, a low compost

treatment of 45 Mg ha^{-1}; (3) HC, a high compost treatment of 269 Mg ha^{-1}; (4) LC+L, low compost (45 Mg ha^{-1}) + 2.24 kg lime as Ca(OH)$_2$ (11.2 Mg ha^{-1}); (5) HC+L, high compost (269 Mg ha^{-1}) + 2.24 kg lime as Ca(OH)$_2$; (6) LC+L+B, low compost (45 Mg ha^{-1}) + 2.24 kg lime as Ca(OH)$_2$ + bentonite applied at 50 g bentonite kg^{-1} compost (0.45 kg); and (7) high compost (269 Mg ha^{-1}) + 2.24 kg lime applied as Ca(OH)$_2$ + bentonite applied at 50 g bentonite kg^{-1} compost (2.69 kg). The addition of bentonite was similar to what may be used to aid in the pelletization process of the compost. All treatments were thoroughly mixed into the plots to a depth of approximately 30 cm; plots were then raked to level the surface.

Site A was established on May 8, 2006 and Site B on May 12, 2006. Soil samples (20 cm depth) were collected from each plot using a small garden shovel on May 26, 2006 (Time 0), October 12, 2006 (139 d after time 0 (DATZ)), May 14, 2007 (353 DATZ), November 12, 2007 (535 DATZ), and May 6, 2008 (711 DATZ). Five sub-samples were taken from different areas within each individual plot and mixed to form a single sample for that plot. Each soil sample was divided into two fractions, one of which was immediately sieved to < 2 mm and stored without drying at < 4° C for microbial assays, while the other fraction was air-dried and sieved to < 2 mm for chemical analysis. After soil sampling on the May 26, 2006, Blackwell Switchgrass (*Panicum virgatum*) (Sharp Brothers Seed Company, Clinton, MO) was seeded into each of the plots at 6.72 kg of pure live seed (PLS) ha^{-1} and then lightly raked into the soil. Unfortunately, for a variety of reasons, vegetation did not establish in 2006. Therefore, annual ryegrass (*Lolium multiflorum* Lam.) was seeded in the plots on October 12, 2006 to act as a protective winter cover. On March 18, 2007 all plots were sprayed with glyphosate to kill the ryegrass. Plots were lightly spaded and again seeded with Blackwell Switchgrass (6.72 kg PLS ha^{-1}) on April 19, 2007.

Mine Waste/Compost Analyses. Mine waste and compost pH was measured in a 1:1 deionized water mixture with a Ross Combination pH electrode (Thermo Orion, Beverly, MA). Electrical conductivities were determined by use of a saturated paste extract (USDA, 1954). Total C and N were measured by dry combustion on a LECO CN-2000 Elemental Analyzer (LECO Corporation, St. Joseph, MI). Samples were pretreated with HCl to remove carbonates before dry combustion analysis. Phosphorus was determined in the compost by using a salicylic-sulfuric acid digestion (Bremner and Mulvaney, 1982). Inorganic N (NH_4^+ and NO_3^-) was extracted by shaking with 1 M KCl solution (1:10) and inorganic P was determined by Mehlich-3 (Mehlich, 1984) then samples were then analyzed colorimetrically. Nitric acid digestable metal concentrations were determined using 2 g of material ($\leq$ 2-mm) with 20 mL of trace metal grade 4 M HNO_3 at 80 to 85°C for 4 h (Sposito et al., 1982). Filtered digests were then analyzed for Cd, Pb, and Zn by inductively coupled plasma optical emission spectroscopy (ICP-OES).

To measure weak electrolyte extractable metals, 2 g of dry material was combined with 40 mL of 0.5 M $Ca(NO_3)_2$ and mixed on a rotary shaker for 4 h at 25°C (Basta and Gradwohl, 2000). Samples were filtered and immediately analyzed for Cd, Pb, and Zn using ICP-OES. Diffusive gradients in Thin Films (DGT) were also used to estimate bioavailability of Cd, Pb, and Zn in this mine waste material. The DGT device (DGT Research, Lancaster, UK) consists of a plastic assembly containing a layer of resin embedded in gel, overlain by a layer of diffusive gel, and a protective filter through which ions can freely diffuse. Details on the preparation of the diffusive and resin gels have been given previously (Zhang and Davison, 1995). The DGT devices were deployed after each sample collection time. Soils were maintained at 100% water holding capacity for 24 hours before the devices were installed. The mass of accumulated metals in the resin layer was measured by eluting the resin with 1 M HNO_3 solution for a minimum of

24 hours. The solution was then analyzed for Cd, Pb, and Zn using ICP-OES. Cation exchange capacity (CEC) was determined using a modified method of Jaynes and Bigham (1986).

Estimated Available Water. Available water capacity was estimated by using water retention curve measurements in the laboratory as described by Cassell and Nielson (1986). We used -1.5 MPa to estimate the permanent wilting point and -10 kPa to estimate field capacity. Water retention measurements were made in pressure-plate extractors (Soilmoisture Equipment Corp., Santa Barbara, Calif.) using a 100 kPA ceramic plate for the -10 kPa estimate (-10 kPA; estimate of field capacity) and a 1.5 MPa ceramic plate (1.5 MPa; estimate of permanent wilting point). Retaining rings (5-cm in diameter and 1-cm tall) were used to contain the material on the plates. Samples from five of the treatments (CO, LC, HC, LCLB, and HCLB) were collected, air-dried, and sieved (2-mm). A select set of samples was used due to availability of the equipment. Subsamples from each of the treatments were placed inside of the rings so that the material was about level with the top of the ring. Two reps for each treatment were measured and soil bulk density was not controlled.

Saturation of the plates and samples was achieved by submerging in 5 mM $CaSO_4$ solution for 24 hours prior to pressurization. Applied pressure was monitored with a calibrated SEC pressure gauge.   Equilibration times for -10 kPa and -1.5 MPa were 3 and 7 days, respectively. Immediately after removal from the pressure apparatus, the samples were weighed, dried for 24 h at 105 ^{o}C, and re-weighed to determine gravimetric water content. To calculate available water capacity for corresponding treatments, the gravimetric water content of the -1.5 MPa samples was subtracted from the gravimetric water content of the -10 kPa samples after equilibration.

Microbial Biomass. Soil microbial biomass was determined using the chloroform fumigation-

incubation method (Horwath and Paul, 1994). Samples of moist soil (20g) were incubated and a gas chromatograph (GC) with a thermal conductivity detector (Shimadzu Gas Chromatograph GC-84, Shimadzu Corp., Japan) was used to measure the amount of CO_2 that evolved over the incubation period. Microbial biomass N was measured by determining the concentration of NH_4^+ and NO_3^- before and after the fumigation/incubation period for each sample. Both fumigated and control samples were prepared, but in plots with high compost additions, the control produced more CO_2 and N than the fumigated samples. Therefore, microbial biomass C and N were calculated without using a control (Franzluebbers et al., 1999). The K_c and K_n values used to calculate microbial biomass C and N are 0.41 and 0.54, respectively (Horwath and Paul, 1994). These values are literature values that estimate the proportion of C and N mineralized during a 10 d incubation in soil.

Nitrification. Nitrification was determined for each sample using the aerobic incubation method (Hart et al., 1994). Two 10 g samples of moist soil for each plot were placed in plastic specimen cups. One sample from each plot was extracted immediately with 100 mL of 2 M KCl. Extracts were filtered using a Whatman No. 2 filter and collected for analysis. The other sample was covered with a lid that had a small hole in it to minimize gas loss, but yet maintain gas exchange. Containers and soil were weighed weekly to monitor water loss. If water was lost, deionized water was added to return the soil to its previous water content. After 28 days, the samples were extracted as described for the initial samples. Nitrate was measured colorimetrically. Net mineralization was then calculated as the change in NO_3^- pool size over the incubation period.

Microbial Enzyme Assays. Soil enzyme activities were assayed within 2 weeks after sampling. During this time, samples were stored at 4 ^{o}C. Activities of β-glucosidase (pH 6, 37 ^{o}C); acid phosphatase (pH 6.5, 37 ^{o}C); alkaline phosphatase (pH 11, 37 ^{o}C); and arylsulfatase (pH 5.8, 37

^{o}C) were assayed as described by Tabatabai (1994). The amount of p-nitrophenol released was determined colorimetrically. Deaminase activity (arginine deamination; 35 ^{o}C) was measured by the amount of ammonia produced and determined colorimetrically (Alef and Kleiner, 1986). All enzyme activities, MBC, MBN, and nitrification were determined on field-moist samples and are reported on a dry-weight basis; moisture content was determined from loss in weight after drying at 105°C for 48 h. Additionally, duplicates were run for every fifth sample.

Soil Microbial Community Analysis. Changes to soil microbial community were assessed at 711 d by measuring the soil phosphlipid fatty acid (PLFA) content. The PLFA are indicators of viable microbial biomass (Kennedy and Gewin, 1997). Immediately after sampling/sieving, approximately 20 g of moist material was frozen at -20 ^{o}C and lyophilized. The total lipids were extracted from the lyophilized material following the methods of White and Ringelberg (1998). The total lipid extract was then separated into PLFA and waste lipids using silicic acid chromatography; the fatty acids were then cleaved from the glycerol backbone of the phospholipids by KOH saponification (0.2 M KOH in methanol); and the harvested fatty acids were then methylated to form fatty acid methyl esters (FAME's) (Allison and Miller, 2005). The resulting FAME's derived from PLFA were analyzed with an Agilent 6890 gas chromatograph (GC) with a DB5-MS column (30 m x 250 μm ID x 0.25 μm film thickness-Agilent #122-5532) and flame ionization detector (FID). Helium was the carrier gas (1.0 ml min^{-1} constant flow) and the temperature program was as follows: 50°-170°C at 20°C min^{-1}; 170°-270°C at 5°C min^{-1}. The injector and detector temperatures were 220 and 300°C, respectively. Bacterial acid methyl esters mix (BAME - Matreya #1114) along with individual FAME standards were used to ID peaks and the internal standard (methyl-nonadecanoate) was used to quantify data. A Thermo Scientific Trace GC – DSQ II mass spectrometer (San Jose, CA) was used to confirm peak

assignments. Parameters for the mass spectrometer were identical to chromatographic parameters in the GC-FID analysis. Analysis was conducted in the electron impact mode. Assignments of FAME peaks not present in the BAME mix were made by mass spectral interpretation and comparison to the NIST Mass Spectral Database version 2.0 (NIST, Gaithersburg, MD). Identified fatty acids were named according to the nomenclature reported by Bossio and Shaw (1998) and assigned to certain microbial markers (Table 3-2)

Data Analyses. The experimental design was a randomized complete block design with treatment as the main factor at each site. Sampling time was the strip plot factor, so the analyses were handled as a strip plot design using PROC MIXED. Sites were separated due to a significant site by treatment interaction ($P \leq 0.05$) for all measurements. The Scheffe method was used to adjust the *P*-values and means were separated at the 0.05 level of significance. Multiple linear regression analyses with backward selection was used on all microbial measurements to determine the variables that have the most influence on microbial communities. Principle components analysis (PCA) was used to analyze PFLA profiles and treatments were compared at the 711 d sampling. All statistical analyses were performed using SAS for Windows version 8.2 (SAS Institute, 2001).

3.4 Results and Discussion

Soil Characterization. Basic chemical properties of the compost are given in Table 3-3. Total C, N, and P of the compost was 126, 13.5, and 7.5 g kg^{-1}. The compost contained low levels of Cd and Pb, but did contain measurable levels of Zn and had a high salt content reflecting the addition of salts and Zn to cattle rations.

As expected, the addition of composted beef manure and lime significantly altered a number of chemical properties of the contaminated mine waste materials (Table 3-4). However,

this increase was usually only significant for the high compost treatments (269 Mg ha^{-1}) as compared to the control or the low compost additions. The addition of lime with compost significantly increased pH over the control. The compost itself increased pH because beef cattle diets include substantial quantities of calcium carbonate, a portion of which gets excreted from the animal (Eghball, 1999), but this increase was not significantly different than the control at time 0. However, at 711 d, the HC treatments do had a significantly higher pH than the control at site B (data not shown). High compost treatments significantly increased NO_3^--N, extractable P and K, and total N at both study sites. Total C was significantly increased by the HC treatment at site A and by all high compost additions at site B.

Microbial Biomass and Nitrification. The addition of composted beef manure led to a significant increase in microbial biomass C (Table 3-5), which was expected since total C was increased by compost amendments. Microbial biomass C was initially higher for all treatments, including the control, at time 0, which was likely due to the disturbance of the study area. At site A, the treatments followed the order of HC > HCL > LC >LCL > CO, but only the HC treatment was significantly higher than the control (Table 3-5). At site B, the order was HC > HCL > LCL > CO > LC. Both the HC and HCL treatments were significantly higher than the LCL, LC, and C treatments. At the 711 d sampling at site A, the HC and HCL treatments had significantly higher microbial biomass C, while at site B the HC treatment had significantly higher microbial biomass C than the control. Microbial biomass N was also significantly increased by compost additions and again treatments were significantly changing with time. Initially microbial biomass N was stimulated by compost additions, gradually decreased with time, and then increased again at 535 and 711 d. At 711 d, the HC treatment at site A and the HC and HCL treatments at site B were the only treatments to have significantly higher microbial biomass N

109

over the control.

The nitrification potential was unaffected by compost amendments until the 353 d at both study sites. At site A, the HC treatment became significantly higher than the control at 353 d and was significantly higher through the last measurement at 711 d. At site B, both the HC and HCL treatments were significantly higher than the control, but at 711 d only the HC treatment remained significantly increased. Measurement of nitrification potential showed high variability throughout the study, which is likely why significant treatment differences were unable to be detected until later in the study.

Multiple linear regression analyses were performed to determine the variables that influence microbial biomass C, biomass N, and nitrification. The model for microbial biomass C (r^2 = 0.50, P < 0.0001) was dependent on total C (slope = 8.01, P < 0.0001), extractable P (slope = 0.10, P = 0.0005), and C to N ratio (slope = -4.17, P = 0.0207). The relationship of total C with microbial biomass C was expected and was similar to the results of Clemente et al. (2007). Interestingly, changes in microbial biomass C were not related to reductions in metal bioavailability upon amendment additions. Clemente et al. (2007) reported no relationship between DTPA extractable metals and microbial biomass. However, studies have shown that microbial biomass sharply decreases as concentrations of Cd and Zn increase, but these investigations were performed on soils and not mine wastes (Kandeler et al., 1996; Leita et al., 1995; Pérez de Mora et al., 2005).

Multiple linear regression analysis for microbial biomass N (r^2 = 0.59, P < 0.0001) was highly dependent on total C (slope = 3.96, P < 0.0001). Again, there was no relationship to the reduction in bioavailable metals upon additions of compost. However, since no relationship was found with bioavailable metals and microbial biomass C, there was no reason to believe that

there would be a relationship to microbial biomass N. Multiple regression for nitrification (r^2 = 0.50, P < 0.0001) found significant relationships with DGT Zn (slope = -0.03, P = 0.0105), electrical conductivity (slope = -0.02, P = 0.0095), and NH_4^+ (slope = 0.02, P = 0.0007). A significant positive relationship with NH_4^+ was expected because nitrification converts NH_4^+ to NO_3^- and therefore, is dependent on the presence of substrate. While the addition of compost supplied the substrate for nitrification, it also increased the electrical conductivity. The negative relationship between electrical conductivity and nitrification was likely due to the harmful osmotic effects that salt content can have on cell membranes. As a result, compost additions would possibly inhibit nitrification until salts were leached from the material. The inhibition of nitrification by Zn has been documented (Kandeler et al., 1996; Stuczynski et al., 2003) and is supported by the negative relationship with DGT Zn. With time nitrification potential increased significantly in the HC treatment as compared to the control, which was likely related to the reduction in Zn bioavailability, a degrease in salts through leaching, and increases in substrate.

Microbial Enzyme Activities. Acid and alkaline phosphatases are extracellular enzymes that catalyze the hydrolysis of organic phosphates, releasing plant and microbial available phosphate. Acid phosphatases are produced by plants and microbes, but alkaline phosphatases are produced primarily by microbes (Tabatabai, 1994). Alkaline phosphatase activity was significantly increased at time 0 for sites A and B by the HC and HCL treatments (Table 3-6). This trend generally remained constant with time. Multiple regression analysis of alkaline phosphatase (r^2 = 0.62, P < 0.0001) showed significant relationships with total C (slope = 50.5, P < 0.0001) and estimated available water (slope = 455.3, P = 0.0058). Inhibition of alkaline phosphatase activity by Cd and Zn has been demonstrated by Kandeler et al. (1996), while Marzadori et al. (1996) concluded that Pb significantly decreased phosphatase activity, but this study does not

support these findings. Increases in phosphatase activity were most related to total C and estimated available water, which were increased upon compost addition and are important in ecosystem function.

Amendment additions did not cause a significant increase in acid phosphatase activity at the first sampling for site A, but by the 353 d sampling the HC treatment had significantly higher activity than the control (Table 3-6). This continued through the last measurement at 711 d. At site B, both the HC and HCL treatments had significantly higher acid phosphatase activity at time 0, but at 711 d there were no significant differences between treatments. Multiple linear regression analysis of acid phosphatase ($r^2 = 0.65$, $P < 0.0001$) showed relationships with total C (slope = 24.6, $P < 0.0001$) and electrical conductivity (slope = -98.1, $P = 0.0056$). The relationship of total C and acid phosphatase was demonstrated in previous research (Claassens et al., 2005). Again, the increased electrical conductivity, which was caused by high salt content of the compost, significantly reduced phosphatase activity. However, with time the salts were leached from the system; therefore, they had less effect on microbial populations.

Arylsulfatase is an extracellular enzyme that catalyzes the hydrolysis of organic sulphate esters, thus releasing available sulfate. Arylsulfatase activities at site A were significantly higher for the HC and HCL treatments compared to the control at time 0 (Table 3-6). However, at 711 d, only the HC treatment was significantly higher than the control. At site B, only the HC treatment had significantly higher activities at time 0, but by 711 d, both HC and HCL were significantly higher than the control. Multiple regression analysis of arylsulfatase activity ($r^2 = 0.69$, $P < 0.0001$) indicated a significant negative relationship with electrical conductivity (slope = -11.4, $P = 0.0006$) and a positive relationship with total C (estimate 12.4, $P < 0.0001$). With time, the influence of salts decreased because they were readily leached from the system

(Chapter 4). Multiple regression analysis did not indicate a relationship with the reduction in bioavailble Cd, Pb, and Zn, which agrees with the results of Stuczynski et al. (2003). However, Pèrez de Mora et al. (2005) showed that arylsulfatase was negatively related to Cd and Zn in an *in situ* remediation study and similar results were obtained by Kandeler et al. (1996), when they found arylsulfatase activity was inhibited by these same elements. In mine wastes, the lack of C, available water, and nutrients significantly reduced microbial activity, while bioavailable metals had much less of an impact.

β-glucosidase activity is the rate-limiting enzyme in the microbial degradation of cellulose to glucose and plays a critical role in C cycling. Mean β-glucosidase values are given in Table 3-5 for each sample time. For both sites at all sample times, only the HC treatment produced a significantly higher β-glucosidase activity than the control. Multiple regression analysis of β-glucosidase activity ($r^2 = 0.77$, $P < 0.0001$) revealed negative relationships with $Ca(NO_3)_2$ extractable Zn (slope = -0.43, $P < 0.0001$) and electrical conductivity (slope = -29.2, $P = 0.0008$) and a positive relationship with total C (slope 15.8, $P = 0.0002$). Claassens et al. (2005) and Eivazi and Tabatabai (1990) reported a significant positive relationship with total C and β-glucosidase activity, which is related to the increase in organic residues (García-Gil et al., 2000). Glucosidase activity was inhibited by Zn as evidenced by the negative relationship with $Ca(NO_3)_2$ extractable Zn. Similarly, Kandeler et al. (1996) found that β-glucosidase activity was reduced by Zn, but only at the highest Zn loadings. In contrast, Pérez de Mora et al. (2005) concluded that high Zn concentrations have very little effect on β-glucosidasebecause microbes require more C for maintenance when stressed; therefore, they produce more β-glucosidase enzyme in heavy metal contaminated soils. We observed an increase in glucosidase activity when compost was applied to contaminated heavy metal mine wastes, which is likely related to

the increase in microbial biomass.

Treatments at site A did not have an effect on deaminase activity, which is a measure of the potential arginine ammonification rate, at the first sample time (Table 3-6). At the 353 d sampling, the HC treatment was significantly higher than the control, but by 711 d there were no treatment differences. At site B, the HC treatment was significantly higher than the control at all sampling times . Multiple regression analysis of deaminase activity did not indicate anysignificant relationships to chemical properties, which is likely due to the high variability of this measurement throughout the study.

To summarize, additions of 269 Mg ha^{-1} composted beef manure increased enzyme activities in heavy metal contaminated mine wastes. This increase in enzyme activity was primarily due to the increases in total C and estimated available water, which is directly related to the organic amendment addition. Claassens et al. (2005) observed that organic C content had significant relationships to several microbial measurements, which emphasizes the importance of organic matter as a soil amendment during rehabilitation. Regression analyses indicated that most enzymes were negatively related to electrical conductivity, thus illustrating the initial negative effects that large additions of animal-based compost had on microbial communities. Nitrification potential and β-glucosidate activity had negative relationships with DGT Zn and Ca(NO$_3$)$_2$ extractable Zn, respectively. This agrees with other studies conducted on enzymes and heavy metals (Kandeler et al., 1996; Leita et al., 1995; Pèrez de Mora et al., 2005; Stuczynski et al., 2003). The additions of C and nutrients to mine wastes appeared to be most important at increasing microbial biomass and stimulating microbial activity. However, the reduction in heavy metal bioavailability caused by compost additions likely contributed to increased activities.

Phospholipid Fatty Acids. At site A, there was a microbial community shift towards Gm^+ bacteria PLFA with increasing amounts of compost (Figure 3-1A). At site B, there was no shift to Gm^+ bacteria PLFA (Figure 3-1B). In fact, there were very few changes in PLFA's upon amendment addition at site B. However, the addition of lime at both study sites (Figures 3-2A and B) slightly shifted microbial communities in favor of Gm^- bacteria PLFA. This agrees with Frostegård et al. (1993a) and Bååth et al. (1995) who discovered increases in Gm^- bacteria PLFA upon liming a forest soil and ash application, respectively. Surprisingly, there were very few changes in the fungal derived PLFA's after amendment addition. This lack of change in fungal PLFA's could be attributed to the increase of P upon compost treatment. Phosphorus has been shown to increase the abundance of bacteria relative to fungal PLFA's (Grayston et al., 2004); therefore, it is plausible that high concentrations of P could impede a microbial community shift to fungi, but disturbance can also negatively impact fungal communities. Kelly et al. (2003) have suggested that successful remediation increases in the mole percents of indicator fatty acids for Gm^+ bacteria, actinomycetes, and fungal derived PLFA's when they compared heavy metal contaminated soils to remediated soils. However, they were dealing with soils and not mine wastes. In this study, only site A had an increase in Gm^+ bacteria PLFA's, which may be an indication that the reclamation/stabilization program was unsuccussful. On the other hand, information is limited on PLFA profiles for remediated mine wastes. In fact, research is still being conducted on how to successfully revegetate and create a self-sustainable system in heavy metal contaminated mine wastes, including this study. A comparison of PLFA profiles to uncontaminated sites was not performed at this time and may not be suitable because mine wastes materials are likely never to behave like undisturbed environments. However, if remediation were to be successful, microbial communities should begin to resemble non-

contaminated areas with time, but currently the succession is still in flux due to large additions of C. As a result, it is currently inappropriate to compare undisturbed environments to the remediated areas.

The PLFA procedure can also provide an estimate of microbial biomass. Results from PLFA analysis for the 711 d sample period indicated that high rates of compost significantly increased total microbial biomass in the contaminated mine waste materials (Table 3-7). At site A, the HC treatment had significantly higher biomass than all other treatments, while at site B the HC treatment had significantly higher biomass than all treatments except for HCLB. At both sites, the HC treatment increased the biomass of Gm^+ bacteria, Gm^- bacteria, and fungal derived PLFA's as compared to the control and low compost additions. High compost treatments did not result in a significant increase in the biomass of actinomycetes over the control, which was unexpected. This could be due to severe metal contamination or improper substrate to support the growth and function of actinomycetes. Actinomycetes are thought to have the lowest degree of tolerance to heavy metals (Hiroki, 1992); therefore, it is possible that amendments did not reduce metal availability sufficiently to support significantly increase the population of this group. In addition, Drenovsky et al. (2004) and Peacock et al. (2001) have reported that additions of C (composted poultry manure/straw/vetch combination or dairy manure) actually decreased the amount of actinomycete biomarkers present in uncontaminated soils, which was likely related to the quality of substrate or how well actinomycetes can or cannot compete with other microbial groups for resources. Feng et al. (2003) suggested that high relative abundances of actinomycetes may reflect a higher proportion of C in recalcitrant forms. As a result, increases in actinomycetes or fungi may not occur, if at all, until later in this study after the more readily available C has been utilized.

The principal component analysis (PCA) of the PLFA profiles indicated that there were differences in the PLFA profiles among the samples and that the samples grouped based on treatment (Figure 3-2). The two extracted components were able to explain 53% of the total variation in the data. There was a significant site interaction ($P < 0.05$), which can be observed below (Figure 3-2), but there was no significant site by treatment interaction. This indicates that sites behaved differently, but PLFA profiles behaved similarly for a given treatment at both sites. For site A, the unamended control and low compost treatments grouped on the left, while the high compost treatments grouped toward the bottom of the plot (Figure 3-2). For site B, the unamended control and low compost treatments grouped in the top right and bottom left quadrants, while the high compost treatments grouped in the bottom right corner (Figure 3-2). The differences in sites could be related to pH (Table 3-1), where pH differs considerably. As a result, high amendment additions at site B caused a greater positive shift in the microbial community. The two highest positive eigenvector values for PC1 are cy17:0 and cy19:0, which are Gm⁻ bacteria PLFA's. This suggests that site B does in fact have a greater shift toward Gm⁻ bacteria.

For PC1, high compost treatments (HC, HCL, and HCLB) had significantly different PLFA profiles ($P < 0.05$) than all other treatments. Multiple regression analysis of PC1 ($r^2 = 0.96$, $P < 0.0001$) was used to help explain differences among treatments. Results indicated negative relationships with $Ca(NO_3)_2$ extractable Cd (slope = -1.27, $P < 0.0001$) and DGT Zn (slope = -0.22, $P = 0.0014$) and positive relationships with total C (slope = 4.45, $P = 0.0054$), extractable NH_4^+ (slope = 0.51, $P = 0.0007$), and estimated available water (slope = 20.6, $P = 0.0012$). Thus as compost additions increased, the PLFA profiles were significantly changed. Regression analyses also indicate that a part of this change were associated with a reduction in

the bioavailability of Zn. Kelly et al. (2003) demonstrated that a mixture of municipal sewage sludge and fly ash (73.5 Mg ha^{-1}) applied to a Zn contaminated soil changed the structure of the soil microbial communities as determined by PFLA profiles, which they attributed to a reduction in heavy metal bioavailability. They found that PLFA profiles of remediated sites had increased Gm$^+$ bacteria, actinomycetes, and fungal derived PLFA's when compared to unremediated sites. They suggested that this was an indication of microbial community recovery. Kiikkilä et al. (2001) did not find a significant change in PLFA profiles when they applied mulch to a Cu/Ni contaminated soil. However, they did report an increase in bacterial growth, which was thought to be related to the reduction in metal availability.

Changes in PLFA profiles upon addition of 269 Mg ha^{-1} of compost were positively affected by total C, extractable NH$_4^+$, and an increase in estimated available water. Drenovsky et al. (2004) concluded that both soil water content and soil C availability were highly correlated with observed differences in microbial community composition. However, Allison et al. (2007) proposed that the effects of C on microbial shifts are likely to be more indirect. Conversely, White and Rice (2009) illustrated that in-field decomposition of grain sorghum residue was observable as a pulse in total, fungal, and Gm$^+$ bacterial PLFA's, suggesting that C was a direct affect. In this study, compost does not appear to dramatically shift the microbial population, but it certainly increased its size. Therefore, in terms of increasing microbial activity to enhance SOM cycling to support plant growth, compost additions to mine waste materials were successful.

Allison et al. (2007) discussed the important direct impact that root biomass had on PLFA's. This suggests that there is a substantial rhizosphere effect. In plots that received the high compost treatments (HC, HCL, and HCLB), plant biomass was significantly greater than

the control and low compost treatments (Chapter 4). Therefore, there will be more root biomass and root exudates to potentially support and perhaps diversify the microbial community. Other research in disturbed environments has suggested that the recovery of microbial communities was closely related to the presence of vegetation (Allen et al., 1999). As a result, vegetation recovery is an important aspect of successful microbial community recovery.

Conclusions. Application of composted beef manure to heavy metal contaminated mine wastes increased microbial activity compared to the contaminated control, which agreed with our hypothesis. However, the HC treatments was needed to produce microbial biomass measurements, enzyme activities, and potential nitrification values that were significantly increased over the control and that lasted for the duration of the study (711 d). These measurements had significant positive relationships with total C and estimated available water, while significant negative relationships existed with electrical conductivity and on occasion with DGT Zn and $Ca(NO_3)_2$ extractable Zn. This suggests that C may be the ultimate variable in establishing and maintaining a healthy microbial population in metal contaminated mine wastes. With time, the microbial biomass and activity measurements declined, which is an indication that the amendments were losing their effectiveness.

The treatments of lime or lime plus bentonite with compost did not increase microbial activity over the compost amendment alone. In fact, on several occasions the treatment of lime or lime plus bentonite with compost actually decreased microbial activity compared to just compost. Therefore, at this time there does not appear to be any advantage of combining these amendments with compost to remediate metal contaminated mine wastes. However, pH values of the mine wastes were only slightly acidic; therefore, under more acidic conditions a lime application may be needed to enhance microbial function.

119

Principal components analysis of the PLFA profiles indicated that high amounts of compost (HC, HCL, and HCLB) alter microbial community structure, but not dramatically. This change is related to the increases in total C and estimated available water content and decreases in heavy metal bioavailability upon compost addition. Community shifts are likely the result of changes in a select few fatty acid signatures and not the entire population. Only high compost additions at site A had increases in Gm$^+$ bacteria PLFA as compared to the control. This study does not involve soils; therefore, it would be difficult to compare successful reclamation of a contaminated soil to mine wastes. Additionally, PLFA estimated microbial biomass for Gm$^+$ bacteria, Gm$^-$ bacteria, and fungi were significantly increased by the HC treatment at 711 d compared to the control. On most occasions, low compost amendments did not significantly increase biomass compared to the control, which supports the hypothesis that large compost additions are needed to significantly increase microbial biomass and activity in mine wastes.

This study provides important information on how soil amendment additions affect microbial communities in severely disturbed systems. After 711 d, a 269 Mg ha^{-1} addition of compost increased microbial activity and slightly shifted the structure of microbial communities. Results suggest that an application of compost between 45 and 269 Mg ha^{-1} is needed to significantly increase microbial activity and biomass compared to an unamended control. Further monitoring of these sites is needed to determine if amendment additions can maintain microbial communities, biomass, and activities, which are key in nutrient cycling processes that support ecosystem function.

3.5 References

Alef, K., and D. Kleiner. 1986. Arginine ammonification, a simple method to estimate microbial activity potential in soils. Soil Biol. Biochem. 18:233-235.

Allen, M.F., E.B. Allen, T.A. Zink, S. Harney, L.C. Yoshida, C. Sigüenza, F. Edwards, C. Hinkson, M. Rillig, D. Bainbridge, C. Doljanin, and R. MacAller. 1999. Soil microorganisms. p. 521-544. *In* L.R. Walker (ed.) Ecosystems of disturbed grounds. Elsevier Science, Amsterdam.

Allison, V.J., and R.M. Miller. 2005. Soil grinding increases the relative abundance of eukaryotic phospholipid fatty acids. Soil Sci. Soc. Am. J. 69:423-426.

Allison, V.J., Z. Yermakov, R.M. Miller, J.D. Jastrow, and R. Matamala. 2007. Using landscape and depth gradients to decouple the impact of correlated environmental variables on soil microbial community composition. Soil Biol. Biochem. 39:505-516.

Bååth, E., Å. Díaz-Raviňa, Å. Frostegård, and C.D. Cambell. 1998. Effect of metal-rich sludge amendments on the soil microbial community. Appl. Environ. Microbiol. 64:238-245.

Bååth, E., Å. Frostegård, T. Pennanen, and J. Fritze. 1995. Microbial community structure and pH response in relation to soil organic matter quality in wood-ash fertilized, clear-cut or burned in conifersous forest soils. Soil Biol. Biochem. 27:229-240.

Bardgett, R.D., and E. McAlister. 1999. The measurement of soil fungal: bacterial-biomass ratios as an indicator of ecosystem self-regulation in temperate meadow grasslands. Biol. Fertil. Soils 29:282-290.

Basta, N.T., and R. Gradwohl. 2000. Remediation of heavy metal-contaminated soil using rock phosphate. Better Crops Plant Food 82:29-31.

Bossio, D.A., and K.M. Scow. 1998. Impacts of carbon and flooding on soil microbial communities: phospholipd fatty acid profiles and substrate untilization patterns. Microbiol. Ecol. 35:265-278.

Bremner, J.M., and C.S. Mulvaney. 1982. Salicylic acid thiosulfate modification of the Kjeldhal method to include nitrate and nitrite. p. 621. *In* R.H. Miller and D.R. Keeney (ed.) Methods of soil analysis. Part 2. Am. Soc. Agron., Madison, WI.

Brookes, P.C. 1995. The use of microbial parameters in monitoring soil pollution by heavy metals. Biol. Fertil. Soils 19:269-279.

Brookes, P.C., and S.P. McGrath. 1994. Effect of metal toxicity on the size of the soil

microbial biomass. J. Soil Sci. 35:341-346.

Brown, S.L., C.L. Henry, R.L. Chaney, H. Compton, and P. DeVolder. 2003. Using municipal biosolids in combination with other residuals to restore metal-contaminated mining areas. Plant Soil 249:203-215.

Cassell, D.K., and D.R. Nielson. 1986. Field capacity and available water capacity. p. 901-926. *In* A. Klute (ed.) Method of soil analysis. Part 1. 2nd ed. Agronomy Monograph 9. ASA and SSSA, Madison, WI.

Chander, K., P.C. Brookes, and S.A. Harding. 1995. Microbial biomass dynamics following addition of metal-enriched sewage sludges to a sandy loam. Soil Biol. Biochem. 27:1409-1421.

Claassens, S., K.J. Riedel, L. Van Rensburg, T.L. Morgenthal, and P.J. Jansen Van Rensburg. 2005. Soil microbial properties in coal mine tailings under rehabilitation. Appl. Ecology Environ. Res. 4:75-83.

Clemente, R., C. Almela, and M.P. Bernal. 2006. A remediation strategy based on active phytoremediation followed by natural attenuation in a soil contaminated by pyrite waste. Environ. Pollut. 143:397-406.

Clemente, R., C. de la Fuente, R. Moral, and M.P. Bernal. 2007. Changes in microbial biomass parameters of a heavy metal-contaminated calcareous soil during a field remediation experiment. J. Environ. Qual. 36:1137-1144.

Drenovsky, R.E., D. Vo, K.J. Graham, and K.M. Scow. 2004. Soil water content and organic carbon availability are major determinants of soil microbial community composition. Microbiol. Ecol. 48:424-430.

Eghball, B. 1999. Liming effects of beef cattle feedlot manure or compost. Commun. Soil Sci. Plant Anal. 30:2563-2570.

Eivazi, F., and M.A. Tabatabai. 1990. Factors affecting glucosidase and galactosidase activities in soils. Soil Biol. Biochem. 22:891-897.

Feng, Y., A.C. Motta, D.W. Reeves, C.H. Burmester, E. van Santen, and J.A. Osborn. 2003. Soil microbial communities under conventional-till and no-till continous cotton systems. Soil Biol. Biochem. 33:1693-1703.

Franzluebbers, A.J., R.L. Haney, F.M. Hons, and D.A. Zuberer. 1999. Assessing biological soil quality with chloroform fumigation-incubation: Why subtract a control? Can. J.

Soil Sci. 79:521-528.

Frostegård, Å., E. Bååth, and A. Tunlid. 1993a. Shifts in structure of soil microbial communities in limed forests as revealed by phospholipid fatty acid analysis. Soil Biol. Biochem. 25:723-730.

Frostegård, Å., A. Tunlid, and E. Bååth. 1993b. Phospholipid fatty acid compostion, biomass, and activity of microbial communities from two soil types experimentally exposed to different heavy metals. Applied and Environ. Microbiol. 59:3605-3617.

García-Gil, J.C., C. Plaza, P. Soler-Rovira, and A. Polo. 2000. Long-term effects of municipal solid waste compost application on soil enzyme activities and microbial biomass. Soil Biol. Biochem. 32:1907-1913.

Gee, G.W., and J.W. Bauder. 1986. Particle size analysis. p. 399-404. *In* A. Klute (ed.) Methods of soil analysis. Part 1. 2nd ed. Agron. Monogr. 9. ASA and SSSA, Madison, WI.

Grayston, S.J., C.D. Campbell, R.D. Bardgett, J.L. Mawdsley, C.D. Clegg, K. Ritz, B.S. Griffiths, J.S. Rodwell, S.J. Edwards, W.J. Davies, D.J. Elston, and P. Millard. 2004. Assessing shifts in microbial community structure across a range of grasslands of differing management intensity using CLPP, PLFA, and community DNA techniques. Appl. Soil Ecol. 25:63-84.

Harris, J.A. 2003. Measurements of the soil microbial community for estimating the success of restoration. Eur. J. Soil Sci. 54:801-808.

Hart, S.C., J.M. Stark, E.A. Davidson, and M.K. Firestone. 1994. Nitrogen mineralization, immobilization, and nitrification. *In* R.W. Weaver et al. (ed.) Methods of Soil Analysis: Microbial and biochemical properties. Part 2. Soil Sci. Soc. Am. 5:985-1018.

Hinojosa, M.B., J.A. Carreira, R. García-Ruíz, and R.P. Dick. 2005. Microbial response to heavy metal-polluted soils: Community analysis from phospholipid-linked fatty acids and ester-linked fatty acids extracts. J. Environ. Qual. 34:1789-1800.

Hiroki, M. 1992. Effects of heavy metal contamination on soil microbial population. Soil Sci. Plant Nutr. 38:141-147.

Horwath, W.R., and E.A. Paul. 1994. Microbial biomass. *In* R.W. Weaver et al. (ed.) Methods of Soil Analysis: Microbial and biochemical properties. Part 2. Soil Sci. Soc. Am. 5:753-773.

Kandeler, E., C. Kampichler, and O. Horak. 1996. Influence of heavy metals on the functional diversity of soil microbial communities. Biol. Fertil. Soils 23:299-306.

Kelly, J.J., M. Håggblom, and R.L. Tate. 2003. Effects of heavy metal contamination and remediation on soil microbial communities in the vicinity of a zinc smelter as indicated by analysis of microbial community phospholipid fatty acid profiles. Biol. Ferti. Soils 38:65-71.

Kennedy, A.C., and V.L. Gewin. 1997. Soil microbial diversity: present and future considerations. Soil Sci. 162:607-617.

Kiikkilä, O., J. Perkiömäki, M. Barnette, J. Derome, T. Pennanen, E. Tulisalo, and H. Fritze. 2001. In situ bioremediation through mulching of soil polluted by a copper-nickel smelter. J. Environ. Qual. 30:1134-1143.

Konopka, A., T. Zakharova, M. Bischoff, L. Oliver, C. Nakatsu, and R.F. Turco. 1999. Microbial biomass and activity of lead-contaminated soil. App. Environ. Microbiol. 65:2256-2259.

Leita, L., M. De Nobili, G. Muhlbachova, C. Mondini, L. Marchiol, and G. Zerbi. 1995. Bioavailability and effects of heavy metals on soil microbial biomass survival during laboratory incubation. Biol. Fertil. Soils 19:103-108.

Lindsay, W.L. 1979. Chemical equilibria in soils. Wiley, New York, NY.

Marzadori, C., C. Ciavatta, D. Montecchio, C. Gessa. 1996. Effects of lead pollution on different soil enzyme activities. Biol. Fertil. Soils 22:53-58.

McKinely, V.L., A.D. Peacock, and D.C. White. 2005. Microbial communit PLFA and PHB responses to ecosystem restoration in tallgrass prairie soils. Soil Biol. Biochem. 37:1946-1958.

Mehlich, A. 1984. Mehlich 3 soil test extractant: A modification of Mehlich-2 extractant. Commun. Soil Sci. Plant Anal. 15(12): 1409-1416.

Parkin, T.B. 1993. Spatial variability of microbial processes in soil: A Review. J. Environ. Qual. 22:409-417.

Peacock, A.D., M.D. Mullen, D.B. Ringelberg, D.D. Tyler, D.B. Hedrick, P.M. Gale, and D.C. White. 2001. Soil microbial community responses to diary manure or ammonium nitrate applications. Soil Biol. Biochem. 33:1011-1019.

Pennanen, T., Á. Frostegård, H. Fritze, and E. Bååth. 1996. Phospholipid fatty acid composition and heavy metal tolerance of soil microbial communities along two heavy metal-polluted gradients in coniferous forests. Appl. Environ. Microbiol. 62:420-428.

Pérez de Mora, A., J.J. Ortega-Calvo, F. Cabrera, and E. Madejón. 2005. Changes in

enzyme activities and microbial biomass after "in situ" remediation of heavy metal contaminated soil. Appl. Soil Ecol. 125-137.

Ponder, F.P., and M. Tadros. 2002. Phospholipid fatty acids in forest soil four years after organic matter removal and soil compaction. Appl. Soil Ecol. 19:173-182.

Rajapaksha, R.M.C.P., M.A. Tobor-Kaplon, and E. Bååth. 2004. Metal toxicity affects fungal and bacterial activities in soil differently. Appl. Environ. Microbiol. 70:2966-2973.

Shi, W., J. Becker, M. Bischoff, R.F. Turco, and A.E. Konopka. 2002. Association of microbial community composition and activity with lead, chromium, and hydrocarbon contamination. Appl. Environ. Microbiol. 68:3859-3866.

Sposito, G., L.J. Lund, and A.C. Chang. 1982. Trace metal chemistry in arid-zone field soils amended with sewage sludge: I. Fractionation of Ni, Cu, Zn, Cd, and Pb in solid phases. Soil Sci. Soc. Am. J. 46:260-264.

Stuczynski, T.I., G.W. McCarty, and G. Siebielec. 2003, Response of soil microbial activities to cadmium, lead, and zinc. J. Environ. Qual. 32:1346-1355.

Tabatabai, M.A. 1994. Soil enzymes. *In* R.W. Weaver et al. (ed.) Methods   of   Soil Analysis: Microbial and biochemical properties. Part 2. Soil Sci. Soc. Am. 5:775-833.

Turco, R.F., A.C. Kennedy, and M.S. Jawson. 1994. Microbial indicators of soil quality. p. 73-90. *In* Defining soil quality for a sustainable environment. SSSA Spec. Publ. 35. SSSA and ASA, Madison, WI.

White, D.C., and D.B. Ringelberg. 1998. Signature lipid biomarker analysis. p. 255-272. *In* R.S. Burlage, R. Atlas, D. Stahl, G. Geesey, and G. Sayler (ed.) Techniques in Microbial Ecology. Oxford University Press, NY.

White, Jr., P.M., and C.W. Rice. 2009. Tillage effects on microbial and carbon dynamics during plant residue decomposition. Soil Science Society of America Journal. In press.

Zhang, H., and W. Davison. 1995. Performance characteristics of diffusion gradients in thin films for the in situ measurement of trace metals in aqueous solutions. Anal. Chem. 67:3391-3400.
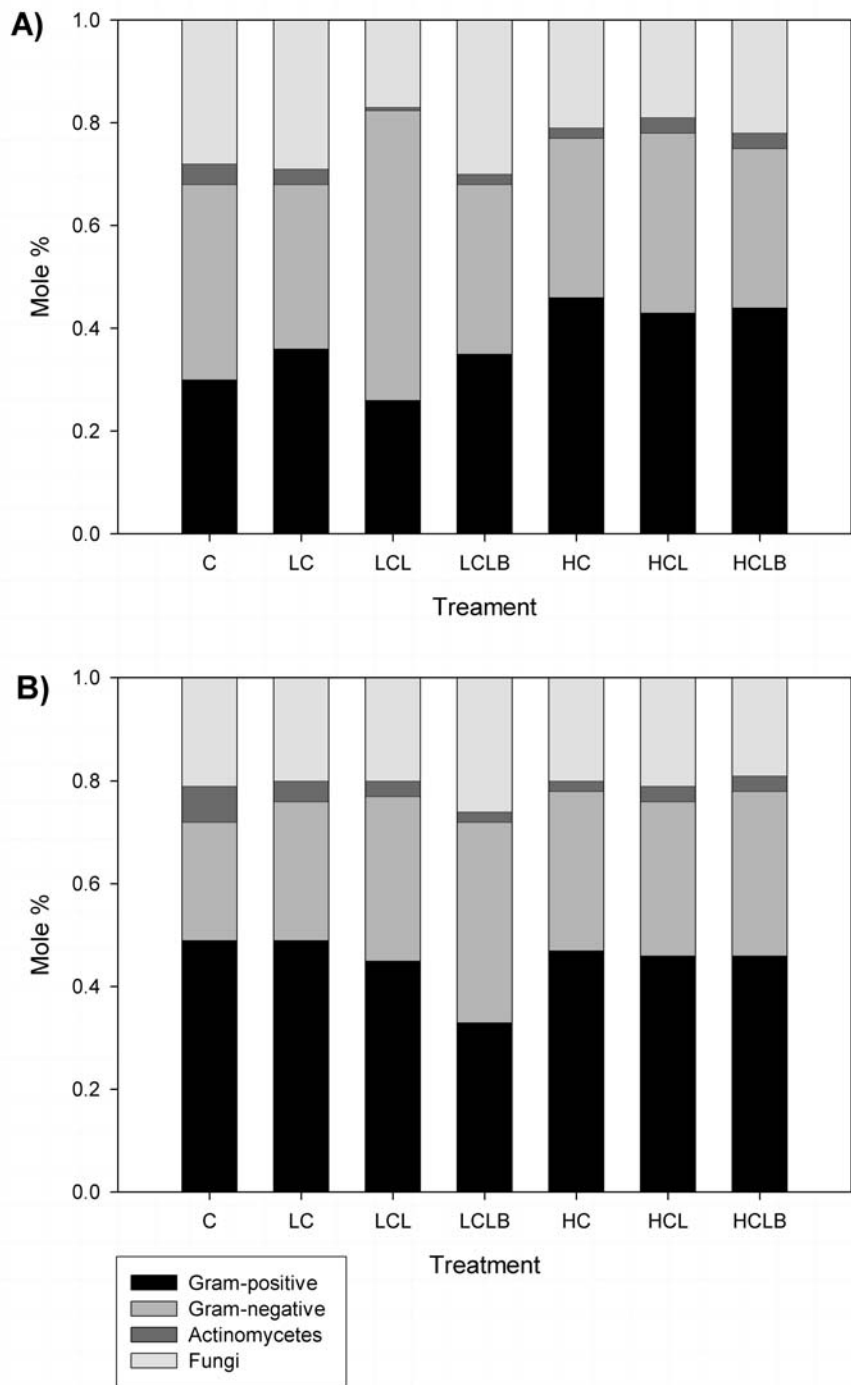
Figure 3-1. Impact of treatments on relative abundance of microbial functional groups at A) site A and B) site B. Gram-positive: Gram-postive bacteria; Gram-negative: Gram-negative bacteria.

126
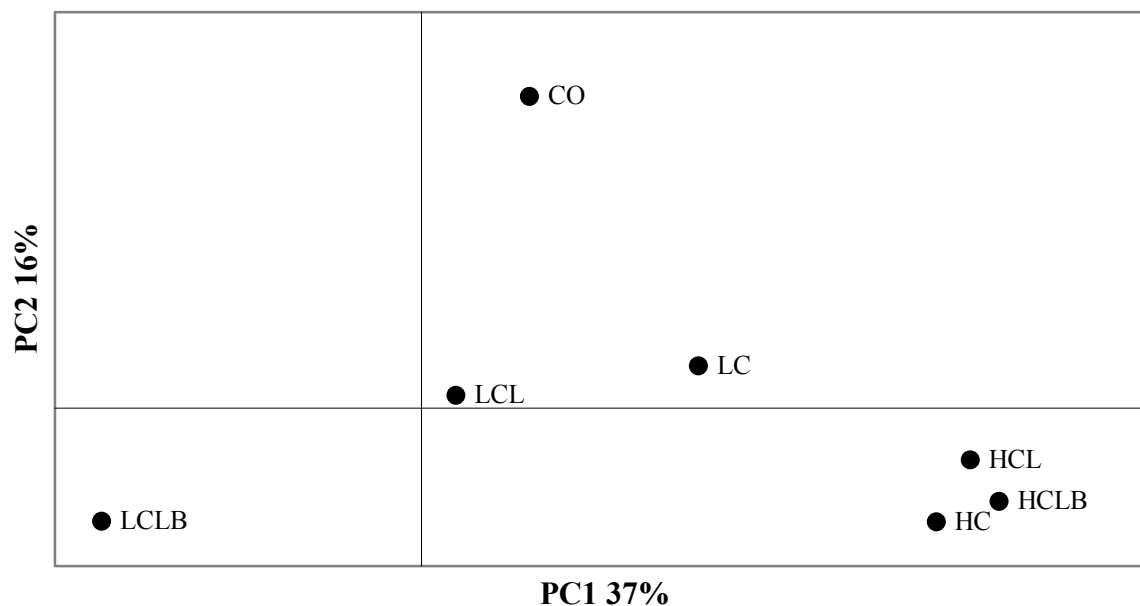
Figure 3-2. Score plot of principal components analysis showing the separation of treatments and sites along the first two principal components (PC1 and PC2) using the PLFA data. Treatments are designated by CO, LC, LCL, LCLB, HC, HCL, and HCLB. The different study sites are indicated as diamonds for site A and circles for site B.

Table 3-1. Basic properties of the contaminated mine waste materials before amendment additions.

Characteristics	Site A	Site B
pH	6.5	4.9
Extractable NH_4^+-N (mg kg^{-1})	2.9	1.7
Extractable NO_3^--N (mg kg^{-1})	5.4	1.5
Extractable P (mg kg^{-1})	55.3	18.9
Extractable K (mg kg^{-1})	80.5	45.4
Total C (g kg^{-1})	3.9	4.2
Total N (g kg^{-1})	0.35	0.33
Total Cd (mg kg^{-1})	30.2	39.8
Total Pb (mg kg^{-1})	3400	2300
Total Zn (mg kg^{-1})	6800	6200
CEC (cmol$_c$ kg^{-1})†	14.7	23.1
Electrical Conductivity (dS m^{-1})	0.08	0.05
Coarse Fragments (g kg^{-1})‡	741	756
Sand (g kg^{-1})	207	204
Silt (g kg^{-1})	44	28
Clay (g kg^{-1})	8	12

† CEC: Cation Exchange Capacity
‡Coarse fragments are considered particles > 2 mm in size

Table 3-2. Phospholipid fatty acid (PLFA) groups used to assign microbial markers. Table adopted from McKinley et al., 2005.

Fatty Acid	Marker
10Me18:0	Actinomycetes
10Me16:0	Actinomycetes, Gram (+)
i14:0	Gram (+)
i15:0	Gram (+)
a15:0	Gram (+)
i16:0	Gram (+)
i17:0	Gram (+)
a17:0	Gram (+)
16:1w9c	Gram (-)
16:1w7c	Gram (-)
16:1w7t	Gram (-)
16:1w5c	Gram (-), Fungi
cy17:0	Gram (-)
18:1w7c	Gram (-)
18:1w7t	Gram (-)
18:1w5c	Gram (-)
cy19:0	Gram (-)
18:1w9c	Fungi, Plants
20:1w9c	Fungi
18:2w6	Fungi, Plants
18:3w3	Fungi, Plants
20:5w3	Fungi, Plants

Table 3-3. Basic chemical properties of the beef manure compost.

Characteristics	Compost
Electrical Conductivity (dS m^{-1})	36.0
pH	8.1
Total C (g kg^{-1})	126
Total N (g kg^{-1})	13.5
Total P (g kg^{-1})	7.5
C:N	9.4
K (g kg^{-1})	21.5
Ca (g kg^{-1})	2.7
Na (g kg^{-1})	5.3
Cd (mg kg^{-1})	1.3
Pb (mg kg^{-1})	nd†
Zn (mg kg^{-1})	496

† not detectable; detection limit for Pb is 8.0 µg kg^{-1}

Table 3-4. Basic chemical properties after amendment addition to contaminated mine waste materials.

Site	Treatment	pH	NH$_4^+$-N	NO$_3^-$-N	P	K	Total C	Total N
			----------------mg kg^{-1}----------------				-----g kg^{-1}-----	
A	C	6.9a	3.3a	8.0a	59a	94a	3.8a	0.3a
	LC	7.9ab	2.7a	12.6a	172a	268a	7.6a	0.9ab
	LCL	9.6b	7.5abc	6.7a	168a	318a	6.8a	0.8ab
	LCLB	9.6b	6.5abc	8.4a	228ab	287a	7.4a	0.8ab
	HC	8.2ab	4.5ab	64.0b	509b	1321b	25.3b	3.2c
	HCL	9.2ab	10.5c	41.0b	469b	1189b	16.2ab	2.0bc
	HCLB	9.2ab	8.9bc	59.0b	446b	1224b	17.1ab	2.2bc
B	C	5.2a	2.1a	1.8a	22a	46a	4.2a	0.3a
	LC	7.3ab	11.0ab	38.4ab	330b	841b	12.1ab	1.5a
	LCL	9.7bc	10.9ab	32.6ab	288b	681b	13.0ab	1.4a
	LCLB	10.6c	10.6ab	28.6ab	315b	624b	9.7ab	1.2a
	HC	7.7abc	6.3ab	165.5c	690c	3162c	31.9b	4.3b
	HCL	9.0bc	17.2b	161.8c	665c	3091c	32.5b	4.3b
	HCLB	8.5bc	9.9ab	103.2bc	584c	2286c	27.9b	3.5b

Note: Mean within a column for a specific site followed by the same letter are not significantly different at $P < 0.05$

Table 3-5. Comparison of mean values for microbial biomass C and N and nitrification at all five sample times for five treatments. Bentonite treatments are left out because they are not significantly different ($P \leq 0.05$) from LCL and HCL treatments.

Time	Treatment	-------------------Site A--			-------------------Site B-------------------		
		MBMC	MBMN	Nitrification	MBMC	MBMN	Nitrification
(d)		-------mg kg^{-1}-------		mg NO$_3^-$-N kg^{-1} d^{-1}	-------mg kg^{-1}-------		mg NO$_3^-$-N kg^{-1} d^{-1}
0	CO	270a	15a	0.24a	344a	9.2a	0.58a
	LC	419ab	26a	0.34a	313a	72ab	0.34a
	HC	641b	93b	0.45a	688b	266b	0.43a
	LCL	304a	30ab	0.38a	346a	74ab	0.27a
	HCL	455ab	81ab	0.31a	606b	237b	0.61a
139	CO	108a	15a	0.17a	70a	5.0a	0.06a
	LC	241ab	17a	0.14a	186ab	33ab	0.19a
	HC	281b	33a	0.33a	356b	91b	0.44a
	LCL	131a	31a	0.23a	115a	31ab	0.26a
	HCL	167a	42a	0.34a	223ab	100b	0.68a
353	CO	45a	5.1a	0.20a	90a	6.3a	0.02a
	LC	115ab	5.0a	0.19a	181ab	6.1a	0.44ab
	HC	222b	29b	0.61b	214ab	47b	0.66b
	LCL	72a	6.3a	0.12a	161ab	8.4a	0.28ab
	HCL	114ab	19ab	0.34ab	240b	30ab	0.70b
535	CO	92a	33a	0.19a	88a	8.6a	0.03a
	LC	197ab	46a	0.24a	247ab	59ab	0.40ab
	HC	574b	219b	0.80b	437b	167b	0.72b
	LCL	277ab	70a	0.29ab	254ab	64ab	0.34ab
	HCL	373ab	103ab	0.67ab	281ab	124ab	0.64b
711	CO	122a	41a	0.02a	113a	28a	0.05a
	LC	137a	35a	0.10ab	185ab	84ab	0.04a
	HC	289b	171b	0.27b	271b	163b	0.24b
	LCL	112a	28a	0.12ab	163ab	46ab	0.09ab
	HCL	171ab	71ab	0.12ab	246ab	148b	0.09ab
	Time	**	**	**	***	***	**
	Treatment x time	*	***	*	**	**	*

MBMC: Microbial biomass carbon, MBMN: Microbial biomass nitrogen

Note: Mean within a column and specific time period followed by the same letter are not significantly different at $P < 0.05$

*, **, and *** indicate significance at $P < 0.05$, 0.01, and 0.0001, respectively

Table 3-6. Comparison of mean values for microbial enzymes at all five sample times for five treatments. Bentonite treatments are left out because they are not significantly different ($P \leq 0.05$) from LCL and HCL treatments.

Time	Treatment	Site A					Site B				
		Alk Phos	Acid Phos	Aryl	β-gluco	Deaminase	Alk Phos	Acid Phos	Aryl	β-gluco	Deaminase
(d)		----------mg p-nitrophenol kg^{-1}----------				mg NH_4^+ kg^{-1}	----------mg p-nitrophenol kg^{-1}----------				mg NH_4^+ kg^{-1}
0	CO	280a	225a	11a	101a	1.1a	350a	365a	7.4a	32a	1.1a
	LC	886ab	344a	43ab	208ab	1.2a	1133ab	108a	59ab	155ab	1.7a
	HC	1986b	926a	116b	477b	2.9a	2560b	1744b	147b	345b	5.7b
	LCL	414ab	243a	8.7a	117a	1.7a	712ab	490ab	7.1a	39a	2.1ab
	HCL	1709b	470a	121b	236ab	2.3a	2160b	1514b	62ab	249ab	4.0ab
139	CO	375a	134a	11a	204ab	1.3a	135a	76a	5.9a	50a	1.7a
	LC	757ab	327a	32ab	218ab	1.7a	714ab	341ab	42a	170ab	2.3ab
	HC	2278b	653a	144b	651b	3.4a	2599b	1222b	213b	507b	8.3b
	LCL	381a	409a	33ab	124a	1.9a	485ab	744ab	74ab	95a	2.4ab
	HCL	1187ab	387a	117b	230ab	2.9a	1885b	1183b	244b	258ab	6.6ab
353	CO	360a	111a	15a	211ab	2.6a	220a	343a	45a	24a	1.9a
	LC	650ab	190ab	42a	152ab	4.4a	710ab	353a	123ab	158ab	7.8ab
	HC	2248b	805b	281b	684b	14.7b	2780b	1100a	241b	552b	16.3b
	LCL	286a	191ab	64ab	76a	5.9ab	995ab	532a	77ab	78a	6.3ab
	HCL	1705b	621ab	161ab	229ab	10.0ab	2665b	903a	250b	372ab	13.3b
535	CO	225a	266a	47a	209ab	2.9a	297a	40a	12a	112a	1.6a
	LC	425ab	715ab	62a	215ab	3.4a	520ab	529ab	95ab	277ab	3.5ab
	HC	2603b	1412b	235b	727b	3.6a	1728b	1309b	201b	657b	7.1b
	LCL	975ab	518ab	79ab	150a	3.3a	1229ab	424ab	85ab	151a	2.9ab
	HCL	2042b	956ab	164ab	323ab	3.6a	1455ab	742ab	196b	426ab	5.0ab
711	CO	287a	277a	25a	80a	1.6a	96a	627a	26a	105a	1.6a
	LC	658ab	345a	39a	151ab	3.1a	712ab	458a	66ab	95a	3.2a
	HC	2000b	1690b	193b	383b	3.6a	2134b	1019a	183b	349b	3.3a
	LCL	390a	316a	30a	73a	2.7a	949ab	426a	67ab	117a	2.2a
	HCL	1067ab	598ab	67ab	186ab	3.3a	2115b	1056a	156b	267ab	3.4a
	Time	***	**	**	**	***	***	ns	**	**	**
	Treatment x time	***	**	*	*	**	**	*	*	**	**

Alk Phos: Alkaline Phosphatase, Acid Phos: Acid Phosphatase, Aryl: Arylsulfatase, β-gluco: β-glucosidase

Note: Mean within a column and specific time period followed by the same letter are not significantly different at $P < 0.05$

*, **, and *** indicate significance at $P < 0.05$, 0.01, 0.0001, respectively

Table 3-7. Comparison of microbial biomass of treatments for selected structural groups extracted by phospholipids-linked fatty acids methods.

Site	Treatment	Gram-positive bacteria	Gram-negative bacteria	Actinomycetes	Fungi	Total‡
		--- µmol kg^{-1} dry soil---				
A	CO	10.2c†	10.1b	1.2abc	8.7cd	30.2c
	LC	9.7c	7.9b	0.8bc	6.9d	25.3c
	LCL	9.2c	26.8a	0.3c	6.4d	42.7bc
	LCLB	8.9c	8.3b	0.6c	8.0d	25.8c
	HC	37.8a	24.1a	2.0a	16.4a	80.3a
	HCL	25.9b	23.2a	1.7ab	11.8bc	62.6b
	HCLB	24.8b	16.7ab	1.6ab	12.8ab	55.9b
B	CO	11.8bc	5.0c	1.5ab	4.8b	23.1d
	LC	18.8b	11.7bc	1.5ab	7.7b	39.7c
	LCL	12.3bc	9.0bc	0.9b	7.3b	29.5d
	LCLB	10.5bc	18.3abc	0.6b	6.4b	35.8cd
	HC	38.2a	28.5a	1.9a	16.3a	84.9a
	HCL	32.9a	20.3ab	1.9a	13.7a	68.8b
	HCLB	34.6a	23.0ab	2.1a	13.4a	73.1ab

† Mean within a column and for a specific site followed by the same letter are not significantly different at $P < 0.05$

‡ Total is the sum of Gram-positive bacteria, Gram-negative bacteria, Actinomycetes, and Fungi for a given treatment

CHAPTER 4 - Revegetation of Pb/Zn Mine Wastes with *Panicum virgatum* using Beef Manure Compost and Other Inorganic Amendments

4.1 Abstract

One method for stabilizing Pb/Zn contaminated waste materials is to apply large quantities of organic matter in order to improve physical, chemical, and biological characteristics, which enhances biogeochemical nutrient cycles. Our hypothesis is that greater than 200 Mg ha^{-1} additions of beef manure compost is needed in order to establish and maintain a vegetative cover over time. Compost was applied at two different quantities (45 or 269 Mg ha^{-1}) with and without lime and bentonite to mine wastes contaminated with heavy metals to investigate the effects on nutrient content, estimated water holding capacity, and success of revegetation at two sites over time. Switchgrass (*Panicum virgatum*) was seeded into plots to establish a vegetative cover, but invasive weed species were also present. Compost additions significantly increased C, N, P, and K contents along with pH values, while significantly reducing Ca(NO$_3$)$_2$ extractable metals and DGT (diffusive gradients in thin films) Zn content. Due to high salt content and minimal rainfall, revegetation was unsuccessful in year one. In years two and three, the 269 Mg ha^{-1} treatment was able to establish and maintain significantly higher plant biomass than the 45 Mg ha^{-1} treatment and the control at both study sites. However, at site A, plant biomass started to decline in year three, which is likely related to significantly higher amounts of bioavailable Zn at site A as compared to site B. At site B, plant biomass decreased in the 45 Mg ha^{-1} treatment, but increased in the 269 Mg ha^{-1} treatment. The addition of lime and lime plus bentonite did not further increase plant biomass production over compost

alone. Therefore, these amendments were not needed for revegetation at these sites at this time. Successful revegetation was related to increases in estimated available water, plant nutrients, and the reduction in bioavailable metals upon amendment additions. In conclusion, a compost addition in the range of 45 to 269 Mg ha^{-1} was needed to establish and maintain vegetation. However, investigations on the efficacy of this remediation strategy are needed, therefore, this study needs long-term monitoring.

4.2 Introduction

The Tri-State Mining Region, located in southwest Missouri, southeast Kansas, and northeast Oklahoma, has a long legacy of Pb and Zn mining. Although mining/smelting of Pb and Zn ceased in the early 1970's, large quantities of waste materials are still present on the surface (Pierzynski et al., 2002). Mine waste materials, which are locally known as chat, are often characterized by their poor physical and chemical characteristics (Wong et al., 1998; Krzaklewski and Pietrzykowski, 2002). Additionally, these materials still have metal concentrations that are sufficiently high enough to adversely affect human health and cause harm to native ecosystems (Adriano et al., 1997; Pierzynski, 1997).

The lack of vegetative cover leaves the mine wastes exposed to erosion processes, direct-contact exposures, and inhibits the development of a functional ecosystem (Martin and Ruby, 2004). As a result, remediation strategies must be designed to reduce metal bioavailability and improve chemical and physical properties of the mine wastes so that they can support a vegetative cover, thus limiting metal mobility and bioavailability. More recently, the use of less invasive and expensive *in situ* solutions has been favored (Iskandar and Adriano, 1997). Such techniques allow for the application of soil amendments, such as organic amendments, alkaline materials, fertilizers, and metal oxide sorbents, which reduce heavy metal bioavailability and

provide more optimum conditions for vegetative growth.

Soil organic matter, nutrients, and biological activity contribute to ecosystem-level process and are important to the productivity of terrestrial ecosystems (Stevenson, 1994). Applications of biosolids or composted materials have recently been used to remediate heavy metal contaminated soils and other materials (Vansgroveld et al., 1995; Li et al., 2000; Brown et al., 2003; Clemente et al., 2005). Such treatments provide large amounts of organic matter, which provide a number of benefits to contaminated soils (Adriano, 2001). The addition of organic materials provide increased metal sorption and favor plant growth through the improvement of soil fertility and water holding capacity, which are lacking in most mine waste materials (Wong et al., 1998; Krzaklewski and Pietrzykowski, 2002). Brown et al. (2004) found that municipal biosolids compost was able to reduce the phyto- and bioavailability of heavy metals in mine tailings. Basta et al. (2001) reported that alkaline organic treatments can reduce human exposure to both Cd and Pb indirectly by reducing Zn phytotoxcity, which facilitates the revegetation of contaminated sites. The combination of calcareous pH and higher organic matter, Fe, and phosphate levels of biosolids compost was able to improve the overall success of vegetation establishment on highly Zn-contaminated soils in Pennsylvania (Li et al., 2000). Similarly, DeVolder et al. (2003) reported that biosolids compost mixed with wood ash allowed for vigorous plant growth in metal contaminated tailings, indicating a reduction in phytotoxicity. Therefore, the addition of inexpensive amendments with compost may help to further improve vegetative growth.

The objective of using organic materials to facilitate the phytostabilization of metal contaminated soils/wastes is to create a self-sustaining environment where nutrients are cycled internally by healthy microbial and plant populations with no further inputs needed. An addition

of beef manure applied at 90 Mg ha^{-1} was able to increase the growth of tall fescue (*Festuca arundinacea* Shreb) in the first year after amendment addition (Pierzynski et al., 2002). However, by the third year plant growth declined and plant tissue analysis suggested that Zn phytotoxicity was a contributing factor. In another study, Brown et al. (2003) made a surface application of high N biosolids (66 Mg ha^{-1}) combined with wood ash. They found that this treatment combination was able to establish and maintain a vegetative cover on heavy metal contaminated mine tailings for two growing seasons. With time they observed a decrease in nutrient content, which led them to believe that much larger organic amendment additions may be required to maintain vegetative communities over a significant period of time. Consequently, further research is needed to investigate the effectiveness of increased additions of organic amendments on permanence and plant growth over time. We hypothesized that higher loadings of an organic amendment (> 200 Mg ha^{-1}) will result in a self-sustaining vegetative cover. The specific objectives of this study are to 1) evaluate the changes in plant nutrient status and pH upon amendment addition over time, 2) ascertain whether increased rates of compost are sufficient to restore and maintain a vegetative cover on mine waste materials, 3) determine if the addition of lime or lime plus bentonite improves the permanence of the compost amendment, and 4) evaluate the effect that lime and bentonite have on plant growth, especially since bentonite is being considered for use in the pelletization process of the compost.

4.3 Materials and Methods

Site and Treatments. The experiment consisted of two field studies. Each study was set up at a different location on mine waste materials contaminated with heavy metals near Galena, KS. Information on the mean annual precipitation and temperature ranges for this region are reported in Chapter 3. The studies consisted of 7 treatments (consisting of 3 amendments with different

amendment combinations and amounts) in plots that were set up using a randomized complete block design with three replicates. The amendments included: composted beef (*Bos taurus*) manure, lime as Ca(OH)$_2$, and Enviroplug Grout (Wyo-Ben, Inc., Billings, MT), which is a Wyoming bentonite. Nutrient content, bioavailable metals, and plant growth were monitored at 139, 535, and 841 d after time 0 (DATZ).

Research plots were established and treatments were the same as described in Chapter 3. A tractor equipped with a front-end loader was used to loosen the waste materials at each location and a representative sample of the waste material was taken from each site to determine particle size distribution (Gee and Bauder, 1986), the intial pH, and background metal concentrations. Galvanized steel borders, that were 1 by 2 meters in size, were installed to limit the amount of interplot contamination. Treatments were then applied to their assigned plot and mixed to a depth of 30 cm using a shovel on May 8 and 12, 2006 for sites A and B, respectively. The treatments were the following: (1) CO, non-amended control plot; (2) LC, a low beef manure compost addition of 45 Mg ha^{-1}; (3) HC, a high compost addition of 269 Mg ha^{-1}; (4) LCL, low compost addition (45 Mg ha^{-1}) + 2.24 kg lime as Ca(OH)$_2$ (11.2 Mg ha^{-1}); (5) HCL, high compost addition (269 Mg ha^{-1}) + 2.24 kg lime as Ca(OH)$_2$; (6) LCLB, low compost addition (45 Mg ha^{-1}) + 2.24 kg lime as Ca(OH)$_2$ + bentonite applied 50 g bentonite kg^{-1} compost (0.45 kg); and (7) HCLB, high compost addition (269 Mg ha^{-1}) + 2.24 kg lime applied as Ca(OH)$_2$ + bentonite applied 50 g bentonite kg^{-1} compost (2.69 kg).

Switchgrass (*Panicum virgatum*) was seeded into all plots on May 26, 2006 at 6.72 kg of pure live seed (PLS) ha^{-1}. Due to high salinity of the compost and lack of rainfall, establishment of vegetation failed in the first year. Plots were then seeded to annual ryegrass (*Lolium multiflorum* Lam.) in the fall of 2006 to serve as a protective winter cover. Glyphosate was used

to kill the annual ryegrass in the spring of 2007, and plots were re-seeded with switchgrass on April 19, 2007.

Soil samples of the material were collected on May 26, 2006 (Time 0), and 139, 353, 535, 711, and 841 DATZ. A composite sample composed of five subsamples was collected with a stainless steel garden shovel for each plot. All samples were analyzed for 1:1 soil to deionized water pH and electrical conductivity (EC) using a saturated paste extract (USDA, 1954). Total C, N and P, inorganic N, extractable P, extractable cations, cation exchange capacity, total metal concentrations, and bioavailable metal concentrations were measured on all samples. Total C and N were measured by dry combustion following pretreatment with HCl to remove inorganic carbonates. Inorganic N was determined by extraction with 1 M KCl and extractable P by Mehlich (1984). Concentrations of N and P in filtered extracts and digests were determined colorimetrically. Cation ion exchange was determined by displacement at the 353 d sampling (Jaynes and Bigham, 1986). Available cations (K, Na, Mg, and Ca) were determined by extraction with 1 M ammonium acetate. Nitric acid digestable metal concentrations were determined using 2 g of material ($\leq$ 2-mm) with 20 mL of trace metal grade 4 M HNO_3 at 80 to 85°C for 4 h (Sposito et al., 1982). Bioavailable metal fractions were estimated using 0.5 M $Ca(NO_3)_2$ to measure weak electrolyte extractable metals (Basta and Gradwohl, 2000) and diffusive gradients in thin films (DGT) as reported in Chapter 3. Details on the preparation of the diffusive and resin gels for the DGT procedure are given by Zhang and Davison (1995). Available cation, HNO_3 metal, and bioavailable metal concentrations in collected solutions were measured using inductively coupled plasma-optical emission spectrometry (ICP-OES). Compost was collected and analyzed for total C, N, and P, available cation (K, Na, Mg, and Ca) content, pH, and total metal concentrations (see Chapter 3). Total P was determined by salicylic-sulfuric

acid digestion (Bremner and Mulvaney, 1982). Basic characteristics of the beef manure compost can be viewed in Table 4-1. Available water capacity estimates were previously determined (Chapter 3) by using water retention curve measurements in the laboratory as described by Cassell and Nielson (1986). Only select samples were used for this analysis (CO, LC, LCLB, HC, and HCLB).

Plant Samples. Due to adverse growing conditions, there was no plant biomass to harvest in year 1. Plant biomass was harvested from all plots on November 12, 2007 (535 DATZ) and September 13, 2008 (841 DATZ) and separated into different species before drying. The plant species present at Site A was switchgrass, tufted hairgrass (*Deschampsia cespitosa*), and smooth pigweed (*Amaranthus hybridus*) for both samplings, while at Site B there was switchgrass and yellow foxtail (*Setaria glauca*) for the 535 DATZ sampling and switchgrass and marestail (*Conyza canadensis*) for the 841 DATZ sampling. Plant materials were thoroughly washed with deionized water, a 5 g kg^{-1} sodium lauryl sulfate solution, and then again with deionized water to remove adhering soil particles. After washing, plants samples were oven-dried at 55 $^{\circ}$C and weighed for biomass. Plant samples were then ground and digested to determine total metal and nutrient uptake. Subsamples of 0.25 g plant material were digested with concentrated H_2SO_4 and 30% H_2O_2 for determination of plant N, P, and K (Thomas et al., 1967). Subsamples of 0.5 g of plant material were digested with trace-metal grade concentrated HNO_3 for 4 h at 120 $^{\circ}$C for determination of plant Cd, Pb, and Zn. Concentrations of K, Cd, Pb, and Zn in digests were determined using ICP-OES, while P and N were determined colorimetrically. Quality assurance and quality control consisted of 10% of samples run as duplicates, blanks, and check samples (NIST standard 1515 apple leaf).

Data Analyses. The experimental design was a randomized complete block design with

treatment as the main factor at each site. Sampling time was the strip plot factor, so the analyses were handled as a strip plot design using PROC MIXED. The Scheffe method was used to adjust the *P*-values and means were separated at the 0.05 level of significance. Principle components analysis (PCA) was used at the 535 and 841 d samplings to determine the influence of the treatments. Multiple linear regression analysis with backward selection was used for all plant species at the 535 and 841 d samplings to determine the variables that were most influential on plant biomass. All statistical analyses were performed using SAS for Windows version 8.2 (SAS Institute, 2001).

4.4 Results and Discussion

Characterization of the Contaminated Mine Wastes. The mine waste materials were comprised mostly of coarse fragments and sand, which contribute to its high porosity (Table 4-2). High porosity also means low water holding capacity, which can limit vegetative growth. The pH was acidic, and nutrient concentrations were low. Additionally, there were elevated levels of Cd, Pb, and Zn. The USEPA (1997) reported that average Pb and Zn concentrations in chat ranged from 360 to 1,500 mg kg^{-1} and 6,000 to 13,000 mg kg^{-1}, respectively, which was similar to our results.

Effects of Amendments on pH. At both study sites, there was a significant increase in pH caused by amendment additions (Table 4-3). This effect can be attributed to both the lime and compost additions. Eghball (1999) demonstrated that composted beef manure could be used independently to increase soil pH. This is possible because calcium carbonate is added to the diets of beef cattle as a source of Ca, but much of the material is excreted in the manure. Therefore, beef manure or composted beef manure can be used to potentially increase the pH of mine wastes. At site A, compost alone did not cause a significant increase in pH. However,

additions of lime with the 45 Mg ha^{-1} compost addition did significantly increase pH at time 0, but at 841 d no treatments were significantly different than the contaminated control. At site B, only the additions of compost with lime caused a significant increase in pH at time 0. At 841 d, all treatments except for the LC treatment had significantly higher pH values than the contaminated control. The fact that the HC treatment had a pH that was similar to the treatments with lime supports the findings of Eghball (1999) in that composted beef manure can increase pH.

Agronomic Measurements. Amendment additions changed a number of chemical properties of the mine waste material at both study sites; however, several of these properties were no longer significantly different than the control at 841 d (Table 4-3). At both study sites, the HC treatment caused a significant increase in extractable NH_4^+, but by 841 d the results were not significantly different from the control. All high compost treatments had significantly higher NO_3^- levels at time 0, but similar to NH_4^+ all treatments had similar NO_3^- concentrations at 841 d. This also is true for K levels at site A. However, at site B all treatments caused a significant increase in K at time 0, but after 841 d, only the high additions of compost still had K levels significantly higher than the contaminated control. This was expected since NH_4^+, NO_3^-, and K^+ are highly mobile elements in this environment and would be readily leached from the porous mine wastes with time. This is mainly due to the lack of clay minerals, which provide the bulk of the cation exchange capacity present in soils. Pierzynski et al. (2002) found that after two years, K levels decreased or were at levels that were insufficient for plant growth when manure was added to a similar mine waste material. Brown et al. (2003) also saw a significant decrease in K after application of high N biosolids to mine tailings, which led to the conclusion that larger applications of organic materials may be needed to maintain sufficient high nutrient levels.

Extractable P concentrations at both study sites were significantly increased by compost additions. At site A, only 269 Mg ha^{-1} additions of compost increased extractable P significantly over the control. For the time 0 measurements at site B, both low and high compost treatments significantly increased extractable P, while at 841 d only the high treatments had significantly higher levels of P. Interestingly, the extractable P values at both sites increased with the high compost addition over the study period. This suggests that either P mineralization or dissolution of P-containing solid phases has released additional extractable P. Total C and N were significantly increased at the high compost additions and remained constant for the duration of the study.

Electrical conductivity (EC) was significantly increased by the high compost additions. However, with time EC decreased such that there were no significant treatment effects. . The increase in EC was expected since manure characteristics are influenced by animal rations, which contain salts (Kissinger et al., 2007). The salts were leached out of the root zone by the end of the first year of the experiment (data not shown). There is some environmental concern if this technique were to be adopted to remediate large mine waste areas. Movement of nutrients into ground or surface waters could lead to both drinking water and ecological issues. Studies have found the movement of N, P, and other constituents contained in manures and composts into water sources when applied in excess of plant nutrient needs on soils (Burkhart and James, 1999; Eghball, 2003; Ferguson et al., 2005). Therefore, loss of nutrients and salts from mine waste materials is an even greater concern due to the high porosity and low water holding capacity of the mine waste materials.

Cation exchange capacity was significantly increased by the HC treatment, but was not influenced by any other amendment (Table 4-4). The increase in CEC was expected since

organic materials and organic matter contains functional groups that are reactive towards cations (Stevenson, 1994). This increase in CEC caused by organic matter addition also increased the potential sorption of heavy metals in the mine wastes making them less available to plants and microbial communities. However, as the organic material decomposes, it is possible that complexed metals would be released leading Beckett et al. (1979) to postulate on the "time bomb" theory. Estimated available water content was determined on soil samples collected from select treatments (CO, LC, LCLB, HC, and HCLB). It was assumed that the addition of lime with compost would not increase estimated available water over compost alone; therefore, available water content was not measured in the LCL and HCL treatments. High quantities of compost significantly increased the amount of available water (Table 4-4), which is important to establishing healthy plant and microbial communities in these porous materials.

Heavy Metal Availability and Plant Biomass. In the first year of the study, there was no plant biomass to harvest reflecting the high EC of the compost and lack of rainfall. However, vegetative growth did occur in years 2 and 3 and treatments had a significant effect on total plant biomass at each site (Figure 4-1). At site A, the HC treatments produce significantly more plant biomass than the 45 Mg ha^{-1} treatments and the control. However, plant biomass decreased at 841 d, which is similar to the findings of Pierzynski et al. (2002). At site B, both the HC and LC treatments produced significantly more plant biomass than the control, while the HC treatments had significantly more biomass than the LC treatments. At the 841 d sampling, plant biomass had decreased in the 45 Mg ha^{-1} treatments, while biomass was still increasing in the 269 Mg ha^{-1} treatments. This is contradictory to site A and could be related to the higher concentrations of bioavailable Zn at site A as compared to site B (Table 4-6).

Switchgrass is a native, warm-season grass that is slow to develop, particularly with the

poor growing conditions that exist in mine waste materials. Early in the study significant competition occurred from weed species such as marestail, smooth pigweed, tufted hairgrass, and yellow foxtail. The weeds probably came from seeds that were deposited on the chat from surrounding vegetated areas and that germinated once more favorable growing conditions were created by the soil amendments. Annual plants are less desirable as vegetative cover as compared to perennials.

At site A, there were no significant differences in switchgrass biomass at 535 d. However, the HCL treatment significantly increased the growth of smooth pigweed and tufted hairgrass, which indicated that the mine wastes were also inhibiting the growth of the invasive species. At site B, all of the 269 Mg ha^{-1} compost treatments significantly increased switchgrass production over the control 45 Mg ha^{-1} treatments. In addition, high compost additions increased the production of yellow foxtail at site B. Interestingly, the HCL treatment produced the most biomass at both sites, although it was not significantly different from the other HC treatments, but it may suggest that the addition of lime with compost stimulated plant growth. At the 841 d sampling, the 269 Mg ha^{-1} treatments produced significantly more switchgrass biomass than the 45 Mg ha^{-1} treatments and the control. Again, the HCL treatment had significantly more tufted hairgrass than the control. At site B, the 269 Mg ha^{-1} treatments had significantly more switchgrass than the 45 Mg ha^{-1} and control treatments at 841 d. In addition, foxtail was not present at the 841 d sampling, but was replaced by marestail in the study areas, which could suggest a vegetative succession. Several studies have indicated that high pH organic amendments are needed to reduce phytotoxicity and establish a vegetative cover in heavy metal contaminated wastes (Brown et al., 2004; DeVolder et al., 2003; Li et al., 2000). In this study, a 269 Mg ha^{-1} addition of compost was needed to support the growth of switchgrass; it also

improved the growth of competing invasive species.

Amendment additions significantly decreased $Ca(NO_3)_2$ extractable heavy metal concentrations by the fall of 2006 (data not shown) and values remained significantly less than the contaminated control throughout the remainder of the study (Table 4-6). At site A, extractable Cd was reduced significantly by all HC treatments, while at site B all amendment additions reduced extractable Cd to below detection limits. Extractable Pb was not significantly reduced at site A, but all amendments reduced extractable Pb to below detection limits at site B. Calcium nitrate extractable Zn was significantly reduced compared to the control by all high compost treatments at site A, while at site B all treatments reduced extractable Zn significantly below the control. Similarly, other studies have found that organic amendments are able to reduce $Ca(NO_3)_2$ extractable Zn compared to an untreated soil (Basta et al., 2001; Brown et al., 2003). All compost treatment combinations were able to significantly reduce DGT Zn concentrations at both sites. A significant site by treatment interaction existed for $Ca(NO_3)_2$ extractable and DGT Zn, which could explain the significant increase in switchgrass biomass at site B where bioavailable Zn is significantly lower than at site A.

The objective of the bioavailability measurements was to relate the concentration of a metal to plant biomass production. Nonlinear relationships that were found for $Ca(NO_3)_2$ extractable and DGT Zn with switchgrass biomass (Figure 4-2). While $Ca(NO_3)_2$ had a slightly better fit, both bioavailability assessments were related to switchgrass biomass. Similar relationships were discovered for foxtail at 535 d (DGT Zn: R^2 = 0.82 with P = 0.0034 and $Ca(NO_3)_2$ Zn: R^2 = 0.92 with P < 0.0001) and smooth pigweed at 535 and 841 d combined (DGT Zn: R^2 = 0.43 with P = 0.9333 and $Ca(NO_3)_2$ Zn: R^2 = 0.62 with P = 0.1212), but no relationships were found for tufted hairgrass or marestail. Nonlinear regression analysis was also

146

applied to total biomass and the bioavailability assessments across all sampling times(DGT Zn: $R^2 = 0.69$ with $P < 0.0001$ and $Ca(NO_3)_2$ Zn: $R^2 = 0.52$ with $P = 0.0514$). In most cases, as treatments reduced bioavailable Zn, the amount of biomass significantly increased. Brown et al. (2003) found that as biosolids amendments reduced $Ca(NO_3)_2$ extractable Zn, a vegetative cover was able to be established on a heavy metal contaminated subsoil. Similarly, Pierzynski and Schwab (1993) discovered that manure and limestone reduced KNO_3 extractable Zn in soil, which led to a subsequent reduction in Zn uptake by soybean [*Glycine max* (L.) Merr.]. Sommez and Pierzynski (2005), using a greenhouse pot study, concluded that increasing Zn concentrations determined by DGT resulted in a decrease in sorghum-sudan grass (*Sorghum vulgare* var. Sudanese) biomass, which is similar to our findings.

Inhibition of vegetative growth is likely due to any number of factors such as pH, nutrient deficiencies, poor physical properties, and metal toxicities (Wong et al., 1998; Krzaklewski and Pietrzykowski, 2002). Therefore, plant biomass was subjected to multiple linear regression analysis to determine the variables that were most influential on plant biomass production (Table 4-7). One has to be careful in interpreting results from such an analysis, especially for invasive species that are already capable of growing in extreme conditions. Switchgrass and yellow foxtail had a significant positive relationship with estimated available water content. Thus, as compost additions increased, so did available water, which resulted in a subsequent increase in plant biomass. Switchgrass also had positive relationships with total N and extractable P and K. Both tufted hairgrass and yellow foxtail biomass production were negatively related to DGT Zn. This relationship is expected since our results and others (Somnez and Pierzynski, 2005) have suggested that as DGT Zn increases, the amount of plant biomass produced decreases. Both switchgrass and smooth pigweed biomass production had significant

147

negative relationships with extractable Na and tufted hairgrass with electrical conductivity, thus illustrating the negative effects that salts can have on plant biomass production. No significant relationships were found for marestail.

To better understand how treatments were behaving, the data from the 535 and 841 d samples were subjected to PCA. Sites were separated for PCA because of a significant site by treatment interaction, which suggested that the sites may need to be reclaimed based on their individual needs. In addition, time was significant at both sites ($P < 0.0001$); therefore, time was also separated for each treatment. Principle components analysis of site A indicated a difference between compost amendment additions (Figure 4-3A). The control, low, and high compost treatments separate along PC1 (X-axis). The greatest negative Eigen vector values for PC1 were for all $Ca(NO_3)_2$ extractable metals and DGT Zn, while the positive Eigen vector values were for extractable P and K, total C, total N, estimated available water, and plant biomass. High compost treatments lie on the positive side of PC1, suggesting that compost reduces bioavailable metals and increases nutrient content, available water, and plant biomass. Additionally, there was separation of treatments along PC2 (Y-axis). A high positive Eigen vector value was found for pH, while the most influential negative values were for extractable Na and NH_4^+. Over time all treatments became more negative along PC1 and PC2, which was likely due to loss of nutrients and a reduction in pH. At site B, the different compost amendment treatments separate along both PC1 and PC2 (Figure 4-3B). The highest positive Eigen vector values for PC1 were pH, P, K, total C, total N, plant biomass, while negative values exist for all $Ca(NO_3)_2$ extractable metals and DGT Zn. Again, high compost treatments are on the more positive side of PC1, thus indicating that compost additions reduced bioavailable metals, increased the amount of plant nutrients, and increased plant biomass production. For PC2, the highest Eigen vector values

148

were for NH_4^+, plant biomass, and available water, while the most negative values were for electrical conductivity, total Cd, Pb, and Zn. Electrical conductivity was heavily weighted on PC2, which caused the LC and HC treatments to be initially negative. Over time the salts leached, which resulted in LC and HC treatments becoming more positive along PC2. Across sites and sample times, the addition of lime and lime plus bentonite to compost did not cause significant treatment differences. Additionally, the CO, LC, and HC treatments were significantly different ($P < 0.0001$) from one another at both sites and sample times. Therefore, at this point in time, an addition of 269 Mg ha^{-1} of compost alone was sufficient to increase nutrient content, available water, and plant biomass in contaminated mine wastes.

Conclusions. A general conclusion of the current study was that a high addition (269 Mg ha^{-1}) of beef manure compost was needed to support a self-sustaining plant cover on mine wastes contaminated with heavy metals. This was especially true for establishment of switchgrass. More specific conclusions can be difficult to make because the different indices used to quantify the success of the amendments gave results that are difficult to interpret. This illustrates the complexities that exist in attempting to revegetate contaminated mine wastes using soil amendments. If plant biomass alone were considered, then the amendments were definitely more successful in the second and third years of the study. This can be attributed to the high salt content of the compost and the lack of rainfall during the first growing season. High compost applications promoted significantly greater plant growth than lower amendment additions. Although the increase in yield is encouraging, it was essential that this be related to other parameters that were measured in the study.

Multiple regression analyses indicated that the increase in estimated available water, total N, extractable P, extactable K, and reduction in bioavailable Zn upon amendment additions were

some of the major components related to the increase in plant biomass yield. Both LC and HC treatments significantly reduced bioavailable Zn in most cases. At site A, lime was needed with the LC treatment to significantly reduce bioavailable Zn over the control. A significant negative relationship was found for DGT Zn with yellow foxtail and tufted hairgrass biomass. As compost and lime decreased bioavailable Zn, plant biomass levels significantly increased. However, low additions of compost still produced significantly less plant biomass than all of the high additions, even though both were able to significantly reduce levels of bioavailable Zn. This suggests that water availability and nutrient content may be the major obstacles to overcome when reclaiming porous mine wastes.

Multiple regression analyses indicated that improved fertility was important in establishing switchgrass. Both LC and HC additions were able to improve fertility, but after three years only the HC treatments were able to maintain this improved fertility, although nutrient concentrations have decreased over time. Similarly, Pierzynski et al. (2002) concluded that the amount of K decreased when manure was applied to heavy metal contaminated soils. They found levels that were insufficient for plant growth after just two years, while the HC treatments in this study maintained sufficient levels of K for plant growth over a three year period. Brown et al. (2003) suggested that higher amendment amounts (> 66 Mg ha^{-1}) may be required to support a self-sustaining vegetative cover. According to this study, a minimum compost addition between 45 and 269 Mg ha^{-1} is necessary to provide sufficient plant nutrients, available water, and reduce levels of bioavailable Zn to maintain plant growth in mine wastes. Furthermore, differences between sites throughout the study suggest that remediation practices need to be designed to address the specific characteristics of a given site.

Despite the complicating factors associated with reclaiming heavy metal contaminated

mine wastes, it appears that a single addition of beef manure compost between 45 and 269 Mg ha^{-1} is sufficient for establishing and maintaining a vegetative cover. The combinations of compost with lime and with lime and bentonite do not provide significant improvements in plant biomass, estimated water content, or further reduce metal bioavailability; therefore, they may not be needed. Continuous long-term monitoring is needed to evaluate the success of this type of remediation technology.

4.5 References

Adriano, D.C. 2001. Trace elements in terrestrial environments: Biogeochemistry, bioavailability, and risks of metals. 2nd ed. Springer-Verlag, New York, NY.

Adriano, D.C., J. Albright, F.W. Whicker, I.K. Iskandar, and C. Sherony. 1997. Remediation of metal- and radionuclide-contaminated soils. p. 27-46. *In* I.K. Iskandar and D.C. Adriano (eds.) Remediation of soils contaminated with metals. Advances in Environmental Science. Science Reviews, Middlesex, UK.

Basta, N.T., and R. Gradwohl. 2000. Remediation of heavy metal-contaminated soil using rock phosphate. Better Crops Plant Food 82:29-31.

Basta, N.T., R. Gradwohl, K.L. Snethen, and J.L. Shroder. 2001. Chemical immobilization of lead, zinc, and cadmium in smelter-contaminated soils using biosolids and rock phosphate. J. Environ. Qual. 30:1222-1230.

Beckett, P.H.T., R.T. Davis, and P. Brindley. 1979. The disposal of sewage sludge onto farmland: The scope of the problems of toxic elements. Water, Pollut. Control (Maidstone, England) 78:419-445.

Bremner, J.M., and C.S. Mulvaney. 1982. Salicylic acid thiosulfate modification of the Kjeldhal method to include nitrate and nitrite. p. 621. *In* R.H. Miller and D.R. Keeney (ed.) Methods of soil analysis. Part 2. Am. Soc. Agron., Madison, WI.

Brown, S.L., R. Chaney, J. Hallfrisch, J.A. Ryan, and W.R. Berti. 2004. In situ soil treatments to reduce the phyto- and bioavailability of lead, zinc, and cadmium. J. Environ. Qual. 33:522-531.

Brown, S.L., C.L. Henry, R.L. Chaney, H. Compton, and P. DeVolder. 2003. Using

municipal biosolids in combination with other residuals to restore metal-contaminated mining areas. Plant Soil 249:203-215.

Burkhart, M.R., and D.E. James. 1999. Agricultural nitrogen contributions to hypoxia in the Gulf of Mexico. J. Environ. Qual. 28:850-859.

Cassell, D.K., and D.R. Nielson. 1986. Field capacity and available water capacity. p. 901-926. *In* A. Klute (ed.) Method of soil analysis. Part 1. 2nd ed. Agronomy Monograph 9. ASA and SSSA, Madison, WI.

Clemente, R., D.J. Walker, and M. Pilar Bernal. 2005. Uptake of heavy metals and As by Brassica juncea grown in a contaminated soil in Aznalcollar (Spain): The effect of soil amendments. Environmental Pollution 138:46-58.

DeVolder, P.S., S.L. Brown, D. Hesterberg, and K. Pandya. 2003. Metal bioavailability and speciation in a wetland tailings repository amended with biosolids compost, wood ash, and sulfate. J. Environ. Qual. 32:851-864.

Eghball, B. 1999. Liming effects of beef cattle feedlot manure or compost. Commun. Soil Sci. Plant Anal. 30:2563-2570.

Eghball, B. 2003. Leaching of phosphorus fractions following manure or compost application. Commun. Soil Sci. Plant Anal. 34:2803-2815.

Ferguson, R.B., J.A. Nienaber, R.A. Eigenberg, and B.L. Woodbury. 2005. Long-term effects of sustained beef feedlot manure application on soil nutrients, corn silage yield, and nutrient uptake. J. Environ. Qual. 34:1672-1681.

Gee, G.W., and J.W. Bauder. 1986. Particle size analysis. p. 399-404. *In* A. Klute (ed.) Methods of soil analysis. Part 1. 2nd ed. Agron. Monogr. 9. ASA and SSSA, Madison, WI.

Iskandar, I.K., and D.C. Adriano. 1997. Remediation of soils contaminated with metals: A review of current practices in the USA. p. 1-26. *In* I.K. Iskandar and D.C. Adriano (eds.) Remediation of soils contaminated with metals. Advances in Environmental Science. Science Reviews, Middlesex, UK.

Jaynes, W.F., and J.M. Bigham. 1986. Multiple cation-exchange capacity measurements on standard clays using a commercial mechanical extractor. Clays Clay Miner. 34:93-98.

Kissinger, W.F., R.K. Koelsch, G.E. Erickson, and T.J. Klopfenstein. 2007. Characteristics of manure harvested from beef cattle feedlots. Appl. Engineering Agric. 23:357-365.

Krzaklewski, W., and M. Pietrzykowski. 2002. Selected physio-chemical properties of zinc and lead ore tailings and the biological stabilization. Water, Air, Soil Pollut. 141:125-142.

Li, Y., R.L. Chaney, G. Siebielec, and B.A. Kerschner. 2000. Response of four turfgrass cultivars to limestone and biosolids-compost amendment of a zinc and cadmium contaminated soil at Palmerton, Pennsylvania. J. Environ. Qual. 29:1440-1447.

Martin, T.A., and M.V. Ruby. 2004. Review of *in situ* remediation technologies for lead, zinc, and cadmium in soil. Remediation J. 14:35-53.

Mehlich, A. 1984. Mehlich 3 soil test extractant: A modification of Mehlich-2 extractant. Commun. Soil Sci. Plant Anal. 15(12): 1409-1416.

Pierzynski, G.M. 1997. Strategies for remediating trace-element contaminated sites. p. 67-84. *In* I.K. Iskandar and D.C. Adriano (eds.) Remediation of soils contaminated with metals. Advances in Environmental Science. Science Reviews, Middlesex, UK.

Pierzynski, G.M., M. Lambert, B.A.D. Hetrick, D.W. Sweeney, and L.E. Erickson. 2002. Phytostabilization of metal mine tailings using tall fescue. Practice Periodical of Hazardous, Toxic, and Radioactive Waste Management 6:212-217.

Pierzynski, G.M., and A.P. Schwab. 1993. Bioavailability of zinc, cadmium, and lead in a metal-contaminated alluvial soil. J. Environ. Qual. 22:247-254.

Sonmez, O., and G.M. Pierzynski. 2005. Assessment of zinc phytoavailability by diffusive gradients in thin films. Environ. Toxicol. Chem. 24:934-941.

Sposito, G., L.J. Lund, and A.C. Chang. 1982. Trace metal chemistry in arid-zone field soils amended with sewage sludge: I. Fractionation of Ni, Cu, Zn, Cd, and Pb in solid phases. Soil Sci. Soc. Am. J. 46:260-264.

Stevenson, F.J. 1994. Humus chemistry: Genesis, composition, reactions. Wiley-Interscience, New York.

Thomas, R.L., R.W. Sheard, and J.R. Moyer. 1967. Comparison of conventional and automated procedures for N, P, and K analysis of plant material using a single digestion. Agron. J. 59:9-10.

USDA. 1954. Diagnosis and improvement of saline and alkali soils. Agric. Handb. No. 60. United States Salinity Laboratory, Riverside, CA.

U.S. Environmental Protection Agency. 1997. EPA Superfund Record of Decision: Cherokee County, Kansas. U.S. Environmental Protection Agency Report

EPA/ROD/R0797/073.

Vangronsveld, J., F.V. Assche, and H. Clijsters. 1995. Reclamation of a bare industrial area contaminated by non-ferrous metals: In situ metal immobilization and revegetation. Environmental Pollution 87:51-59.

Wong, J.W.C., C.M. Ip, and M.H. Wong. 1998. Acid-forming capacity of lead-zinc mine tailings and its implications for mine rehabilitation. Env. Geochem. Hlth. 20:149-155.

Zhang, H., and W. Davison. 1995. Performance characteristics of diffusion gradients in thin films for the in situ measurement of trace metals in aqueous solutions. Anal. Chem. 67:3391-3400.
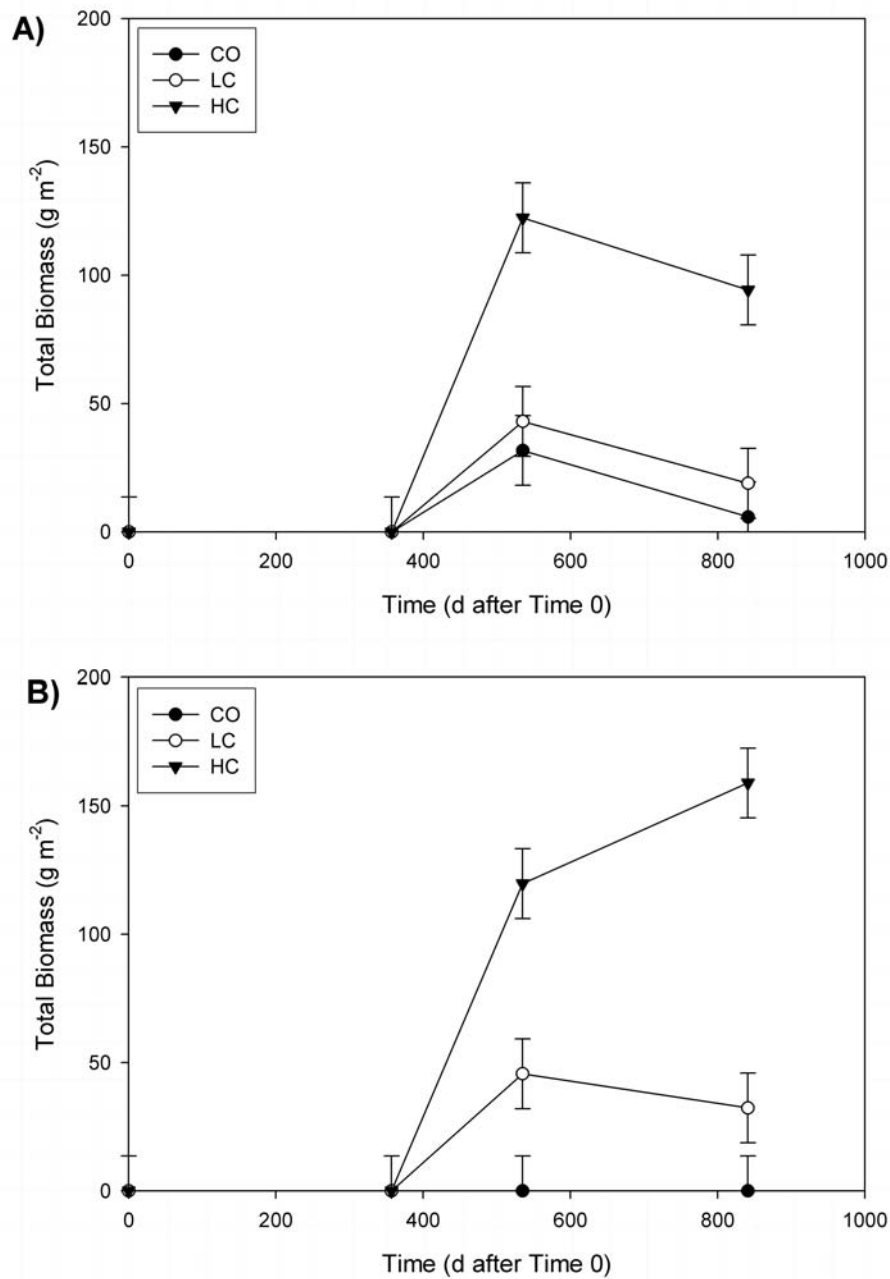
Figure 4-1. Total plant biomass of vegetated plots over time. A) is for site A and B) for is site B. Sites are significantly different (*P* < 0.0001) at all sample times. CO is the control, LC is the average of LC, LCL, and LCLB since these treatments are not signficanly different, and HC is the average of HC, HCL, and HCLB since these treatments are not significantly different.
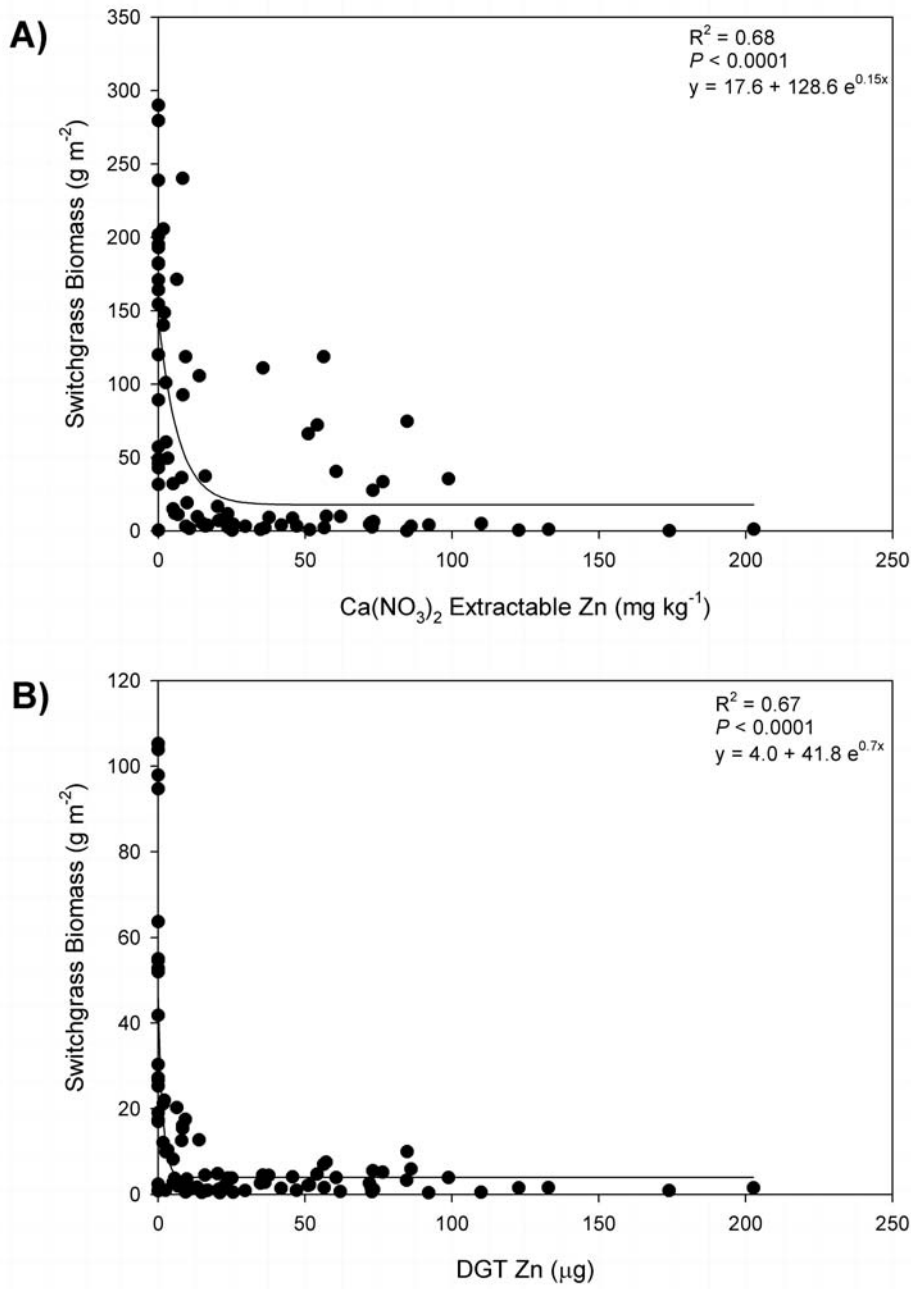
Figure 4-2. Relationship between switchgrass biomass with A) Ca(NO₃)₂ extractactable Zn in waste materials and B) DGT Zn in waste materials for both study sites.
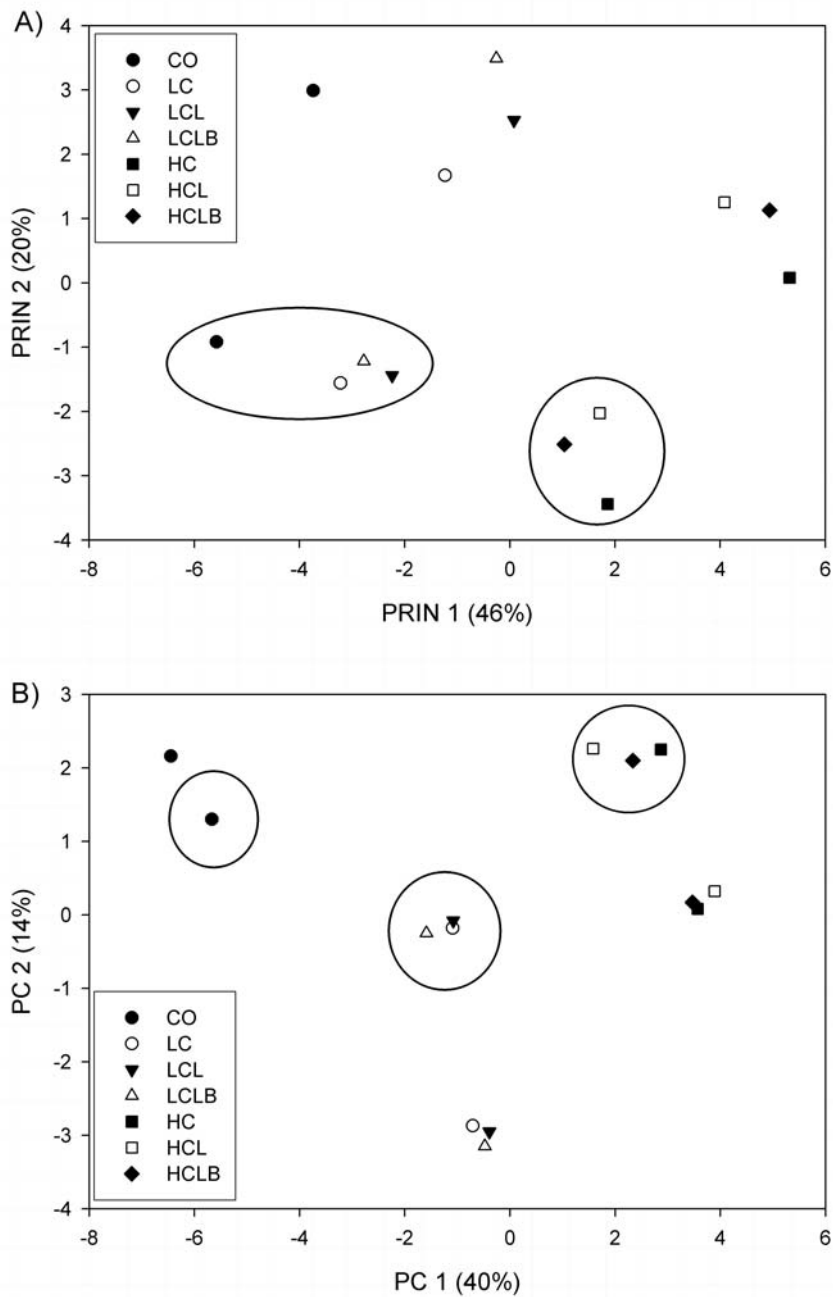
Figure 4-3. Principle components analysis of agronomy-based measurements for all treatments at both study sites. A) At site A, principle components (PC) 1 and 2 account for 46 and 20% of the variation, respectively. B) At site B, PC 1 and 2 account for 40 and 14% of the variation. Circles around treatments indicate a sampling time of 841 d. Treatments not included in circles are treatments sampled at 535 d.

Table 4-1. Basic characteristics of the beef manure compost.

Characteristics	Compost
Electrical Conductivity (dS m^{-1})	36
pH	8.1
Total C (g kg^{-1})	126
Total N (g kg^{-1})	14
Total P (g kg^{-1})	7.5
C:N	9.4
K (g kg^{-1})	22
Ca (g kg^{-1})	2.7
Na (g kg^{-1})	5.3
Cd (mg kg^{-1})	1.3
Pb (mg kg^{-1})	nd†
Zn (mg kg^{-1})	496

† nd = not detectable; 8.0 µg kg^{-1} detection limit for Pb

Table 4-2. General properties of the chat material before amendment application.

Characteristics	Site A	Site B
pH	6.5	4.9
Extractable NH_4^+-N (mg kg^{-1})	2.9	1.7
Extractable NO_3^--N (mg kg^{-1})	5.4	1.5
Extractable P (mg kg^{-1})	55	19
Extractable K (mg kg^{-1})	81	45
Total C (g kg^{-1})	3.9	4.2
Total N (g kg^{-1})	0.35	0.33
Total Cd (mg kg^{-1})	30	40
Total Pb (mg kg^{-1})	3400	2300
Total Zn (mg kg^{-1})	6800	6200
CEC (cmol$_c$ kg^{-1})†	15	23
Electrical Conductivity (dS m^{-1})	0.08	0.05
Coarse Fragments (g kg^{-1})‡	741	756
Sand (g kg^{-1})	207	204
Silt (g kg^{-1})	44	28
Clay (g kg^{-1})	8	12

† CEC: Cation Exchange Capacity
‡Coarse fragments are considered particles > 2 mm in size

Table 4-3. Selected agronomy-based measurements at Time 0 and 841 days.

Time (d)	Site	Treatment	pH	NH$_4^+$-N	NO$_3^-$-N	P	K	Total C	Total N	EC
				---------------mg kg^{-1}---------------				-----g kg^{-1}-----		mS cm^{-1}
0	A	CO	6.9a	3.3a	8.0a	59a	94a	3.8a	0.3a	1.3a
		LC	7.9ab	2.7a	12a	172a	268a	7.6a	0.9ab	1.3a
		LCL	9.6b	7.5abc	6.7a	168a	318a	6.8a	0.8ab	1.9ab
		LCLB	9.6b	6.5abc	8.4a	228ab	287a	7.4a	0.8ab	1.8a
		HC	8.2ab	4.5ab	64b	509b	1321b	25b	3.2c	4.2bc
		HCL	9.2ab	10c	41b	469b	1189b	16ab	2.0bc	4.5bc
		HCLB	9.2ab	8.9bc	59b	446b	1224b	17ab	2.2bc	5.5c
841		CO	6.5a	0.5a	3.7a	50a	68a	3.3a	0.2a	0.2a
		LC	7.3a	1.4a	5.7a	130ab	87a	5.3a	0.3a	0.2a
		LCL	7.7a	0.5a	4.5a	214ab	84a	7.3a	0.5a	0.1a
		LCLB	7.7a	0.9a	5.5a	158ab	74a	5.6a	0.4a	0.2a
		HC	7.3a	0.6a	8.3a	870b	193a	23b	2.4b	0.3a
		HCL	7.8a	0.9a	3.4a	922b	163a	18ab	1.9ab	0.3a
		HCLB	7.8a	1.0a	4.7a	908b	132a	18ab	1.9ab	0.3a
		Treatment x time	***	***	**	*	***	NS†	NS	**
0	B	CO	5.2a	2.1a	1.8a	22a	46a	4.2a	0.3a	0.3a
		LC	7.3ab	11ab	38ab	330b	841b	12ab	1.5a	4.5a
		LCL	9.7bc	10ab	32ab	288b	681b	13ab	1.4a	4.1a
		LCLB	9.8c	10ab	28ab	315b	624b	10ab	1.2a	4.1a
		HC	7.7abc	6.3ab	165c	690c	3162c	32b	4.3b	14b
		HCL	9.0bc	17b	161c	665c	3091c	33b	4.3b	13b
		HCLB	8.5bc	10ab	103bc	584c	2286c	28b	3.5b	8.7b
841		CO	4.6a	1.9a	3.3a	56a	64a	3.6a	0.1a	0.2a
		LC	6.8ab	0.5a	3.6a	290ab	185ab	9.2ab	0.8a	0.4a
		LCL	7.7b	1.3a	3.9a	230a	199ab	11ab	0.8a	0.4a
		LCLB	7.4b	0.3a	3.8a	262ab	151ab	8.7ab	0.7a	0.2a
		HC	7.7b	0.6a	3.2a	1359bc	331b	28b	3.1b	0.4a
		HCL	7.8b	0.4a	4.4a	1574c	464b	30b	3.2b	0.5a
		HCLB	7.7b	0.4a	3.1a	1487c	426b	28b	3.0b	0.4a
		Treatment x time	***	**	***	***	***	NS	NS	***

Note: Mean within a column and specific time period followed by the same letter are not significantly different at $P < 0.05$

*, **, and *** indicate significance at $P < 0.05$, 0.01, 0.0001, respectively

† NS: not significant

Table 4-4. Estimates of cation exchange capacity and available water after amendment additions.

Treatment	Cation Exchange Capacity	Available Water Capacity†
	$cmol_c\ kg^{-1}$	$g\ g^{-1}$
CO	20a	0.09a
LC	36a	0.10ab
LCL	32a	nd‡
LCLB	30a	0.11b
HC	60b	0.15c
HCL	66b	nd
HCLB	61b	0.15c

Note: Mean within a column and specific time period followed by the same letter are not significantly different at $P < 0.05$

† Estimate of available water capacity in the laboratory determined by the difference in water content at -10 kPa and -1.5 MPa

‡ nd: not determined

Table 4-5. Plant biomass yield for the fall of 2007 and 2008 (535 and 841 d after time 0, respectively). Biomass is divided into individual species.

		-----Site A-----			-----Site B-----	
Time	Treatment	Switchgrass	Smooth Pigweed	Tufted Hairgrass	Switchgrass	Yellow Foxtail
d		-----$g\ m^{-2}$-----				
535	CO	0.0a	23.0b	8.7b	0.0b	0.0d
	LC	2.7a	24.6b	23.6ab	19.2b	32.6abc
	LCL	4.4a	22.6b	14.1b	18.0b	21.3cd
	LCLB	5.5a	11.1b	20.6ab	16.6b	29.1bc
	HC	29.5a	59.2ab	32.3ab	54.1a	52.2ab
	HCL	14.3a	90.2a	46.1a	70.7a	59.5a
	HCLB	27.7a	44.0ab	23.5ab	75.6a	46.9abc

		-----Site A-----			-----Site B-----	
Time	Treatment	Switchgrass	Smooth Pigweed	Tufted Hairgrass	Switchgrass	Marestail
d		-----$g\ m^{-2}$-----				
841	CO	0.0b	5.8a	0.0b	0.0b	0.0b
	LC	0.0b	9.5a	7.8ab	29.5b	8.1ab
	LCL	5.2b	16.0a	1.9ab	32.1b	6.5b
	LCLB	2.8b	11.6a	1.9ab	11.4b	9.1ab
	HC	61.8a	7.5a	6.1ab	71.0a	53.4a
	HCL	62.3a	25.8a	11.6ab	86.8a	42.7a
	HCLB	51.2a	25.2a	6.1ab	99.8a	53.0a
	Time	**	*	**	**	-
	Time x Treatment	**	ns	ns	**	-

Note: Mean within a column followed by the same letter are not significantly different at $P < 0.05$.

*, **, and *** indicate significance at $P < 0.05$, 0.01, 0.0001, respectively

† NS: not significant

Table 4-6. Mean extractable Ca(NO₃)₂ Cd, Pb, and Zn and diffusive gradients in thin films (DGT) Zn content of the control and amendment treated mine waste material 841 d (fall 2008) after time 0.

| Site | Treatment | Ca(NO₃)₂ Extractable Metals | | | DGT |
		Cd	Pb	Zn	Zn
		------------mg kg⁻¹------------			µg
A	CO	5.1a	11.5a	239.9a	70.4a
	LC	3.7ab	2.9a	192.5a	22.7b
	LCL	2.4ab	1.9a	65.8ab	7.8b
	LCLB	3.6ab	2.5a	99.8ab	15.9b
	HC	0.4b	1.3a	19.6b	4.3b
	HCL	0.6b	1.9a	21.6b	3.7b
	HCLB	0.5b	2.0a	22.0b	6.6b
B	CO	1.4	23.5	64.0a	26.0a
	LC	nd†	nd	9.4b	1.4b
	LCL	nd	nd	4.7b	1.7b
	LCLB	nd	nd	4.3b	1.5b
	HC	nd	nd	4.5b	1.2b
	HCL	nd	nd	4.5b	2.0b
	HCLB	nd	nd	5.4b	1.6b

Note: Mean within a column and for a specific site followed by the same letter are not significantly different at $P < 0.05$.
† nd: not detectable.

Table 4-7. Results of multiple linear regression analysis for each plant species.

---------------Switchgrass---------------			------------Smooth Pigweed------------		
Parameter	Estimate	r^2	Parameter	Estimate	r^2
Intercept	-49.23**	0.77***	Intercept	335.25***	0.68***
K	0.16***		K	-1.31***	
P	0.13***		Ca	-0.01*	
Na	-0.78*		Na	-63.22***	
Total N	21.68**		Total C	-12.64*	
Available Water	298.64*		Total N	94.65**	
			CEC	1.47*	

-------------Yellow Foxtail-------------			-----------Tufted Hairgrass-----------		
Parameter	Estimate	r^2	Parameter	Estimate	r^2
Intercept	268.52***	0.67***	Intercept	-51.68*	0.60***
DGT Zn	-282.74*		pH	10.20**	
Mg	0.06*		DGT Zn	-33.34*	
Total C	7.80*		Ca	0.02*	
CN Ratio	-5.77**		Mg	0.04*	
Available Water	223.16*		Electrical Conductivity	-38.10*	
			Total C	1.50*	

*, **, and *** indicate significance at $P < 0.05$, 0.01, 0.0001, respectively

CHAPTER 5 - Spectroscopic Investiation of Pb Speciation after the Addition of Different P Amendments to a Smelter-Contaminated Soil

5.1 Abstract

The stabilization of Pb upon additions of P to contaminated soils and mine spoil materials has been well documented. We hypothesized that the differences in efficacy of Pb stabilization in contaminated soils upon fluid or granular P amendment addition is due to different P reaction processes in and around fertilizer granules and fluid droplets. We used a combination of several synchrotron-based techniques, namely, spatially resolved micro-x-ray fluorescence (μ-XRF), micro-x-ray absorption near edge structure spectroscopy (μ-XANES), micro-extended-x-ray absorption fine structure spectroscopy (μ-EXAFS), and micro-x-ray diffraction (μ-XRD) to speciate Pb at two incubation times in a smelter-contaminated soil upon addition of several fluid and granular P amendments. The results indicated that the Pb phosphate mineral plumbogummite was an intermediate phase of pyromorphite formation. Additionally, all fluid and granular P sources were able to induce Pb phosphate formation, but fluid phosphoric acid (PA) was the most effective with time and distance from the treatment. Granular phosphate rock (PR) and triple super phosphate (TSP) amendments reacted to generate Pb phosphate minerals, with TSP being more effective at greater distances from the point of application. As a result, PA and TSP were the most effective P amendments for inducing Pb phosphate formation, but caution needs to be exercised when adding large additions of soluble P to the environment.

5.2 Introduction

Lead (Pb) is a natural constituent of all soils (Adriano, 2001). Soil concentrations of Pb continue to increase through mining, sewage sludge application, fossil fuel combustion, and

many chemical and other manufacturing industries (Adriano, 2001; Basta et al., 2005). A wide variety of health effects for Pb have been recognized (ATSDR, 2005), and the bioavailability of Pb in natural environments primarily depends on its chemical speciation. In contaminated soils and mine wastes, large fractions of Pb can exist in potentially bioavailable fractions. Therefore, considerable effort has been focused on developing cost-effective remediation technologies to reduce metal bioavailability and mobility in natural environments.

Previously, remediation efforts have principally consisted of removal of the contaminated material with subsequent back-filling with clean soil. However, this process is costly, time consuming, and requires a source of clean soil. Current research involves the potential to change the bioavailability of Pb *in situ* by altering its chemical speciation (Mench et al., 1994). Much of this research has been focused on the addition of P amendments to Pb contaminated soils to form Pb phosphates, particularly pyromorphite, which is one of the most stable Pb minerals under a wide range of environmental conditions (Nriagu, 1974). As a result, P amendments could be used to reduce the bioavailability/bioaccessibility of Pb in contaminated soils and mine wastes.

Immobilizing Pb as pyromorphite in soils has been extensively studied in the literature (Cao et al., 2003; Chappell and Scheckel, 2007; Chen et al., 2006; Cotter-Howells and Caporn, 1996; Hettiarachchi and Pierznyski., 2004; Hettiarachchi et al., 2000; Hettiarachchi et al., 2001; Lin et al., 2005; Ma et al., 1993, 1995; McGowen et al., 2001; Ruby et al., 1994; Scheckel and Ryan, 2002; Scheckel and Ryan, 2004; Yang et al., 2001; Yoon et al., 2007). Research has continued to explore the effect of different P sources on metal phosphate formation. These sources include phosphate rock (PR), diammonium phosphate (DAP), triple superphosphate (TSP), and phosphoric acid (PA) (Cao et al., 2003; Chappell and Scheckel, 2007; Hettiarachchi et al., 2000; Hettiarachchi et al., 2001; McGowen et al., 2001; Yang et al., 2001). All P sources

have resulted in the reduction of Pb bioavailability to a variety of organisms. This decline is hypothesized to be the result of metal phosphate formation. However, treatments could vary across soils due to the chemical heterogeneity of soil environments. Additionally, it is not well understood how the metal phosphate species formed might be influenced by P source or by distance in the soil from P-containing materials, which has implications for the amount of P that needs to be added and the degree of mixing that is required. For example, fluid P delivery systems should be more effective at producing metal phosphates due to the greater availability of P for reaction and a larger reaction zone. However, research in this area is lacking and is needed to better understand the influence of P sources in the Pb sequestration process.

One goal of Pb stabilization research is to measure the amount of available Pb that is converted to less soluble phosphate phases, but this is problematic in heterogeneous, non-equilibrated systems (Scheckel and Ryan, 2004). More recently, speciation of metals in complex environments has been achieved by using spatially-resolved synchrotron-based techniques, such as X-ray absorption spectroscopy (XAS), coupled with statistical analysis via linear combination fitting (LCF) or principal component analysis (PCA) (Isaure et al., 2002, Roberts et al., 2002, Scheckel and Ryan, 2004). This experimental approach combines the *in situ* capabilities of synchrotron-based techniques with thorough statistical analysis that allows one to compare unknown samples to well-characterized reference compounds (Scheckel and Ryan, 2004). Concerns with this procedure do exist because of the limited number of reference mineral compounds, but it has been suggested that the combined use of different synchrotron-based techniques could enhance mineral species identification (Manceau et al., 2002a). Therefore, a combination of μ-X-ray fluorescence (μ-XRF), μ-XAS, and μ-X-ray diffraction (μ-XRD) would allow one to locate trace-metal enriched areas (μ-XRF), determine the chemical environment (μ-

XAS), and identify the mineral form (μ-XRD). This approach was employed to accomplish the following objectives: 1) investigate how different P sources influence the Pb phosphate species formed, 2) quantify the amount of Pb phosphate minerals formed at a given distance from the P amendment, and 3) observe how speciation changes with reaction time.

5.3 Materials and Methods

Materials. The material used in this study was collected from an abandoned Pb/Zn smelter near Dearing, KS and is a smelter slag/soil mixture that has been previously studied (Hettiarachchi et al., 2001; Hettiarachchi et al., 2000). The material was collected from the upper 20 cm, sieved through a stainless steel 2-mm screen, air dried, and stored in plastic containers at room temperature.

Soil pH was measured in a 1:1 deionized water:soil mixture with a Ross Combination pH electrode (Thermo Orion, Beverly, MA). Total organic C was measured by dry combustion on a LECO CN-2000 Elemental Analyzer (LECO Corporation, St. Joseph, MI). Total P for contaminated soil and P amendments were determined by salicylic-sulfuric acid digestion (Bremner and Mulvaney, 1982) and extractable P by Mehlich-3 (Mehlich, 1984). Filtered digests/extracts were then analyzed colorimetrically for P content. Cation exchange capacity (CEC) was determined by ion displacement (Jaynes and Bigham, 1986). Nitric acid metal conctentrations were determined by digesting 2 g of material ($\leq$ 2-mm) with 20 mL of 4 *M* HNO_3 (trace metal grade) acid at 80 to 85°C for 4 h (Sposito et al., 1982). Filtered digests were then analyzed for Cd, Pb, and Zn by inductively coupled plasma-optical emission spectrometry (ICP-OES). Total "free" iron oxide content was estimated using the Na-citrate bicarbonate-dithionite method (Na-CBD) (Jackson et al., 1986). Extracts were analyzed for Fe using ICP-OES. Soil was analyzed for sand, silt and clay content by the pipette method as described by

Gee and Bauder (1986). See Table 5-1 for details. For bulk X-ray analyses, fractionation of sand, silt, and clay was done according to Jackson (1975). The bulk X-ray analyses were conducted with a Phillips X-ray diffractormeter (Phillips Electronic Instruments, Mahwah, NJ) with a theta compensating slit and curved crystal graphite monochromator. Measurements were taken using Cu Kα radiation at a wavelength of 1.54 Å and were made using a continuous scanning technique at a speed of 2° 2θ per minute. The potential was 35 kV, and the amperage 20mA.

Sample Preparation for X-ray Techniques. The treatments in this study included several P sources and a control that were reacted over two different time periods (4 and 52 weeks). The P sources included fluid phosphoric acid (PA) and ammonium polyphosphate (APP) and the granular sources phosphate rock (PR), monammonium phosphate (MAP), and triple super phosphate (TSP). In addition, a contaminated non-P amended control was prepared for comparison. MAP, APP, and TSP were commercially available fertilizer grade P sources and contained 221, 133, and 199 g P kg^{-1}, respectively. MAP and APP contain N in the ammonium form and each delivered 115 and 102 g N kg^{-1}, respectively. The PR was from Occidental Corp. (White Springs, FL) and had 144 g P kg^{-1}, while PA was technical grade phosphoric acid containing 314 g P kg^{-1}. For each treatment combination, a small amount of contaminated waste material (25% gravimetric water content) was placed in a plastic container. The P sources were added in a line across the center of the container so that 20 mg of P were provided by each source. The P additions were clearly marked with plastic toothpicks and covered by additional contaminated material. The containers were packed to a bulk density of 1.35 g cm^{-3}. The plastic containers were covered and allowed to incubate in the moist condition for 4 or 52 weeks. Once incubation time was 24 hours from being complete, the covers were removed from the plastic

containers, and they were placed in the greenhouse to air dry. The air-dried samples were then impregnated with Buehler EpoThin® two part (epoxy/hardener) resin (Beuhler LTD., Lake Bluff, IL, USA) and allowed to cure overnight. The hardened resin was then cut using a petrographic trim saw to expose the P treatments and surrounding waste material. Once exposed, the surface was polished to remove saw markings, cleaned with deionized water, dried, and cemented to polystyrene plastic (0.5-mm thick) using Hillquist Thin Section Epoxy A-B (Hillquist Inc., Denver, CO, USA). Polystyrene plastic was chosen instead of glass in an attempt to eliminate as much background noise in μ-XRD measurements. Once the cement was dry, thin sections were polished to a thickness of approximately 25-μm.

Synchrotron-based μ-XRF, -XAS, and -XRD Data Collection/Analyses. Micro-XRF maps, μ-XAS, and μ-XRD were collected at beamline 13-BM (GeoSoilEnviro Consortium of Advanced Radiation Sources) at the Advanced Photon Source at Argonne National Laboratory, Argonne, IL. All data were collected at ambient temperature in fluorescence mode with a Ge solid-state 13-element detector (Canberra Inc., Meriden, CT, USA) and μ-XRD spectra were collected with a MAR 345 Image Plate detector (MarUSA Inc., Evanston, IL, USA).

The samples were mounted on an x-y-θ stepping-motor stage. Fluorescence data for Pb were collected at ambient temperature for a given area (map sizes typically range from 3000- by 6000-μm) for all fluid and granular P treatments with a step size of 50-μm. Using the XRF maps, further investigation of four to six points of interest (POIs) (high relative concentrations) for Pb were determined moving outward from the point of P application. Figure 5-1 illustrates how POIs were selected. For granular sources, the centers of the point of application for different treatments were defined by the granule. Whereas in fluid treatments, the center of the point of application was estimated by distance from a plastic marker (toothpick) installed at the

time of P application.

For each sample, three replicates of μ-XAS spectra for each defined Pb POI were collected across the range of -200 to 600 eV above the L-edge of Pb (~13035 eV) in fluorescence mode. The μ-XAS spectra were also collected for several known standard Pb compounds. Standard Pb compounds include galena [PbS], anglesite [$PbSO_4$], cerussite [$PbCO_3$], hydrocerussite [$Pb_3(CO_3)_2(OH)_2$], leadhillite [$Pb_4(SO_4)(CO_3)_2(OH)_2$], magnetoplumbite [$PbFe_6Mn_6O_{19}$], plumboferrite [$Pb_2Mn_{0.2}Mg_{0.1}Fe_{10.6}O_{18.4}$], plumbojarosite [$PbFe_6(SO_4)_4(OH)_{12}$], plumbogummite [$PbAl_3(PO_4)_2(OH)_5 \cdot H_2O$], vaquelinite [$Pb_2Cu(CrO_4)(PO_4)(OH)$], hinsdalite [$PbAl_3(PO_4)(SO_4)(OH)_6$], and pyromorphite [$Pb_5(PO_4)_3Cl$]. In addition, the μ-XAS spectra were also colleted for Pb sorbed to ferrihydrite at pH of 6.

The collected Pb μ-XAS spectra for P treatments and reference compounds were processed using the IFEFFIT software package (Ravel and Newville, 2005). Due to high levels of background noise only μ-XANES spectra could be used for Pb data analysis. Processed experimental spectra were analyzed in a two-step process using Labview software for principal components analysis (PCA) and the IFEFFIT software package for linear combination fitting (LCF) (Ravel and Newville, 2005). Principal components analysis was used only to test the consistency of the fitting procedure and, therefore, results from PCA will not be presented. The region of 12985 to 13135 eV for Pb was isolated for Pb LCF. The linear combination procedure attempted to reconstruct the contaminated soil-P amendment spectra using all of the combinations of the reference spectra indicated by PCA.

For the LCF procedure, the combination with the lowest reduced χ^2 was chosen as the most likely set of components. The accuracy of LCF depends on the data quality and how well the reference spectra fit the experimental samples (Roberts et al., 2002). A reduced χ^2 value near

1 indicates a reliable fit. Because there are a limited number of reference spectra and problems obtaining ideal standards to use in the fits, the best-fit compositions may not give the true composition, but the results can be used to describe and compare the differences between treatments. To help remedy this problem, synchrotron-based μ-XRD can be teamed with μ-XAS to enhance mineral species identification (Manceau et al., 2002a; 2002b). X-ray diffraction is a more definitive technique than XAS, but minerals have to be crystalline in order to utilize XRD. Therefore, a μ-XRD (~17,500 eV) pattern was taken at each Pb POI to assist in species identification. For μ-XRD spectra, the data were processed using the Fit2D software package for integrating 2D Debye-Scherer rings to one-dimensional 2θ scans (Hammersley et al., 1996). The compound cerium dioxide (CeO_2) was used as the calibrant. Cerium was chosen because it is a relatively heavy element, so it will diffract higher energy X-rays very strongly. D-spacings were calculated using Fit2D software and matched to the d-spacings of known mineral species using the powder diffraction file search manual (JCPDS-International Centre for Diffraction Data, 1987).

To elucidate information on the movement and distribution of P upon the addition of P amendments, μ-XRF maps were collected at beamline 2-ID-D at the Advanced Photon Source, Argonne, IL. Thin sections, previously used at 13-BM, were peeled from the plastic slides and mounted onto a sample holder, which provided a sample thickness of approximately 25-μm. The sample holder was then placed on an x-y-θ stepping-motor stage. Fluorescence data for the P K-edge (2145.5 eV) were collected at ambient temperature for a 300- by 2000-μm area for all fluid and granular P treatments. A beam size of 500- by 500-nm with a step size of 5-μm was used and data were collected with a silicon drift detector. In addition, XRF spectra for two thin-film NIST multi-element standard reference materials (SRM 1832 and SRM 1833 for X-ray

fluorescence spectrometry) were collected for conversion of XRF signals to relative elemental concentrations, which allows for the quantification of elements. MAPS software version 1.6.0.4 was used to quantify the distribution of P for each XRF map. Data was used to produce a plot of concentrations as a function of distance from the P amendment.

5.4 Results and Discussion

Bulk Mineralogical Analyses. Bulk XRD techniques can only detect crystalline materials present in concentrations $\geq$ 10 to 20 g kg^{-1} (Ma et al., 1994), and direct identification of solid forms of many elements was not always possible by XRD. The mineralogy of the silt- (0.05 mm to 0.002) and clay-sized (< 0.002 mm) fractions indicated the presence of quartz, willemite, and galena, but peak intensities for these minerals were weak, suggesting that the minerals were present at concentrations near the detection limit or were amorphous. In fact, the clay-sized fraction consists largely of amorphous Fe oxide minerals (Table 5-1). This could have an impact on the movement of P and the formation of Pb phosphates since Fe oxide compounds have a high affinity for phosphates (Sims and Pierzynski, 2005). There was no evidence for the existence of Pb phosphate minerals in either mineral fraction analyzed.

Synchrotron-based Pb speciation in non-amended soil. The major Pb species present in non-amended soils include cerussite, galena, and sorbed Pb with smaller amounts of anglesite, magnetoplumbite, and plumboferrite. (Table 5-2) Because there were a limited number of standard spectra, there was some uncertainty associated with the LCF procedure, but μ-XRD analysis was used to further aid in species identification. Micro-XRD analysis of these samples confirmed the presence of cerussite (d-spacings of 3.59, 3.50, 2.49, 1.86, and 1.93) and galena (d-spacings of 2.97, 3.43, 2.10, and 1.79), for the control samples. No other Pb minerals were identified by μ-XRD in the control samples. Other studies, using either bulk or molecular

techniques, have established that galena, anglesite, cerussite, pyromorphite, and sorbed Pb species are the dominant forms of Pb present in non-amended contaminated soils/mine tailings (Cao et al., 2002; Ostergren et al., 1999; Scheckel and Ryan, 2004), which generally agrees with our data. Our results were most similar to those of Scheckel and Ryan (2004) where Pb phosphate minerals were not identified in untreated material.

Synchrotron-based speciation changes of Pb upon P amendment addition. The LCF analysis of the Pb μ-XANES spectra for different P amendments indicated the presence of Pb phosphate minerals for all treatments in the contaminated soil (Table 5-2). This implied that all P amendments were successful at converting Pb from more soluble species to the less soluble Pb phosphate minerals, namely plumbogummite and pyromorphite. However, results vary by P amendment, incubation time, and distance from the point of P application.

For PR incubated for 4 weeks, plumbogummite (54.6%) was the major Pb species adjacent to the granule. However, Pb phosphate minerals became an insignificant part of the fit as the distance from the PR granule increased, which was anticipated due to the low solubility of PR (Lindsay, 1979). After 52 weeks, the same trend still existed. There were significant amounts of Pb phosphates present adjacent to the granule, 25.8% plumbogummite and 19.4% pyromorphite, but as distance increased from 900 to 1200 μm the amount of plumbogummite decreased from 49.7% to 4.9%, respectively, which can again be attributed to the low solubility of PR.

To better illustrate the differences in P solubility, Figure 5-2 compares the average concentration of P with distance from the edge of a PR or TSP granule, and to PA droplet, relative to background soil P concentrations at 52 weeks. Phosphorus concentrations in the PR treatment reached background levels at approximately 1250 μm, which was the point where

plumbogummite was estimated to be 4.9% of the Pb species present. In contrast, P concentrations for the fluid PA amendment were evenly dispersed and at appreciably higher concentrations than background levels up to 2000 μm. Distribution of P in granular MAP (data not shown) and TSP (Figure 5-2) were intermediate to PR and PA, while P concentration distribution in APP, another fluid P source, (data not shown) was similar to PA. These results support other studies that indicated reduced lability of granular P compared to liquid fertilizer formulations (Hettiarachchi et al., 2006; Lombi et al., 2005). This may influence the effectiveness of the P amendment at immobilizing Pb. In particular, greater available P concentrations created by both fluid and highly soluble granular P sources could enhance the probability of Pb phosphate formation. However, more soluble P sources could increase eutrophication risk if P amended soil or mine waste were moved off site into surface waters.

Linear combination fitting for the PA amendment incubated for 4 weeks showed a relatively even distribution of Pb phosphates with distance from the point of P application (Table 5-2). However, the identity of the P solid phases did vary. At the 52 week sampling, pyromorphite (38.5%) became the dominant Pb mineral adjacent to the droplet, while the amount of plumbogummite increased at 1500 and 3300 μm when compared to similar distances at the 4 week period. Additionally, it appeared as if the P gradient was nonexistent at 52 weeks in the PA treatment, which was supported by the μ-XRF generated radial P distribution plot (Figure 5-2). As a result, the same amount of P applied through fluid PA versus that applied in granular PR influenced the Pb chemistry of a much larger area. However, there is concern that PA will lower soil pH (Cao et al., 2003), which could subsequently alter the bioavailability of Pb and other potentially toxic metals (Yoon et al., 2007).

Fluid APP could be used to supply P for reaction with less acidity, but it has not been

studied. After a 4 week incubation period, Pb phosphate minerals dominated the Pb speciation at 300 and 2400 μm from the point of APP application (Table 5-2). Additionally, this was the only amendment, either granular or fluid, besides TSP that induced pyromophite formation within weeks of application. At 3600 μm, the amount of Pb phosphates was significantly reduced as compared to 300 and 2400 μm, which suggested that P had not yet diffused to this point or P availability was limited by another variable. At 52 weeks, pyromorphite was the principal Pb mineral adjacent to the droplet, while at 1700 and 4200 μm the amount of Pb phosphates decreased. In contrast, the radial distribution plot for APP at 52 weeks showed an even distribution pattern similar to PA (Figure 5-2), suggesting that Pb phosphate formation was limited by other factors such as P sorption to Fe oxides (Sims and Pierzynski, 2005), lack of Pb for reaction, or competition of other metals for P (Lindsay, 1979; Nriagu, 1984).

Triple super phosphate, which is mostly monocalcium phosphate [$Ca(H_2PO_4)_2*H_2O$], was the only granular P source to induce pyromorphite formation at the 4 week incubation period (Table 5-2). This could be attributed to the small amount of acidity produced during granule dissolution that could potentially release Pb for reaction. In addition, the amount of Pb phosphate minerals produced by TSP during this time period was rather homogenous over distance, which suggested P movement similar to the fluid P sources. At 52 weeks, the amount of pyromorphite present increased with a subsequent decrease in plumbogummite when compared to the 4 week incubation. However, the amount of Pb phosphate minerals formed over the entire area did not increase dramatically with time, which suggested a rather rapid initial reaction with TSP followed by a slow transformation of existing Pb-phosphates. Results for granular MAP indicated the presence of Pb phosphates at all distances and incubation times. At the 4 week incubation period, the amount of Pb phosphates was lowest adjacent to the granule

and highest at 2300 μm. One possible explanation for this was that another phase was controlling the availability of Pb or P in the vicinity of the granule, thus limiting Pb phosphate formation. At 52 weeks, there was an increase in Pb phosphate minerals present, but the increase occurred at 1600 μm from the granule where pyromorphite was present suggesting that some other phase was limiting P or Pb availability for reaction.

Hettiarachchi et al. (2001) used the same soil contaminated by a Pb/Zn smelter slag and found that PA and a high application of TSP were more effective at reducing bioavailable Pb as measured by the physiologically-based extraction procedure (PBET) than PR. However, in the other four contaminated materials studied, PR was equally effective as compared to both PA and TSP. This study confirmed the findings of Hettiarachchi et al. (2001) in that PA and TSP were more effective than PR at reducing Pb bioavailability through the formation of insoluble Pb phosphate minerals in the smelter slag contaminated soil. We propose that the smelter slag soil contains more discrete Pb minerals that are dissolved by the acidity created by both PA and TSP, thus allowing more Pb to react with P resulting in more Pb phosphate minerals. Phosphate rock does not produce this acidity; therefore, less Pb phosphates are formed.

It has been suggested that pyromorphite formation is kinetically rapid and aging increases crystallinity in a pure system (Scheckel and Ryan, 2002). However, this study indicated that pyromorphite formation in natural soil environments may actually be rather slow. In contaminated soils, there are a number of potential constraints that could delay pyromorphite formation such as P availability, pH, presence of competing cations, the accessibility of Pb for reaction, and soil water content, and which could lead to the formation of intermediate Pb phosphate phases.

The formation of the Pb phosphate mineral plumbogummite has not been documented in

any study using P amendments to stabilize Pb contaminated soils or wastes. However, studies have not attempted to speciate and quantify Pb phosphate formation around individual P granules or droplets. According to Nriagu (1984), the precipitation of plumbogummite during soil formation processes cannot be ignored since the mineral is expected to be more stable than pyromorphite at near neutral pH, provided that both Pb and phosphate activities are low and Al is available for reaction. Pyromorphite is favored by acidic environments and high P/Pb availabilities. In previous studies, researchers saturated the soil solution with respect to phosphate to induce pyromorphite formation and the systems were homogenized by mixing (Chappell and Scheckel, 2007; Cotter-Howells and Caporn, 1996; Hettiarachchi et al., 2001; Ma et al., 1993, 1995; Scheckel and Ryan, 2002; Scheckel and Ryan, 2004; Yang et al., 2001), which would favor pyromorphite. It was acknowledged that under normal environmental conditions it is inevitable that Pb or P availability could be a rate limiting component for pyromorphite formation (Scheckel and Ryan, 2002), which could lead to the formation of other Pb phosphate minerals. This study was aimed to investigate the Pb speciation changes in the vicinity of an individual P source at the molecular level, which ultimately led to the identification of both plumbogummite and pyromorphite.

For most P sources, the amount of plumbogummite decreased with time with a subsequent increase in pyromorphite (Table 5-2). This suggests that plumbogummite may be a metastable Pb phosphate mineral that transforms into pyromorphite as P concentrations increase. Plumbogummite is not stable in acid soil environments with elevated Pb and P concentrations (Nriagu, 1984). Therefore, with increasing distance from the point of P application, plumbogummite remains the only Pb phosphate mineral present and this is likely due to low P availability.

Micro-XRD Analysis. Galena was the major mineral species detected by μ-XRD analysis (Table 5-3). This also was the major mineral species identified using XAS (Table 5-2). Other minerals that were identified by μ-XRD include cerussite, plumboferrite, magnetoplumbite, plumbogummite, and pyromorphite. Figure 5-3 is an example μ-XRD pattern for PA incubated for 52 weeks that indicates the presence of chloropyromorphite (d-spacings of 2.97, 2.89, 4.13, 3.27, 2.06, and 1.92) and plumboferrite (d- spacings of 2.64, 2.97, 2.44, and 1.68). Most interestingly, XRD was able to confirm many of the same trends that were discovered using XAS. For example, at the 4 week incubation, identification of plumbogummite and pyromorphite (Pb phosphates) by XRD was limited primarily to the area adjacent to the point of application, which was similar to the results using XAS. However, XAS on many occasions identified Pb phosphates at much greater distances than XRD, but XAS can determine mineral speciation on both amorphous and crystalline materials, while XRD was limited to only crystalline species. Crystallinity of Pb phosphates may be an issue at early incubation times At the 52 week incubation, Pb phosphate minerals can be identified by XRD at greater distances from the point of application indicating an increase in crystallinity. Pyromorphites have increased crystallinity, more distinguishable morphology, and greater stability with time after formation (Scheckel and Ryan, 2002; Stack et al., 2004), which would facilitate identification by XRD.

We have proposed that plumbogummite or plumbogummite-like minerals could be metastable Pb phases during the formation of pyromorphite. In addition, species could be poorly crystalline or amorphous in nature and would not strongly defract X-rays making them more difficult to detect by XRD. However, μ-XRD is a quick and powerful tool when coupled with μ-XAS. The use of μ-XRD supported the findings of the XAS work and reduced the inherent

uncertainty in the linear combination fitting procedure.

Environmental Implications. All P amendments were able to induce Pb phosphate formation *in situ*, thus potentially reducing Pb bioavailability. Pyromorphite formation is preceded by the formation of other metastable Pb phosphate minerals, such as plumbogummite, which was not been previously reported. This further suggests that Pb bioavailability may change with time. Fluid P amendments are superior at inducing Pb phosphate formation over a much greater area than granular P sources. Due to the amount of water that was added with fluid sources, the degree of P diffusion was much greater than in granular sources where the outward rate of P movement was slowed by the osmotic effects of the granule (Hettiarachchi et al., 2006). In general, PA was the most effective P amendment at producing Pb phosphates. This can be attributed to high levels of available P and the acidity of PA that can make Pb more readily available for reaction through the dissolution of discrete Pb minerals (Cao et al., 2003). Triple super phosphate was the most effective granular source at forming Pb phosphates. As a result, PA and TSP were the most effective P amendments at inducing Pb phosphate formation in this material, but monitoring is necessary to assure stability of Pb phosphates over time and to limit the impact of P on the environment.

5.5 References

Adriano, D.C. 2001. Trace elements in terrestrial environments: Biogeochemistry, bioavailability, and risks of metals. 2nd ed. Springer-Verlag, New York, NY.

Agency for Toxic Substances and Disease Registry. 2005. ToxFAQS for lead [Online]. Available at www.atsdr.cdc.gov/tfacts13.html (accessed 10 Oct. 2006). ATSDR, Atlanta, GA.

Basta, N.T., J.A. Ryan, and R.F. Chaney. 2005. Trace element chemistry in residual-treated soil: Key concepts and metal bioavailability. J. Environ. Qual. 34:49-63.

Bremner, J.M., and C.S. Mulvaney. 1982. Salicylic acid thiosulfate modification of the Kjeldhal method to include nitrate and nitrite. p. 621. *In* R.H. Miller and D.R. Keeney (ed.) Methods of soil analysis. Part 2. Am. Soc. Agron., Madison, WI.

Cao, X., L.Q. Ma, M. Chen, S.P. Singh, and W.G. Harris. 2002. Impacts of phosphate amendments on lead biogeochemistry at a contaminated site. Environ. Sci. Technol. 36:5296-5304.

Cao, R.X., L.Q. Ma, M. Chen, S.P. Singh, and W.G. Harris. 2003. Phosphate-induced metal immobilization in a contaminated site. Environ. Pollut. 122:19-28.

Chappell, M.A., and K.G. Scheckel. 2007. Pyromorphite formation and stability after quick lime neutralization in the presence of soil and clay sorbents. Environ. Chem. 4:109-113.

Chen, S.B., Y.G. Zhu, and Y.B. Ma. 2006. The effect of grain size of rock phosphate amendment on metal immobization in contaminated soils. J. Hazard Mater. 134:74-79.

Cotter-Howells, J., and S. Caporn. Remediation of contaminated land by formation of heavy metal phosphates. Appl. Geochem. 11:335-342.

Gee, G.W., and J.W. Bauder. 1986. Particle size analysis. p. 399-404. *In* A. Klute (ed.) Methods of soil analysis. Part 1. 2nd ed. Agron. Monogr. 9. ASA and SSSA, Madison, WI.

Hammersley, A.P., S.O. Svensson, M. Hanfland, A.N. Fitch, and D. Häusermann. 1996. Two-dimensional detector software: From real detector to idealized image or two-theta scan. High Press. Res. 14:235-248.

Hettiarachchi, G.M., E. Lombi, M.J. McLaughlin, D. Chittleborough, and P. Self. 2006. Density changes around phosphorus granules and fluid bands in a calcareous soil. Soil Sci. Soc. Am. J. 70:960-966.

Hettiarachchi, G.M., and G.M. Pierzynski. 2004. Soil lead bioavailabililty and in situ remediation of lead-contaminated soils: A review. Environ. Prog. 23:78-93.

Hettiarachchi, G.M., G.M. Pierzynski, and M.D. Ransom. 2000. In situ stabilization of soil lead using phosphorus and manganese oxide. Environ. Sci. Tech. 34:4614-4619.

Hettiarachchi, G.M., G.M. Pierzynski, and M.D. Ransom. 2001. In situ stabilization of lead using phosphorus. J. Environ. Qual. 30:1214-1221.

Isaure, M.-P., A. Laboudigue, A. Manceau, G. Sarret, C. Tiffreau, P. Trocellier, G. Lamble, J.-L. Hazemann, and D. Chateigner. 2002. Quantitative Zn speciation in a contaminated dredged sediment by μ-PIXE, μ-SXRF, EXAFS spectroscopy and principal components analysis. Geochim. Cosmochim. Acta 66:1549-1567.

Jackson, M.L. 1975. Soil chemical analysis-advanced course. 2nd ed. Dep. Soil Sci., Univ. of Wisconsin, Madison, WI.

Jackson, M.L., C.H. Lim, and L.W. Zelazny. 1986. Oxides, hydroxides and aluminosilicates. p. 101-150. *In* A. Klute (ed.) Methods of soil analysis. Part 1. 2nd ed. Agron. Monogr. 9. ASA and SSSA, Madison, WI.

Jaynes, W.F., and J.M. Bigham. 1986. Multiple cation-exchange capacity measurements on standard clays using a commercial mechanical extractor. Clays Clay Miner. 34:93-98.

JCPDS-International Centre for Diffraction Data. 1987. Powder diffraction file inorganic phases search manual (Hanawalt method). JCPDS, Swarthmore, PA.

Lin, C.W., J. Lian, and H.H. Fang. 2005. Soil lead immobilization using phosphate rock. Water Air Soil Pollut. 161:113-123.

Lindsay, W.L. 1979. Chemical equilibria in soils. Wiley, New York, NY.

Kilgour, D.W., R.B. Moseley, M.O. Barnett, K.S. Savage, and P.M. Jardine. Potential negative consequences of adding phosphorus-based fertilizers to immobilize lead in soil. J. Environ. Qual. 37:1736-1740.

Lombi, E., M.J. McLaughlin, C. Johnston, R.D. Armstrong, and R.E. Holloway. 2005. Mobility, solubility, and lability of fluid and granular forms of P fertilizer in caclcareous and non-calcareous soils under laboratory conditions. Plant Soil 269:25-34.

Ma, Q.Y., T.J. Logan, and S.J. Traina. 1995. Lead immobilization from aqueous solutions and contaminated soils using phosphate rocks. Environ. Sci. Technol. 29:1118-1126.

Ma, Q.Y., T.J. Logan, S.J. Traina, and J.A. Ryan. 1994. Effects of NO_3^-, Cl^-, F^-, SO_4^{2-}, and CO_3^{2-} on Pb^{2+} immobilization by hydroxyapatite. Environ. Sci. Technol. 28:408-418.

Ma, Q.Y., S.J. Traina, T.J. Logan, and J.A. Ryan. 1993. In situ lead immobilization by

apatite. Environ. Sci. Technol. 27:1803-1810.

Manceau, A., M.A. Marcus, and N. Tamura. 2002a. Quantitative speciation of heavy metals in soils and sediments by X-ray techniques. Rev. Mineral. Geochem. 49:321-428.

Manceau, A., N. Tamura, M.A. Marcus, A.A. MacDowell, R.S. Celestre, R.E. Sublett, G. Sposito, and H.A. Padmore. 2002b. Deciphering Ni sequestration in soil ferromanganese nodules by combining X-ray fluorescence, absorption, and diffraction at micrometer scales of resolution. Am. Mineral. 87:1494-1499.

Mehlich, A. 1984. Mehlich 3 soil test extractant: A modification of Mehlich-2 extractant. Commun. Soil Sci. Plant Anal. 15(12): 1409-1416.

Mench, M., V. Didier, M. Loffler, Am. Gomez, and P. Masson. 1994. A mimicked in-situ remediation study of metal-contaminated soils with emphasis on Cd and Pb. J. Environ. Qual. 23:58-63.

McGowen, S.L., N.T. Basta, and G.O. Brown. 2001. Use of diammonium phosphate to reduce heavy metal solubility and transport in smelter-contaminated soil. J. Environ. Qual. 30:493-500.

Nriagu, J.O. 1974. Lead orthophosphates-IV. Formation and stability in the environment. Geochim. Cosmochim. Acta 38:887-989.

Nriagu, J.O. 1984. Formation and stability of base metal phosphates in soils and sediments. p. 318-329. *In* J.O. Nriagu and P.B. Moore (ed.) Phosphate Minerals. Springer, London.

Ostergren, J.D., G.E. Brown Jr., G.A. Parks, and T.N. Tingle. 1999. Quantitative speciation of lead in selected mine tailings from Leadville, CO.

Ravel, B., and M. Newville. 2005. ATHENA, ARTEMIS, HEPHAESTUS: Data analysis for X-ray absorption spectroscopy using IFEFFIT. J. Synchrotron Radiat. 12:537-541.

Roberts, D.R., A.C. Scheinost, D.L. Sparks. 2002. Zinc speciation in a smelter-contaminated soil profile using bulk and microspectroscopic techniques. Envron. Sci. Technol. 36:1742-1750.

Ruby, M.V., A. Davis, and A. Ncholson. 1994. In situ formation of lead phosphates in soils as a method to immobilize lead. Environ. Sci. Technol. 28:646-654.

Scheckel, K.G., and J.A. Ryan. 2002. Effects of aging and pH on dissolution kinetics and stability of chloropyromorphite. Environ. Sci. Technol. 36:2198-2204.

Scheckel, K.G., and J.A. Ryan. 2004. Spectroscopic sceciation of lead in phosphate-amended soils. J. Environ. Qual. 33:1288-1295.

Sims, J.T., and G.M. Pierzynski. 2005. Chemistry of phosphorus in soils. *In* M.A. Tabatabai and D.L. Sparks (ed.) Chemical processes in soils. SSSA Book Ser. 8. SSSA. Madison, WI.

Sposito, G., L.J. Lund, and A.C. Chang. 1982. Trace metal chemistry in arid-zone field soils amended with sewage sludge: I. Fractionation of Ni, Cu, Zn, Cd, and Pb in solid phases. Soil Sci. Soc. Am. J. 46:260-264.

Stack, A.G., R. Erni, N.D. Browning, and W.H. Casey. 2004. Pyromorphite growth on lead-sulfide surfaces. Environ. Sci. Technol. 38:5529-5534.

Yang, J., D.E. Mosby, S.W. Casteel, and R.W. Blanchar. 2001. Lead immobilization using phosphoric acid in a smelter-contaminated urban soil. Environ. Sci. Technol. 35:3553-3559.

Yoon, J.K., X.D. Cao, and L.Q. Ma. 2007. Application methods affect phosphorus-induced lead immobilization from a contaminated soil. J. Environ. Qual. 36:373-378.
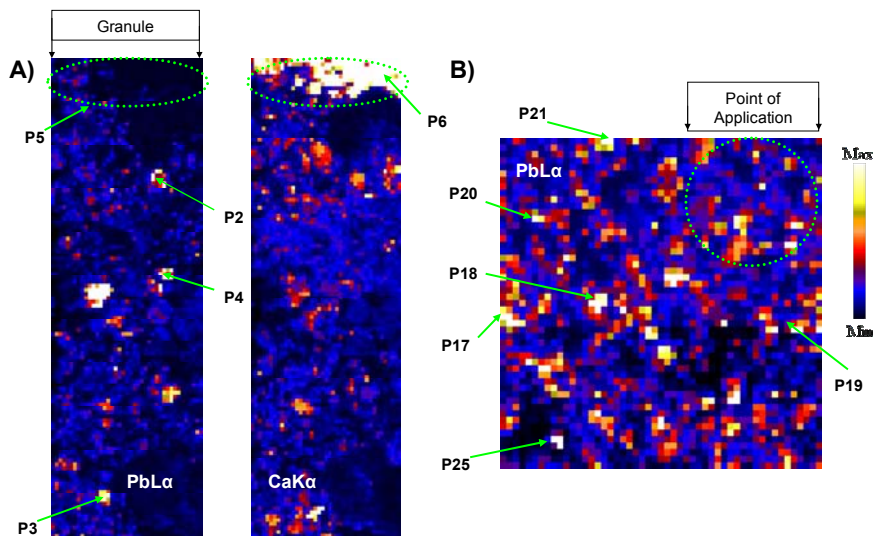
Figure 5-1. Micro-X-ray fluorescence maps of a) Pb and Ca for soil incubated with PR for 1 month and b) Pb for soil incubated with PA for 1 month. Area of a single map is a) 2000- by 6000-µm and b) 2500- by 2500- µm. The color scheme used ranges from white or yellow for high fluorescence signal to blue or black for low fluorescence signal. Shading is relative across each map. The markers P1 to P6 in a) and P17 to P25 in b) represent locations for which µ-X-ray absorption near-edge structure (XANES) and µ-X-ray diffraction (XRD) analyses were conducted. Calcium is shown in a) to illustrate the location of a PR granule.
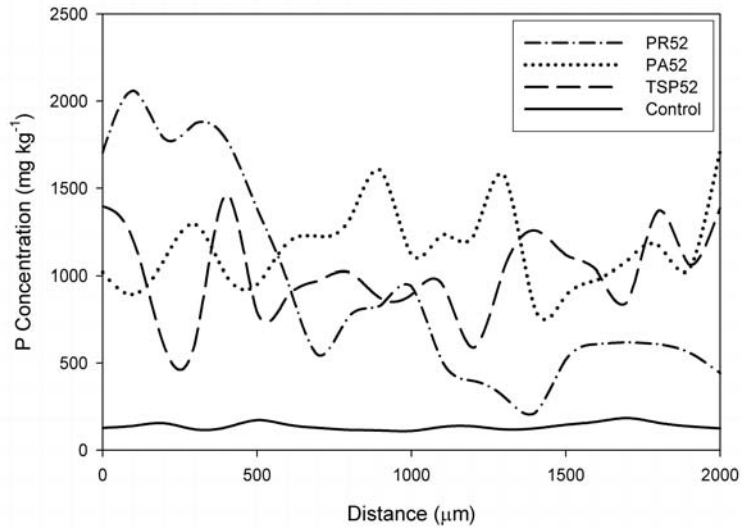
Figure 5-2. A radial distribution plot at 52 weeks for P generated by using μ-XRF maps for soils treated with PR, PA, and TSP. Point of application is at 0 μm. The solid line represents the background P concentration measured across the control soil. PR52: phosphate rock at 52 weeks, PA52: phosphoric acid at 52 weeks, TSP52: triple super phosphate at 52 weeks, and control: amended sample.
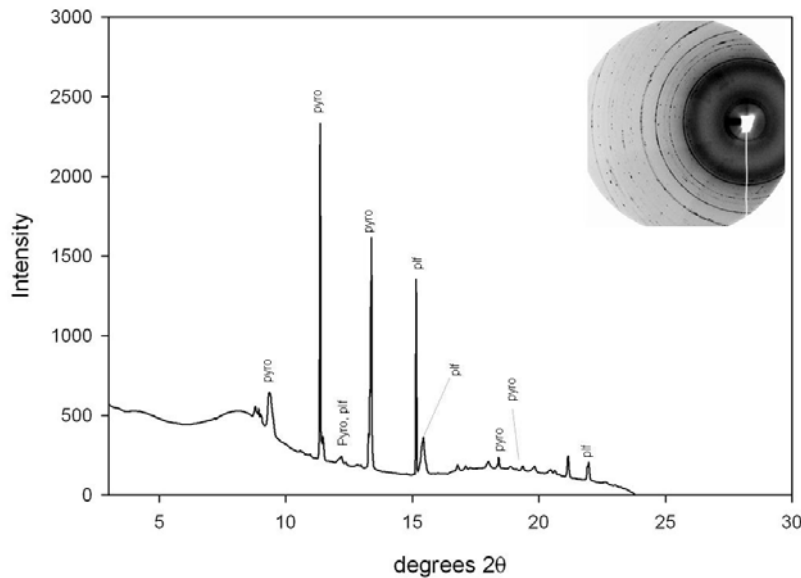
Figure 5-3. Micro-XRD pattern for treatment PA52 at 400 μm from the center of treatment. Original Debye-Sherer rings are located in the top-right hand corner of the graph. Species detected are pyro (chloropyromorphite [$Pb_5(PO_4)_3(Cl)$] with d-spacings of 2.97, 2.89, 4.13, 3.27, 2.06, and 1.92) and plf (plumboferrite [$Pb_2Mn_{0.2}Mg_{0.1}Fe_{10.6}O_{18.4}$] with d-spacings of 2.64, 2.97, 2.44, and 1.68).

186

Table 5-1. Selected soil properties.

Property	Value
pH	6.4
Total organic C, g kg^{-1}	39.7
Total P, mg kg^{-1}	152
Mehlich-3 extractable P, mg kg^{-1}	18.0
Na-CBD Fe mg kg^{-1}	38000
Total Pb, mg kg^{-1}	24300
Total Zn, mg kg^{-1}	72900
Total Cd, mg kg^{-1}	103
Cation exchange capacity, cmolc kg^{-1}	42.3
Sand, mg kg^{-1}	764
Silt, mg kg^{-1}	164
Clay, mg kg^{-1}	72

Table 5-2. Percentages of Pb species from selected POIs for control and P treated soils as determined by linear combination fitting of µ-X-ray absorbtion near-edge structure (µ-XANES) spectra 4 and 52 weeks after P amendment addition. Typical uncertainties in the percentages listed for each standard component are 5%.

Sample †	Distance ‡	Ce#	Ga	Pg	Py	Mp	Pf	Ag	SPb	χ2††
Control	--	54.2	3.1	--	--	42.7	--	--	--	0.18
Control	--	--	13.9	--	--	--	3.9	17.8	64.4	0.62
Control	--	--	51.2	--	--	--	9.4	39.4	--	0.58
PR4	100	--	36.3	54.6	--	5.8	3.3	--	--	0.72
PR4	2200	62.3	30.1	10.5	--	--	--	--	--	0.22
PR4	5100	--	55.3	1.2	--	15.4	--	--	28.1	0.28
PR52	100	--	21.7	25.8	19.4	--	33.1	--	--	0.19
PR52	900	36.3	14.1	49.7	--	--	--	--	--	0.15
PR52	1200	--	43.7	4.9	--	--	22.6	28.7	--	0.23
TSP4	100	--	43.1	35.2	8.4	--	13.2	--	--	0.30
TSP4	1800	--	59.3	31.2	--	9.5	--	--	--	0.55
TSP4	5200	--	47.1	30.7	--	16.6	5.7	--	--	0.17
TSP52	200	67.2	--	13.5	19.3	--	--	--	--	0.66
TSP52	2000	--	45.1	32.6	--	--	--	22.3	--	0.27
TSP52	3100	39.5	24.2	36.3	--	--	--	--	--	0.19
MAP4	200	--	47.7	16.6	--	35.7	--	--	--	0.24
MAP4	1500	--	--	7.7	--	--	28.2	25.3	38.8	0.86
MAP4	2300	--	59.9	31.5	--	--	8.6	--	--	0.39
MAP52	100	--	51.4	31.1	--	17.5	--	--	--	0.10
MAP52	1600	30.9	--	42.5	15.3	11.3	--	--	--	0.86
MAP52	3600	--	63.4	29.6	--	--	--	--	7.0	0.28
PA4	300	--	49.0	31.8	--	--	19.2	--	--	0.28
PA4	1800	--	72.6	27.4	--	--	--	--	--	0.11
PA4	2500	36.0	46.6	17.4	--	--	--	--	--	0.83
PA52	400	--	17.5	--	38.5	8.5	35.4	--	--	0.81
PA52	1500	--	43.1	56.9	--	--	--	--	--	0.10
PA52	3300	--	51.8	48.2	--	--	--	--	--	0.13
APP4	300	29.5	11.4	37.6	21.5	--	--	--	--	0.50
APP4	2400	--	36.9	56.0	7.1	--	--	--	--	0.37
APP4	3600	--	89.4	10.6	--	--	--	--	--	0.38
APP52	300	--	20.6	--	56.4	4.5	18.5	--	--	0.56
APP52	1700	--	45.0	9.7	--	37.0	--	--	8.3	0.17
APP52	4200	--	65.0	13.6	--	21.4	--	--	--	0.11

† Control: non-P amended; PR: Phophate rock; TSP: Triple super phosphate; MAP: Monammonium phosphate; PA: Phosphoric acid; APP: Ammonium polyphosphate. Number following treatment indicates incubation time (4 or 52 weeks).

‡ Distance in µm from the P treatment. For fluid sources (PA and APP) this distance begins at the approximate center of the point of application. For granular sources (PR, TSP, and MAP) this distance begins at the edge of the granule. Points of interest for the controls were taken randomly where high relative Pb concentrations were present.

Ce: Cerussite, Ga: Galena, Pg: Plumbogummite, Py: Pyromorphite, Mp: Magnetoplumbite, Pf: Plumboferrite, Ag: Anglesite, SPb: Sorbed Pb

†† Values closer to 1 indicate more reliable fits.

Table 5-3. A summary of μ-XRD analysis for Pb POI's that corresponds to Pb POI's selected for μ-XAS in Table 5-2.

Sample†	Distance ‡	Minerals Detected by μ-XRD Analysis
PR4	100	Galena, Plumbogummite
PR4	2200	Cerussite
PR4	5100	Galena
PR52	100	Pyromorphite, Plumboferrite
PR52	900	Cerussite, Plumbogummite
PR52	1200	Galena, Plumboferrite
TSP4	100	Galena, Plumbogummite
TSP4	1800	Galena
TSP4	5200	Galena
TSP52	200	Cerussite, Pyromorphite
TSP52	2000	Galena
TSP52	3100	Cerussite, Plumbogummite
MAP4	200	Galena, Magnetoplumbite
MAP4	1500	Plumboferrite
MAP4	2300	Galena
MAP52	100	Galena
MAP52	1600	Plumbogummite
MAP52	3600	Galena
PA4	300	Galena
PA4	1800	Galena
PA4	2500	Cerussite, Galena
PA52	400	Pyromorphite, Plumboferrite
PA52	1500	Galena, Plumbogummite
PA52	3300	Galena, Plumbogummite
APP4	300	Plumbogummite, Pyromorphite
APP4	2400	Galena, Plumbogummite
APP4	3600	Galena
APP52	100	Pyromorphite
APP52	1700	Galena, Magnetoplumbite
APP52	4200	Galena, Magnetoplumbite

† Control: non-P amended; PR: Phophate rock; TSP: Triple super phosphate; MAP: Monammonium phosphate; PA: Phosphoric acid; APP: Ammonium polyphosphate. Number following treatment indicates incubation time (4 or 52 weeks).

‡ Distance in μm from the P treatment. For fluid sources (PA and APP) this distance begins at the approximate center of the point of application. For granular sources (PR, TSP, and MAP) this distance begins at the edge of the granule. Points of interest for the controls were taken randomly where high relative Pb concentrations were present.

CHAPTER 6 - Speciation of Zn as Influenced by P addition in a Pb/Zn Smelter-Contaminated Soil

6.1 Abstract

The use of P to immobilize Pb in contaminated soils has been well documented. However, the influence of P on Zn speciation has not been documented, and these two metals often occur as co-contaminants. We hypothesized that additions of P would induce Zn phosphate formation and fluid P sources would be more effective. A combination of different synchrotron-based techniques, namely, spatially resolved micro-x-ray fluorescence (μ-XRF), extended micro-x-ray absorption fine structure spectroscopy (μ-EXAFS), and micro-x-ray diffraction (μ-XRD) was used to speciate Zn at two incubation times in a soil contaminated from a Pb/Zn smelter after addition of fluid and granular P amendments. Phosphate rock (PR), triple super phosphate (TSP), monammonium phosphate (MAP), and fluid ammonium polyphosphate (APP) induced Zn phosphate formation. APP was more effective at greater distances from the point of P application. Phosphoric acid increased the presence of soluble Zn species because of increased acidity. This has implications for enhanced Zn bioavailability, which may negatively impact vegetation and other sensitive organisms. While additions of P immobilize Pb, this practice needs close monitoring due to potential increases in Zn solubility in Pb/Zn co-contaminated soils and wastes.

6.2 Introduction

Zinc is a natural constituent of all soils and is ubiquitous in the environment (Adriano, 2001). Soil concentrations of Zn continue to increase through mining and smelting operations, tire wear, agricultural production, sewage sludge application, use of fossil fuels, and other industrial practices (Adriano, 2001; Basta et al., 2005; Councell et al., 2004). The primary risk

associated with Zn is phytotoxicity (Brown et al., 2003; Chaney, 1993), which can leave soils devoid of vegetation, thus increasing the exposure and movement of Zn and other contaminants commonly associated with Zn, most notably Cd and Pb. The bioavailability of heavy metals in natural environments primarily depends on their chemical speciation. Considerable effort has been put forth to develop cost-effective remediation strategies to reduce metal mobility and bioavailability in the environment.

Heavy metals present an unacceptable risk to human and ecological health and often are causative agents for soil remediation. Commonly used methods have involved excavation and disposal of contaminated materials, but recently less expensive and less invasive *in situ* solutions have been favored (Iskandar and Adriano, 1997). *In situ* stabilization using P has the potential to decrease metal solubility through the formation of metal-phosphate precipitates, thus increasing long-term stability by forming less soluble, more stable compounds (Mench et al., 1998). The use of P to immobilize Pb in soils, presumably through the formation of Pb phosphates such as pyromorphite has been extensively studied (Cao et al., 2003; Hettiarachchi and Pierzynski, 2004; Hettiarachchi et al., 2000; Kilgour et al., 2008; Scheckel and Ryan, 2004; Yoon et al., 2007). However, the immobilization of Zn has been researched less, although, it has been included in a few studies because of its close geologic association with Pb (Cao et al., 2003; Cotter-Howells and Caporn, 1996; Hettiarachchi and Pierzynski, 2002; Ma et al., 1994; McGowen et al., 2001). Under normal environmental conditions, it was proposed that Zn phosphates form when P is added (Nriagu, 1984). However, evidence for Zn phosphate formation has been inconclusive. Thus, the influence of added P and different P amendments on Zn speciation is not known, but needs to be investigated. It is hypothesized that added P will be able to induce Zn phosphate formation and fluid P delivery systems will be more effective at this process. Research in this

area is lacking and is needed to understand how P additions could impact Zn speciation in Pb/Zn contaminated soils.

The arrival of spatially resolved synchrotron-based techniques, such as extended X-ray absorption fine structure (EXAFS) spectroscopy, coupled with linear combination fitting (LCF) has allowed researchers to speciate metals in complex environments, which was difficult to achieve in the past (Roberts et al., 2002; Scheckel and Ryan, 2004). This technique combines the *in situ* capabilities of synchrotron-based techniques with statistical analysis to compare unknown samples to known compounds (Scheckel and Ryan, 2004). Concerns with this procedure do exist because of the limited number of reference mineral compounds, but it has been suggested that multiple synchrotron-based techniques could be paired to enhance mineral species identification (Manceau et al., 2002a). For example, μ-X-ray fluorescence (μ-XRF), μ-EXAFS, and μ-X-ray diffraction (μ-XRD) would allow one to locate trace-metal enriched areas (μ-XRF), determine the chemical environment (μ-EXAFS), and identify the mineral form (μ-XRD). This approach was employed to achieve the following objectives: 1) investigate if added P induces Zn phosphate formation in a Pb/Zn contaminated soil, 2) determine if different P sources influence Zn speciation differently, and 3) observe how speciation changes with distance from the amendment and reaction time.

6.3 Materials and Methods

Materials. The contaminated material used in this study was collected from an abandoned Pb/Zn smelter near Dearing, KS and is a smelter slag contaminated soil that has been previously studied (Hettiarachchi and Pierzysnki, 2002; Hettiarachchi et al., 2001; Hettiarachchi et al., 2000). The material was collected from the upper 20 cm, sieved through a stainless steel 2-mm screen, air dried, and stored in plastic containers at room temperature.

192

Soil pH was measured in a 1:1 deionized water:soil mixture with a Ross Combination pH electrode (Thermo Orion, Beverly, MA). Total organic C was measured by dry combustion on a LECO CN-2000 Elemental Analyzer (LECO Corporation, St. Joseph, MI). Total P for contaminated soil and P amendments was determined by salicylic-sulfuric acid digestion (Bremner and Mulvaney, 1982). Filtered digests were then analyzed colorimetrically for P content. Cation exchange capacity (CEC) was determined by ion displacement (Jaynes and Bigham, 1986). Nitric acid extractable metals were determined by digesting 2 g of material ($\leq$ 2-mm) with 20 mL of 4 M HNO_3 (trace metal grade) acid at 80 to 85°C for 4 h (Sposito et al., 1982). Filtered digests were then analyzed for Pb and Zn by inductively coupled plasma-optical emission spectrometry (ICP-OES). Total "free" iron oxide content was estimated using the Na-citrate bicarbonate-dithionite method (Na-CBD) (Jackson et al., 1986). Extracts were analyzed for Fe using ICP-OES. Soil was analyzed for sand, silt, and clay content by the pipette method as described by Gee and Bauder (1986). For bulk X-ray analyses, fractionation of sand, silt, and clay was done according to Jackson (1975). The bulk X-ray analyses were conducted with a Phillips X-ray diffractormeter (Phillips Electronic Instruments, Mahwah, NJ) with a theta compensating slit and curved crystal graphite monochromator. Measurements were taken using Cu Kα radiation at a wavelength of 1.54 Å and were made using a continuous scanning technique at a speed of 2° 2θ per minute. The potential was 35 kV, and the amperage 20mA.

Sample Preparation for X-ray Techniques. The treatments in this study included several P sources and a control that were reacted over two time periods (4 and 52 weeks). The P sources included fluid phosphoric acid (PA) and ammonium polyphosphate (APP) and the granular sources phosphate rock (PR), triple super phosphate (TSP), and monammonium phosphate (MAP). In addition, a contaminated non-P amended control was prepared for comparison. APP,

MAP, and TSP were commercially available fertilizer grade P sources containing 133, 221, and 199 g P kg^{-1}, respectively. In addition, MAP and APP contain N, which is in the ammonium form and deliver 115 and 102 g N kg^{-1}, respectively. The PR was from Occidental Corp. (White Springs, FL) and had 144 g P kg^{-1}, while PA was technical grade phosphoric acid containing 314 g P kg^{-1}. For each treatment combination, a small amount of contaminated waste material (25% gravimetric water content) was placed in a plastic container. The P sources were added in a line across the center of the container so that 20 mg of P were provided by each source. The P additions were clearly marked with plastic toothpicks and covered by additional contaminated material. The containers were packed to a bulk density of 1.35 g cm^{-3}. The plastic containers were covered and allowed to incubate in the moist condition for 4 or 52 weeks. Once incubation time was 24 hours from being complete, the covers were removed from the plastic containers, and they were placed in the greenhouse to air dry. The air-dried samples were then impregnated with Buehler EpoThin® two part (epoxy/hardener) resin (Beuhler LTD., Lake Bluff, IL, USA) and allowed to cure overnight. The hardened resin was then cut using a petrographic trim saw to expose the P treatments and surrounding waste material. Once exposed, the surface was polished to remove saw markings, cleaned with deionized water, dried, and cemented to polystyrene plastic (0.5-mm thick) using Hillquist Thin Section Epoxy A-B (Hillquist Inc., Denver, CO, USA). Polystyrene plastic was chosen instead of glass in an attempt to eliminate background noise in μ-XRD analysis. When the cement was dry, thin sections were polished to a thickness of approximately 25-μm.

Synchrotron-based μ-XRF, -EXAFS, and -XRD Data Collection/Analyses. Micro-XRF maps, -EXAFS, and -XRD were collected at beamline 13-BM (GeoSoilEnviro Consortium of Advanced Radiation Sources) at the Advanced Photon Source at Argonne National Laboratory,

Argonne, IL. All data were collected in fluorescence mode with a Ge solid-state 13-element detector (Canberra Inc., Meriden, CT, USA), while μ-XRD spectra were collected with a MAR 345 Image Plate detector (MarUSA Inc., Evanston, IL, USA).

The samples were mounted on an x-y-θ stepping-motor stage. Fluorescence data for Zn were collected at ambient temperature for a given area (commonly 3000- by 6000-μm) for all fluid and granular P treatments with a step size of 50-μm. Using the XRF maps, further investigation of four to six points of interest (POIs) (high relative concentrations) for Zn were selected moving outward from the point of fertilizer application. Figure 6-1 illustrates how POIs were collected. For granular sources, the centers of the point of application for different treatments were defined by the granule, while in fluid treatments; the center of the point of application was estimated by distance from a plastic marker installed at the time of P application.

For each sample, three replicates of μ-EXAFS spectra for each defined Zn POI were collected across the range of -200 to 600 eV above the K-edge of Zn (~9659 eV) in fluorescence mode. The μ-EXAFS spectra were also collected for several known Zn compounds for comparison. Known Zn compounds include: Zn sorbed to ferrihydrite [$Fe_2^{3+}O_3 \cdot 0.5H_2O$], aqueous Zn, $ZnSO_4$, $Zn(OH)_2$, synthetic ZnS, sphalerite [ZnS], smithsonite [$ZnCO_3$], zincite [ZnO], gahnite [$ZnAl_2O_4$], hydrozincite [$Zn_5(CO_3)_2(OH)_6$], willemite [Zn_2SiO_4], franklinite [$Zn_{0.6}Mn_{0.3}^{2+}Fe_{0.1}^{2+}Fe_{1.5}^{3+}Mn_{0.5}^{3+}O_4$], hemimorphite [$Zn_4Si_2O_7(OH)_2 \cdot H_2O$], Zn-Al layered double hydroxide (LDH) with a nitrate interlayer, Zn-Al LDH with a silicate interlayer, zinc aluminum silicate [$ZnAl_2Si_2O_8$], scholzite [$CaZn_2(PO_4)_2 \cdot 2H_2O$], and hopeite [$Zn_3(PO_4)_2 \cdot 4H_2O$]. The Zn-Al layered double hydroxides have the basic formula [$Zn_{x-1}Al_x(OH)_2$](A^{m-})$_{x/m}$ * nH_2O, where A^{m-} is the exchangeable interlayer anion (Drits and Bookin, 2001).

The collected Zn μ-EXAFS spectra for P treated materials and reference compounds were

processed using the IFEFFIT software package (Newville, 2001; Ravel and Newville, 2005). The Zn spectra were averaged, normalized, background corrected, and then transformed to k space (where k is the photoelectron number) and weighted to k^3 to reduce dampening. Processed experimental spectra were analyzed in a two-step procedure using Labview software for principal components analysis (PCA) and the IFEFFIT software package for linear combination fitting (LCF). Principal components analysis was used only to test the consistency of the fitting procedure and, therefore, results from PCA are not presented. Experimental Zn spectra were fit between 2 and 10 k space. The linear combination procedure attempted to reconstruct the contaminated soil-P amendment spectra using all of the combinations of the reference spectra that were identified by PCA. Due to detector failure, EXAFS data for MAP and APP at 52 and MAP at 4 weeks are not available. However, μ-XRD data were collected for these treatments.

For the LCF procedure, the combination with the lowest reduced χ^2 was chosen as the most likely set of components. The accuracy of LCF procedure depends on the data quality and how well the reference spectra fit the experimental samples (Roberts et al., 2002). A reduced χ^2 near a value of 1 indicates a reliable fit. Because there are a limited number of reference spectra and problems obtaining standards to use in the fits, the best-fit compositions may not give the true composition, but the results can be used to describe and compare treatment differences. To enhance the certainty in mineral identification, synchrotron-based μ-XRD can be teamed with μ-EXAFS (Manceau et al., 2002a; 2002b). Therefore, μ-XRD (~17,500 eV) patterns were taken at each Zn POI to assist in Zn species identification. X-ray diffraction is a more definitive technique than EXAFS, but minerals have to be crystalline in order to utilize XRD, while EXAFS can identify both crystalline and non-crystalline species. Micro-XRD spectra were processed using the Fit2D software package for integrating 2D Debye-Scherer rings to one-

dimensional 2θ scans (Hammersley et al., 1996). D-spacings were calculated using Fit2D software and matched to the d-spacings of known mineral species using the powder diffraction file search manual (JCPDS-International Centre for Diffraction Data, 1987).

6.4 Results and Discussion

Soil Analysis and Bulk Mineralogy. The Pb and Zn concentrations were 24,300 and 72,900 mg kg^{-1}, respectively, in the contaminated material. The pH was 6.4, total P was 152 mg kg^{-1}, and organic C content was 40 g kg^{-1}. The P content was much lower than the average P content (600 mg kg^{-1}) reported in soils and was therefore, unlikely to act as a control on Zn speciation due to the high concentration of Zn in the material (Lindsay, 1979). Particle size analysis revealed that the sand, silt, and clay contents were 764, 164, and 72 g kg^{-1}, respectively. The CEC was estimated to be 42 $cmol_c$ kg^{-1} and the Na-CBD extractable Fe 38,000 mg kg^{-1}, which could influence Zn sorption. High levels of Fe were also detected in μ-XRF analyses (Chapter 5).

Bulk XRD techniques of the sand, silt, and clay sized fractions indicated the presence of quartz and willemite. However, peak intensities for these minerals were weak, suggesting that minerals were present at concentrations at or near the detection limit or were poorly crystalline. Ma et al. (1994) acknowledged that crystalline materials need to be present in concentrations ≥10 to 20 g kg^{-1} to be detected by bulk XRD. The presence of organic C and amorphous Fe oxide minerals could cause Zn to be sorbed rather than in discrete mineral phases, thus making them undetectable by XRD. Additionally, the occurrence of Fe could impact Zn phosphate formation since Fe oxides have high affinities for P (Sims and Pierzynski, 2005). No Zn phosphate minerals were detected before treatment with P in bulk XRD analyses.

Zn Speciation by μ-EXAFS. The k^3-weighted Zn μ-EXAFS spectra and their LCF's (dashed lines) for a control sample and Zn POI's at distances of 100- to 400-μm from the center of a

197

droplet or the edge of a granule at two incubation times (4 and 52 weeks) are given in Figure 6-2. The spectra from the treated soils appear to be different than the control, which is an indication that P amendments were affecting Zn speciation. Estimates of the amounts of Zn species present in the control sample are given in Table 6-1. Major Zn species identified were willemite, hemimorphite, franklinite, $ZnSO_4$, and Zn-Al LDH nitrate. Micro-XRD analyses of these same POI's confirmed the presence of willemite and hemimorphite, which are both Zn silicate minerals. Other studies using EXAFS discovered that Zn primarily exists as willemite, hemimorphite, gahnite, franklinite, sphalerite, and incorporated into the interlayers of phyllosilicate minerals in smelter contaminated soils (Manceau et al., 2000; Nategaal et al., 2005; Roberts et al., 2002). The minerals willemite, hemimorphite, franklinite, and gahnite are all high temperature Zn minerals that were likely formed during the smelting process, which causes them to be highly crystalline and easily identified by XRD (Nachtegaal et al., 2005; Roberts et al., 2002). Interestingly, no Zn phosphate minerals were identified in this study or the others previously mentioned.

Estimates of the amounts of Zn mineral species as determined by k^3-weighted EXAFS spectra for PR, TSP, and PA treatments after 4 and 52 week incubation periods and APP at the 4 week incubation period are given in Table 6-1. Results for APP at 52 weeks and MAP at 4 and 52 weeks were lost due to detector error. Linear combination fits of treated samples identified Zn minerals similar to the control. In sample PR4 (i.e. PR incubated for 4 weeks), the Zn phosphate mineral scholzite (11.2%) was discovered in the area adjacent to the granule. Scholzite (Zn, Ca phosphate) is much more stable mineral than hopeite, but Ca must be available for formation (Nriagu, 1984). Since PR was mostly composed of $Ca_5(PO_4)_3F$, it is expected that a significant amount of Ca would be available upon granule dissolution and therefore, the

formation of scholzite was likely. In a study investigating the effects of aqueous Zn on Pb immobilization by hydroxyapatite, it was found that both Zn and Ca disappeared from solution (Ma et al., 1994). Therefore, it was hypothesized that mixed metal phosphates precipitated, although this could not be proven by XRD. At greater distances from the granule in PR4, there were no formation of Zn phosphate minerals. At the 52 week incubation time, the mineral hopeite (23.5%) was found adjacent to the granule; while at 800-μm scholzite (25.5%) was present. No Zn phosphates were found at 1400-μm from the granule. This can be attributed to PR's limited solubility, which affects the amount of P that was available for reaction, especially at increasing distances from the granule (Lindsay, 1979).

Triple super phosphate, which was mostly monocalcium phosphate [$Ca(H_2PO_4)_2*H_2O$], induced the formation of hopeite at both incubation times, but formation of scholzite was not detected (Table 6-1). For TSP4, hopeite was present at both 300 and 1300-μm from the granule with greater amounts occurring in the immediate vicinity of the granule, while no Zn phosphates were identified at 2800-μm. Larger quantities of Zn phosphates were expected to occur adjacent to the treatment zone in granular sources, because P had to diffuse from the granule and through the soil for reaction. At the 52 week incubation period (TSP52), hopeite was discovered at 100 and 1100-μm from the granule at 56.7 and 57.5%, respectively, but no other Zn phosphate minerals were found with increased distance. The increased Zn phosphate production by TSP over PR is likely related to two things. First, TSP provided a more available source of P than PR. Second, TSP produced a small amount of acidity during granule dissolution that could potentially release Zn for reaction with P. No scholzite was detected in TSP samples, which could be due to low levels of available Ca.

Results for PA indicated no formation of Zn phosphate minerals at any distance or

reaction time. Interestingly, at the 4 week incubation period Zn sulfate and hydroxide species became important, while at 52 weeks aqueous Zn and Zn sulfates were significant components. This suggested that PA was actually increasing the presence of more soluble Zn species. It is well known that as pH decreases the solubility of Zn significantly increases (Lindsay, 1979). Therefore, in the remediation of smelter contaminated soils the use of PA could be problematic because while PA works well at immobilizing Pb (see Chapter 5) it may potentially increase Zn availability. Zinc is not considered toxic to humans, but can be to plants (Chaney, 1993). Increased Zn availability could negatively impact plant cover, thus increasing the potential of exposure of other heavy metal contaminants to multiple organisms. Additionally, materials treated with highly soluble fluid P sources may require special management to reduce the potential of P movement into surface water sources, which can cause eutrophication.

To reduce the pH effects caused by PA and still provide a highly available fluid source of P, APP could be used. However, research on APP to reduce metal bioavailability in contaminated environments is lacking. With APP, there is still the concern of using a highly soluble fluid P source because of its potential to influence surface water. Nevertheless, the application of APP induced the formation of Zn phosphates (Table 6-1). As distance increased from the point of application so did the amount of hopeite present, this was not expected. This phenomenon may be related to the availability of Zn rather than the lack of P to form Zn phosphate minerals, but can not be determined for sure. The use of APP illustrated the advantage of fluid P sources over granular sources in that a greater area was affected upon application. After just 4 weeks, LCF determined hopeite to be the major mineral species at 3700-μm from the point of application. Unfortunately, 52 week data for APP were lost due to unknown detector problems, but it is anticipated that the amount of Zn phosphate minerals would

increase with time.

Micro-XRD Analysis. Micro-XRD analysis was able to detect several Zn mineral species (Table 6-2). Willemite was the most common Zn mineral identified by XRD, which corresponded with the EXAFS data (Table 6-1). Other minerals that were identified by μ-XRD include hemimorphite, franklinite, zincite, gahnite, smithsonite, and hopeite. Figure 6-3 gives an example μ-XRD pattern for APP incubated at 52 weeks where willemite (d-spacings of 2.63, 2.84, 3.48, 2.32, 1.86, 1.42, 4.02, and 1.34) and hopeite (d-spacings of (4.57, 2.85, 9.12, 3.46, 3.39, 4.41, 1.94, and 4.85) were identified. It was interesting that μ-XRD analyses were able to confirm the majority of the Zn minerals identified by μ-EXAFS, which justifies the use of multiple synchrotron-based techniques in mineral speciation.

No Zn phosphate minerals were detected in the PR or PA treatments by μ-XRD. This was expected in PA since EXAFS suggested that more soluble forms of Zn existed. Hopeite was detected in the TSP samples at both incubation times at 1300 and 1100-μm from the sample, which confirmed EXAFS estimates. However, it was not detected in areas adjacent to the granule. Micro-XRD established the presence of hopeite in APP4 at 3700-μm, but not at 1700-μm. Micro-EXAFS data for APP52 was not available, but XRD analysis detected hopeite at 400-μm from the center of the droplet, which was anticipated since hopeite was found at the 4 week incubation time. Micro-XRD analysis for MAP showed the presence of hopeite at 100-μm from the edge of the granule after a 4 week incubation and at 200 and 800-μm after a 52 week incubation period. This implied that the presence of Zn phosphates increased with time. Additionally, the results suggested that MAP may be just as effective or similar to the TSP treatment at inducing Zn phosphate formation, although additional speciation data (EXAFS) is needed to confirm this.

Micro-XRD analysis was not able to confirm the presence of Zn phosphates at all POI's where EXAFS identified their presence. This was expected because Zn phosphates could be undetectable do to their poor crystallinity, or Zn could be sorbed to phosphate instead of occurring in a discrete mineral form (Cao et al., 2003; Xu and Schwartz, 1994). Additionally, Zn phosphate phases may be amorphous in character; therefore, they would be detected by EXAFS, but not by XRD. Cotter-Howells (1996) was able to identify hopeite in a Zn-contaminated soil, treated with soluble P using bulk-XRD. However, their system, which was purposely saturated with P, did not include speciation around an individual granule or droplet as in this study. Zinc phosphate minerals were not detected in PR samples by μ-XRD, which was related to the limited diffusion of P and minimal effects on pH. If P diffusion was slow and limited Zn was available for reaction (i.e. high pH), there was a greater chance to form poorly crystalline mixed metal phosphates were not detectable by μ-XRD. Overall, μ-XRD was a quick, useful tool that can be utilized to help confirm results of EXAFS analyses.

Environmental Impact. Other studies proposed the formation of Zn phosphates (Cao et al., 2003; Cotter-Howells, 1996; Ma et al., 1994), but only one confirmed the presence of Zn phosphate formation (Cotter-Howells, 1996) until now. No other studies attempted to speciate Zn at the molecular level in the vicinity of different P amendments in a Pb/Zn contaminated material, which makes this study unique. PA was the most effective amendment at inducing Pb phosphate formation (Chapter 5), but in the same material aqueous Zn became an important component after PA addition. This suggested an increase in Zn solubility. Therefore, in the remediation of Pb/Zn contaminated soils, the use of PA would not be recommended or may need to be accompanied with lime to reduce the potential to increase available Zn. Other metal contaminants that occur with Pb would be of concern too. For example, Kilgour et al. (2008)

determined that the addition of soluble P sources to immobilize Pb in soils containing As and Sb can mobilize these elements. As a result, the presence of other contaminants needs to be considered before using P to immobilize Pb.

PR, TSP, APP, and MAP were able to produce Zn phosphates. Theoretically, these treatments immobilized Zn by forming less soluble Zn phosphate minerals, thus making Zn less bioavailable. However, Zn phosphates are generally considered to be less soluble than Zn oxides, hydroxides, sulfates, and carbonates, but still expected to supply available P and Zn in soil (Lindsay, 1979). Research conducted by Fomina et al. (2006) demonstrated that ectomycorrhizal and non-mycorrhizal pine trees were able to dissolve Zn phosphates and acquire mobilized P in non-contaminated soils. This suggests that plants growing in contaminated soils have the potential to mobilize Zn through Zn phosphate dissolution. This is important if P amendments are changing the speciation of Zn from less soluble silicate and spinel (i.e. $ZnFe_2O_4$, $ZnAl_2O_4$) forms to more soluble phosphate forms, which can not be determined for sure in this study, but needs to be addressed in the future. If P amendments were to alter Zn from silicate and spinel forms to more soluble Zn phosphates, then the potential exists to release Zn into the system. While Zn is not considered toxic to humans, it is highly toxic to plants (Chaney, 1993). Lack of vegetation increases the risk for human exposure and the potential for contaminants to spread. Additionally, Pb is known to have a much higher affinity for P than Zn (Cao et al., 2003). It has been reported that P amendments are less effective at stabilizing Zn in contaminated media (Ma et al., 1994). Therefore, using P to immobilize Pb in multi-element contaminated soils needs to be managed carefully and intelligently.

This study demonstrated that PR, TSP, MAP, and APP can be added to Pb/Zn contaminated soils to form Zn phosphate minerals, which supported our hypothesis. However,

fluid sources were not necessarily more effective than granular treatments. When PA was added, more soluble Zn species become significant components of the soil P amendment mixture. This suggested that PA increased Zn solubility, which is most likely related to changes in pH. As distance increased from the point of application, APP was most effective at forming Zn phosphates. However, concerns exist over adding large amounts of highly soluble fluid P sources to soils because of the potential for eutrophication. Therefore, PR, TSP, or MAP may be better choices to use in immobilization of Pb in a soil contaminated by a Pb/Zn smelter, but monitoring it required.

6.5 References

Adriano, D.C. 2001. Trace elements in terrestrial environments: Biogeochemistry, bioavailability, and risks of metals. 2nd ed. Springer-Verlag, New York, NY.

Basta, N.T., J.A. Ryan, and R.F. Chaney. 2005. Trace element chemistry in residual-treated soil: Key concepts and metal bioavailability. J. Environ. Qual. 34:49-63.

Bremner, J.M., and C.S. Mulvaney. 1982. Salicylic acid thiosulfate modification of the Kjeldhal method to include nitrate and nitrite. p. 621. *In* R.H. Miller and D.R. Keeney (ed.) Methods of soil analysis. Part 2. Am. Soc. Agron., Madison, WI.

Brown, S.L., C.L. Henry, R.L. Chaney, H. Compton, and P. DeVolder. 2003. Using

municipal biosolids in combination with other residuals to restore metal-contaminated mining areas. Plant Soil 249:203-215.

Cao, R.X., L.Q. Ma, M. Chen, S.P. Singh, and W.G. Harris. 2003. Phosphate-induced metal immobilization in a contaminated site. Environ. Pollut. 122:19-28.

Chaney, R.L. 1993. Zinc phytotoxicity. p. 135-150. *In* A.D. Robson (ed.) Zinc in soils and plants. Kluwer Academic Publ., Dordrecht, The Netherlands.

Cotter-Howells, J. 1996. Lead phosphate formation in soils. Environ. Pollut. 93:9-16.

Cotter-Howells, J., and S. Caporn. Remediation of contaminated land by formation of heavy metal phosphates. Appl. Geochem. 11:335-342.

Councell, T.B., K.U. Duckenfield, E.R. Landa, and E. Callender. 2004. Tire-wear particles as a source of zinc to the environment. Environ. Sci. Technol. 38:4206-4214.

Drits, V.A., and A.S. Bookin. 2001. Crystal structure and X-ray identification of layered double hydroxides. p. 41-100. *In* V. Rives (ed.) Layered double hydroxides: Present and future. Nova Science Publishers, Inc., New York.

Fomina, M., J.M. Charnock, S. Hillier, I.J. Alexander, and G.M. Gadd. 2006. Zinc phosphate transformations by the *Paxillus involutus*/Pine ectomycorrhizal association. Microbiol. Ecol. 52:322-333.

Gee, G.W., and J.W. Bauder. 1986. Particle size analysis. p. 399-404. *In* A. Klute (ed.) Methods of soil analysis. Part 1. 2nd ed. Agron. Monogr. 9. ASA and SSSA, Madison, WI.

Hammersley, A.P., S.O. Svensson, M. Hanfland, A.N. Fitch, and D. Häusermann. 1996. Two-dimensional detector software: From real detector to idealized image or two-theta scan. High Press. Res. 14:235-248.

Hettiarachchi, G.M., G.M. Pierzynski, and M.D. Ransom. 2000. In situ stabilization of

soil lead using phosphorus and manganese oxide. Environ. Sci. Tech. 34:4614-4619.

Hettiarachchi, G.M., G.M. Pierzynski, and M.D. Ransom. 2001. In situ stabilization of lead using phosphorus. J. Environ. Qual. 30:1214-1221.

Hettiarachchi, G.M., and G.M. Pierzynski. 2002. In situ stabilization of soil lead, cadmium, and zinc using phosphorus and manganese oxide: Influence on plant growth. J Environ. Qual. 31:564-572.

Hettiarachchi, G.M., and G.M. Pierzynski. 2004. Soil lead bioavailabililty and in situ remediation of lead-contaminated soils: A review. Environ. Prog. 23:78-93.

Iskandar, I.K., and D.C. Adriano. 1997. Remediation of soils contaminated with metals: A review of current practices in the USA. p. 1-26. *In* I.K. Iskandar and D.C. Adriano (eds.) Remediation of soils contaminated with metals. Advances in Environmental Science. Science Reviews, Middlesex, UK.

Jackson, M.L. 1975. Soil chemical analysis-advanced course. 2nd ed. Dep. Soil Sci., Univ. of Wisconsin, Madison, WI.

Jackson, M.L., C.H. Lim, and L.W. Zelazny. 1986. Oxides, hydroxides and aluminosilicates. p. 101-150. *In* A. Klute (ed.) Methods of soil analysis. Part 1. 2nd ed. Agron. Monogr. 9. ASA and SSSA, Madison, WI.

Jaynes, W.F., and J.M. Bigham. 1986. Multiple cation-exchange capacity measurements on standard clays using a commercial mechanical extractor. Clays Clay Miner. 34:93-98.

JCPDS-International Centre for Diffraction Data. 1987. Powder diffraction file inorganic phases search manual (Hanawalt method). JCPDS, Swarthmore, PA.

Kilgour, D.W., R.B. Moseley, M.O. Barnett, K.S. Savage, P.M. Jardine. 2008. Potential negative consequences of adding phosphorus-based fertilizers to immobilize lead in soil. J.

Environ. Qual. 37:1733-1740.

Ma, Q.Y., T.J. Logan, S.J. Traina, and J.A. Ryan. 1994. Effects of NO_3^-, Cl^-, F^-, SO_4^{2-}, and CO_3^{2-} on Pb^{2+} immobilization by hydroxyapatite. Environ. Sci. Technol. 28:408-418.

Manceau, A., B. Lanson, M.L. Schlegel, J.C. Hargè, M. Musso, L. Eybert-Bèrard, J. Hazemann, D. Chateigner, and G.M. Lamble. Quantitative Zn speciation in smelter-contaminated soils by EXAFS spectroscopy. Am. J. Sci. 300:289-343.

Manceau, A., M.A. Marcus, and N. Tamura. 2002a. Quantitative speciation of heavy metals in soils and sediments by X-ray techniques. Rev. Mineral. Geochem. 49:321-428.

Manceau, A., N. Tamura, M.A. Marcus, A.A. MacDowell, R.S. Celestre, R.E. Sublett, G. Sposito, and H.A. Padmore. 2002b. Deciphering Ni sequestration in soil ferromanganese nodules by combining X-ray fluorescence, absorption, and diffraction at micrometer scales of resolution. Am. Mineral. 87:1494-1499.

McGowen, S.L., N.T. Basta, and G.O. Brown. 2001. Use of diammonium phosphate to reduce heavy metal solubility and transport in smelter-contaminated soil. J. Environ. Qual. 30:493-500.

Mench, J., J. Vansgroveld, N.W. Lepp, and R. Edwards. 1998. Physico-chemical aspects and efficiency of trace element immobilization by soil amendments. *In* J. Vansgroveld and S.D. Cunningham (eds.) Metal-contaminated soils: In situ inactivation and phytorestoration. Springer-Verlag, Berlin.

Nachtegaal, M., M.A. Marcus, J.E. Sonke, J. Vangronsveld, K.J.T. Livi, D. Van Der Lelie, and D.L. Sparks. 2005. Effects of in situ remediation on the speciation and bioavailability of zinc in a smelter contaminated soil. Geochim. Cosmochim. Acta 69:4649-4664.

Newville, M. 2001. IFEFFIT: Interactive EXAFS analysis and FEFF fitting. J.

Synchrotron Radiat. 8:322-324.

Nriagu, J.O. 1984. Formation and stability of base metal phosphates in soils and sediments. p. 318-329. *In* J.O. Nriagu and P.B. Moore (ed.) Phosphate Minerals. Springer, London.

Ravel, B., and M. Newville. 2005. ATHENA, ARTEMIS, HEPHAESTUS: Data analysis for X-ray absorption spectroscopy using IFEFFIT. J. Synchrotron Radiat. 12:537-541.

Roberts, D.R., A.C. Scheinost, D.L. Sparks. 2002. Zinc speciation in a smelter-contaminated soil profile using bulk and microspectroscopic techniques. Envron. Sci. Technol. 36:1742-1750.

Scheckel, K.G., and J.A. Ryan. 2004. Spectroscopic sceciation of lead in phosphate-amended soils. J. Environ. Qual. 33:1288-1295.

Sims, J.T., and G.M. Pierzynski. 2005. Chemistry of phosphorus in soils. *In* M.A. Tabatabai and D.L. Sparks (ed.) Chemical processes in soils. SSSA Book Ser. 8. SSSA. Madison, WI.

Sposito, G., L.J. Lund, and A.C. Chang. 1982. Trace metal chemistry in arid-zone field soils amended with sewage sludge: I. Fractionation of Ni, Cu, Zn, Cd, and Pb in solid phases. Soil Sci. Soc. Am. J. 46:260-264.

Xu, Y., and F.W. Schwartz. 1994. Lead immobilization by hydroxyapatite in aqueous solutions. J. Contam. Hydrol. 15:187-206.

Yoon, J.K., X.D. Cao, and L.Q. Ma. 2007. Application methods affect phosphorus-induced lead immobilization from a contaminated soil. J. Environ. Qual. 36:373-378.
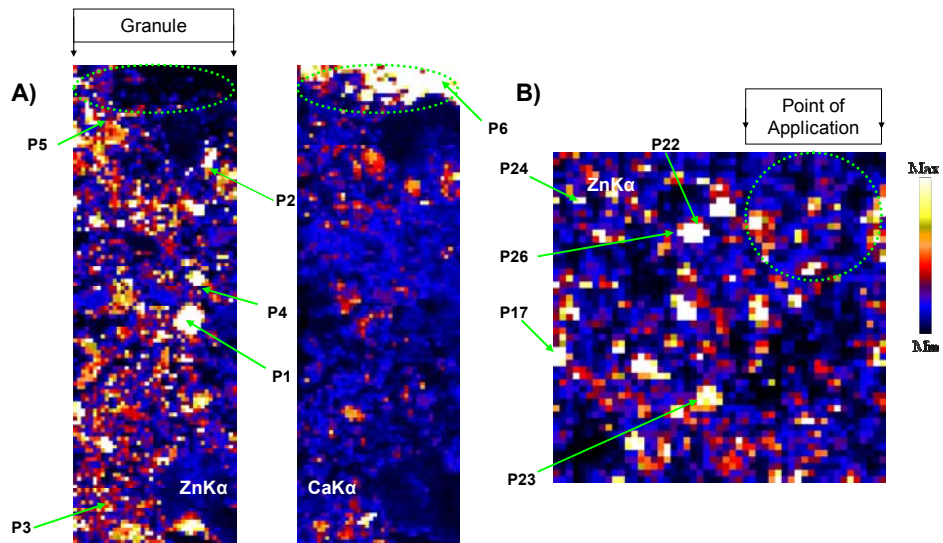
Figure 6-1. Micro-X-ray fluorescence maps of a) Zn and Ca for soil incubated with PR for 4 weeks and b) Zn for soil incubated with PA for 4 weeks. Area of a single map is a) 2000-by 6000-µm and b) 2500- by 2500- µm. The color scheme used ranges from white or yellow for high fluorescence signal to blue or black for low fluorescence signal. Shading is relative across each map. The markers P1 to P6 in a) and P17 to P26 in b) represent locations for which either extended µ-X-ray absorption fine structure (EXAFS) and µ-X-ray diffraction (XRD) analyses were conducted. Calcium is shown in a) to illustrate the location of a PR granule.
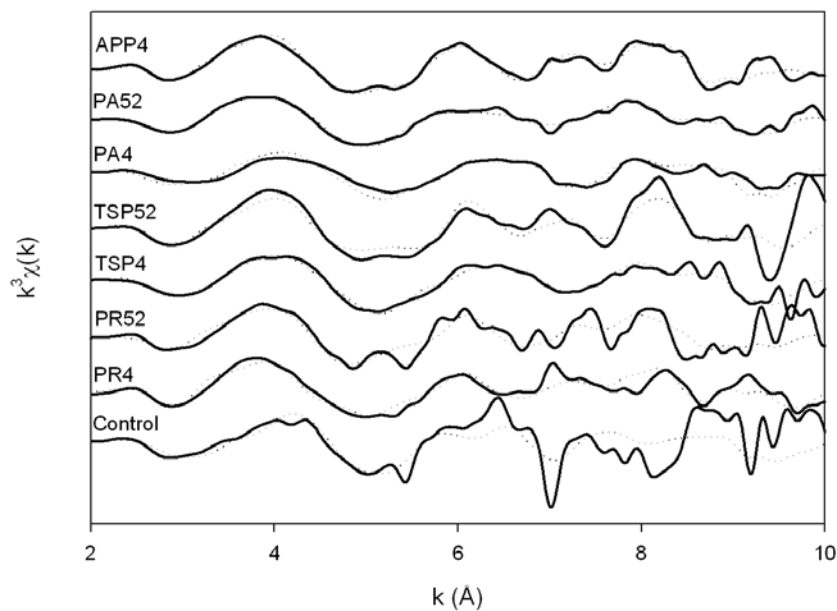
Figure 6-2. The raw Zn k^3-weighted (where k is the photoelectron wavenumber) μ-extended X-ray absorption fine structure (μ-EXAFS) spectra (solid lines) for the Zn K-edge X-ray absorption spectroscopic data. Data were collected from points 100- to 400-μm from the edge of a granule or the center of a droplet. Dotted lines indicate the best linear combination fits using all the standard Zn mineral compounds. Control: unamended sample, PR: phosphate rock, TSP: triple super phosphate, PA: phosphoric acid, APP: ammonium polyphosphate. The numbers 4 and 52 indicate the incubation period.
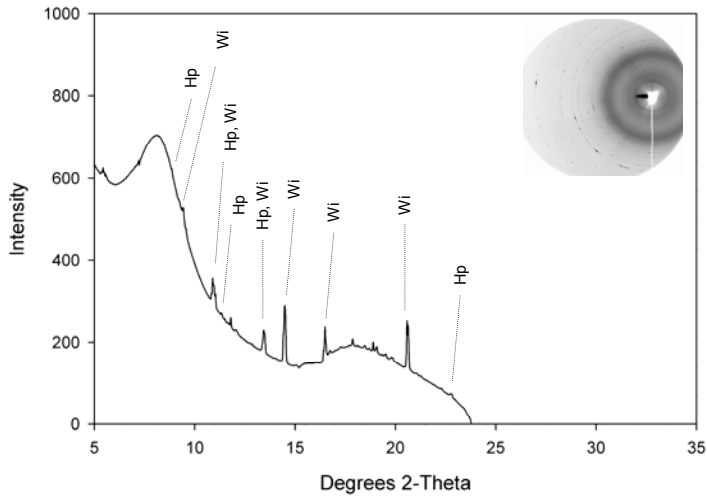
Figure 6-3. Micro-XRD pattern for treatment APP52 at 3700 μm from the center of treatment. Original Debye-Sherer rings are located in the top-right hand corner of the graph. Species detected are Wi (willemite with d-spacings of 2.63, 2.84, 3.48, 2.32, 1.86, 1.42, 4.02, and 1.34) and Hp (hopeite with d-spacings of 4.57, 2.85, 9.12, 3.46, 3.39, 4.41, 1.94, and 4.85).

Table 6-1.   Percentages of Zn species from selected POIs for control and P treated soils as determined by linear combination fitting of extended μ-X-ray absorbtion fine structure (μ-EXAFS) spectra at 4 and 52 weeks after P amendment addition. Typical uncertainties in the percentages listed for each standard component are 5%.

Sample †	Distance ‡	Ga #	Wi	Zi	Ho	Sch	ZnA	Fr	Zs	ZnN	Zo	He	χ^2
Control	--	--	61.2	--	--	--	--	--	--	--	--	38.8	2.20
Control	--	6.0	26.0	--	--	--	--	33.9	--	34.1	--	--	2.62
Control	--	--	22.5	--	--	--	--	--	33.7	--	--	43.8	3.56
PR4	100	11.8	--	38.3	--	11.2	--	--	--	--	--	38.7	1.91
PR4	2200	21.2	40.2	--	--	--	--	--	--	38.6	--	--	0.47
PR4	2700	17.0	--	20.7	--	--	--	--	41.9	--	20.4	--	1.50
PR52	100	--	--	7.2	23.5	--	--	14.5	--	54.8	--	--	0.99
PR52	800	7.6	40.7	--	--	25.5	--	--	--	26.3	--	--	3.83
PR52	1400	6.5	--	--	--	--	67.5	26.0	--	--	--	--	4.16
TSP4	300	14.0	1.2	--	84.8	--	--	--	--	--	--	--	3.66
TSP4	1300	--	--	18.6	40.1	--	--	7.3	--	--	--	34.0	1.05
TSP4	2800	--	65.9	--	--	--	--	--	31.1	--	--	16.9	0.82
TSP52	100	--	--	25.4	56.7	--	--	17.9	--	--	--	--	0.65
TSP52	1100	--	12.5	--	57.5	--	18.5	11.5	--	--	--	--	3.62
TSP52	2300	31.1	43.3	10.6	--	--	--	--	--	--	15.1	--	4.02
PA4	1100	--	--	27.4	--	--	--	15.9	--	--	22.3	34.4	4.82
PA4	1600	11.2	--	--	--	--	--	--	16.8	62.5	9.5	--	2.27
PA4	2300	27.1	36.1	--	--	--	--	--	11.9	--	24.9	--	2.67
PA52	1000	--	23.7	--	--	--	65.6	--	--	--	--	10.7	0.33
PA52	3200	--	59.3	--	--	--	15.1	--	25.6	--	--	--	2.21
PA52	3400	--	39.1	--	--	--	23.1	12.9	24.9	--	--	--	2.92
APP4	300	6.5	23.3	--	--	--	--	10.1	--	60.1	--	--	0.73
APP4	1700	9.5	--	49.8	22.4	--	--	18.3	--	--	--	--	4.77
APP4	3700	5.0	24.4	10.9	59.7	--	--	--	--	--	--	--	2.67

† Control: non-P amended; PR: Phophate rock; TSP: Triple super phosphate; PA: Phosphoric acid; APP: Ammonium polyphosphate. Number following treatment indicates incubation time (4 or 52 weeks).

‡ Distance in μm from the P treatment. For fluid sources (PA and APP) this distance begins at the approximate center of the point of application. For granular sources (PR, and TSP) this distance begins at the edge of the granule. Points of interest for the controls were taken randomly where high relative Pb concentrations were present.

Ga: gahnite; Wi: Willemite; Zi: Zincite; Ho: Hopeite; Sch: Scholzite; ZnA: Aqueous zinc; Fr: Franklinite; Zs: Zinc sulfate; ZnN: Zinc-aluminum layered double hydroxide with a nitrate interlayer; Zo: Zinc hydroxide; He: Hemimorphite

Table 6-2. A summary of μ-XRD analysis for Zn POI's that corresponds to Zn POI's selected for μ-XAS in Table 6-1.

Sample †	Distance ‡	Minerals Detected by μ-XRD Analysis
Control	--	Hemimorphite, Willemite
Control	--	Willemite
Control	--	Hemimorphite
PR4	100	None Detected
PR4	2200	Willemite
PR4	2700	None Detected
PR52	400	None Detected
PR52	800	Willemite
PR52	1400	None Detected
TSP4	300	None Detected
TSP4	1300	Franklinite, Hopeite
TSP4	2800	None Detected
TSP52	100	Franklinite, Zincite
TSP52	1100	Franklinite, Hopeite, Willemite
TSP52	2300	Gahnite, Willemite
PA4	1100	Hemimorphite, Zincite
PA4	1600	Gahnite
PA4	2300	Franklinite, Willemite
PA52	1000	Willemite
PA52	3200	Willemite
PA52	3400	Franklinite
APP4	300	None Detected
APP4	1700	Franklinite, Zincite
APP4	3700	Hopeite, Willemite
APP52	400	Franklinite, Hopeite, Smithsonite
APP52	1500	None Detected
APP52	2600	None Detected
MAP4	100	Hopeite, Willemite
MAP4	1100	Willemite
MAP4	2900	Gahnite
MAP52	200	Gahnite, Hopeite
MAP52	800	Hopeite, Willemite
MAP52	2300	Smithsonite, Gahnite

†Control: non-P amended; PR: Phophate rock; TSP: Triple super phosphate; MAP: Monammonium phosphate; PA: Phosphoric acid; APP: Ammonium polyphosphate. Number following treatment indicates incubation time (4 or 52 weeks).
‡Distance in μm from the P treatment. For fluid sources (PA and APP) this distance begins at the approximate center of the point of application. For granular sources (PR, TSP, and MAP) this distance begins at the edge of the granule. Points of interest for the controls were taken randomly where high relative Pb concentrations were present.

CHAPTER 7 - Summary and Conclusions

Application of composted beef manure to mine wastes contaminated with heavy metals increased microbial activity as compared to the non-amended control. The result supported the hypothesis that compost additions would increase microbial activity. However, a 269 Mg ha^{-1} addition was needed to significantly increase microbial biomass measurements, enzyme activities, and potential nitrification measurements over the non-amended control for the duration of the study (711 d). Increases in microbial activity and biomass were significantly and positively related to increases in total C, estimated available water, and extractable P. However, significant negative relationships were found with electrical conductivity and bioavailable Zn. These relationships were influenced by compost additions. As the amount of compost increased total C, estimated available water, and extractable P content increased, while bioavailable Zn decreased; thus increasing the size and activity of the microbial population.

A negative aspect of using beef manure compost in remediation is its high salt content. High salts initially caused increases in electrical conductivy, which were detrimental to microbial communities as indicated through the significant negative relationship with electrical conductivity. With time, the salts were leached from the materials, and their impact became negligible.

Phospholipid fatty analyses (PLFA) of treatments indicated that the 269 Mg ha^{-1} compost treatments alter microbial community structure as determined by principal components. This alteration was not overly dramatic, but was related to a shift to Gram-negative bacteria (Gm^{-}). Furthermore, PLFA estimated microbial biomass indicated significant increases in Gram-positive (Gm^{+}), Gm^{-}, and fungal biomass in the 269 Mg ha^{-1} treatments over the non-amended control. Interestingly, additions of lime or lime plus bentonite with the compost do not further enhance

microbial activity or biomass at this time, suggesting that these amendments may not be needed when a large application of an organic amendment is made. With time, microbial activity and biomass measurements have begun to decrease slightly, which is likely related to loss of easily mineralizable C and some readily available nutrients. However, we do expect microbial activity and biomass to come to a new steady state that is significantly higher than the non-amended control.

The 269 Mg ha^{-1} compost addition was also able to significantly increase plant biomass over the non-amended control. However, high salt content and limited rainfall resulted in no vegetation production in the first year of the study. Plant communities became established in the second and third years, although they were a mixture of species even though switchgrass was the only species seeded into the study area. Switchgrass is a warm season native grass species that is slow to develop, especially under extreme growing conditions such as mine wastes. As a result, switchgrass is at a disadvantage to invasive weed species that can survive some of the most adverse growing conditions. Over time (0 to 841 d), plant biomass has started to decrease at site A, but is still increasing at site B. This is likely due to the higher bioavailable Zn levels at site A as compared to site B, which can significantly impact plant biomass production.

Switchgrass production was significantly related to improved fertility, increased available water content, and reduced bioavailable Zn. Both the 45 and 269 Mg ha^{-1} compost treatments were able to improve fertility, but after three years only the 269 Mg ha^{-1} treatment was able to maintain significantly higher nutrient concentrations as compared to the non-amended control. Similarly to the microbial study, the addition of lime and lime plus bentonite was unable to further enhance plant biomass growth over compost alone.

The additions of different P sources to a Pb contaminated soil were able to induce Pb

phosphate formation *in situ*, which will reduce the bioavailability of Pb to the environment. Furthermore, it appears as if the formation of pyromorphite in this contaminated system is preceded by the formation of other metastable Pb phosphate minerals, such as plumbogummite or plumbogummite-like minerals, which has not been reported until now.

These results support the hypothesis that fluid P amendments are superior at inducing Pb phosphate formation over a greater area than granular sources. This can be attributed to greater amount of water added with fluid P sources, which increases the degree of P diffusion as compared to granular sources where P movement is slowed by osmotic effects. Phosphoric acid (PA) was the most effective fluid source, which is related to the high levels of available P for reaction and the acidity of PA that can dissolve discrete Pb minerals, thus making Pb more available for reaction. Triple super phosphate (TSP) was the most effective granular P source at inducing Pb phosphate formation, which is related to high available levels of P and the acidity produced upon fertilizer granule dissolution. Therefore, PA and TSP could effectively be used to reduce Pb bioavailability through Pb phosphate formation in a smelter-contaminated soil. However, monitoring is necessary to assure stability of the newly formed Pb phosphate minerals over time and to limit the impact of P on the environment.

While PA was the most effective P amendment in Pb phosphate formation, the acidity from this treatment increased the presence of soluble Zn species in a soil co-contaminated with Pb/Zn, which could increase Zn bioavailability. This was problematic because Zn is known to have negative impacts on ecosystems. Increased levels of bioavailable Zn is likely to result in reduced vegetation, which will increase the exposure of Zn and other elements that commonly occur with Zn, namely Pb and Cd, to the environment. Therefore, lime may need to be applied after the application of PA to reduce the impacts of the acidity. Phosphate rock (PR), ammonium

polyphosphate (APP), monoammonium phosphate (MAP), and TSP were able to produce Zn phosphates, which supports our hypothesis that the addition of P amendments will induce the formation of Zn phosphate minerals. APP was the most effective treatment at forming Zn phosphate minerals especially at greater distances from the treatment. There is concern, however, because Zn phosphates are less soluble than Zn silicate and Zn spinel minerals. Therefore, Zn phosphate minerals would be expected to supply Zn and P to organisms over time. Currently, it is unknown whether the addition of P can change Zn from less soluble Zn silicate and spinel forms to more soluble Zn phosphates.

Both Pb and Zn are toxic to organisms. Lead has negative impacts on human health, whereas high concentrations of Zn can influence ecosystem function. As a result, areas contaminated by these elements need to be cleaned up. Remediation of these contaminants typically consists of removal, landfilling, and then back-filling with uncontaminated material. However, this is costly, labor intensive, and time consuming. Therefore, new reclamation technologies are needed. Our results suggest that both organic and inorganic P amendments can be used to stabilize/immobilize metals in contaminated materials. These practices will not remove the contaminants, but the practices will reduce their bioavailability through sorption and precipitation reactions. These reactions limit plant uptake, movement into surface waters, and bioavailability of Pb and Zn, thus minimizing the accumulation of metals in higher organisms.

The use of organic amendments to stabilize mine wastes or P to reduce metal bioavailability are practical techniques. We have shown that organic amendments increase nutrient content, total C, and estimated available water, while reducing metal availability in mine wastes resulting in an increase in plant production and microbial biomass/activity. However, this study has only addressed the short-term recovery of these systems and long-term stability is an

issue with organic amendments. Therefore, long-term evaluation studies are needed.

Organic amendments are available in many areas in various forms that include: biosolids, yard wastes, animal manures, and composted materials. Many areas that have metal contamination problems are areas of low population density and livestock production. As a result, fresh organic materials may not be available for application and transporting the material over long distances at current fuel prices would be expensive. Composts are better options because composting procedures reduce C to nutrient ratios and remove water; thus, making the material more valuable. Again, availability of composts in contaminated areas would be problematic; therefore, transport and its associated costs would be an issue. However, the risk level (human, animal, ecosystem, ect…) as affected by cost will be a significant concern that governmental regulation and funding agencies will need to evaluate. Additionally, research is needed to investigate risk assessment and the economics of using organic amendments for the remediation of heavy metal contaminated areas.

Using P to form highly insoluble metal phosphate mineral species will reduce the risk of transfer of metals through the food chain and to humans. Furthermore, P additions could be used to treat areas where metals pose a slight risk to human health, but would not otherwise be remediated via excavation due to lower overall metal concentrations. In a sense, we could reduce the risk to more people by having a lower-cost treatment option. If this technology were adopted, information is needed on metal phosphate stability in the presence of plants (rhizosphere chemistry). Over time, we would hypothesize that Pb and other metals would become more bioavailable due to P removal through plant uptake and biomass removal. Therefore, special management practices are likely to be needed to maintain metals in less soluble/bioavailable phosphate forms.

When using soil amendments to immobize metals or stabilize metal contaminants it is necessary to recognize that these materials contain elements that can damage ecosystem function. For example, high loadings of P from P amendments or organic materials can increase the eutrophication potential. Therefore, areas treated with these materials need to be managed carefully and intelligently. Research addressing risk assessment of soil amendments needs to be included before permanently adopting alternative reclamation techniques. It is critical to understand both the positive and negative effects that amendment additions can have on reducing the risk of metal contamination and on ecosystem health.

Alternative reclamation techniques are needed because removal is not an option in many situations. Our research has shown that both organic and inorganic soil additives can be used to immobilize metals (metal phosphate formation), increase vegetative growth, and improve microbial activity and function. While soil amendments reduce the exposure risk to metals and improve ecosystem function in mine wastes, offsite movement of elements (N, P, etc…) associated with the soil amendments have the potential to degrade ecosystems. Therefore, amendment additions to reduce metal exposure need to be carefully managed. These studies support the use of alternative remedation methods, but research is still needed to address the issue of permanence before these technologies can be adopted. As a result, amendments can be added when they are needed if they are cost effective at the time.

7.1 Final Thoughts

One thing that we need to ask ourselves is how do we end up in these situations? We all strive for a higher standard of living, but at what cost is this having on the environment? As population continues to grow, every person wants to improve the lifestyle for themselves and their families. Unfortunately, this requires resources. However, at what point does the earth run

out of resources? We need to remember that the earth is a resource limited system and the persistence of life in that system demands that we manage it well for ourselves and for all other species. Unfortunately, there is not a "new resource delivery truck or garbage man" that stops by to bring us fresh supplies and remove the waste and contamination that we have created to achieve this improved lifestyle. Whether it is soil, air, or water, these resources are all finite. Therefore, we need to protect what we have and try to reclaim what has not been irreversibly damaged. Life as we know depends on us to make the right decisions.

Appendix A - Synchrotron Research Data
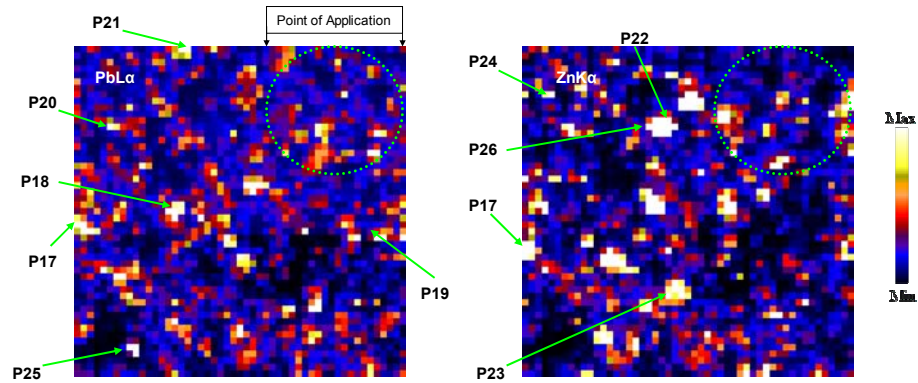
Figure A-1. Micro-X-ray fluorescence maps of Pb and Zn for soil incubated with PA for 4 weeks. Area of a single map is 2500- by 2500- µm. The color scheme used ranges from white or yellow for high fluorescence signal to blue or black for low fluorescence signal. Shading is relative across each map. The arrows represent locations for which either µ-X-ray absorption near-edge structure (XANES), extended µ-X-ray absorption fine structure (EXAFS), and/or µ-X-ray diffraction (XRD) analyses were conducted.
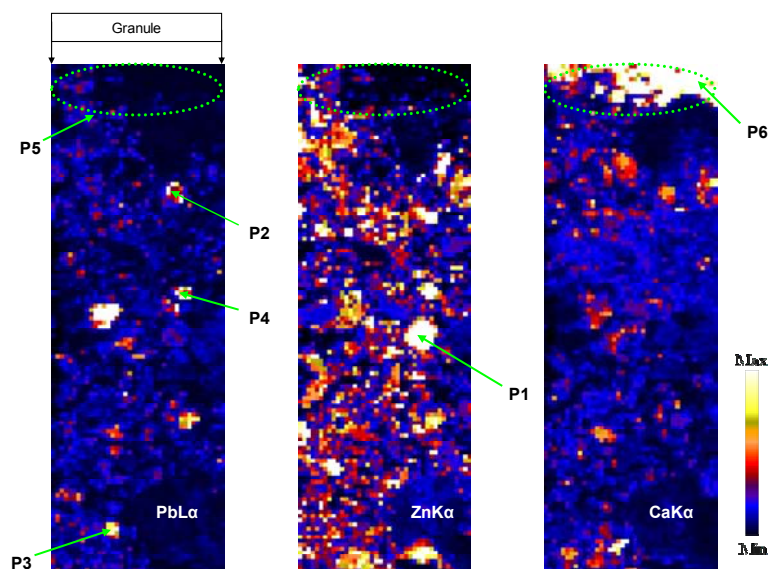
Figure A-2. Micro-X-ray fluorescence maps of Pb, Zn, and Ca for soil incubated with PR for 4 weeks. Area of a single map is 2000- by 6000-μm. The color scheme used ranges from white or yellow for high fluorescence signal to blue or black for low fluorescence signal. Shading is relative across each map. The arrows represent locations for which either μ-X-ray absorption near-edge structure (XANES), extended μ-X-ray absorption fine structure (EXAFS), and/or μ-X-ray diffraction (XRD) analyses were conducted.
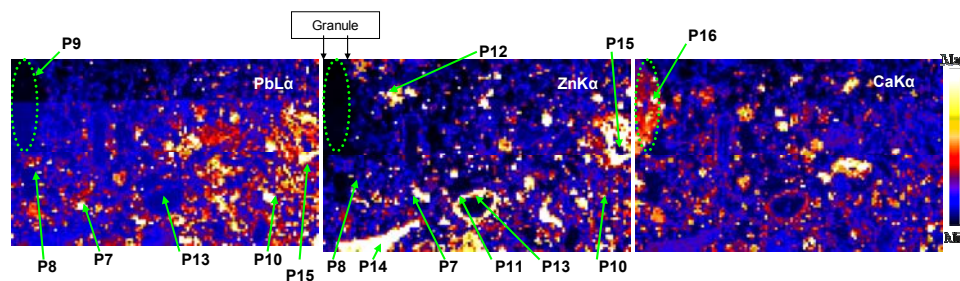
Figure A-3. Micro-X-ray fluorescence maps of Pb, Zn, and Ca for soil incubated with TSP for 4 weeks. Area of a single map is 4000- by 6000- μm. The color scheme used ranges from white or yellow for high fluorescence signal to blue or black for low fluorescence signal. Shading is relative across each map. The arrows represent locations for which either μ-X-ray absorption near-edge structure (XANES), extended μ-X-ray absorption fine structure (EXAFS), and/or μ-X-ray diffraction (XRD) analyses were conducted.
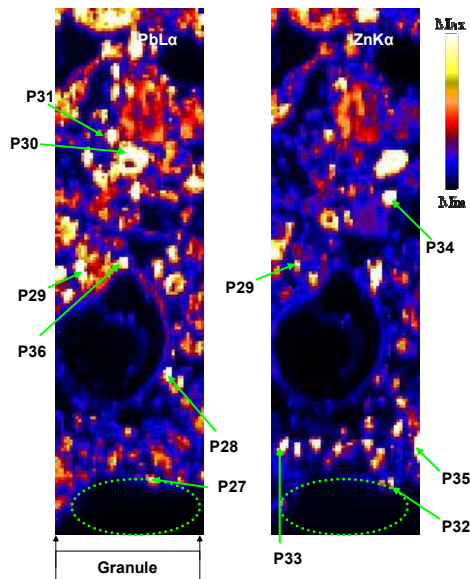
Figure A-4. Micro-X-ray fluorescence maps of Pb and Zn for soil incubated with MAP for 4 weeks. Area of a single map is 2000- by 4000- µm. The color scheme used ranges from white or yellow for high fluorescence signal to blue or black for low fluorescence signal. Shading is relative across each map. The arrows represent locations for which either µ-X-ray absorption near-edge structure (XANES), extended µ-X-ray absorption fine structure (EXAFS), and/or µ-X-ray diffraction (XRD) analyses were conducted.
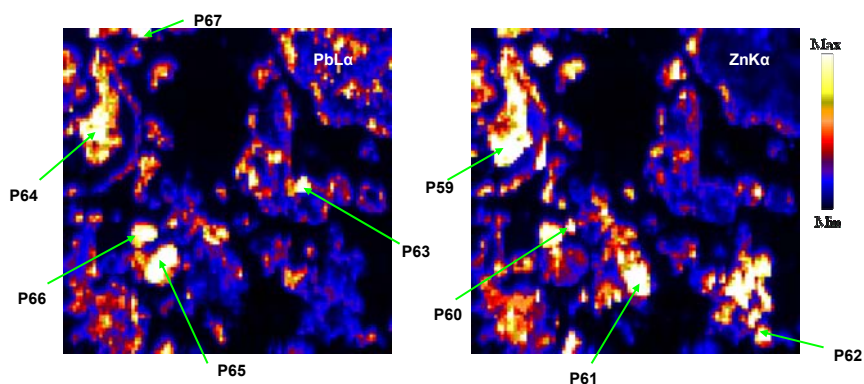
Figure A-5. Micro-X-ray fluorescence maps of Pb and Zn for soil for the contaminated control. Area of a single map is 2500- by 2500- µm. The color scheme used ranges from white or yellow for high fluorescence signal to blue or black for low fluorescence signal. Shading is relative across each map. The arrows represent locations for which either µ-X-ray absorption near-edge structure (XANES), extended µ-X-ray absorption fine structure (EXAFS), and/or µ-X-ray diffraction (XRD) analyses were conducted.
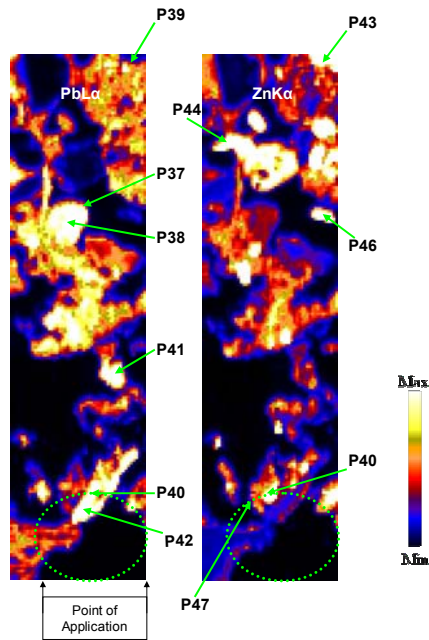
Figure A-6. Micro-X-ray fluorescence maps of Pb and Zn for soil incubated with APP for 4 weeks. Area of a single map is 2000- by 4000- µm. The color scheme used ranges from white or yellow for high fluorescence signal to blue or black for low fluorescence signal. Shading is relative across each map. The arrows represent locations for which either µ-X-ray absorption near-edge structure (XANES), extended µ-X-ray absorption fine structure (EXAFS), and/or µ-X-ray diffraction (XRD) analyses were conducted.
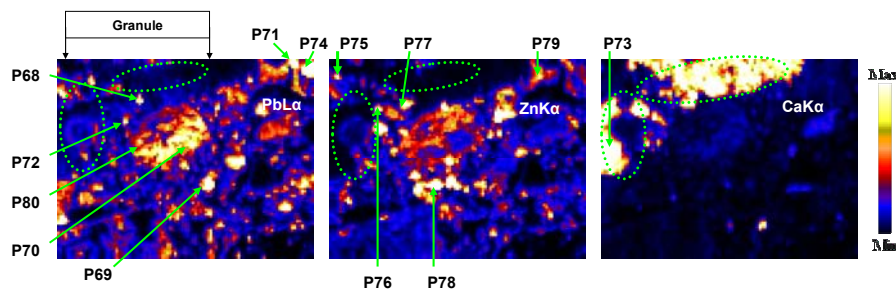
Figure A-7. Micro-X-ray fluorescence maps of Pb, Zn, and Ca for soil incubated with PR for 52 weeks. Area of a single map is 2000- by 3000-µm. The color scheme used ranges from white or yellow for high fluorescence signal to blue or black for low fluorescence signal. Shading is relative across each map. The arrows represent locations for which either µ-X-ray absorption near-edge structure (XANES), extended µ-X-ray absorption fine structure (EXAFS), and/or µ-X-ray diffraction (XRD) analyses were conducted.
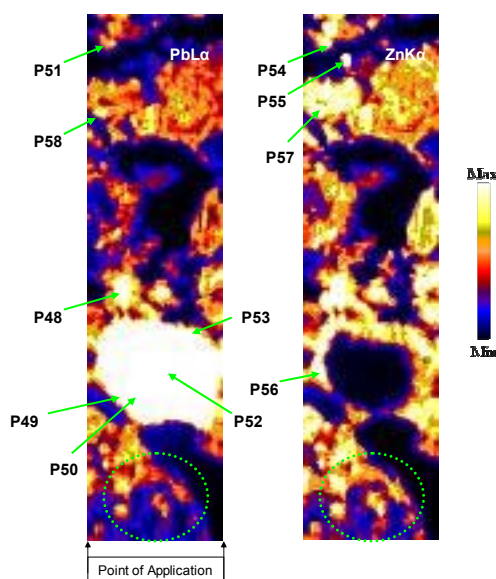
Figure A-8. Micro-X-ray fluorescence maps of Pb and Zn for soil incubated with PA for 52 weeks. Area of a single map is 1000- by 4000- µm. The color scheme used ranges from white or yellow for high fluorescence signal to blue or black for low fluorescence signal. Shading is relative across each map. The arrows represent locations for which either µ-X-ray absorption near-edge structure (XANES), extended µ-X-ray absorption fine structure (EXAFS), and/or µ-X-ray diffraction (XRD) analyses were conducted.
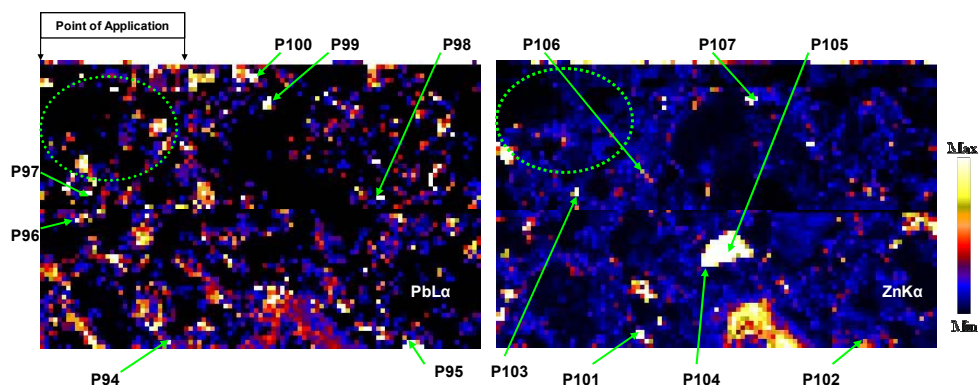
Figure A-9. Micro-X-ray fluorescence maps of Pb and Zn for soil incubated with APP for 52 weeks. Area of a single map is 2000- by 5000- µm. The color scheme used ranges from white or yellow for high fluorescence signal to blue or black for low fluorescence signal. Shading is relative across each map. The arrows represent locations for which either µ-X-ray absorption near-edge structure (XANES), extended µ-X-ray absorption fine structure (EXAFS), and/or µ-X-ray diffraction (XRD) analyses were conducted.
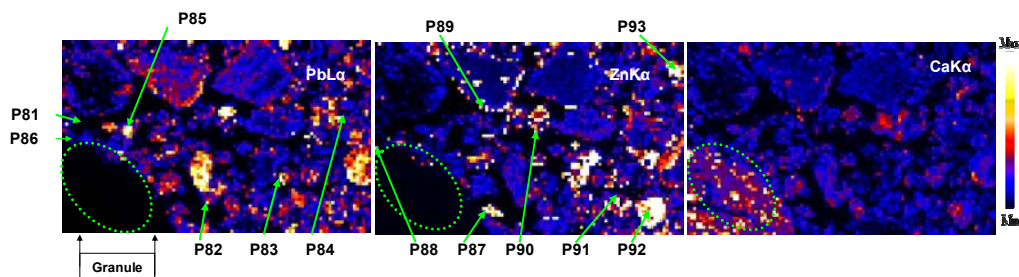
Figure A-10. Micro-X-ray fluorescence maps of Pb, Zn, and Ca for soil incubated with TSP for 52 weeks. Area of a single map is 3000- by 5000- µm. The color scheme used ranges from white or yellow for high fluorescence signal to blue or black for low fluorescence signal. Shading is relative across each map. The arrows represent locations for which either µ-X-ray absorption near-edge structure (XANES), extended µ-X-ray absorption fine structure (EXAFS), and/or µ-X-ray diffraction (XRD) analyses were conducted.
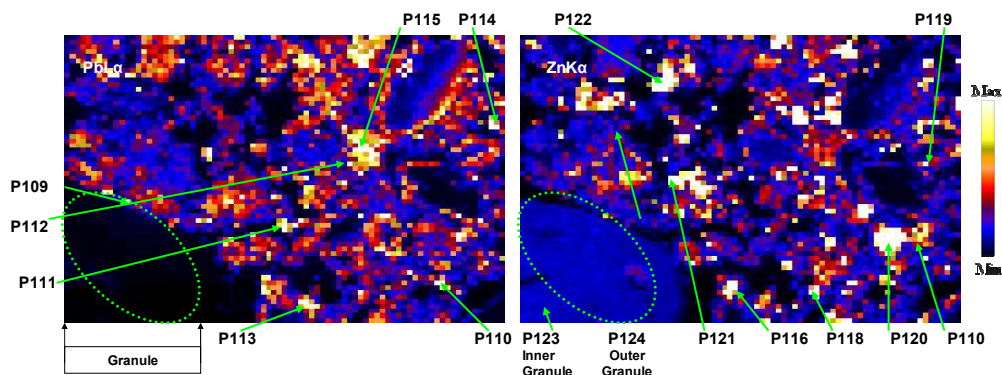
Figure A-11. Micro-X-ray fluorescence maps of Pb and Zn for soil incubated with MAP for 52 weeks. Area of a single map is 3000- by 4000- µm. The color scheme used ranges from white or yellow for high fluorescence signal to blue or black for low fluorescence signal. Shading is relative across each map. The arrows represent locations for which either µ-X-ray absorption near-edge structure (XANES), extended µ-X-ray absorption fine structure (EXAFS), and/or µ-X-ray diffraction (XRD) analyses were conducted.
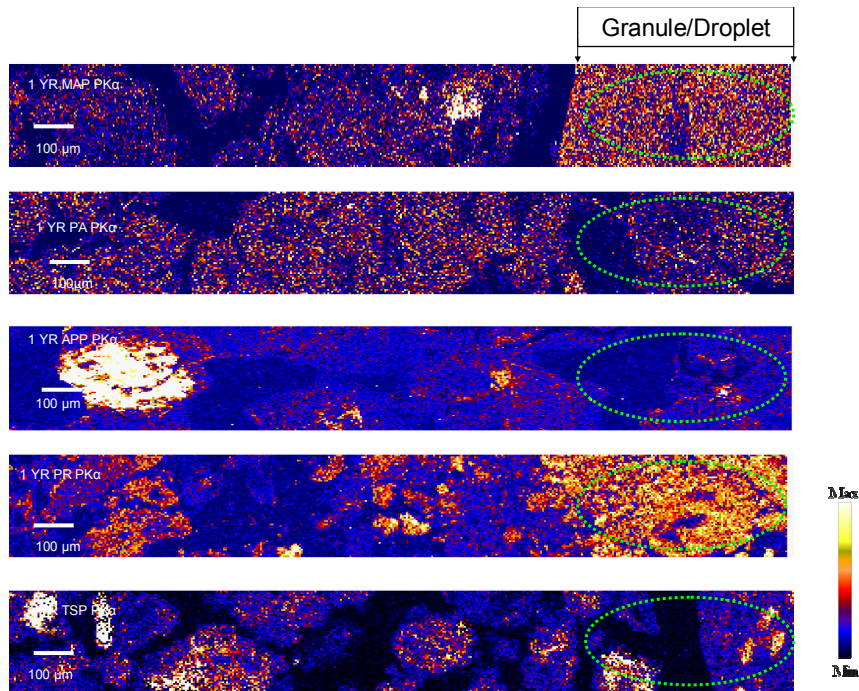
Figure A-12. Micro-X-ray fluorescence maps of P for soil incubated with MAP, PA, APP, PR, and TSP for 52 weeks. Area of a single map is 250- by 2000- μm. The color scheme used ranges from white or yellow for high fluorescence signal to blue or black for low fluorescence signal. Shading is relative across each map. The green circle represents the area where a P granule or droplet was applied.
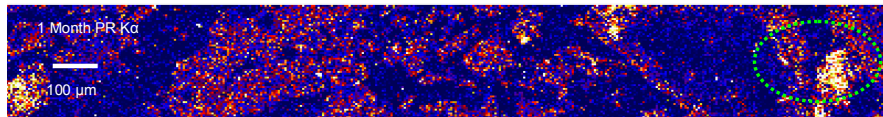
Figure A-13. Micro-X-ray fluorescence maps of P for soil incubated with PR for 52 weeks. Area of a single map is 250- by 2000- μm. The color scheme used ranges from white or yellow for high fluorescence signal to blue or black for low fluorescence signal. Shading is relative across each map. The green circle represents the area where PR was applied.
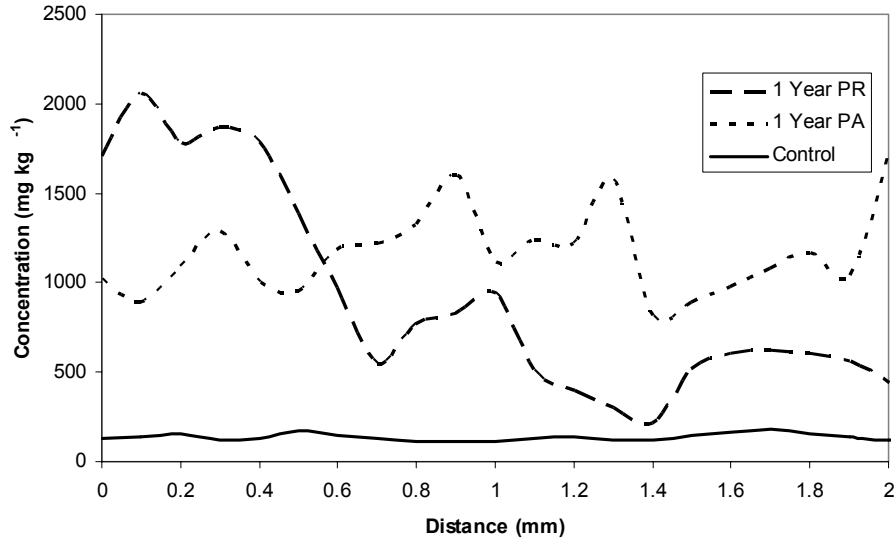
Figure A-14. A radial distribution plot for P generated by using µ-XRF maps for soils treated with PR and PA at the 52 week incubation period. Point of application is at 0 mm. The solid line at the bottom represents the background P concentration measured across the control soil using µ-XRF.
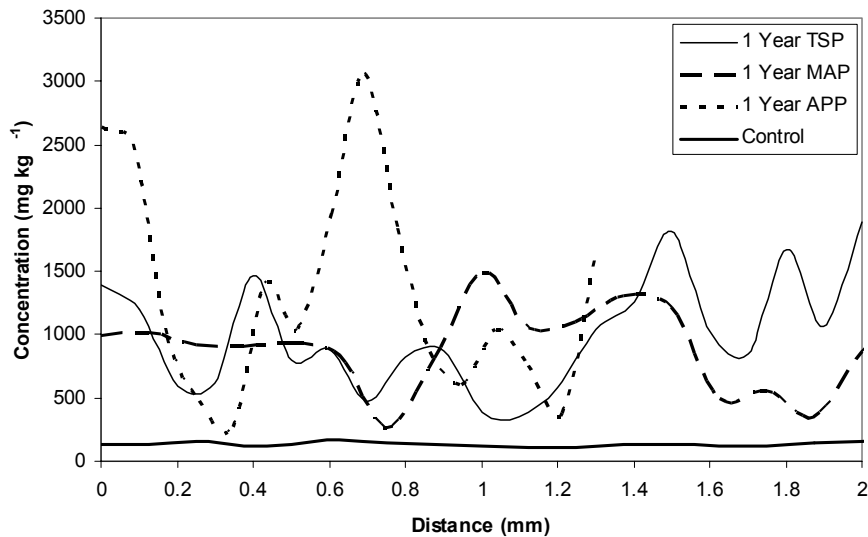
Figure A-15. A radial distribution plot for P generated by using µ-XRF maps for soils treated with TSP, APP, and MAP at the 52 week incubation period. Point of application is at 0 mm. The solid line at the bottom represents the background P concentration measured across the control soil using µ-XRF.
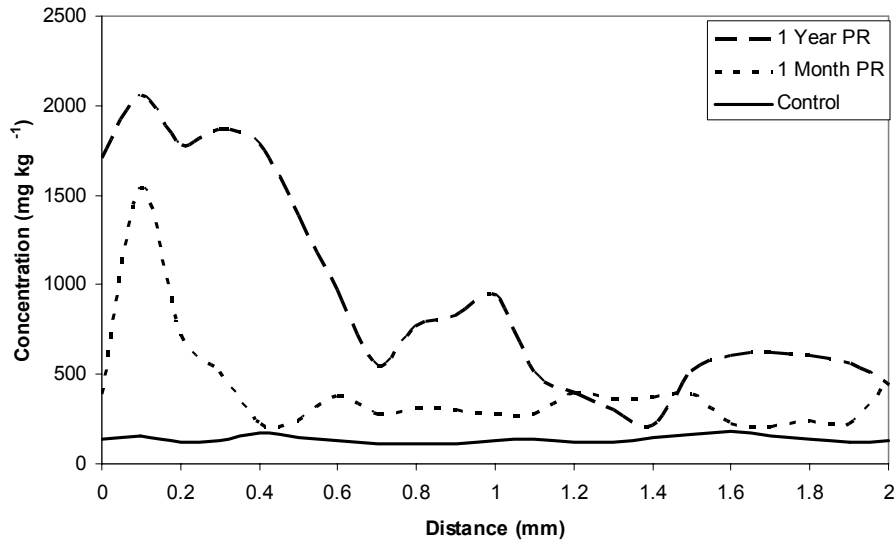
Figure A-16. A radial distribution plot for P generated by using μ-XRF maps for soils treated with PR comparing the 4 and 52 week incubation periods. Point of application is at 0 mm. The solid line at the bottom represents the background P concentration measured across the control soil using μ-XRF.
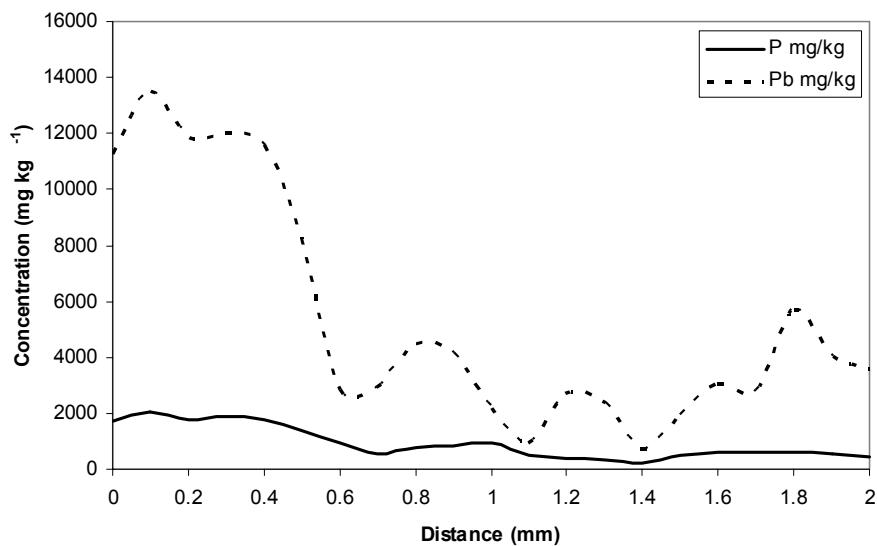
Figure A-17. A radial distribution plot for P and Pb generated by using μ-XRF maps for soil treated with PR at the 52 week incubation period. Point of application is at 0 mm. The solid line at the bottom represents the background P concentration measured across the control soil using μ-XRF. Figure illustrates the movement of Pb towards PR.

Figure A-18. **Micro-XRD pattern for treatment PR4 point P1. Original Debye-Sherer rings are located in the top-right hand corner of the graph. Species detected are willemite (d-spacings of 2.63, 2.84, 3.48, 1.86, 1.42, 4.02, and 1.34) and $PbH_2P_2O_8 * H_2O$ (d-spacings of 2.15, 7.82, 3.47, 2.48, 4.21, 3.16, 2.65, and 2.33).**

Figure A-19. **Micro-XRD pattern for treatment PR4 point P2. Original Debye-Sherer rings are located in the top-right hand corner of the graph. Species detected is franklinite (d-spacings of 2.55, 1.50, 2.99, 1.63, 1.10, 0.98, 2.12, 1.73).**

230

Figure A-20. Micro-XRD pattern for treatment PR4 point P3. Original Debye-Sherer rings are located in the top-right hand corner of the graph. No mineral speices were identified.

Figure A-21. Micro-XRD pattern for treatment PR4 point P4. Original Debye-Sherer rings are located in the top-right hand corner of the graph. No mineral speices were identified.

Figure A-22. **Micro-XRD pattern for treatment PR4 point P5.** **Original Debye-Sherer rings are located in the top-right hand corner of the graph.** **No mineral speices were identified.**

Figure A-23. **Micro-XRD pattern for treatment PR4 point P6.** **Original Debye-Sherer rings are located in the top-right hand corner of the graph.** **No mineral speices were identified.**

Figure A-24. Micro-XRD pattern for treatment TSP4 point P7. Original Debye-Sherer rings are located in the top-right hand corner of the graph. No mineral speices were identified.

Figure A-25. Micro-XRD pattern for treatment TSP4 point P8. Original Debye-Sherer rings are located in the top-right hand corner of the graph. No mineral speices were identified.

Figure A-26. Micro-XRD pattern for treatment TSP4 point P9. Original Debye-Sherer rings are located in the top-right hand corner of the graph. The mineral species detected is gahnite (d-spacings of 2.86, 2.44, 1.43, 1.56, 1.65, 0.83, 1.05, and 1.86).

Figure A-27. Micro-XRD pattern for treatment TSP4 point P10. Original Debye-Sherer rings are located in the top-right hand corner of the graph. The mineral species detected is vuagnatite (d-spacings of 2.22, 2.52, 3.00, 2.67, 2.45, 2.14, 2.40, and 3.93).

234

Figure A-28. Micro-XRD pattern for treatment TSP4 point P11. Original Debye-Sherer rings are located in the top-right hand corner of the graph. No mineral speices were identified.

Figure A-29. Micro-XRD pattern for treatment TSP4 point P12. Original Debye-Sherer rings are located in the top-right hand corner of the graph. No mineral speices were identified.

Figure A-30. Micro-XRD pattern for treatment TSP4 point P13. Original Debye-Sherer rings are located in the top-right hand corner of the graph. No mineral speices were identified.

Figure A-31. Micro-XRD pattern for treatment TSP4 point P14. Original Debye-Sherer rings are located in the top-right hand corner of the graph. No mineral speices were identified.

Figure A-32. Micro-XRD pattern for treatment TSP4 point P15. Original Debye-Sherer rings are located in the top-right hand corner of the graph. The likely mineral species is quartz (d-spacings of 3.34, 4.26, 1.82, 1.54, 2.46, 2.28, 1.37, and 1.38).

Figure A-33. Micro-XRD pattern for treatment TSP4 point P16. Original Debye-Sherer rings are located in the top-right hand corner of the graph. No mineral speices were identified.

Figure A-34. Micro-XRD pattern for treatment TSP4 point P17. Original Debye-Sherer rings are located in the top-right hand corner of the graph. The mineral species identified include willemite (d-spacings of 2.63, 2.84, 2.73, 3.32, 1.86, 1.42, 4.02, and 1.34), gahnite (d-spacings of 2.86, 2.44, 1.43, 1.56, 1.65, 0.83, 1.05, and 1.86), and franklinite (d-spacings of 2.55, 1.50, 2.99, 1.63, 1.10, 0.98, 2.12, and 1.73).

Figure A-35. Micro-XRD pattern for treatment PA4 point P18. Original Debye-Sherer rings are located in the top-right hand corner of the graph. The mineral species identified include plumbogummite (d-spacings of 2.97, 5.70, 3.51, 2.22, 2.21, 1.90, 3.42, and 5.57) and plumboferrite (d-spacings of 2.64, 2.83, 2.96, 1.68, 1.64, 1.48, 3.91, and 2.44).

Figure A-36. Micro-XRD pattern for treatment PA4 point P19. Original Debye-Sherer rings are located in the top-right hand corner of the graph. The mineral species identified include plumbogummite (d-spacings of 2.97, 5.70, 3.51, 2.22, 2.21, 1.90, 3.42, and 5.57) and galena (d-spacings of 2.97, 3.43, 2.10, 1.77, 1.33, 1.71, 1.48, 1.36).

Figure A-37. Micro-XRD pattern for treatment PA4 point P20. Original Debye-Sherer rings are located in the top-right hand corner of the graph. The mineral species identified include plumbogummite (d-spacings of 2.97, 5.70, 3.51, 2.22, 2.21, 1.90, 3.42, and 5.57) and galena (d-spacings of 2.97, 3.43, 2.10, 1.77, 1.33, 1.71, 1.48, 1.36).

239

Figure A-38. Micro-XRD pattern for treatment PA4 point P21. Original Debye-Sherer rings are located in the top-right hand corner of the graph. The mineral species identified could be plumbogummite or galena because both have a major d-spacing at 2.97.

Figure A-39. Micro-XRD pattern for treatment PA4 point P22. Original Debye-Sherer rings are located in the top-right hand corner of the graph. The mineral species identified include willemite (d-spacings of 2.63, 2.84, 3.48, 2.32, 1.86, 1.42, 4.02, and 1.34) and smithsonite (d-spacings of 2.75, 3.55, 1.70, 2.33, 1.95, 2.11, 1.52, and 1.49).

Figure A-40. Micro-XRD pattern for treatment PA4 point P23. Original Debye-Sherer rings are located in the top-right hand corner of the graph. The mineral species identified include gahnite (d-spacings of 2.86, 2.44, 1.43, 1.56, 1.65, 0.83, 1.05, and 1.86) and kehoeite (d-spacings of 3.35, 4.28, 2.97, 1.91, 7.61, 2.21, 1.63, and 1.38).

Figure A-41. Micro-XRD pattern for treatment PA4 point P24. Original Debye-Sherer rings are located in the top-right hand corner of the graph. There were no mineral species that were able to be identified.

Figure A-42. Micro-XRD pattern for treatment PA4 point P25. Original Debye-Sherer rings are located in the top-right hand corner of the graph. The mineral species identified include cerussite (d-spacings of 3.59, 3.50, 2.49, 2.08, 3.07, 1.86, 2.52, and 1.93), plumbogummite has a major d-spacing at 3.51, and galena has a d-spacing at 1.33.

Figure A-43. Micro-XRD pattern for treatment PA4 point P26. Original Debye-Sherer rings are located in the top-right hand corner of the graph. The mineral species identified include zincite (d-spacings of 2.48, 2.81, 2.60, 1.62, 1.48, 1.91, 1.38, and 1.36) and hemimorphite (d-spacings of 6.60, 3.10, 3.29, 3.30, 5.36, 2.40, 2.56, and 4.62).

Figure A-44. Micro-XRD pattern for treatment MAP4 point P27. Original Debye-Sherer rings are located in the top-right hand corner of the graph. There were no mineral species that were able to be identified.

Figure A-45. Micro-XRD pattern for treatment MAP4 point P28. Original Debye-Sherer rings are located in the top-right hand corner of the graph. The mineral species identified was willemite (d-spacings of 2.63, 2.84, 3.48, 2.32, 1.86, 1.42, 4.02, and 1.34).

Figure A-46. Micro-XRD pattern for treatment MAP4 point P29. Original Debye-Sherer rings are located in the top-right hand corner of the graph. The mineral species identified include plumboferrite (d-spacings of 2.64, 2.81, 2.96, 1.68, 1.64, 1.48, 3.91, and 2.44) and plumbogummite (d-spacings of 2.97, 5.70, 3.50, 2.22, 2.21, 1.90, 3.44, and 5.57).

Figure A-47. Micro-XRD pattern for treatment MAP4 point P30. Original Debye-Sherer rings are located in the top-right hand corner of the graph. The mineral species identified was galena (d-spacings of 2.97, 3.43, 2.10, 1.79, 1.33, 1.71, 1.48, and 1.36).

244

Figure A-48. Micro-XRD pattern for treatment MAP4 point P31. Original Debye-Sherer rings are located in the top-right hand corner of the graph. The mineral species identified include pyromorphite (d-spacings of 2.99, 2.96, 2.89, 4.13, 3.27, 2.06, 3.38, and 1.92) and franklinite (d-spacings of 2.55, 2.98, 1.50, 1.63, 2.12, 1.72, 1.10, and 1.29).

Figure A-49. Micro-XRD pattern for treatment MAP4 point P32. Original Debye-Sherer rings are located in the top-right hand corner of the graph. The mineral species identified was willemite (d-spacings of 2.63, 2.84, 3.48, 2.32, 1.86, 1.42, 4.02, and 1.34).

Figure A-50. Micro-XRD pattern for treatment MAP4 point P33. Original Debye-Sherer rings are located in the top-right hand corner of the graph. The mineral species identified was gahnite (d-spacings of 2.86, 2.44, 1.43, 1.56, 1.65, 0.83, 1.05, and 1.86).
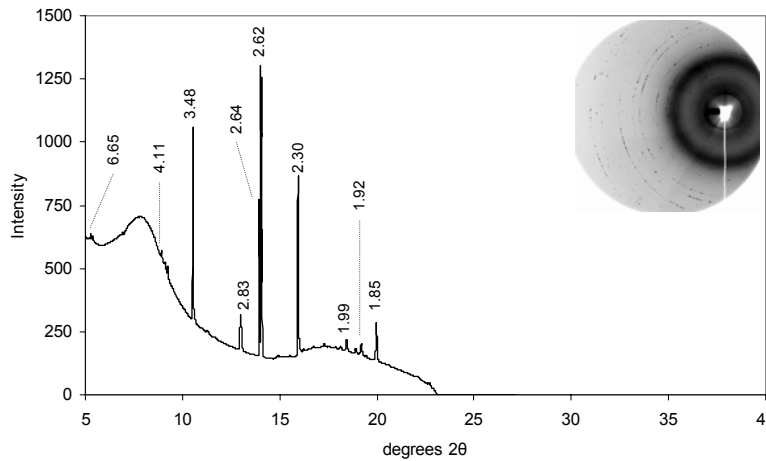
Figure A-51. Micro-XRD pattern for treatment MAP4 point P34. Original Debye-Sherer rings are located in the top-right hand corner of the graph. The mineral species identified include willemite (d-spacings of 2.63, 2.84, 3.48, 2.32, 1.86, 1.42, 4.02, and 1.34) and hopeite (d-spacings of 4.57, 2.85, 9.12, 3.46, 3.39, 4.41, 1.94, and 4.85).

246
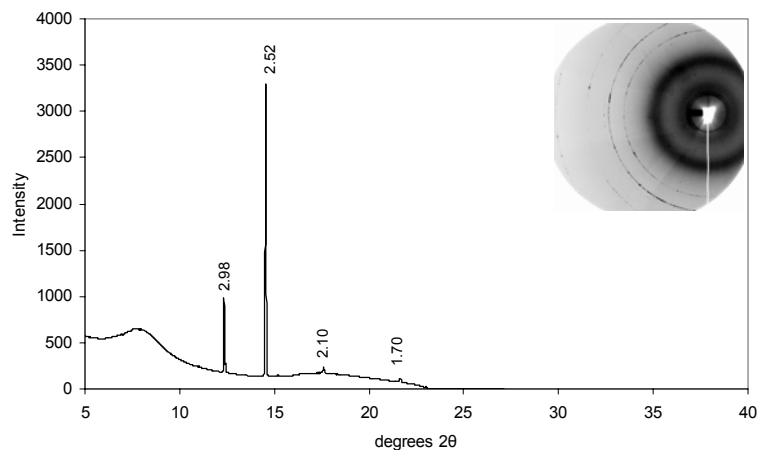
Figure A-52. Micro-XRD pattern for treatment MAP4 point P35. Original Debye-Sherer rings are located in the top-right hand corner of the graph. The mineral species identified was franklinite (d-spacings of 2.55, 1.50, 2.99, 1.63, 1.10, 0.98, 2.12, and 1.73).
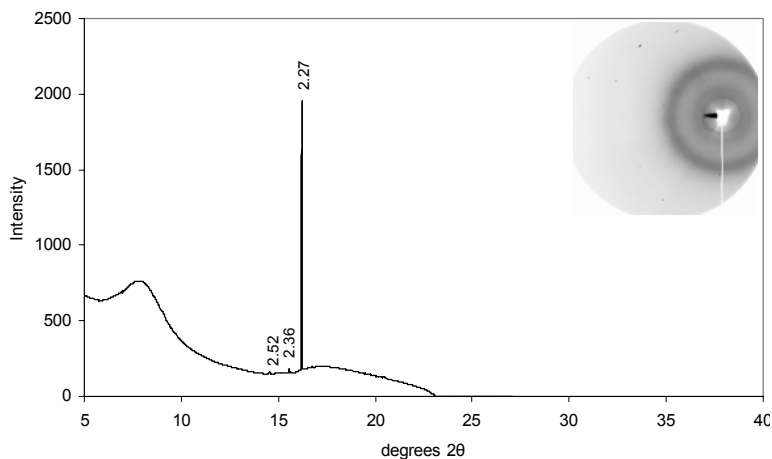
Figure A-53. Micro-XRD pattern for treatment MAP4 point P36. Original Debye-Sherer rings are located in the top-right hand corner of the graph. Mineral species are difficult to determine from this pattern. However, quartz has a strong d-spacing at 2.27.
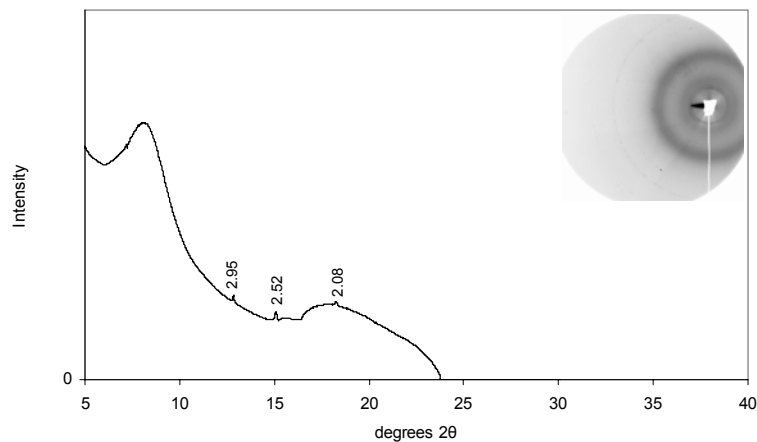
Figure A-54. Micro-XRD pattern for treatment MAP4 point P37. Original Debye-Sherer rings are located in the top-right hand corner of the graph. Mineral species identified was galena (d-spacings of 2.97, 3.43, 2.10, 1.79, 1.33, 1.71, 1.48, and 1.36).
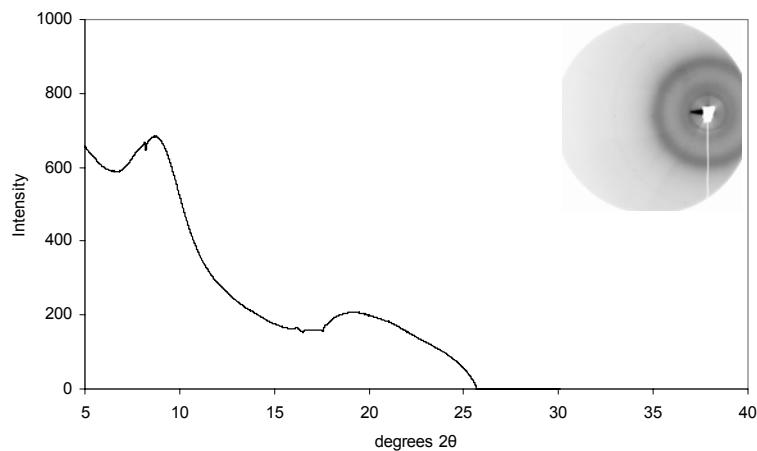
Figure A-55. Micro-XRD pattern for treatment APP4 point P38. Original Debye-Sherer rings are located in the top-right hand corner of the graph. No mineral species were identified.
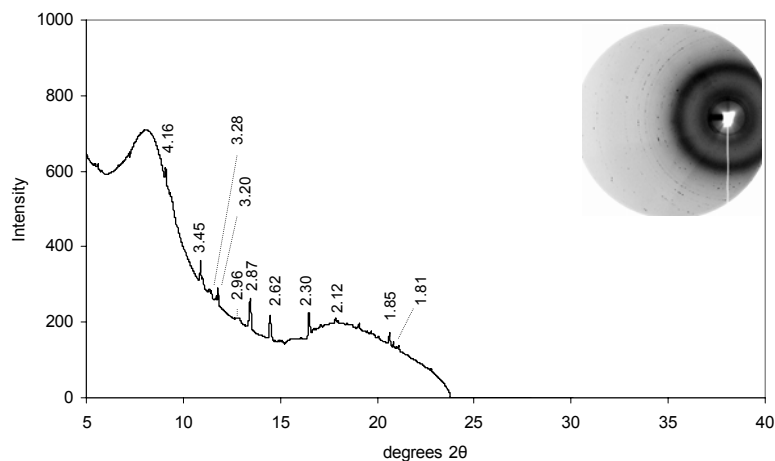
Figure A-56. Micro-XRD pattern for treatment APP4 point P39. Original Debye-Sherer rings are located in the top-right hand corner of the graph. The mineral species identified include galena (d-spacings of 2.97, 3.43, 2.10, 1.79, 1.33, 1.71, 1.48, and 1.36) and pyromorphite (d-spacings of 2.99, 2.96, 2.89, 4.13, 3.27, 2.06, 3.38, and 1.92).
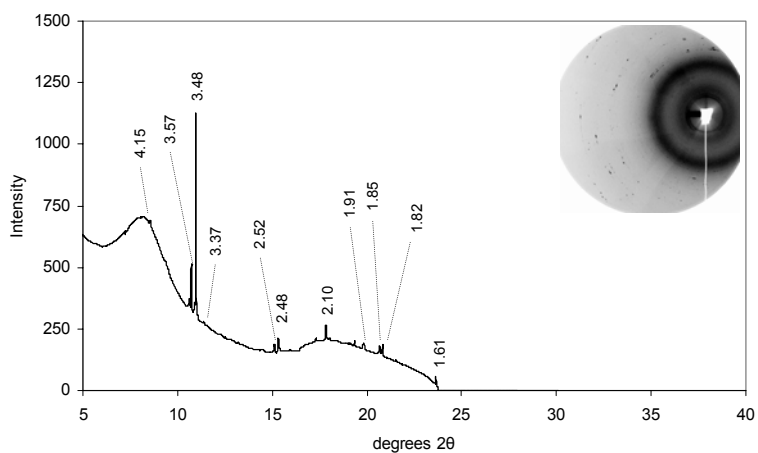
Figure A-57. Micro-XRD pattern for treatment APP4 point P40. Original Debye-Sherer rings are located in the top-right hand corner of the graph. The mineral species identified include galena (d-spacings of 2.97, 3.43, 2.10, 1.79, 1.33, 1.71, 1.48, and 1.36) and cerussite (d-spacings of 3.59, 3.50, 2.49, 2.08, 3.07, 1.86, 2.52, and 1.93).

249
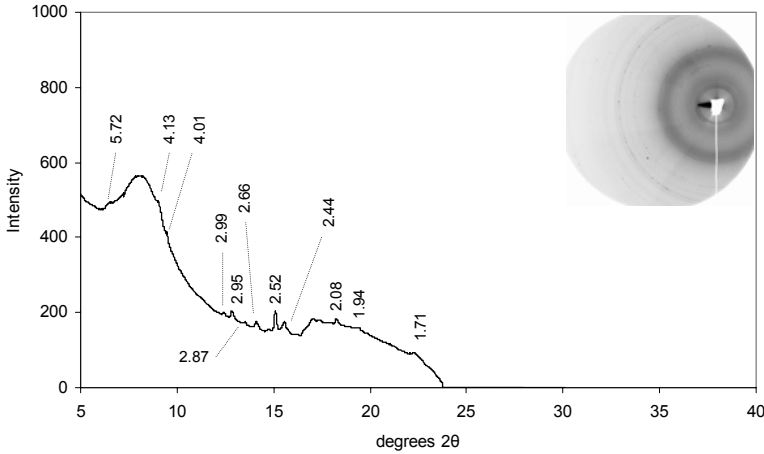
Figure A-58. Micro-XRD pattern for treatment APP4 point P41. Original Debye-Sherer rings are located in the top-right hand corner of the graph. The mineral species identified include galena (d-spacings of 2.97, 3.43, 2.10, 1.79, 1.33, 1.71, 1.48, and 1.36), pyromorphite (d-spacings of 2.99, 2.96, 2.89, 4.13, 3.27, 2.06, 3.38, 1.92), and plumboferrite (d-spacings of 2.64, 2.81, 2.96, 1.68, 1.64, 1.48, 3.91, and 2.44).
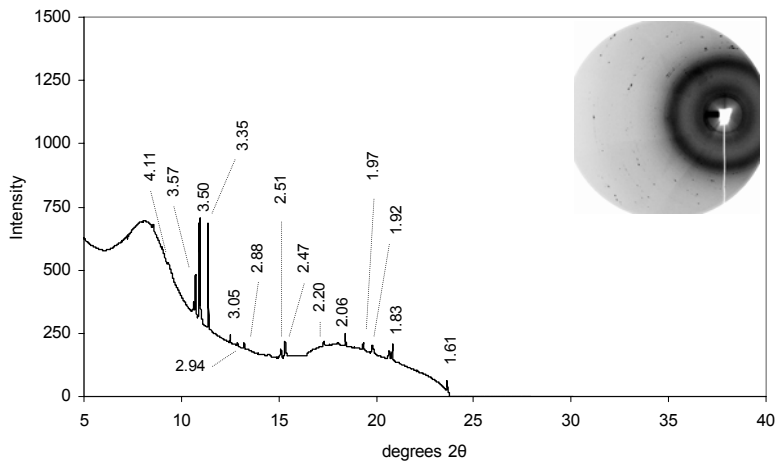
Figure A-59. Micro-XRD pattern for treatment APP4 point P42. Original Debye-Sherer rings are located in the top-right hand corner of the graph. The mineral species identified include galena (d-spacings of 2.97, 3.43, 2.10, 1.79, 1.33, 1.71, 1.48, and 1.36), pyromorphite (d-spacings of 2.99, 2.96, 2.89, 4.13, 3.27, 2.06, 3.38, 1.92), and cerussite (3.59, 3.50, 2.49, 2.08, 3.07, 1.86, 2.52, 1.93)
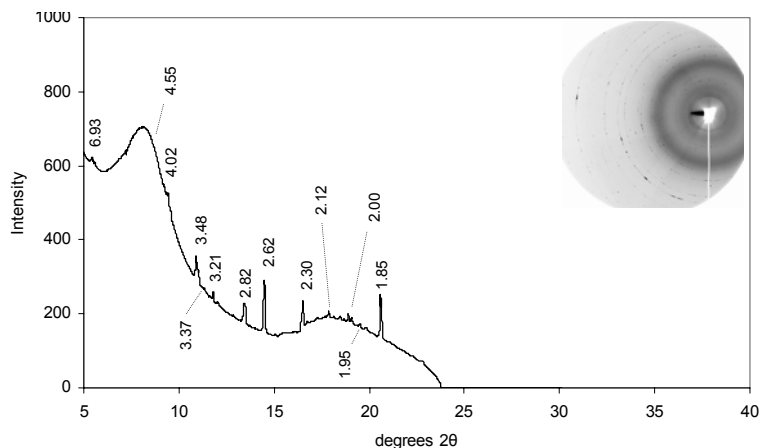
Figure A-60. Micro-XRD pattern for treatment APP4 point P43. Original Debye-Sherer rings are located in the top-right hand corner of the graph. The mineral species identified include willemite (2.63, 2.84, 3.48, 2.32, 1.86, 1.42, 4.02, 1.34), and hopeite (4.57, 2.85, 9.12, 3.46, 3.39, 4.41, 1.94, 4.85)
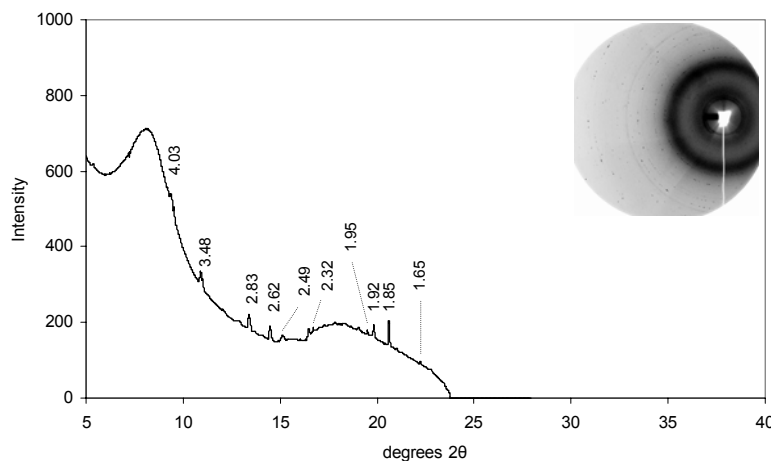
Figure A-61. . Micro-XRD pattern for treatment APP4 point P44. Original Debye-Sherer rings are located in the top-right hand corner of the graph. The mineral species identified include zincite (2.48, 2.81, 2.60, 1.62, 1.48, 1.91, 4.38, 1.38); hopeite (4.57, 2.85, 9.12, 3.46, 3.39, 4.41, 1.94, 4.85); willemite (2.63, 2.84, 3.48, 2.32, 1.86, 1.42, 4.02, 1.34)
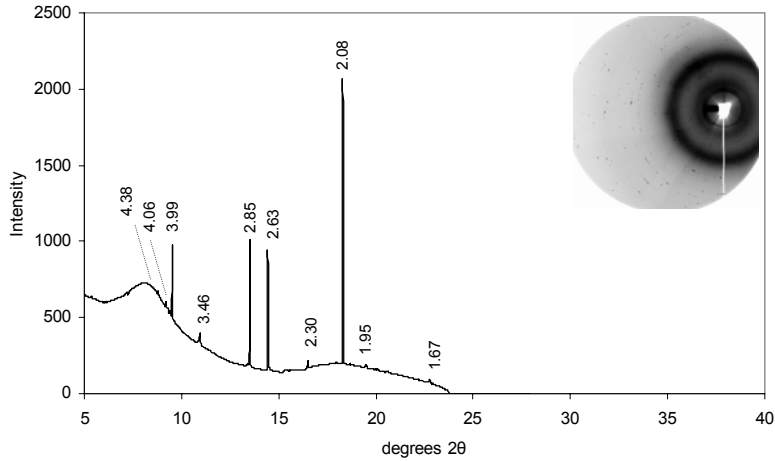
Figure A-62. Micro-XRD pattern for treatment APP4 point P45. Original Debye-Sherer rings are located in the top-right hand corner of the graph. The mineral species identified include willemite (2.63, 2.84, 3.48, 2.32, 1.86, 1.42, 4.02, 1.34), and hopeite (4.57, 2.85, 9.12, 3.46, 3.39, 4.41, 1.94, 4.85)
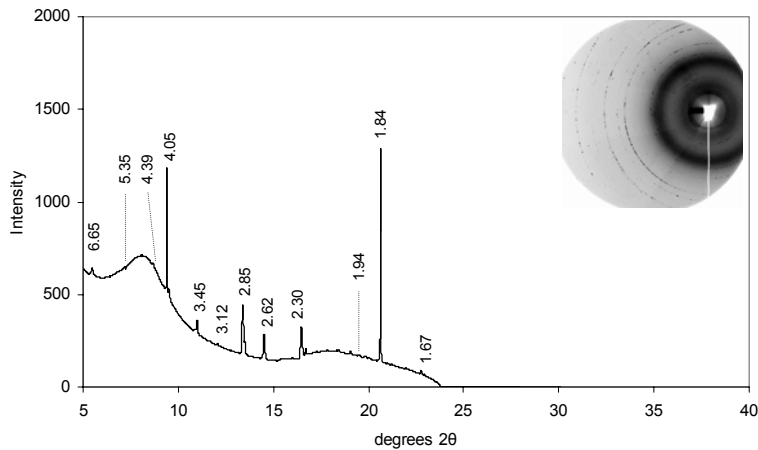
Figure A-63. Micro-XRD pattern for treatment APP4 point P46. Original Debye-Sherer rings are located in the top-right hand corner of the graph. The mineral species identified include willemite (2.63, 2.84, 3.48, 2.32, 1.86, 1.42, 4.02, 1.34), hopeite (4.57, 2.85, 9.12, 3.46, 3.39, 4.41, 1.94, 4.85), and hemimorphite (6.60, 3.10, 3.29, 3.30, 5.36, 2.40, 2.56, 4.62).
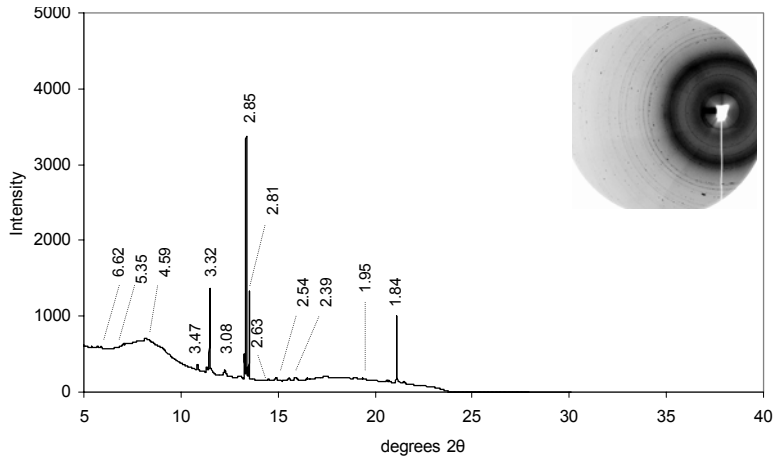
Figure A-64. Micro-XRD pattern for treatment APP4 point P47. Original Debye-Sherer rings are located in the top-right hand corner of the graph. The mineral species identified include willemite (2.63, 2.84, 3.48, 2.32, 1.86, 1.42, 4.02, 1.34), hopeite (4.57, 2.85, 9.12, 3.46, 3.39, 4.41, 1.94, 4.85), and hemimorphite (6.60, 3.10, 3.29, 3.30, 5.36, 2.40, 2.56, 4.62).
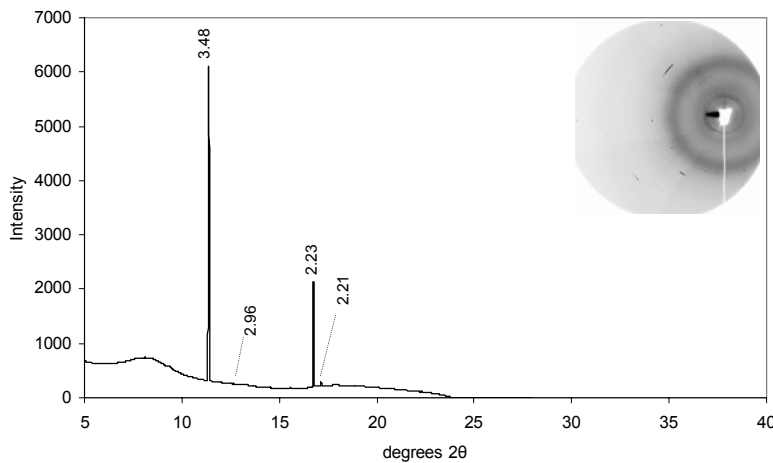
Figure A-65. Micro-XRD pattern for treatment PA52 point P48. Original Debye-Sherer rings are located in the top-right hand corner of the graph. The mineral species identified include plumbogummite (2.97, 5.70, 3.50, 2.22, 2.21, 1.90, 3.44, 5.57).
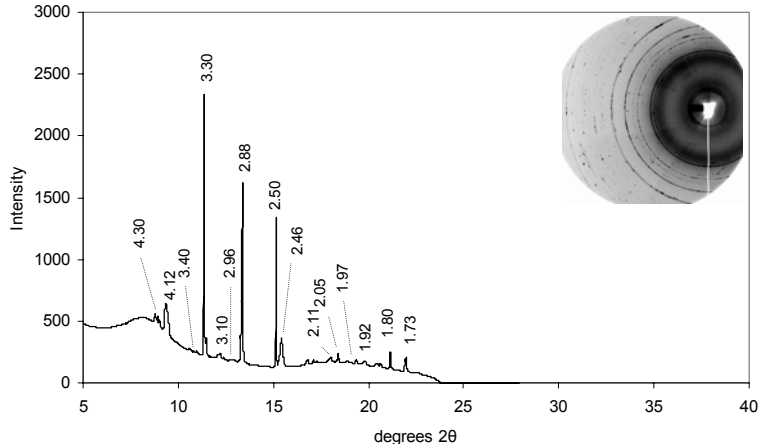
Figure A-66. Micro-XRD pattern for treatment PA52 point P49. Original Debye-Sherer rings are located in the top-right hand corner of the graph. The mineral species identified include galena (d-spacings of 2.97, 3.43, 2.10, 1.79, 1.33, 1.71, 1.48, and 1.36) and pyromorphite (d-spacings of 2.99, 2.96, 2.89, 4.13, 3.27, 2.06, 3.38, and 1.92).
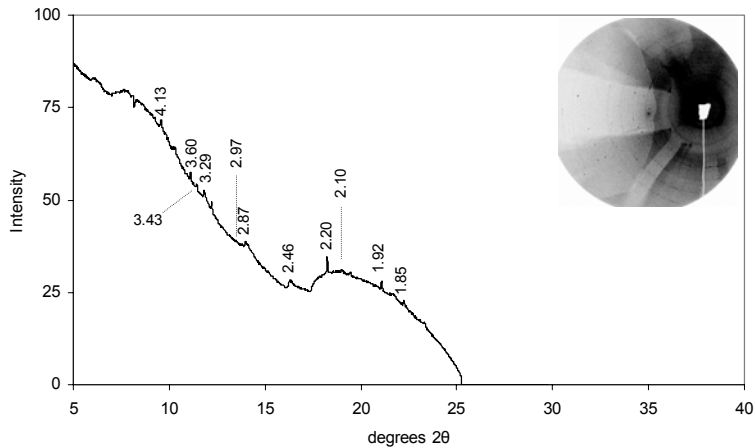
Figure A-67. Micro-XRD pattern for treatment PA52 point P50. Original Debye-Sherer rings are located in the top-right hand corner of the graph. The mineral species identified include galena (d-spacings of 2.97, 3.43, 2.10, 1.79, 1.33, 1.71, 1.48, and 1.36) and pyromorphite (d-spacings of 2.99, 2.96, 2.89, 4.13, 3.27, 2.06, 3.38, and 1.92).
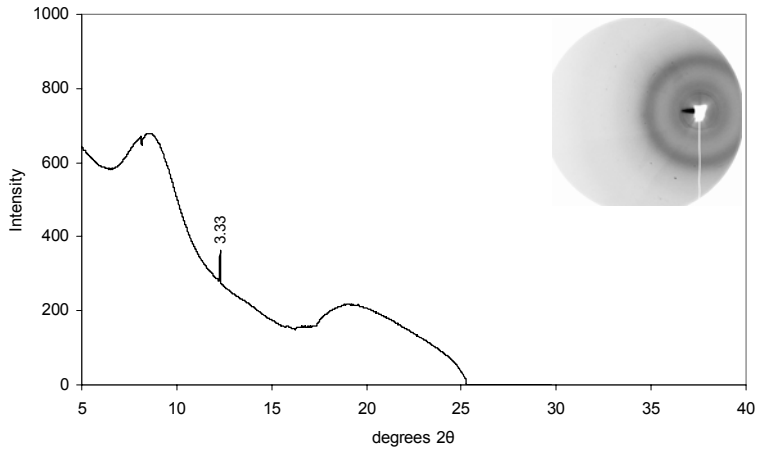
Figure A-68. Micro-XRD pattern for treatment PA52 point P51. Original Debye-Sherer rings are located in the top-right hand corner of the graph. No mineral species were identified.
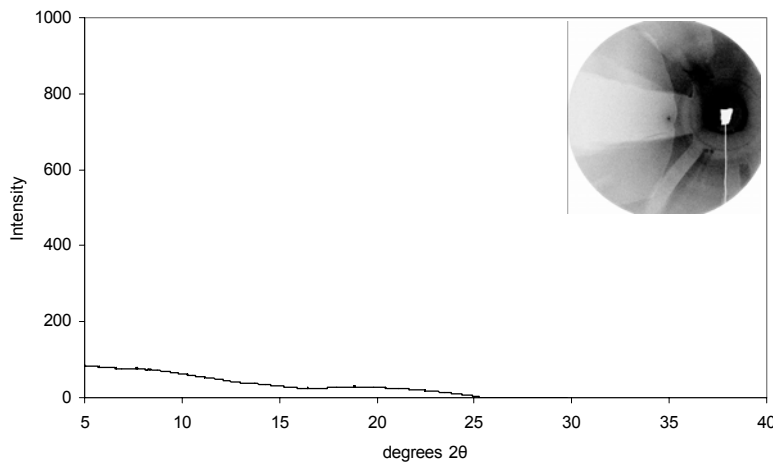
Figure A-69. Micro-XRD pattern for treatment PA52 point P52. Original Debye-Sherer rings are located in the top-right hand corner of the graph. No mineral species were identified.
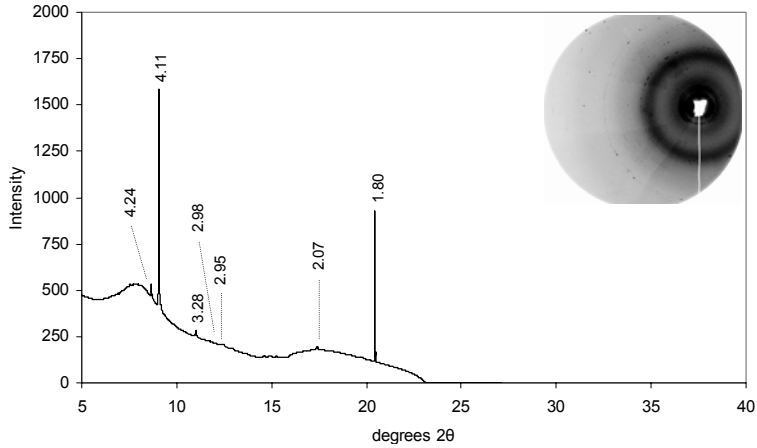
Figure A-70. Micro-XRD pattern for treatment PA52 point P53. Original Debye-Sherer rings are located in the top-right hand corner of the graph. The mineral species identified include galena (d-spacings of 2.97, 3.43, 2.10, 1.79, 1.33, 1.71, 1.48, and 1.36) and pyromorphite (d-spacings of 2.99, 2.96, 2.89, 4.13, 3.27, 2.06, 3.38, and 1.92).
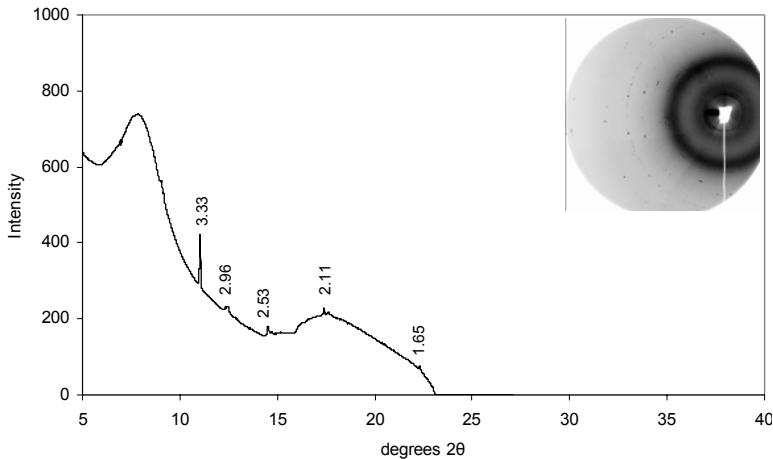
Figure A-71. Micro-XRD pattern for treatment PA52 point P54. Original Debye-Sherer rings are located in the top-right hand corner of the graph. The mineral species identified include franklinite (2.55, 2.98, 1.50, 1.63, 2.12, 1.72, 1.10, 1.29)

256
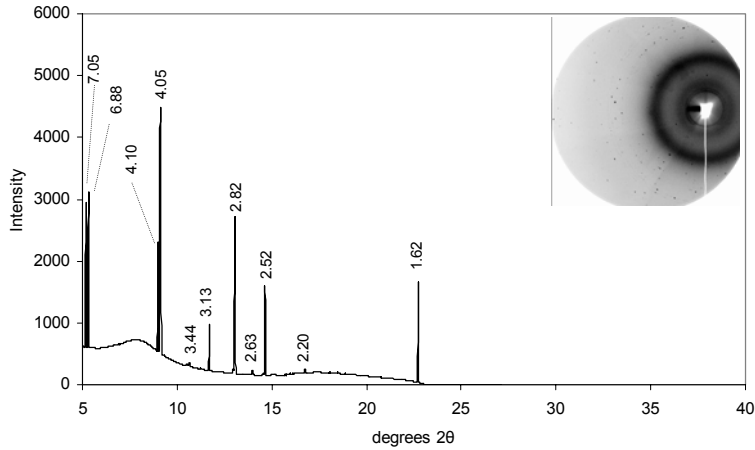
Figure A-72. Micro-XRD pattern for treatment PA52 point P55. Original Debye-Sherer rings are located in the top-right hand corner of the graph. The mineral species identified include willemite (2.63, 2.84, 3.48, 2.32, 1.86, 1.42, 4.02, 1.34).
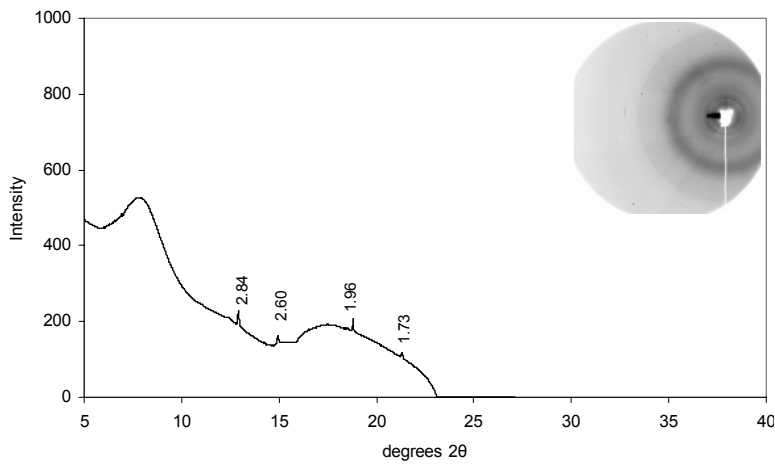
Figure A-73. Micro-XRD pattern for treatment PA52 point P56. Original Debye-Sherer rings are located in the top-right hand corner of the graph. The mineral species identified include willemite (2.63, 2.84, 3.48, 2.32, 1.86, 1.42, 4.02, 1.34).
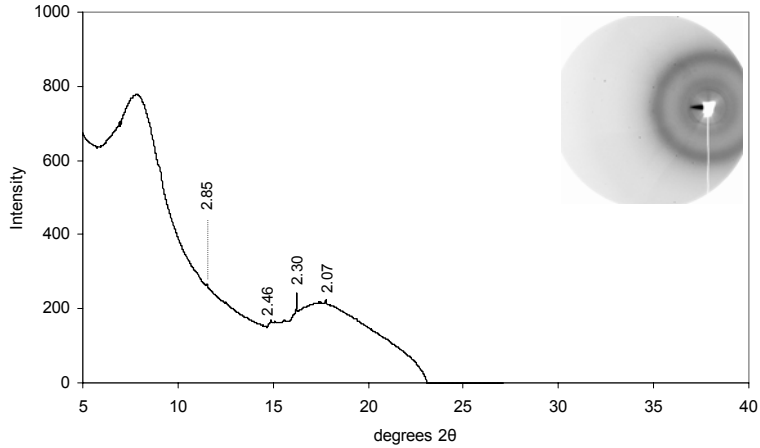
Figure A-74. Micro-XRD pattern for treatment PA52 point P57. Original Debye-Sherer rings are located in the top-right hand corner of the graph. The mineral species identified include willemite (2.63, 2.84, 3.48, 2.32, 1.86, 1.42, 4.02, 1.34).
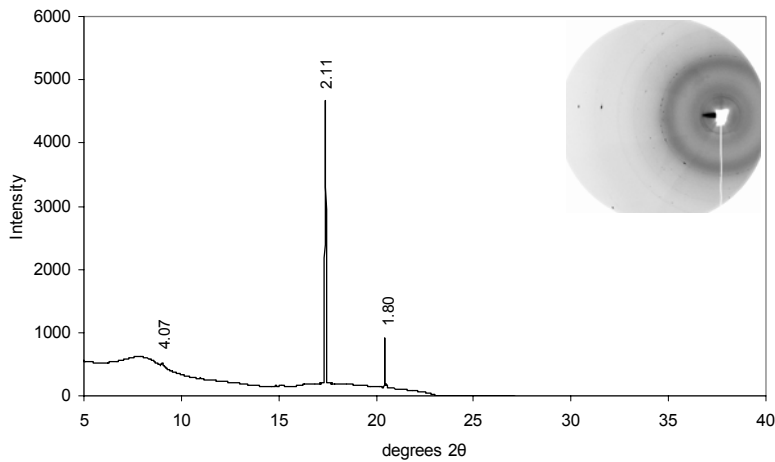
Figure A-75. Micro-XRD pattern for treatment PA52 point P58. Original Debye-Sherer rings are located in the top-right hand corner of the graph. The mineral species identified include galena (d-spacings of 2.97, 3.43, 2.10, 1.79, 1.33, 1.71, 1.48, and 1.36).

258
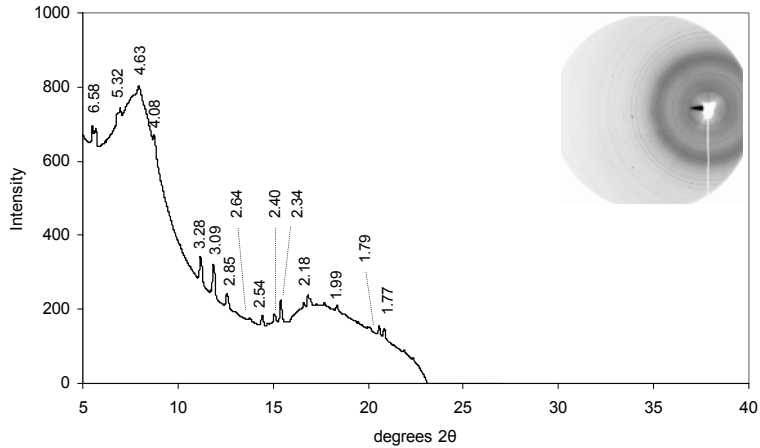
Figure A-76. Micro-XRD pattern for the contol treatment P59. Original Debye-Sherer rings are located in the top-right hand corner of the graph. The mineral species identified include hemimorphite (6.60, 3.10, 3.29, 3.30, 5.36, 2.40, 2.56, 4.62), and willemite (2.63, 2.84, 3.48, 2.32, 1.86, 1.42, 4.02, 1.34)
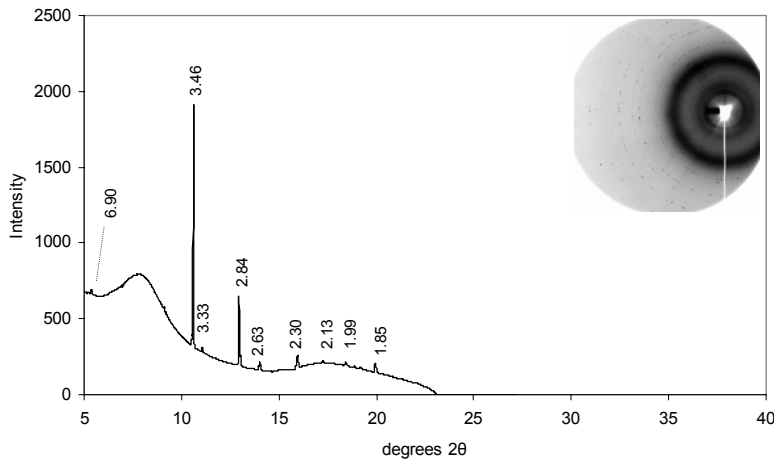
Figure A-77. Micro-XRD pattern for the contol treatment P60. Original Debye-Sherer rings are located in the top-right hand corner of the graph. The mineral species identified include willemite (2.63, 2.84, 3.48, 2.32, 1.86, 1.42, 4.02, 1.34)
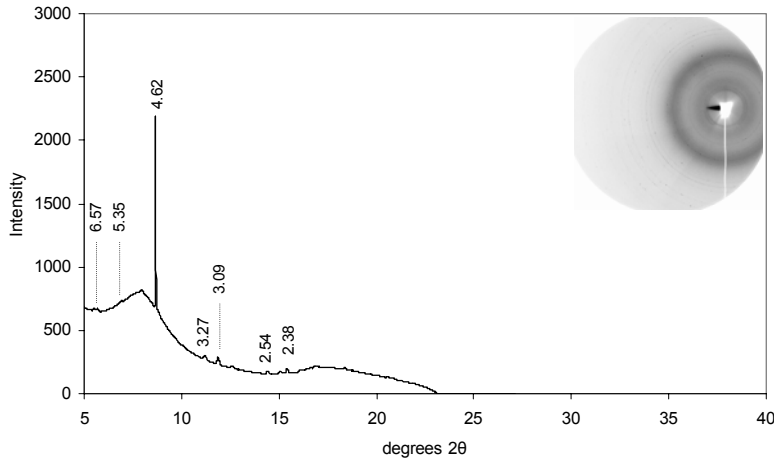
Figure A-78. **Micro-XRD pattern for the contol treatment P61. Original Debye-Sherer rings are located in the top-right hand corner of the graph. The mineral species identified include hemimorphite (6.60, 3.10, 3.29, 3.30, 5.36, 2.40, 2.56, 4.62).**
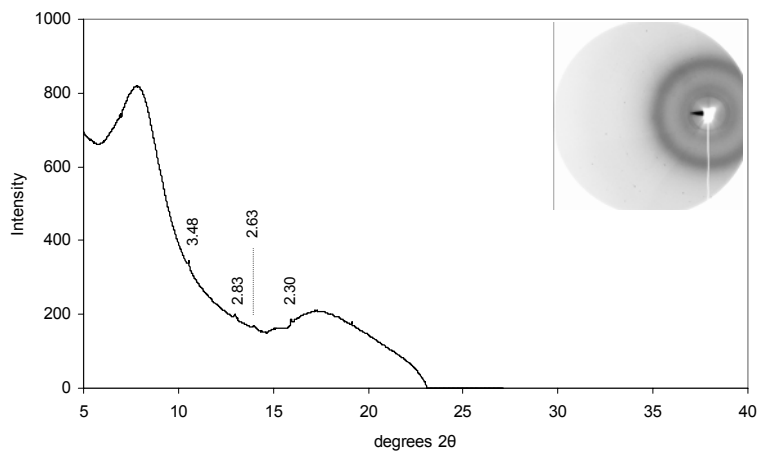
Figure A-79. **Micro-XRD pattern for the contol treatment P62. Original Debye-Sherer rings are located in the top-right hand corner of the graph. The mineral species identified include willemite (2.63, 2.84, 3.48, 2.32, 1.86, 1.42, 4.02, 1.34).**

260
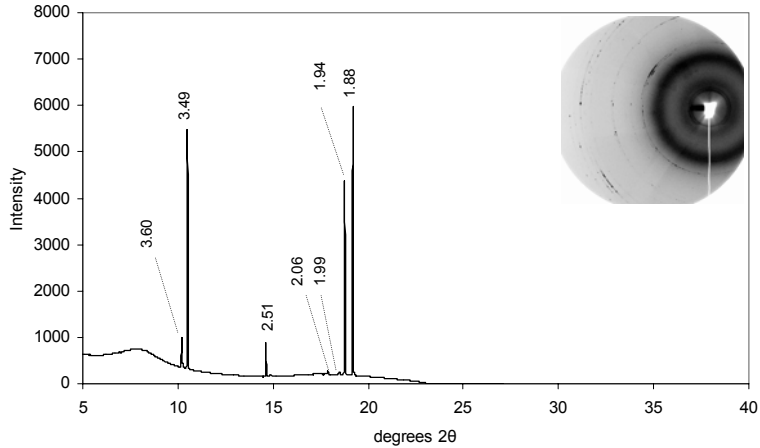
Figure A-80. **Micro-XRD pattern for the contol treatment P63. Original Debye-Sherer rings are located in the top-right hand corner of the graph. The mineral species identified include cerussite (3.59, 3.50, 2.49, 2.08, 3.07, 1.86, 2.52, 1.93).**
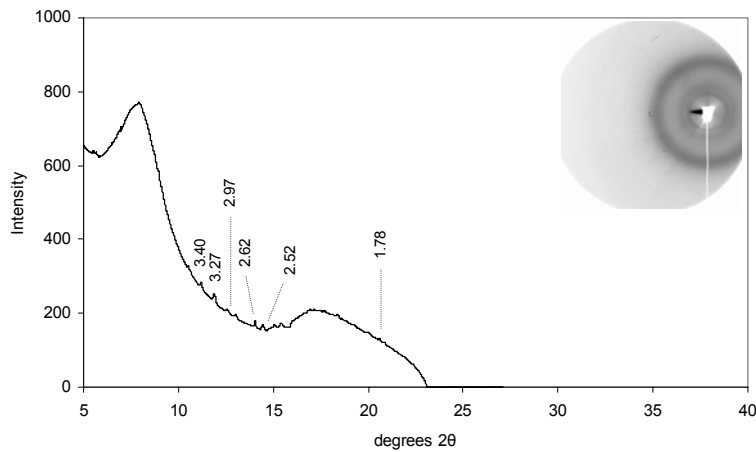
Figure A-81. **Micro-XRD pattern for the contol treatment P64. Original Debye-Sherer rings are located in the top-right hand corner of the graph. The mineral species identified include galena (2.97, 3.43, 2.10, 1.79, 1.33, 1.71, 1.48, 1.36).**
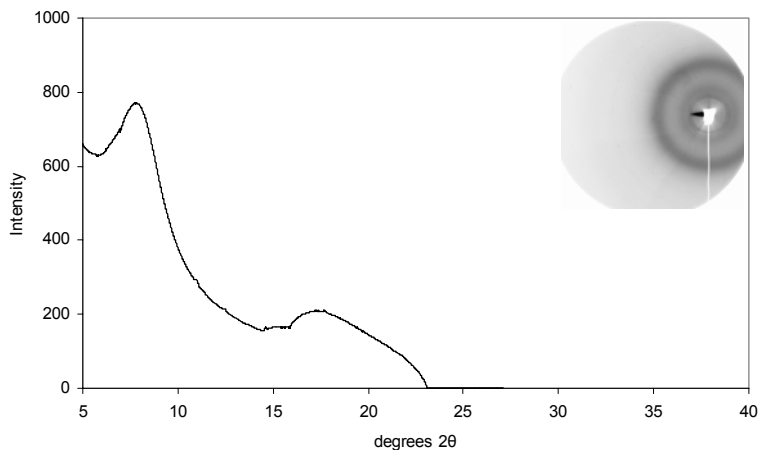
Figure A-82. **Micro-XRD pattern for the contol treatment P65. Original Debye-Sherer rings are located in the top-right hand corner of the graph. There were no mineral species that were able to be identified.**
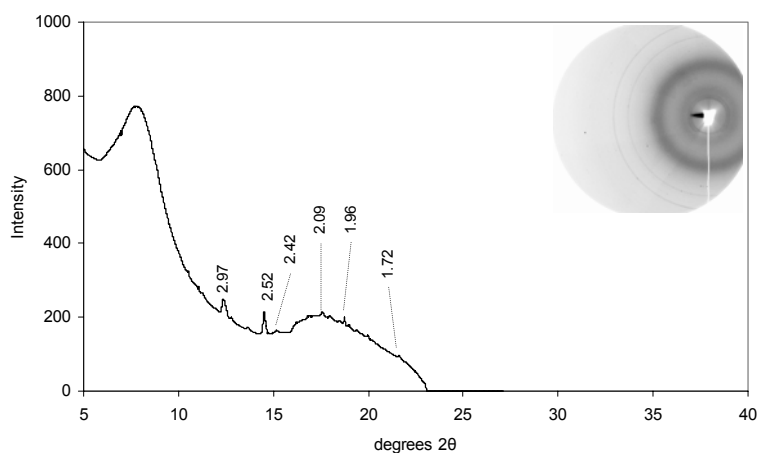
Figure A-83. **Micro-XRD pattern for the contol treatment P66. Original Debye-Sherer rings are located in the top-right hand corner of the graph. The mineral species identified include franklinite (2.55, 1.50, 2.99, 1.63, 1.10, 0.98, 2.12, 1.73).**
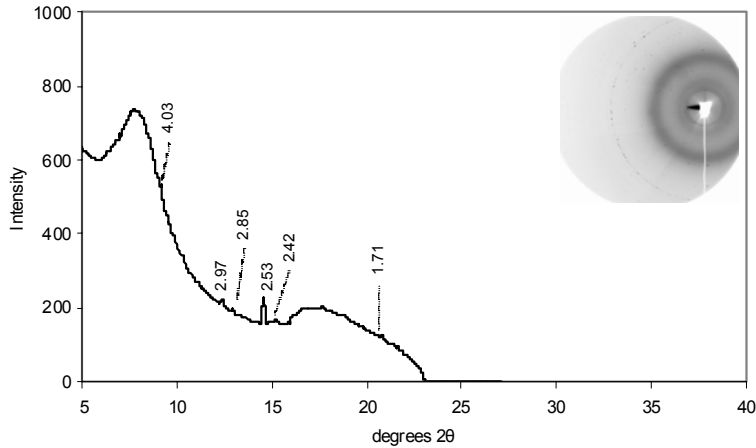
Figure A-84. Micro-XRD pattern for the contol treatment P67. Original Debye-Sherer rings are located in the top-right hand corner of the graph. The mineral species identified include gahnite (2.86, 2.44, 1.453, 1.56, 1.65, 0.83, 1.05, 1.86), and willemite (2.63, 2.84, 3.48, 2.32, 1.86, 1.42, 4.02, 1.34).
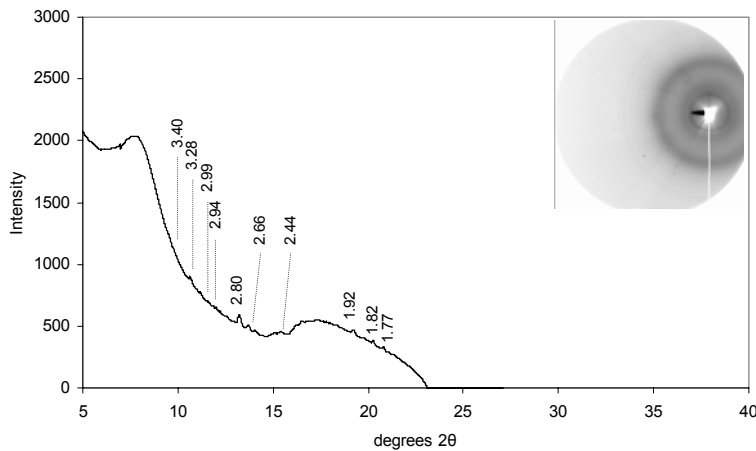
Figure A-85. Micro-XRD pattern for treatment PR52 point P68. Original Debye-Sherer rings are located in the top-right hand corner of the graph. The mineral species identified include plumboferrite (2.64, 2.81, 2.96, 1.68, 1.64, 1.48, 3.91, 2.44) and pyromorphite (2.99, 2.96, 2.89, 4.13, 3.27, 2.06, 3.38, 1.92).
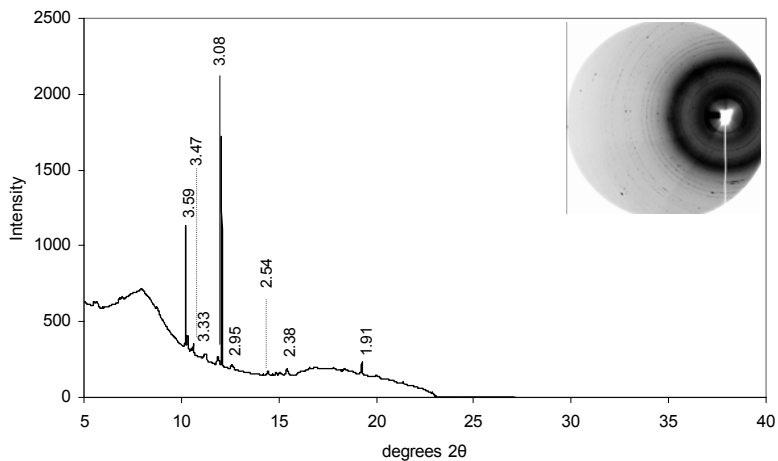
Figure A-86. Micro-XRD pattern for treatment PR52 point P69. Original Debye-Sherer rings are located in the top-right hand corner of the graph. The mineral species identified include cerussite (3.59, 3.50, 2.49, 2.08, 3.07, 1.86, 2.52, 1.93) and plumbogummite (2.97, 5.70, 3.50, 2.22, 2.21, 1.90, 3.44, 5.57) .
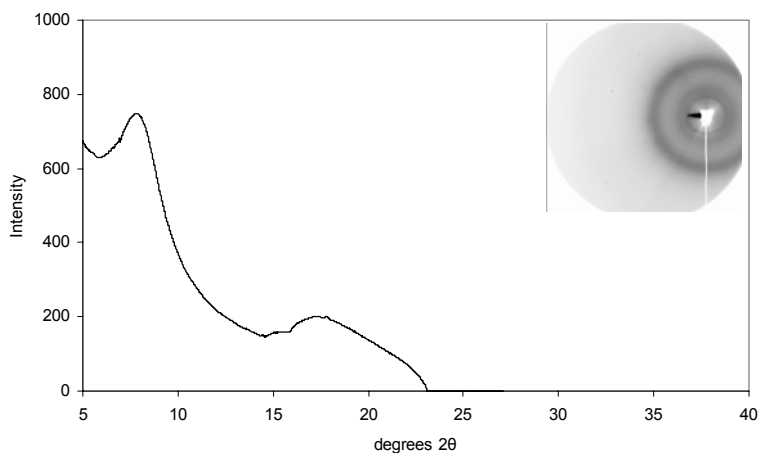
Figure A-87. Micro-XRD pattern for treatment PR52 point P70. Original Debye-Sherer rings are located in the top-right hand corner of the graph. There were no mineral species that were able to be identified.
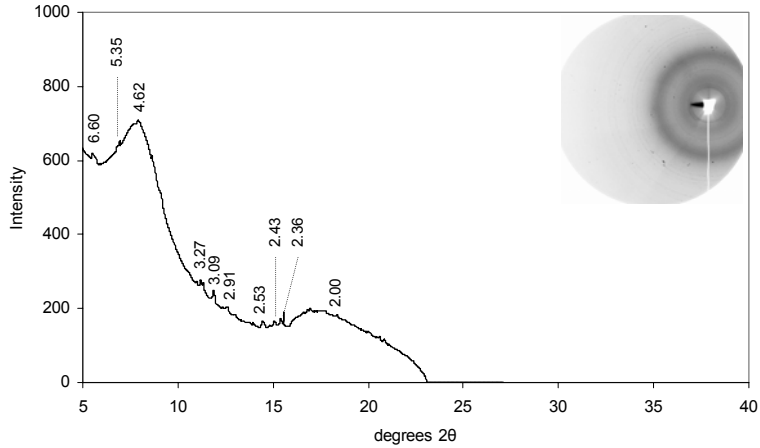
Figure A-88. Micro-XRD pattern for treatment PR52 point P71. Original Debye-Sherer rings are located in the top-right hand corner of the graph. The mineral species identified include hemimorphite (6.60, 3.10, 3.29, 3.30, 5.36, 2.40, 2.56, 4.62).
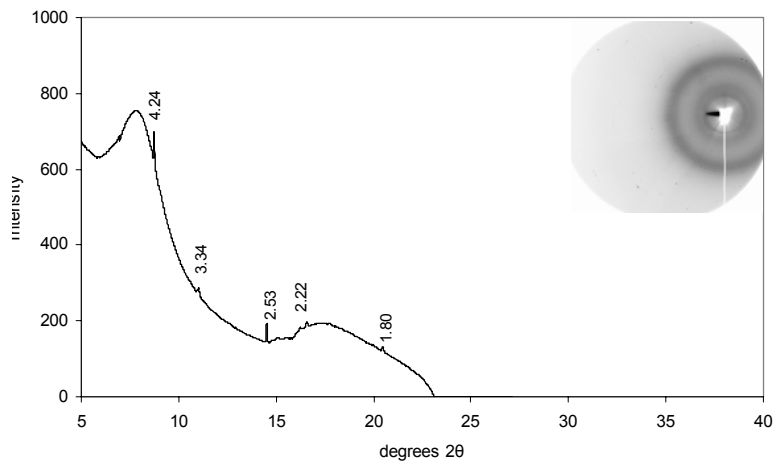
Figure A-89. Micro-XRD pattern for treatment PR52 point P72. Original Debye-Sherer rings are located in the top-right hand corner of the graph. The mineral species identified include anglesite (3.00, 4.26, 3.33).
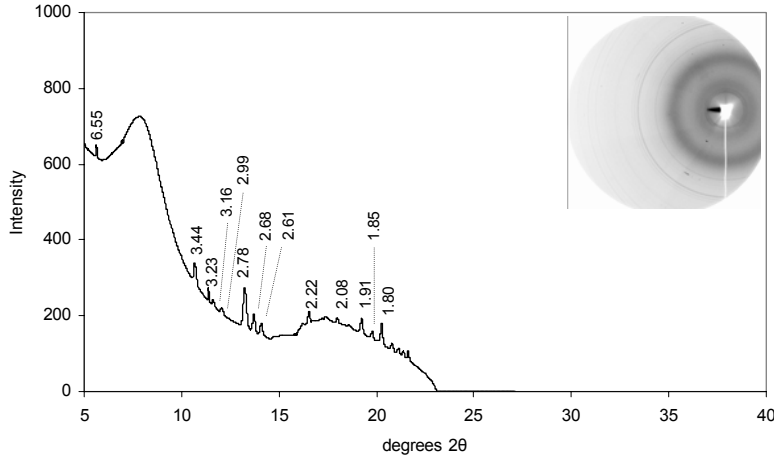
Figure A-90. Micro-XRD pattern for treatment PR52 point P73. Original Debye-Sherer rings are located in the top-right hand corner of the graph. The mineral species identified include galena (2.99, 3.43, 2.10, 1.79, 1.33, 1.71, 1.48, 1.36), plumboferrite (2.64, 2.81, 2.96, 1.68, 1.64, 1.48, 3.91, 2.44) and hemimorphite (6.60, 3.10, 3.29, 3.30, 5.36, 2.40, 2.56, 4.62).
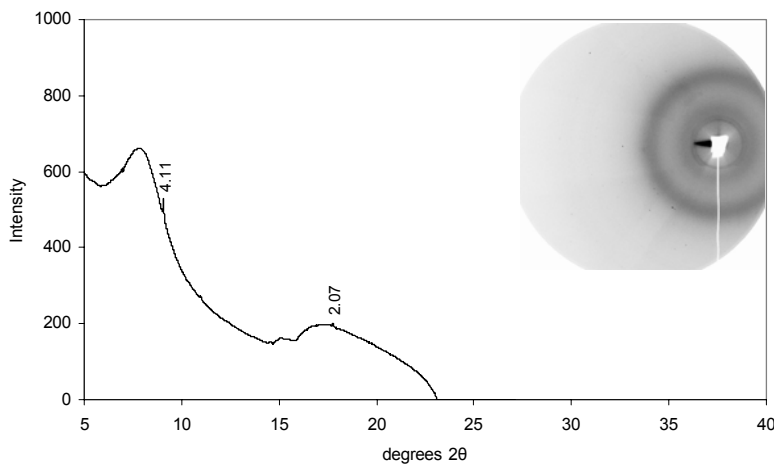
Figure A-91. Micro-XRD pattern for treatment PR52 point P74. Original Debye-Sherer rings are located in the top-right hand corner of the graph. The mineral species identified include pyromorphite has peaks at 4.13 and 2.06 (Inconclusive).
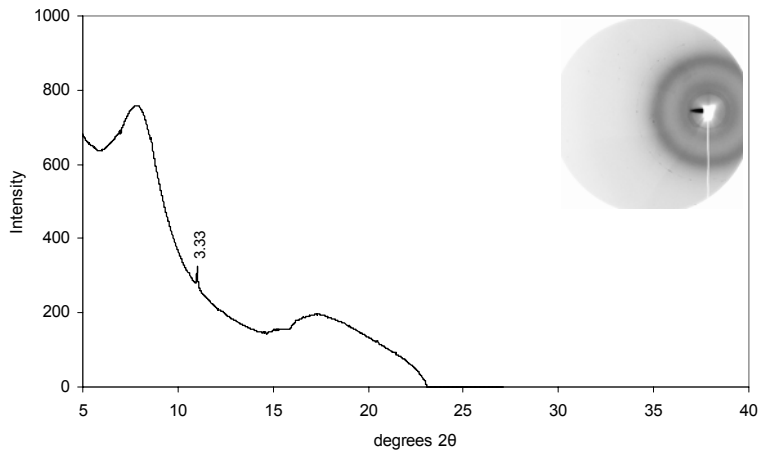
Figure A-92. Micro-XRD pattern for treatment PR52 point P75. Original Debye-Sherer rings are located in the top-right hand corner of the graph. There were no mineral species that were able to be identified.
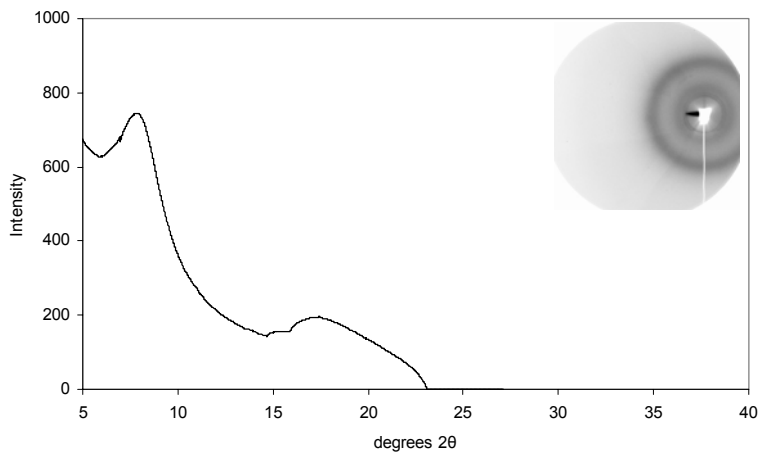
Figure A-93. Micro-XRD pattern for treatment PR52 point P76. Original Debye-Sherer rings are located in the top-right hand corner of the graph. There were no mineral species that were able to be identified.

267
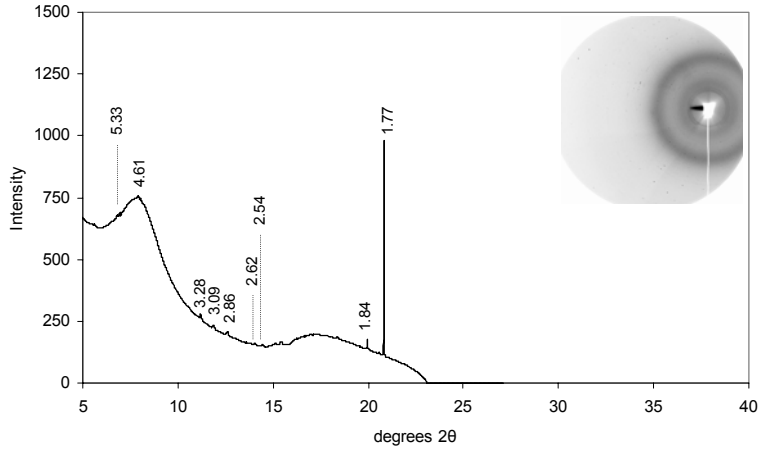
Figure A-94. Micro-XRD pattern for treatment PR52 point P77. Original Debye-Sherer rings are located in the top-right hand corner of the graph. The mineral species identified include willemite (2.63, 2.84, 3.48, 2.32, 1.86, 1.42, 4.02, 1.34).
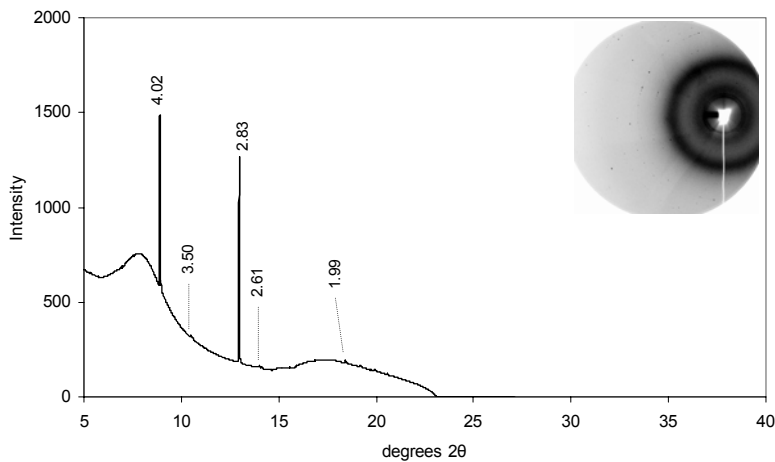
Figure A-95. Micro-XRD pattern for treatment PR52 point P78. Original Debye-Sherer rings are located in the top-right hand corner of the graph. The mineral species identified include willemite (2.63, 2.84, 3.48, 2.32, 1.86, 1.42, 4.02, 1.34).
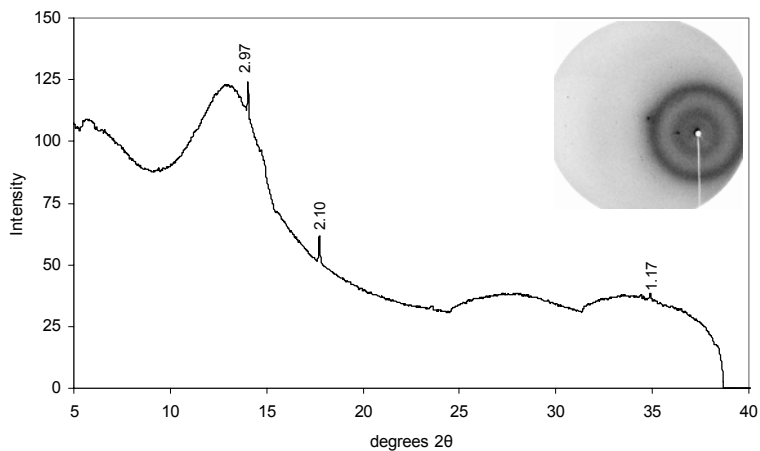
Figure A-96. Micro-XRD pattern for treatment TSP52 point P79. Original Debye-Sherer rings are located in the top-right hand corner of the graph. The mineral species identified could be pyromorphite (2.99, 2.97, 2.89, 4.13, 3.27, 2.06, 3.38, 1.92).
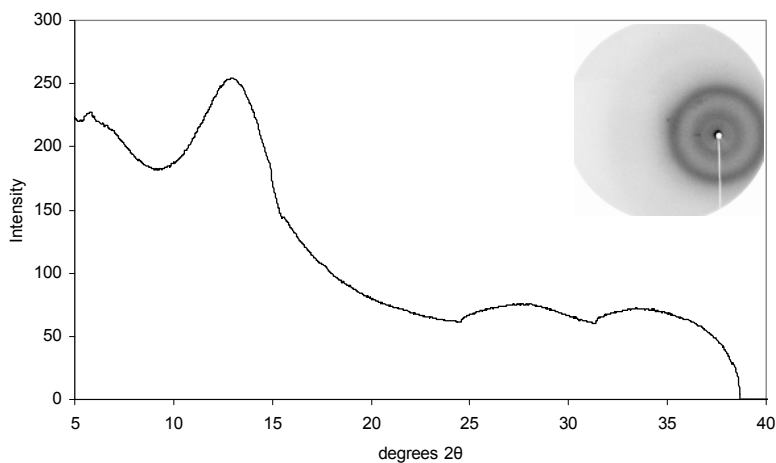
Figure A-97. Micro-XRD pattern for treatment TSP52 point P80. Original Debye-Sherer rings are located in the top-right hand corner of the graph. There were no mineral species that were able to be identified.
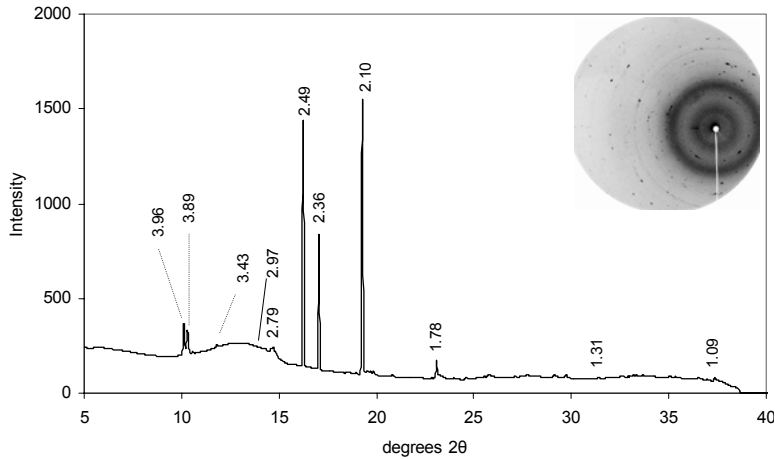
Figure A-98. Micro-XRD pattern for treatment TSP52 point P81. Original Debye-Sherer rings are located in the top-right hand corner of the graph. The mineral species identified include galena (2.97, 3.43, 2.10, 1.79, 1.33, 1.71, 1.48, 1.36), and zincite (2.48, 2.81, 2.10, 1.62, 1.48, 1.91, 1.38, 1.36).
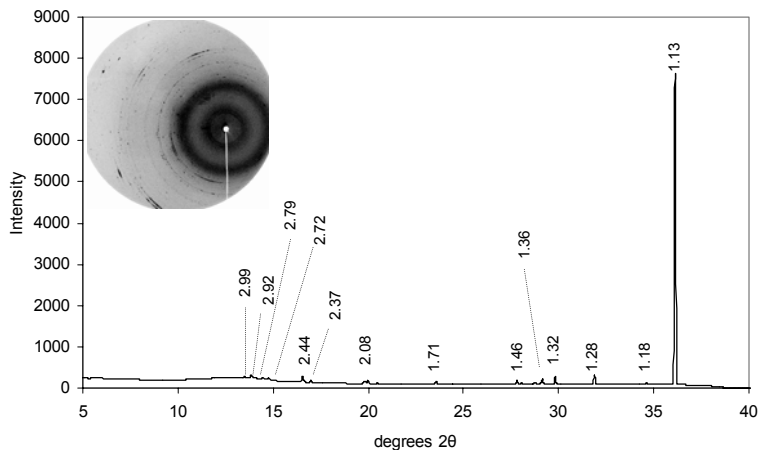
Figure A-99. Micro-XRD pattern for treatment TSP52 point P82. Original Debye-Sherer rings are located in the top-right hand corner of the graph. The mineral species identified include galena (2.97, 3.43, 2.10, 1.79, 1.33, 1.71, 1.48, 1.36).
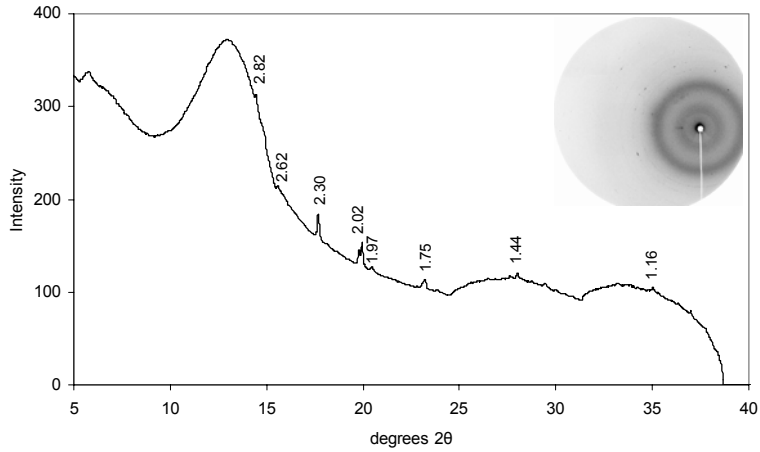
Figure A-100. Micro-XRD pattern for treatment TSP52 point P83. Original Debye-Sherer rings are located in the top-right hand corner of the graph. The mineral species identified include willemite (2.63, 2.84, 3.48, 2.32, 1.86, 1.42, 4.02, 1.34).
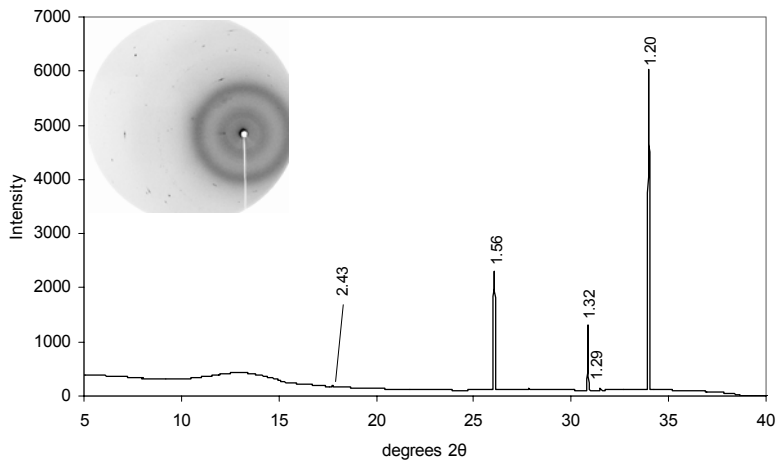
Figure A-101. Micro-XRD pattern for treatment TSP52 point P84. Original Debye-Sherer rings are located in the top-right hand corner of the graph. There were no mineral species that were able to be identified.
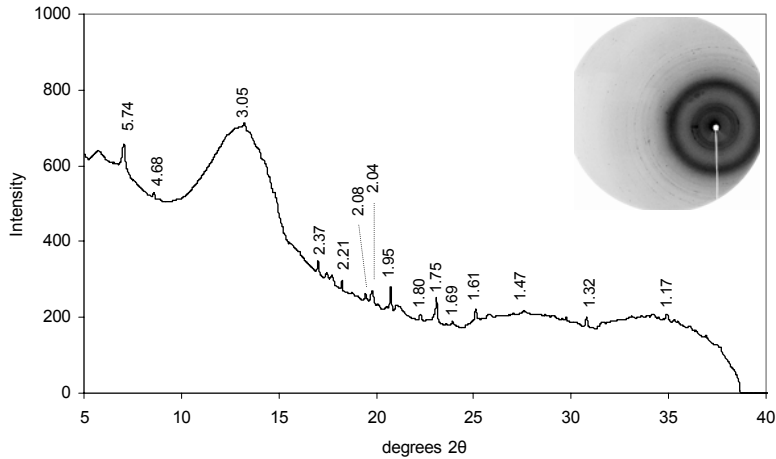
Figure A-102. Micro-XRD pattern for treatment TSP52 point P85. Original Debye-Sherer rings are located in the top-right hand corner of the graph. The mineral species identified include zincite (2.48, 2.81, 2.60, 1.62, 1.48, 1.91, 1.38, 1.36), and franklinite (2.55, 2.98, 1.50, 1.63, 2.12, 1.72, 1.10, 1.29)
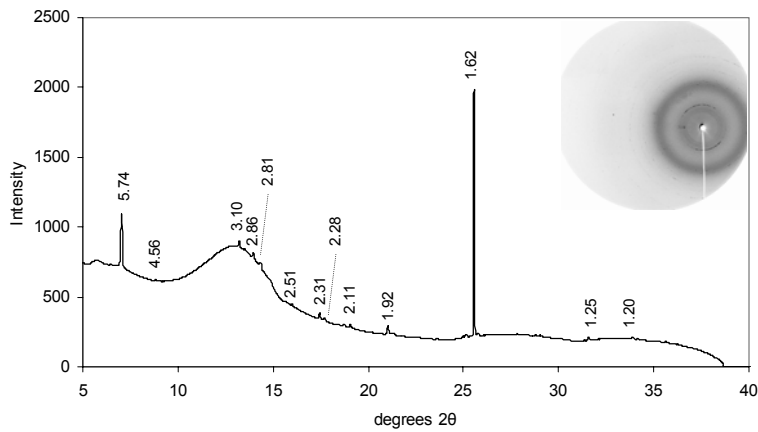
Figure A-103. Micro-XRD pattern for treatment TSP52 point P86. Original Debye-Sherer rings are located in the top-right hand corner of the graph. The mineral species identified include hopeite (4.57, 2.85, 9.12, 3.46, 3.39, 4.41, 1.94, 4.85) and sphalerite (3.12, 1.91, 1.63, 2.71, 1.24).
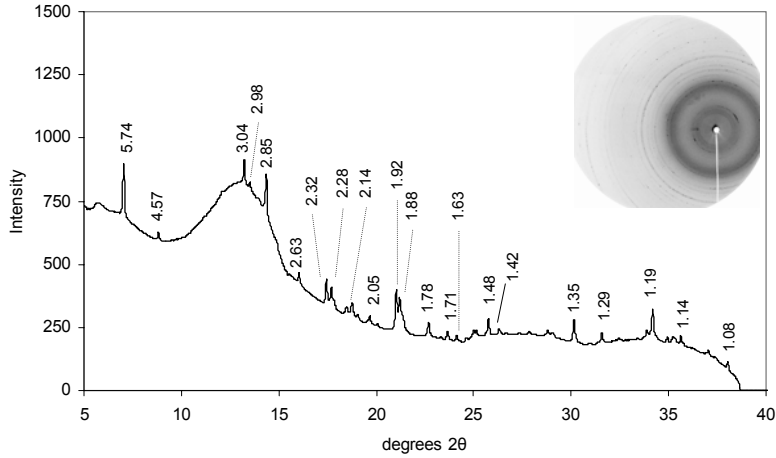
Figure A-104. Micro-XRD pattern for treatment TSP52 point P87. Original Debye-Sherer rings are located in the top-right hand corner of the graph. The mineral species identified include franklinite (2.55, 2.98, 1.50, 1.63, 2.12, 1.72, 1.10, 1.29), hopeite (4.57, 2.85, 9.12, 3.46, 3.39, 4.41, 1.94, 4.85) and willemite (2.63, 2.84, 3.48, 2.32, 1.86, 1.42, 4.02, 1.34)
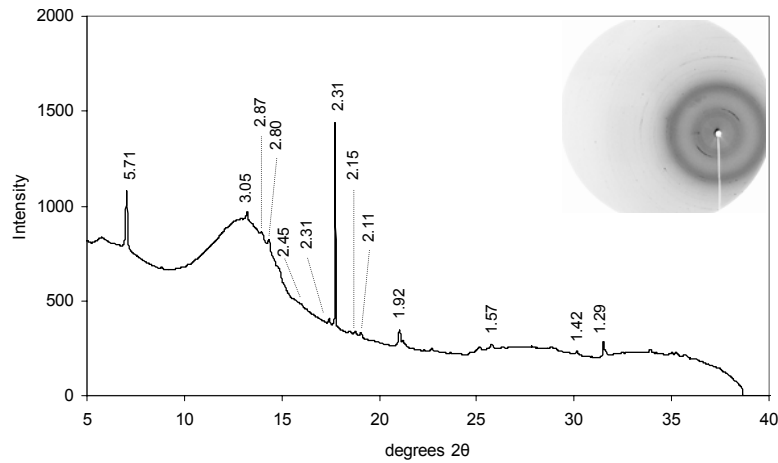
Figure A-105. Micro-XRD pattern for treatment TSP52 point P88. Original Debye-Sherer rings are located in the top-right hand corner of the graph. The mineral species identified include gahnite (2.86, 2.44, 1.43, 1.56, 1.65, 0.83, 1.05, 1.86) and willemite 2.63, 2.84, 3.48, 2.32, 1.86, 1.42, 4.02, 1.34)

273
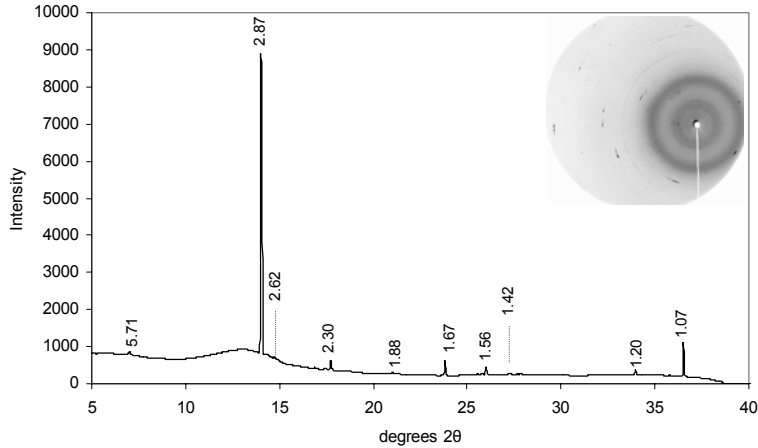
Figure A-106. Micro-XRD pattern for treatment TSP52 point P89. Original Debye-Sherer rings are located in the top-right hand corner of the graph. The mineral species identified include gahnite (2.86, 2.44, 1.43, 1.56, 1.65, 0.83, 1.05, 1.86) and willemite 2.63, 2.84, 3.48, 2.32, 1.86, 1.42, 4.02, 1.34)
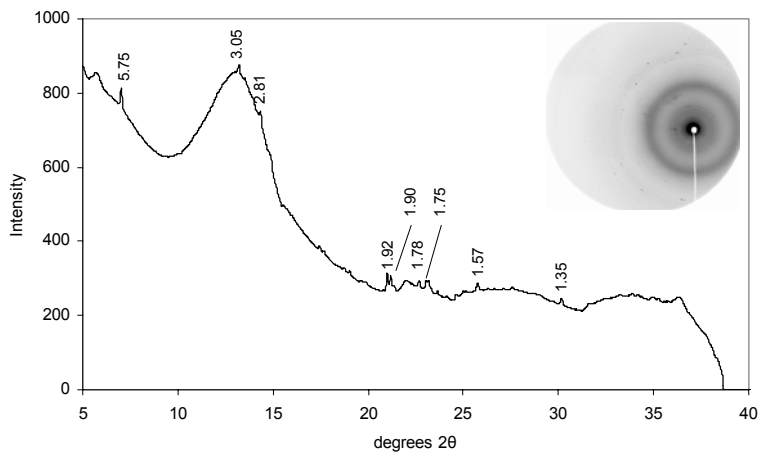
Figure A-107. Micro-XRD pattern for treatment TSP52 point P90. Original Debye-Sherer rings are located in the top-right hand corner of the graph. There were no mineral species that were able to be identified.
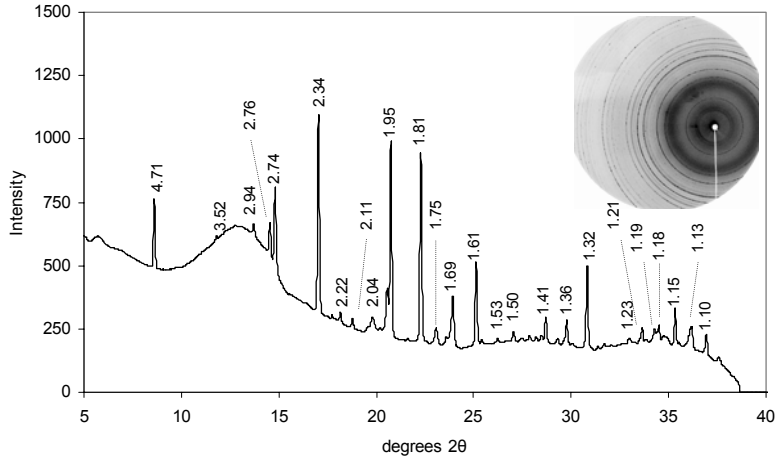
Figure A-108. Micro-XRD pattern for treatment TSP52 point P91. Original Debye-Sherer rings are located in the top-right hand corner of the graph. The mineral species identified include smithsonite (2.75, 3.55, 1.70, 2.33, 1.95, 2.11, 1.52, 1.49) and galena (2.97, 3.43, 2.10, 1.79, 1.33, 1.71, 1.48, 1.36)
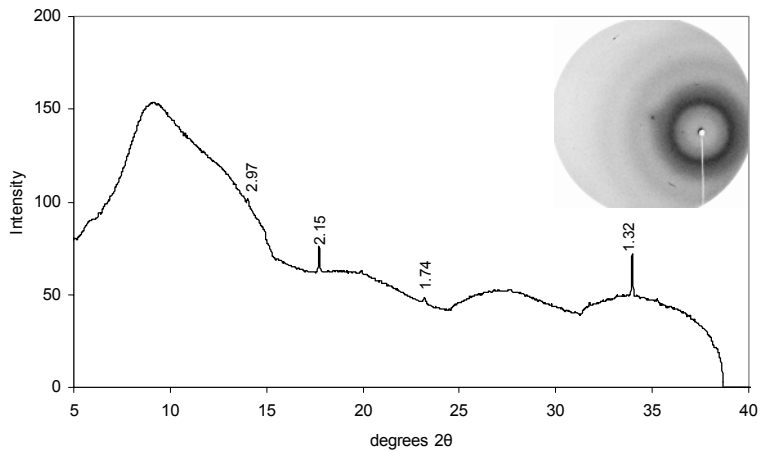
Figure A-109. Micro-XRD pattern for treatment APP52 point P92. Original Debye-Sherer rings are located in the top-right hand corner of the graph. The mineral species identified include galena (2.97, 3.43, 2.10, 1.79, 1.33, 1.71, 1.48, 1.36).
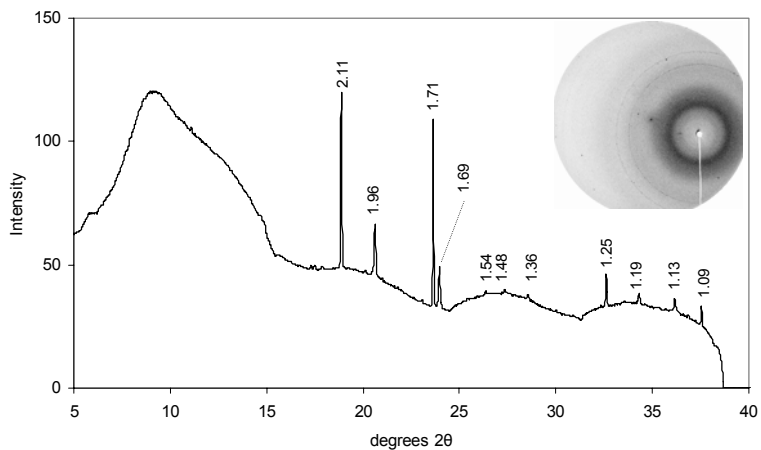
Figure A-110. Micro-XRD pattern for treatment APP52 point P93. Original Debye-Sherer rings are located in the top-right hand corner of the graph. The mineral species identified include galena (2.97, 3.43, 2.10, 1.79, 1.33, 1.71, 1.48, 1.36).
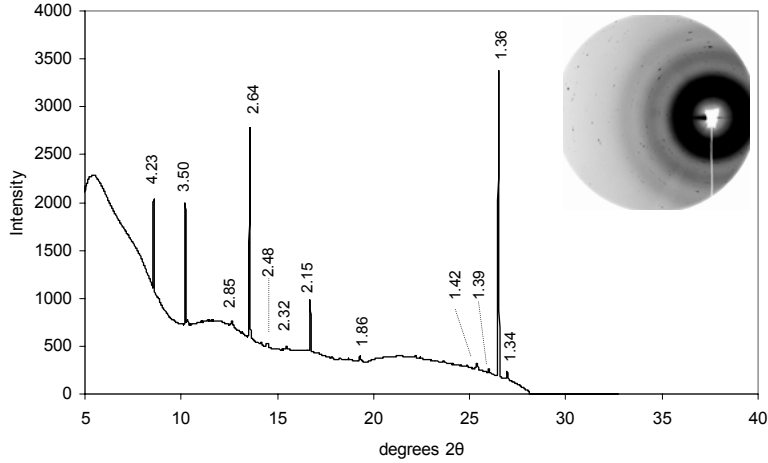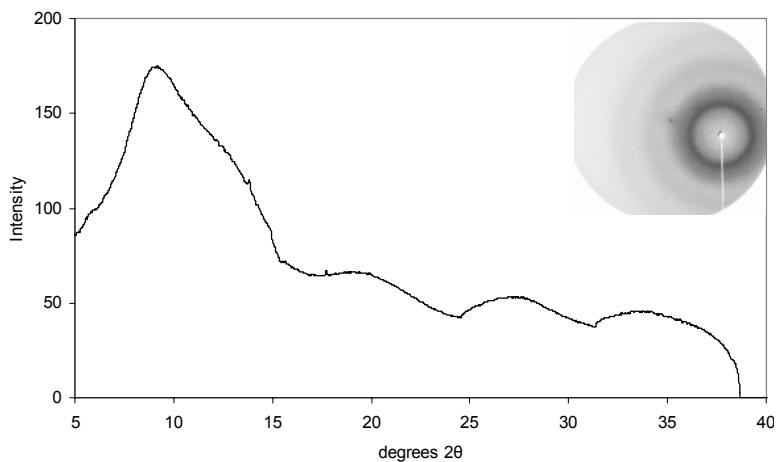

Figure A-111. Micro-XRD pattern for treatment APP52 point P94. Original Debye-Sherer rings are located in the top-right hand corner of the graph. There were no mineral species that were able to be identified.
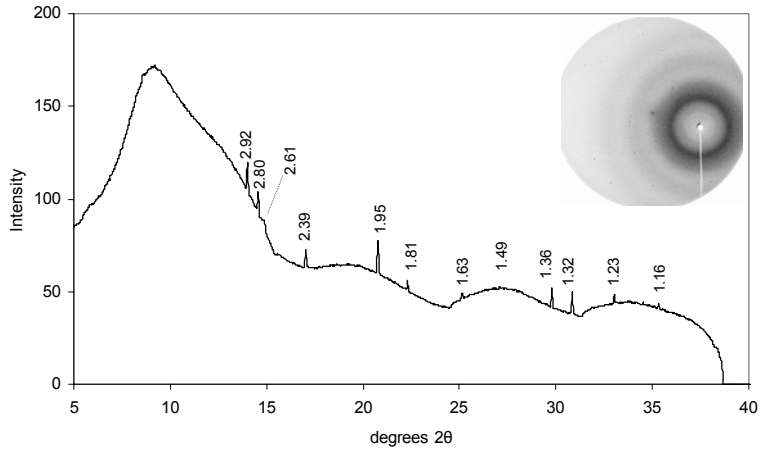
Figure A-112. Micro-XRD pattern for treatment APP52 point P95. Original Debye-Sherer rings are located in the top-right hand corner of the graph. The mineral species identified include plumboferrite (2.64, 2.81, 2.96, 1.68, 1.64, 1.48, 3.91, 2.44) and magnetoplumbite (2.76, 2.62, 2.93, 2.41, 1.62, 4.97, 2.88, 2.23).
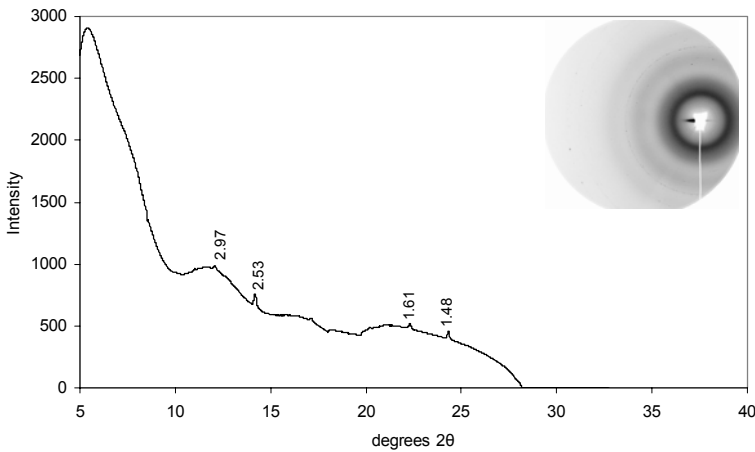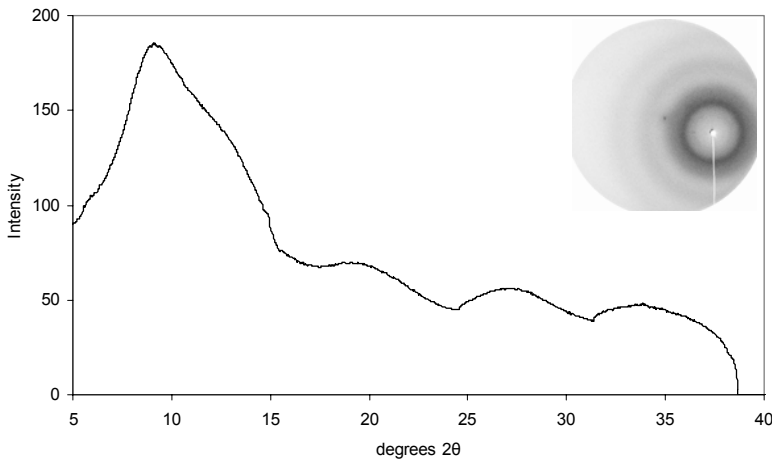

Figure A-113. Micro-XRD pattern for treatment APP52 point P96. Original Debye-Sherer rings are located in the top-right hand corner of the graph. There were no mineral species that were able to be identified.
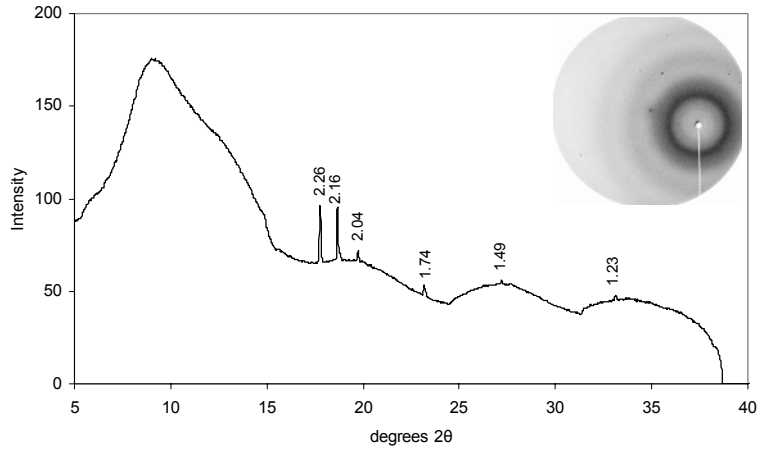
Figure A-114. Micro-XRD pattern for treatment APP52 point P97. Original Debye-Sherer rings are located in the top-right hand corner of the graph. There were no mineral species that were able to be identified.
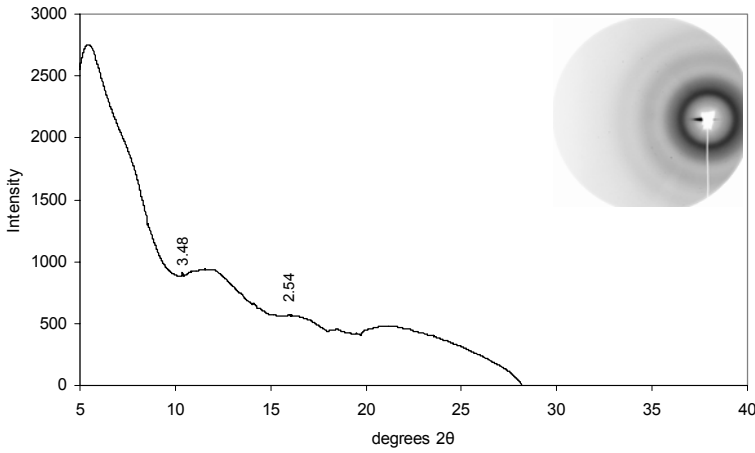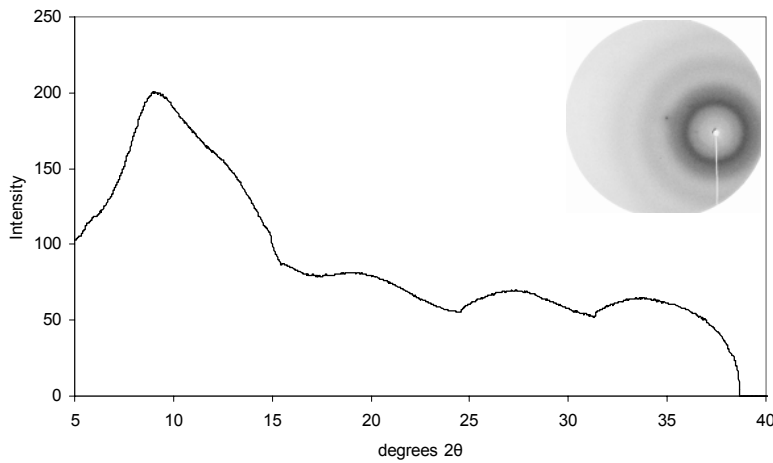

Figure A-115. Micro-XRD pattern for treatment APP52 point P98. Original Debye-Sherer rings are located in the top-right hand corner of the graph. There were no mineral species that were able to be identified.
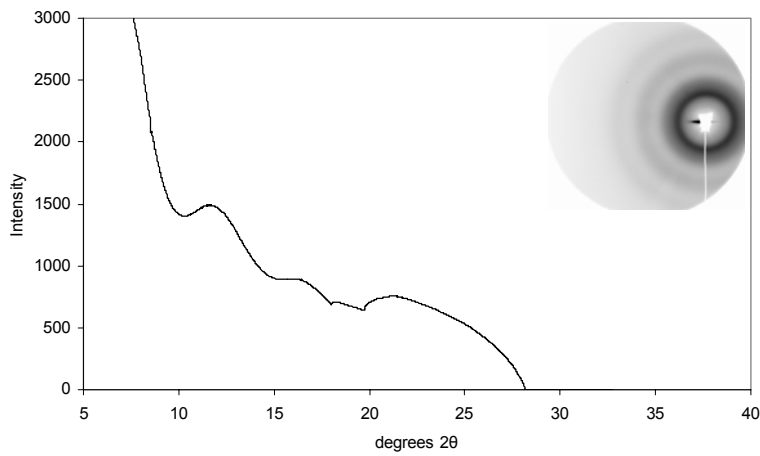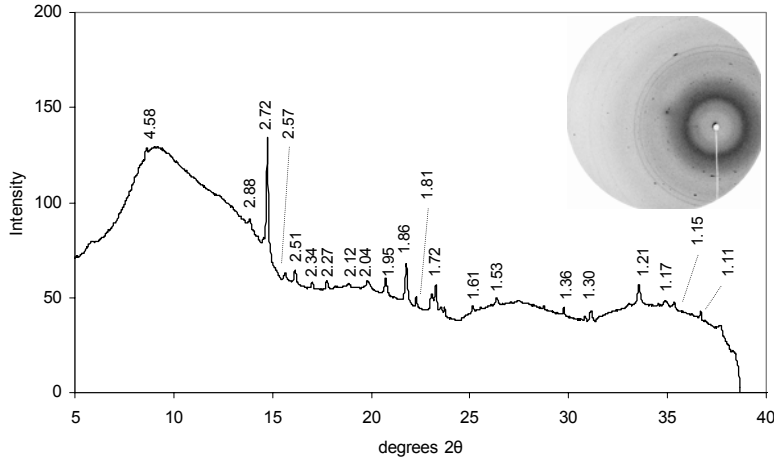
Figure A-116. Micro-XRD pattern for treatment APP52 point P99. Original Debye-Sherer rings are located in the top-right hand corner of the graph. The mineral species identified include franklinite (2.55, 2.98, 1.50, 1.63, 2.12, 1.72, 1.10, 1.29), smithsonite (2.75, 3.55, 1.70, 2.33, 1.95, 2.11, 1.52, 1.49) and hopeite (4.57, 2.85, 9.12, 3.46, 3.39, 4.41, 1.94, 4.85).
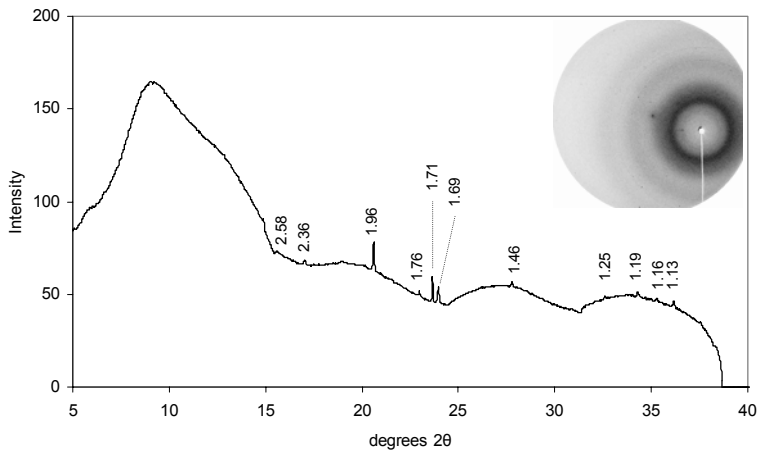
Figure A-117. Micro-XRD pattern for treatment APP52 point P100. Original Debye-Sherer rings are located in the top-right hand corner of the graph. There were no mineral species that were able to be identified.
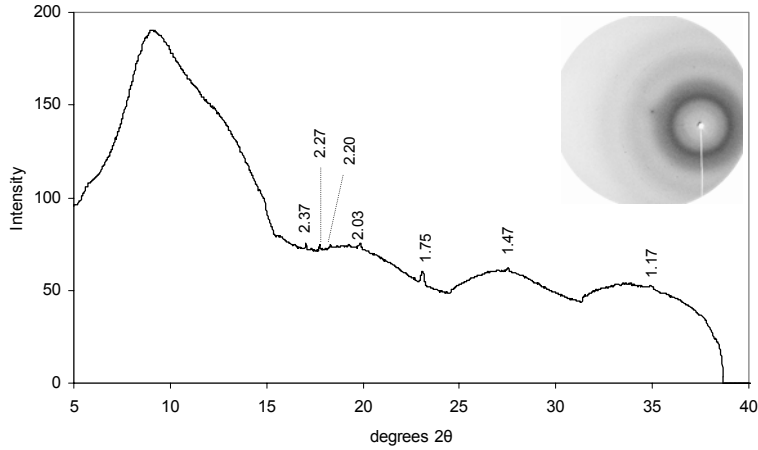
Figure A-118.   Micro-XRD pattern for treatment APP52 point P101. Original Debye-Sherer rings are located in the top-right hand corner of the graph. There were no mineral species that were able to be identified.
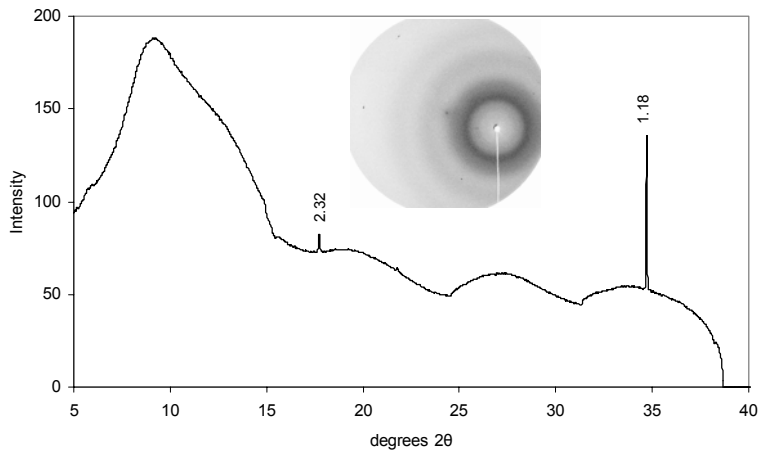
Figure A-119.   Micro-XRD pattern for treatment APP52 point P102. Original Debye-Sherer rings are located in the top-ri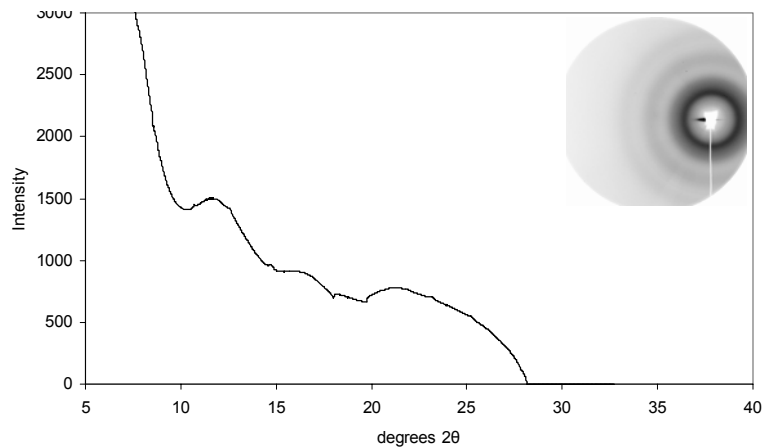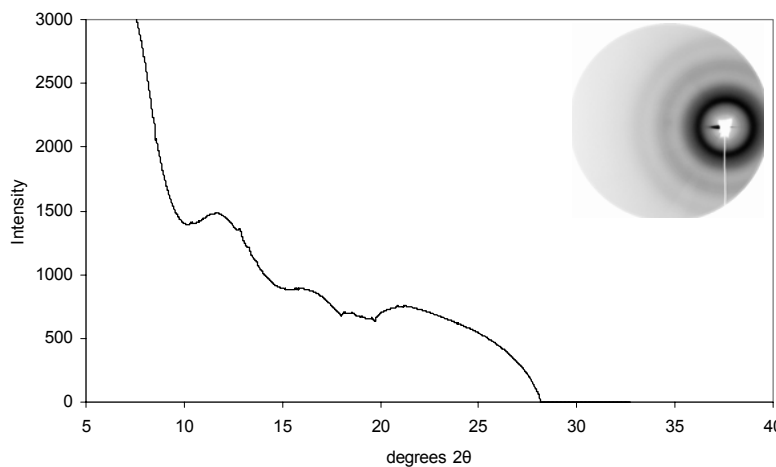ght hand corner of the graph. The mineral species identified include heterosite (3.46, 2.45, 2.31, 1.18, 1.85, 4.26, 1.41, 1.49).
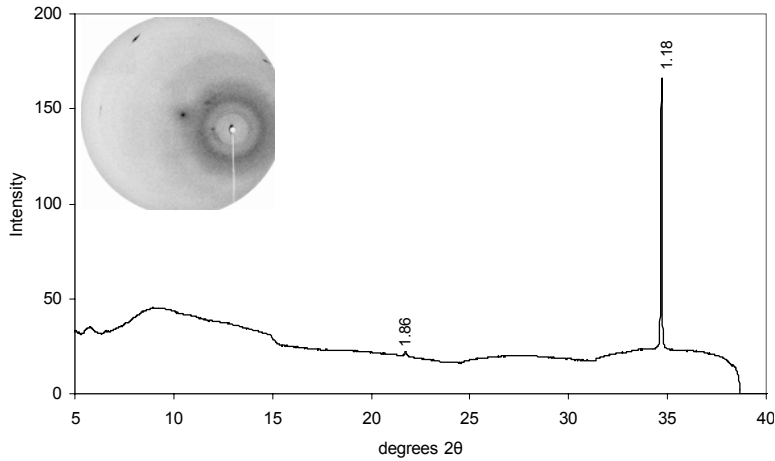
Figure A-120. Micro-XRD pattern for treatment APP52 point P103. Original Debye-Sherer rings are located in the top-ri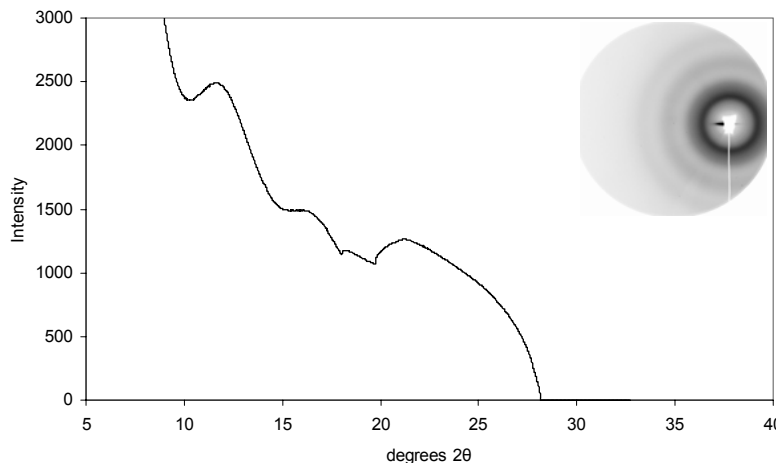ght hand corner of the graph. The mineral species identified include heterosite (3.46, 2.45, 2.31, 1.18, 1.85, 4.26, 1.41, 1.49).
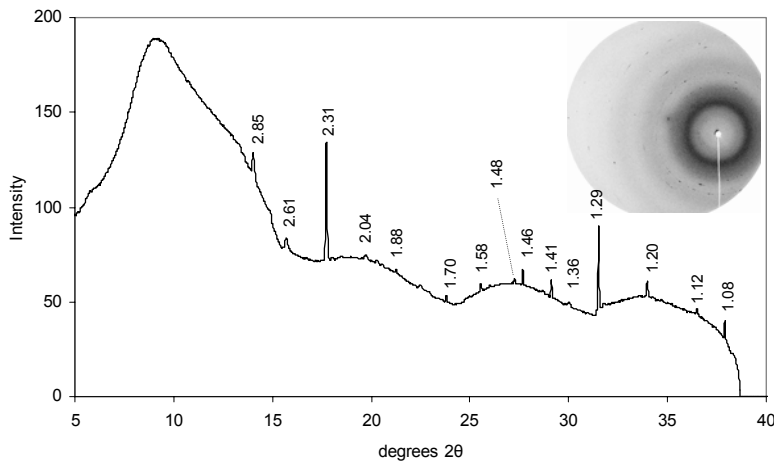
Figure A-121. Micro-XRD pattern for treatment APP52 point P104. Original Debye-Sherer rings are located in the top-right hand corner of the graph. The mineral species identified include willemite (2.63, 2.84, 3.48, 2.32, 1.86, 1.42, 4.02, 1.34).
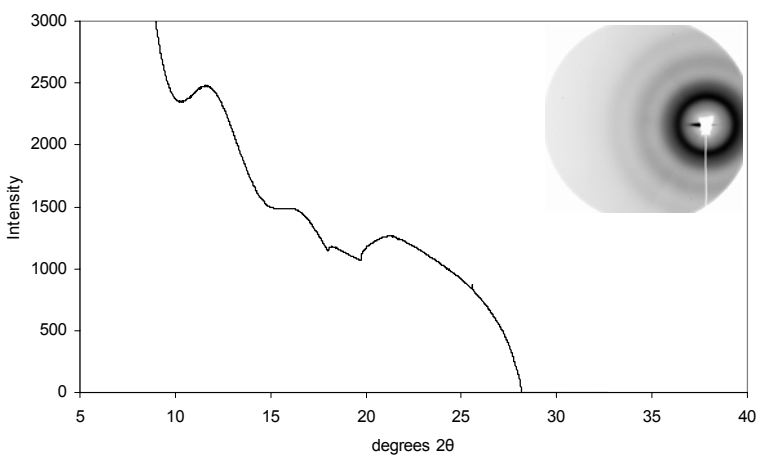
281
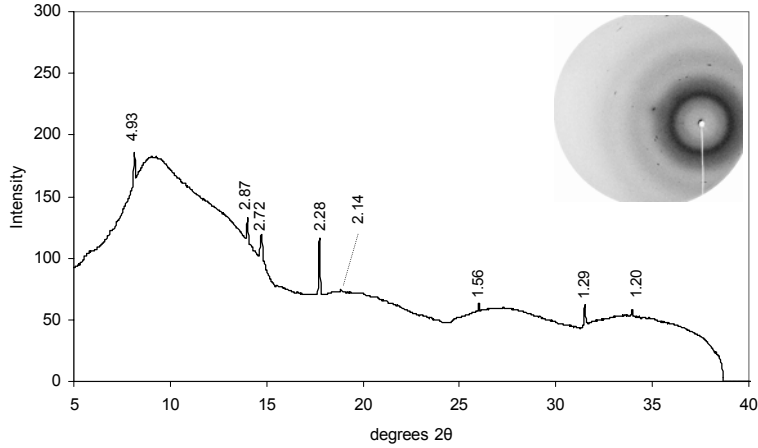
Figure A-122. **Micro-XRD pattern for treatment APP52 point P105. Original Debye-Sherer rings are located in the top-right hand corner of the graph. There were no mineral species that were able to be identified.**
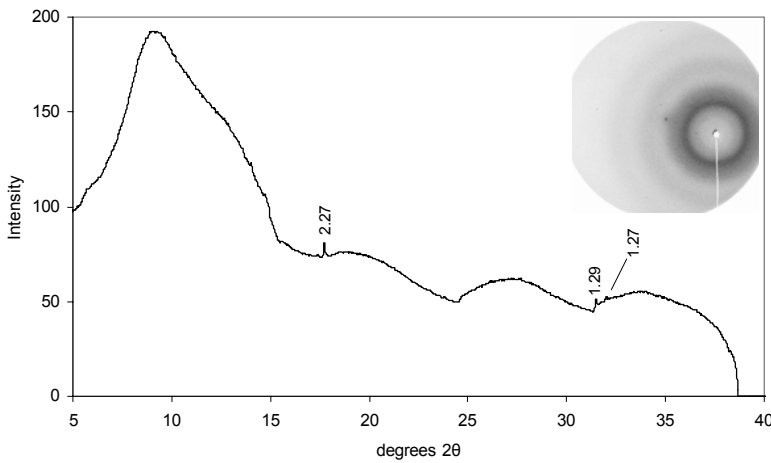
Figure A-123. **Micro-XRD pattern for treatment APP52 point P106. Original Debye-Sherer rings are located in the top-right hand corner of the graph. There were no mineral species that were able to be identified.**
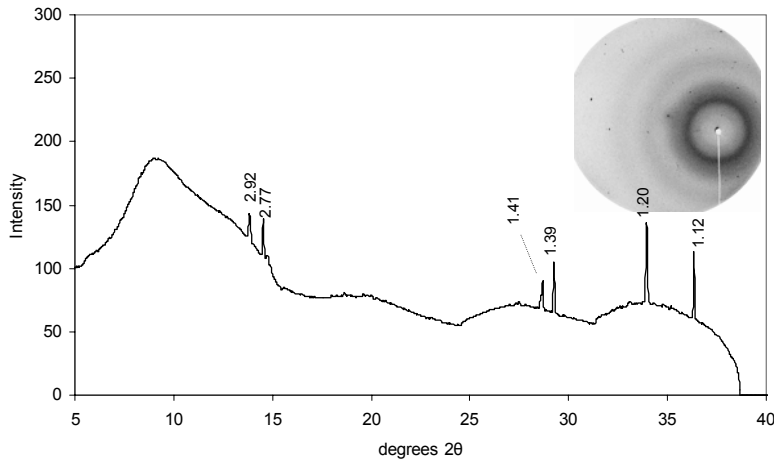
Figure A-124. **Micro-XRD pattern for treatment MAP52 point P107. Original Debye-Sherer rings are located in the top-ri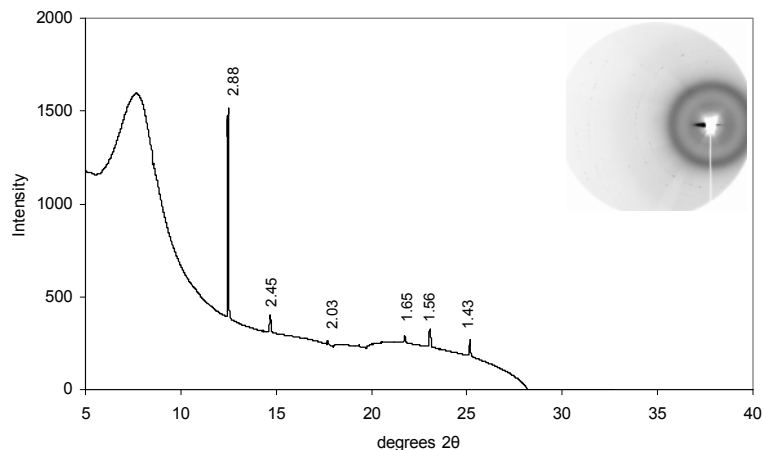ght hand corner of the graph. The mineral species identified include magnetoplubmite (2.76, 2.62, 2.93, 2.41, 1.62, 4.97, 2.88, 2.23).**
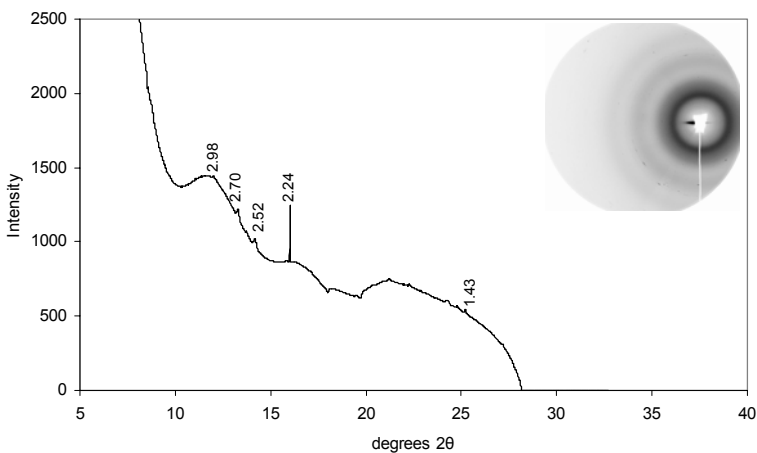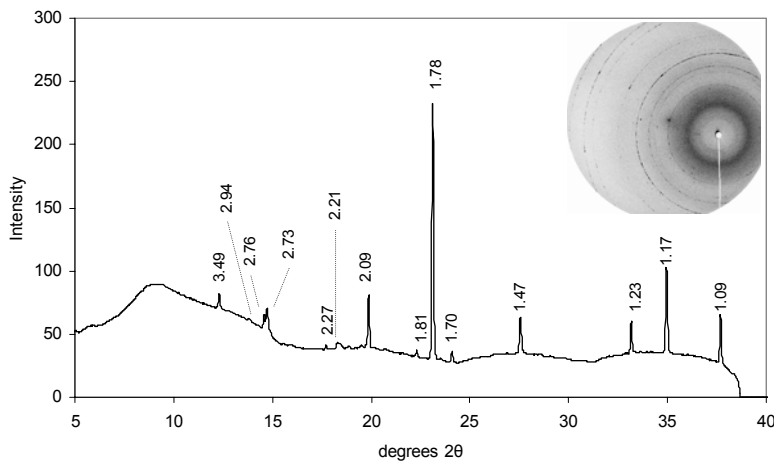

Figure A-125. **Micro-XRD pattern for treatment MAP52 point P108. Original Debye-Sherer rings are located in the top-right hand corner of the graph. The mineral species identified include galena (2.97, 3.43, 2.10, 1.79, 1.33, 1.71, 1.48, 1.36) and plumbogummite (2.97, 5.70, 3.50, 2.22, 2.21, 1.90, 3.44, 5.57).**
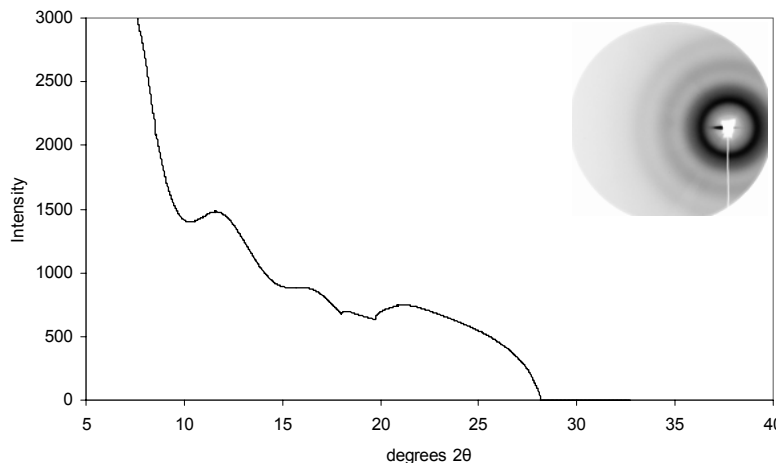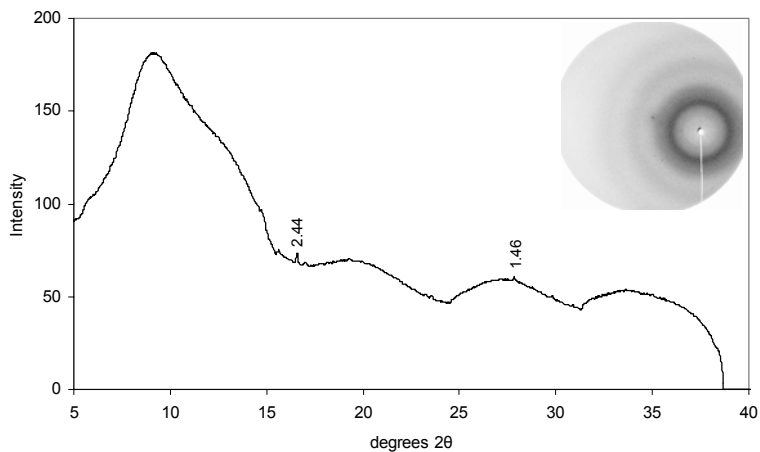
Figure A-126. Micro-XRD pattern for treatment MAP52 point P109. Original Debye-Sherer rings are located in the top-right hand corner of the graph. There were no mineral species that were able to be identified.
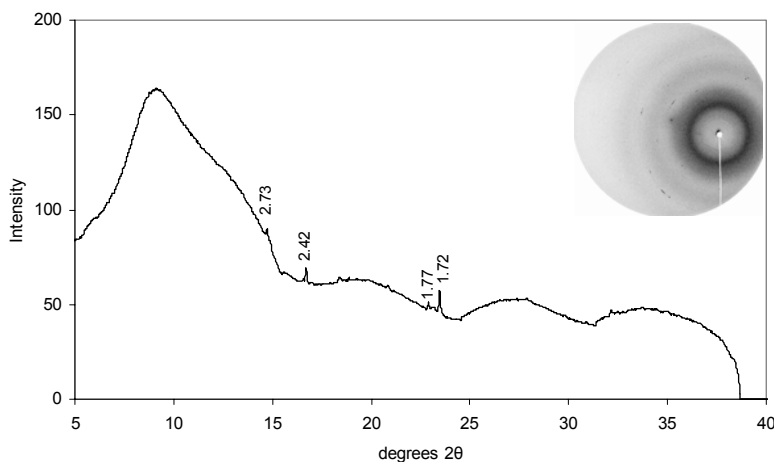
Figure A-127. Micro-XRD pattern for treatment MAP52 point P110. Original Debye-Sherer rings are located in the top-right hand corner of the graph. The mineral species identified include galena (2.97, 3.43, 2.10, 1.79, 1.33, 1.71, 1.48, 1.36).
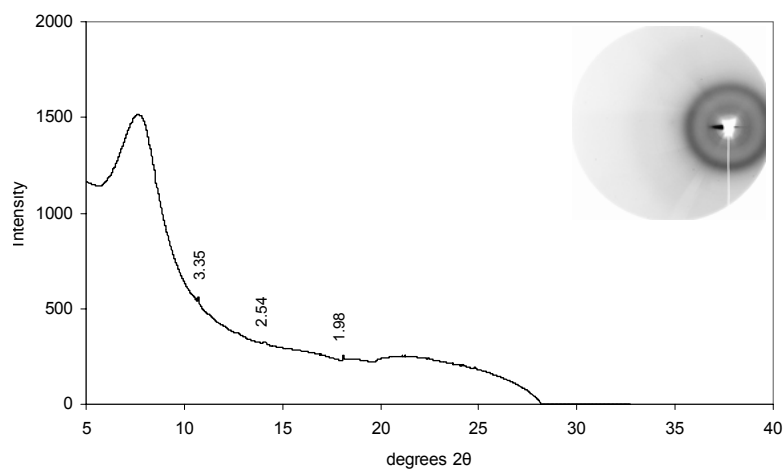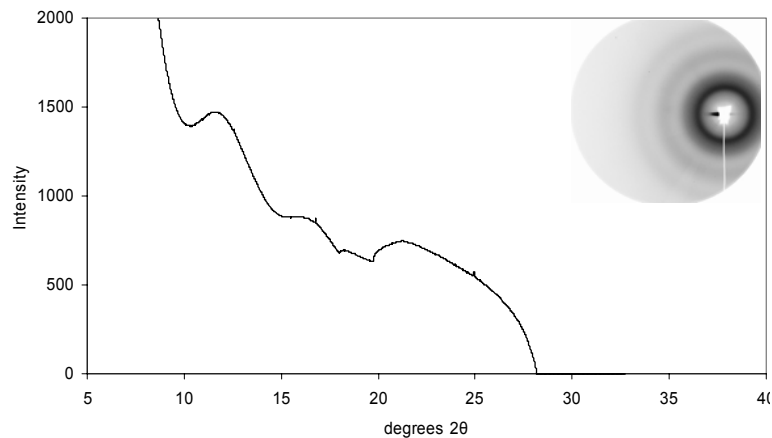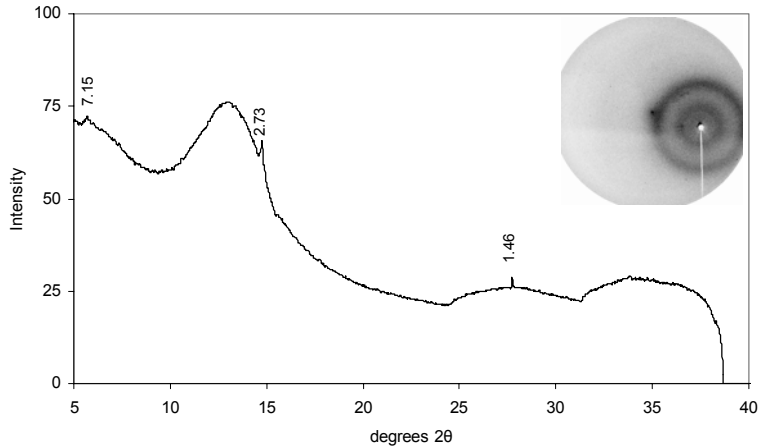
Figure A-128. Micro-XRD pattern for treatment MAP52 point P111. Original Debye-Sherer rings are located in the top-right hand corner of the graph. The mineral species identified include magnetoplumbite which has a peak at 2.76
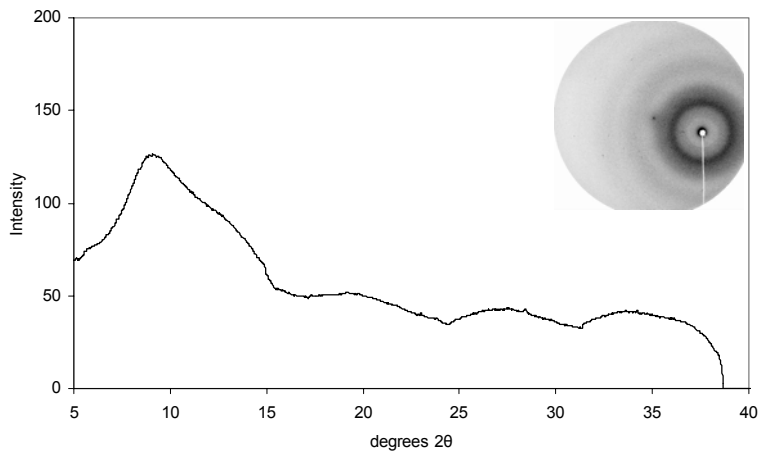
Figure A-129. Micro-XRD pattern for treatment MAP52 point P112. Original Debye-Sherer rings are located in the top-right hand corner of the graph. There were no mineral species that were able to be identified.
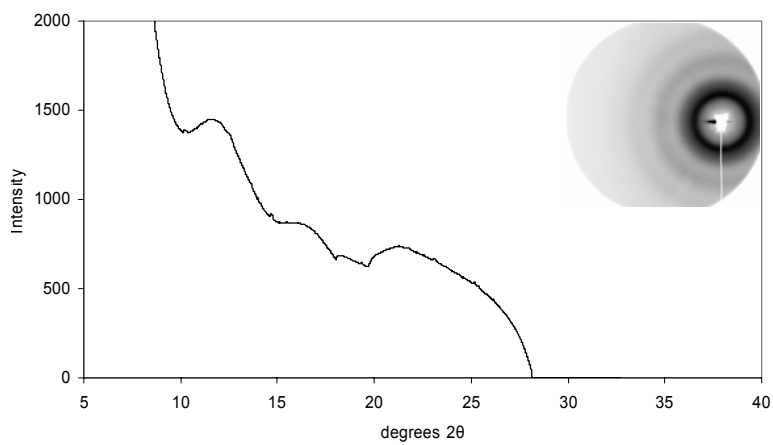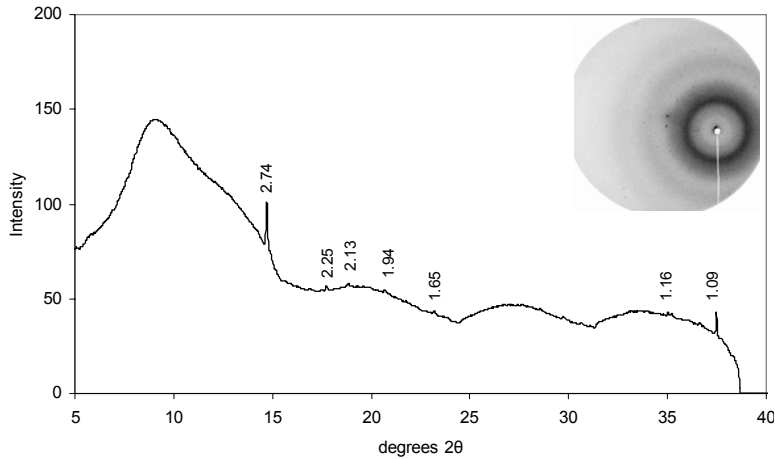
Figure A-130. Micro-XRD pattern for treatment MAP52 point P113. Original Debye-Sherer rings are located in the top-right hand corner of the graph. The mineral species identified include magnetoplumbite (2.76, 2.62, 2.93, 2.41, 1.62, 4.97, 2.88, 2.23) and franklinite has a peak at 1.10.
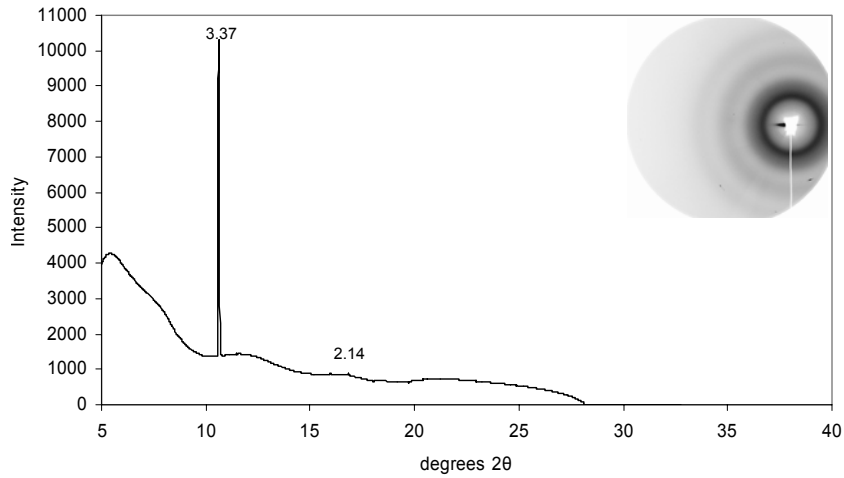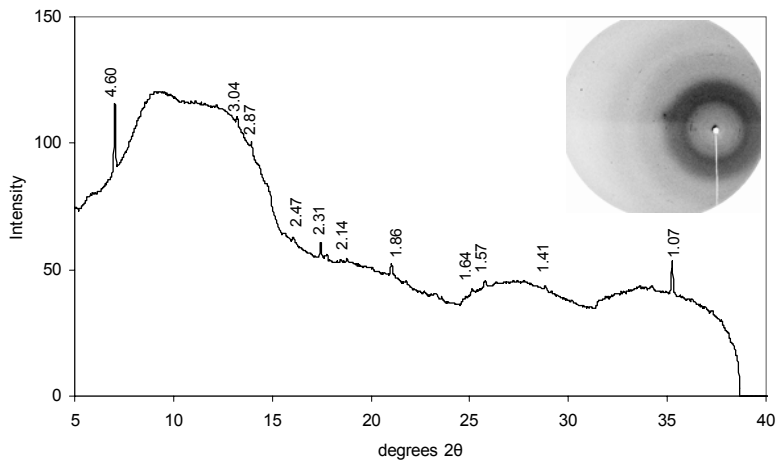

Figure A-131. Micro-XRD pattern for treatment MAP52 point P114. Original Debye-Sherer rings are located in the top-right hand corner of the graph. The mineral species identified include gahnite (2.86, 2.44, 1.43, 1.56, 1.65, 0.83, 1.05, 1.86) and hopeite (4.57, 2.85, 9.12, 3.46, 3.39, 4.41, 1.94, 4.85).
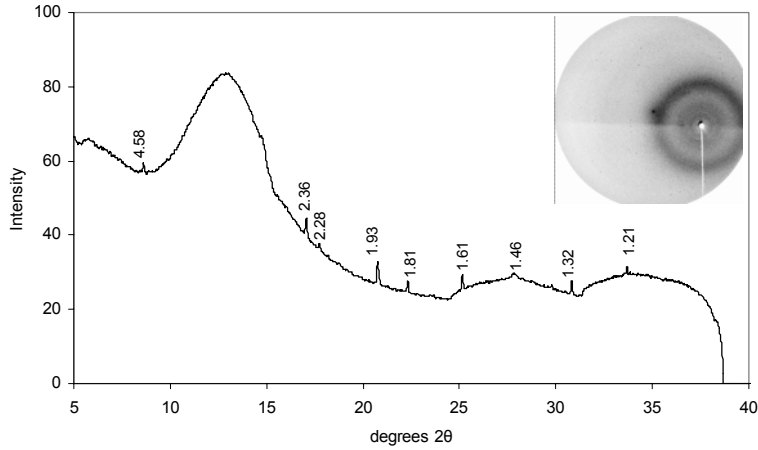
Figure A-132. **Micro-XRD pattern for treatment MAP52 point P115. Original Debye-Sherer rings are located in the top-right hand corner of the graph. The mineral species identified include 4.57 is hopeite (probably not crystalline enough to give a good pattern); sphalerite (3.12, 1.91, 1.63, 2.71, 1.24)**
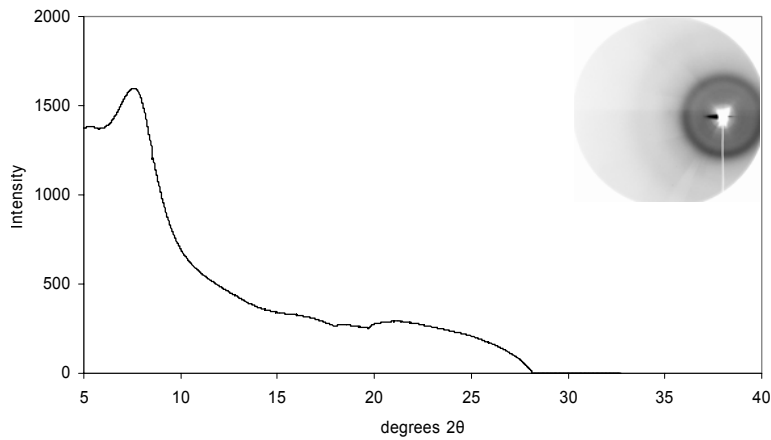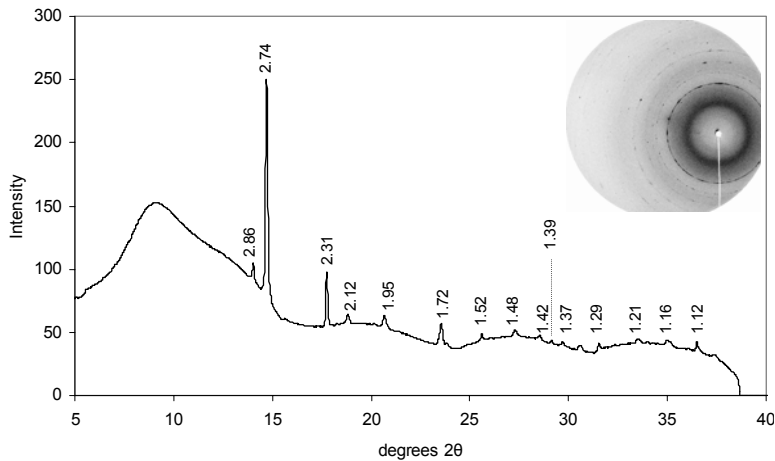

Figure A-133. **Micro-XRD pattern for treatment MAP52 point P116. Original Debye-Sherer rings are located in the top-right hand corner of the graph. The mineral species identified include smithsonite (2.75, 3.55, 1.70, 2.33, 1.95, 2.11, 1.52, 1.49) and 2.86 is probably gahnite.**
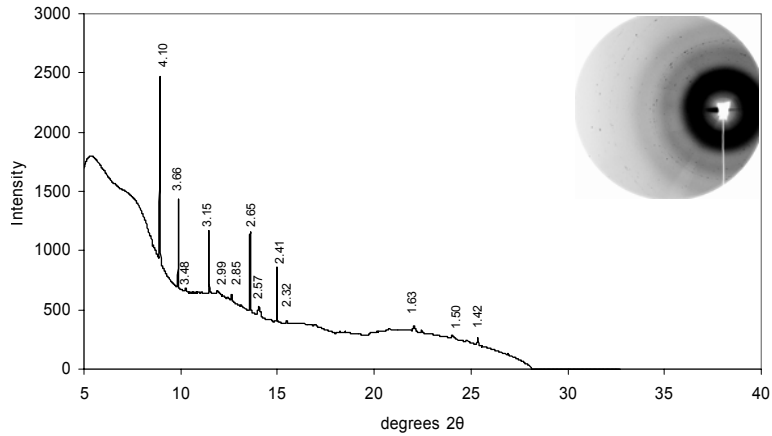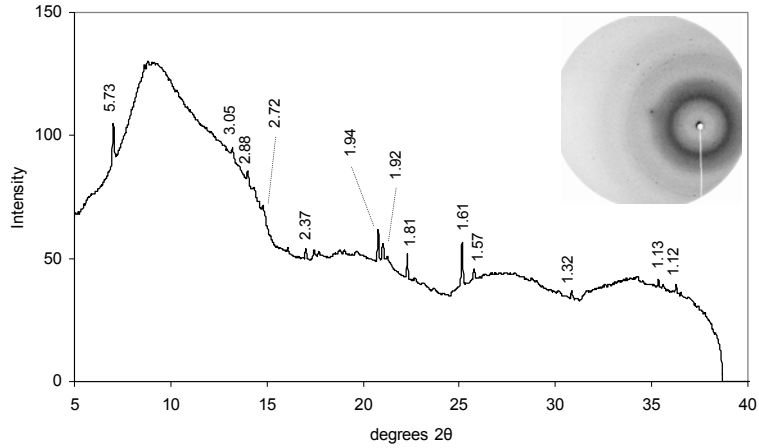
Figure A-134. **Micro-XRD pattern for treatment MAP52 point P117. Original Debye-Sherer rings are located in the top-right hand corner of the graph. There were no mineral species that were able to be identified.**
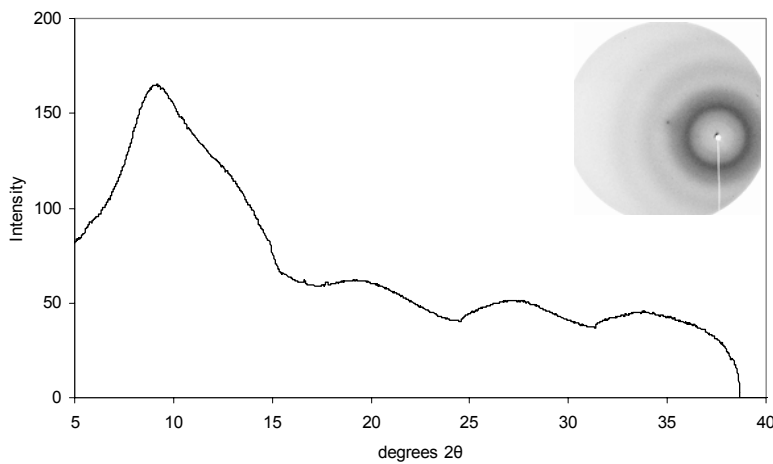
Figure A-135. **Micro-XRD pattern for treatment MAP52 point P118. Original Debye-Sherer rings are located in the top-right hand corner of the graph. There were no mineral species that were able to be identified.**
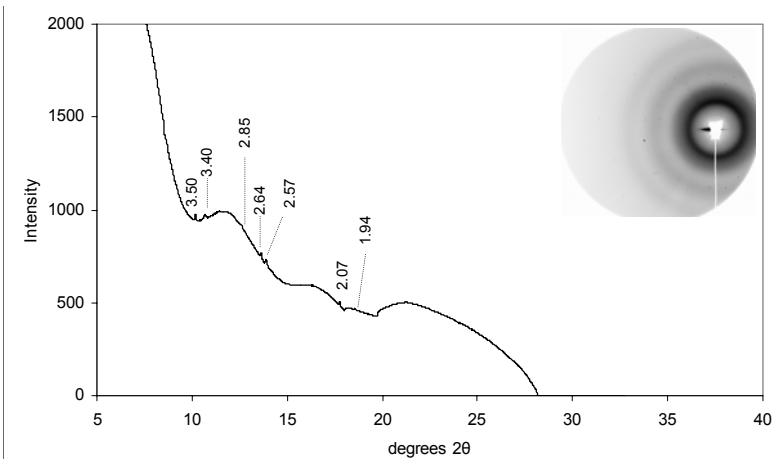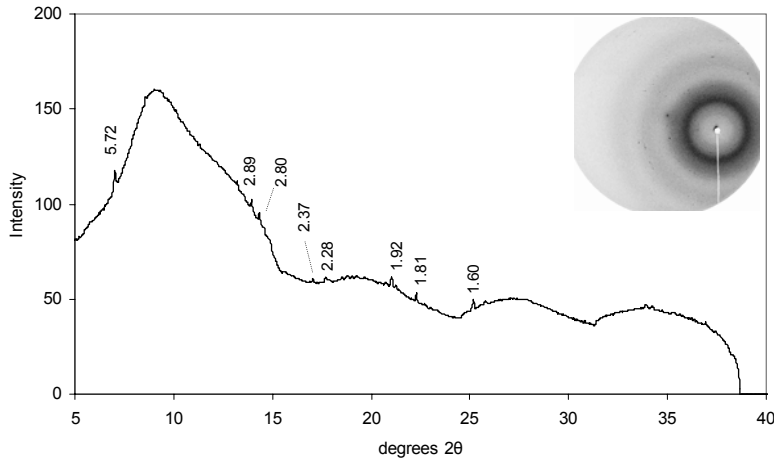
Figure A-136.   Micro-XRD pattern for treatment MAP52 point P119. Original Debye-Sherer rings are located in the top-right hand corner of the graph. There were no mineral species that were able to be identified.
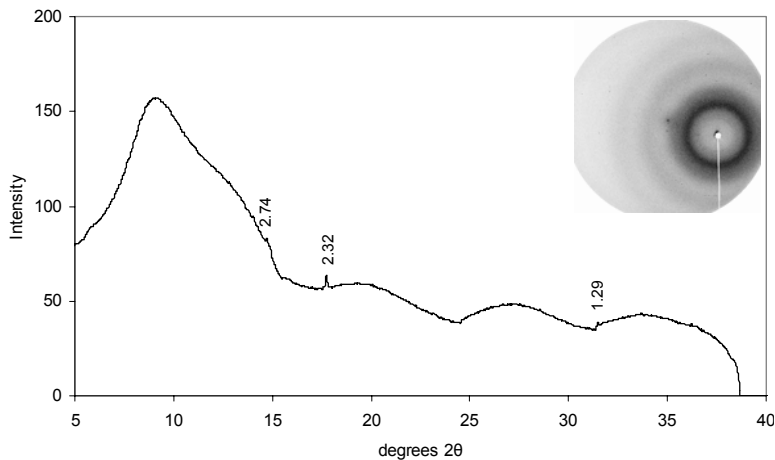
Figure A-137.   Micro-XRD pattern for treatment MAP52 inside of granule point P120. Original Debye-Sherer rings are located in the top-right hand corner of the graph. The mineral species identified include smithsonite (2.75, 3.55, 1.70, 2.33, 1.95, 2.11, 1.52, 1.49).
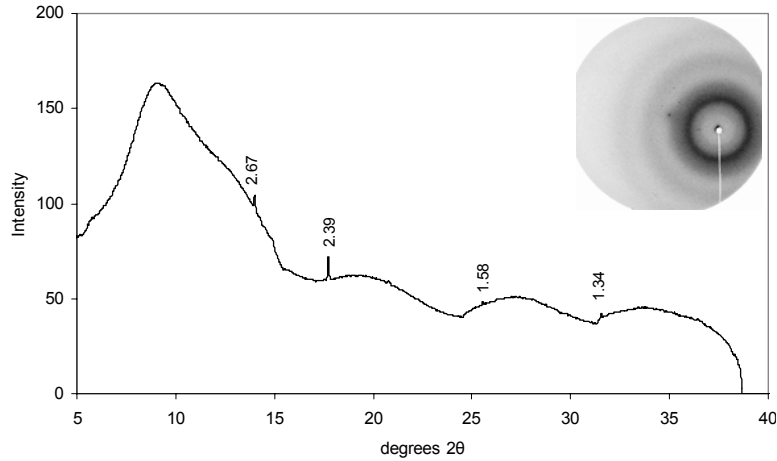
Figure A-138. **Micro-XRD pattern for treatment MAP52 outside of granule point P121. Original Debye-Sherer rings are located in the top-right hand corner of the graph. The mineral species identified include diphosphammite (3.07, 5.32, 3.06, 3.75, 2.01, 2.66, 2.65, 2.39).**
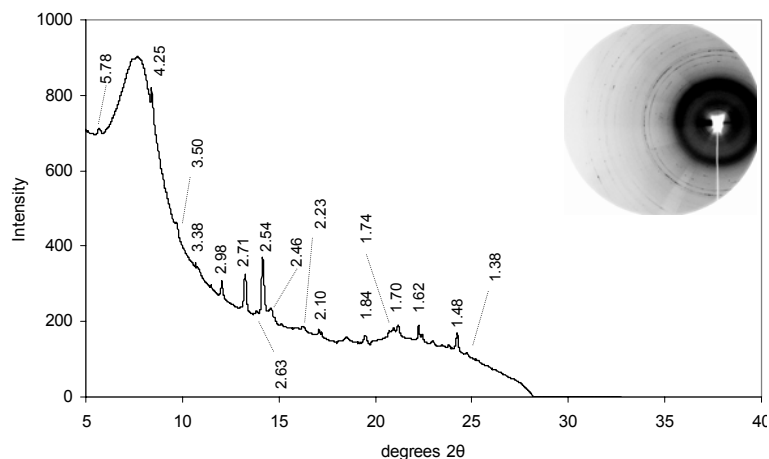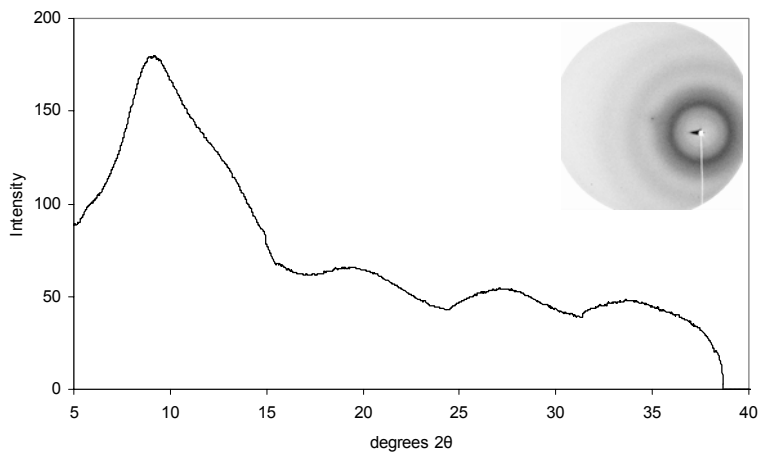

Figure A-139. **Micro-XRD pattern for treatment PA 24hr point P122. Original Debye-Sherer rings are located in the top-right hand corner of the graph. There were no mineral species that were able to be identified.**
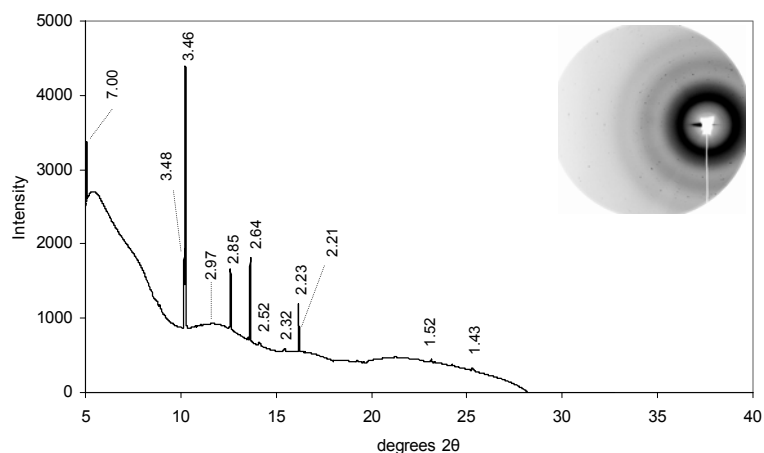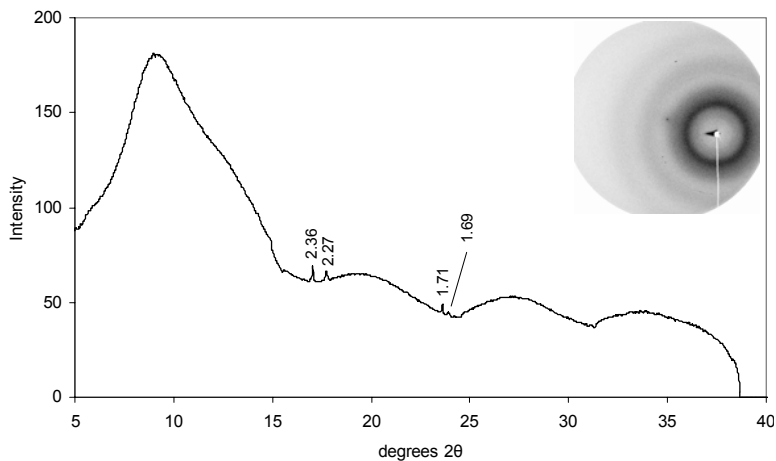
Figure A-140. Micro-XRD pattern for treatment PA 24hr point P123. Original Debye-Sherer rings are located in the top-right hand corner of the graph. There were no mineral species that were able to be identified.
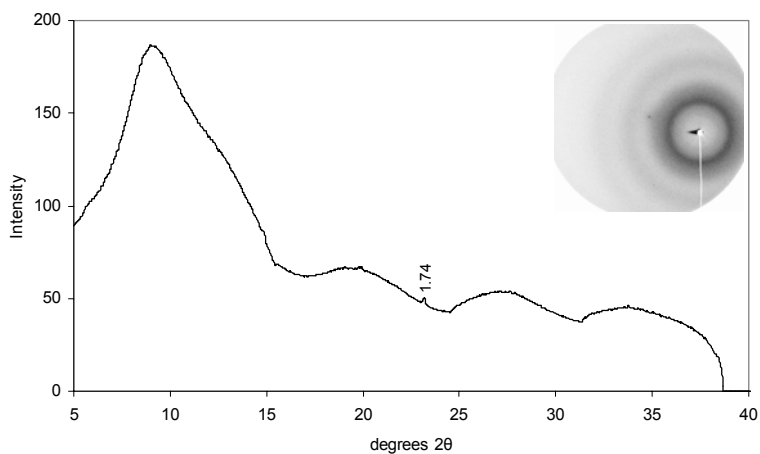
Figure A-141. Micro-XRD pattern for treatment PA 24hr point P124. Original Debye-Sherer rings are located in the top-right hand corner of the graph. There were no mineral species that were able to be identified.
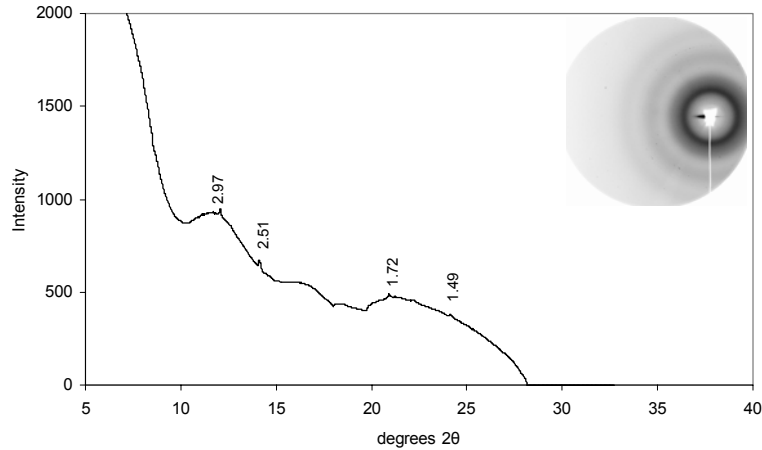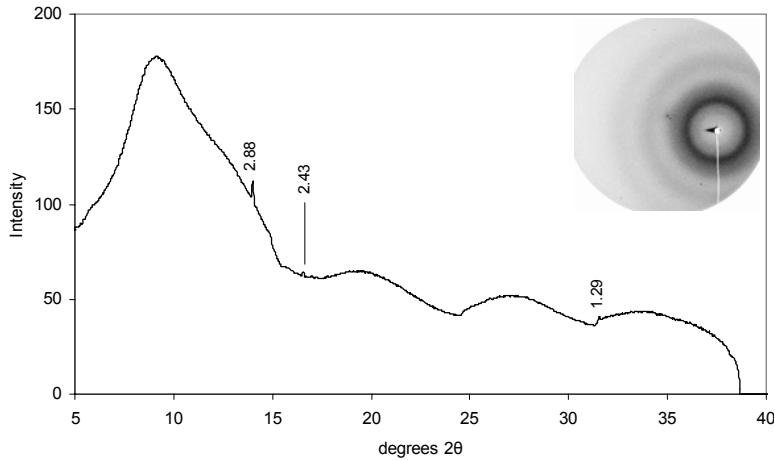
Figure A-142.   Micro-XRD pattern for treatment PA 24hr point P125. Original Debye-Sherer rings are located in the top-right hand corner of the graph. The mineral species identified include gahnite (2.86, 2.44,…).
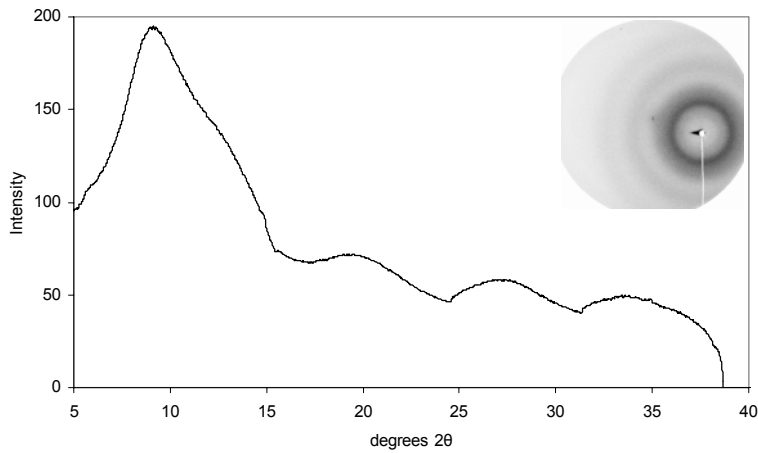
Figure A-143.   Micro-XRD pattern for treatment PA 24hr High Fe Spot point P126. Original Debye-Sherer rings are located in the top-right hand corner of the graph. The mineral species identified include no Peaks, must indicate amorphous iron species.
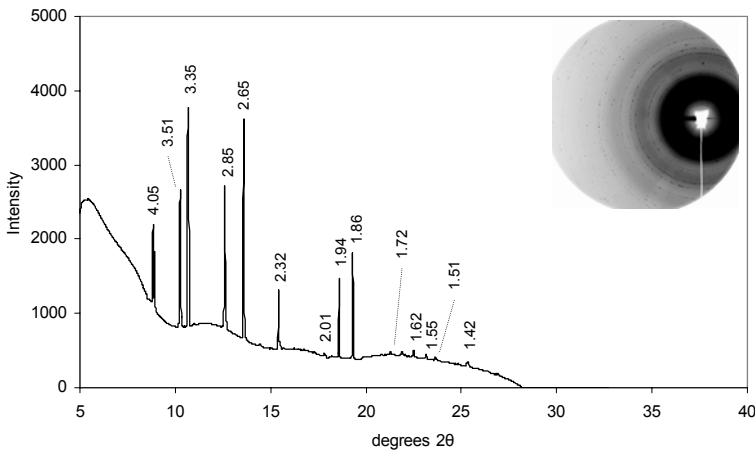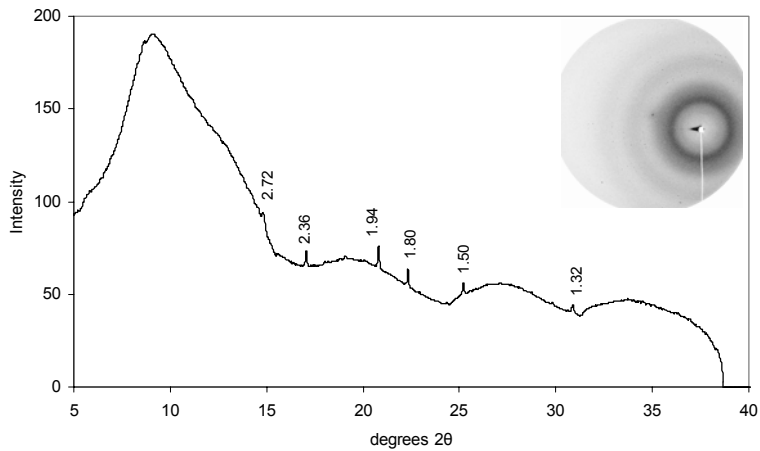
Figure A-144. Micro-XRD pattern for treatment PA 24hr point P127. Original Debye-Sherer rings are located in the top-right hand corner of the graph. The mineral species identified include Smithsonite (2.75, 3.55, 1.70, 2.33, 1.95, 2.11, 1.52, 1.49).
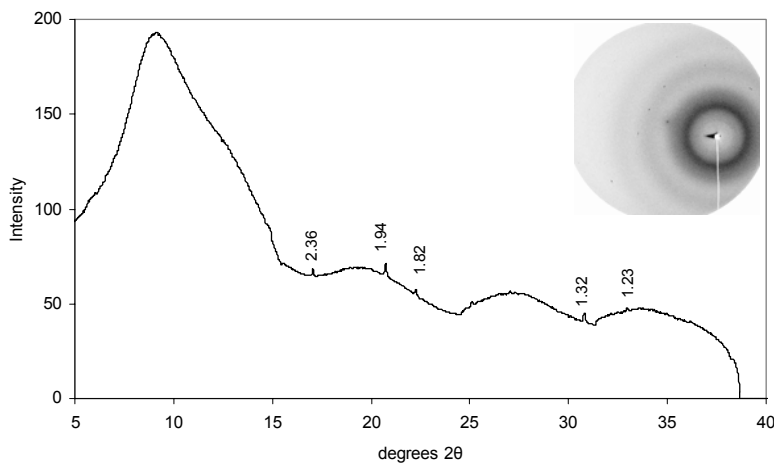
Figure A-145. Micro-XRD pattern for treatment PA 24hr point P128. Original Debye-Sherer rings are located in the top-right hand corner of the graph. There were no mineral species that were able to be identified.
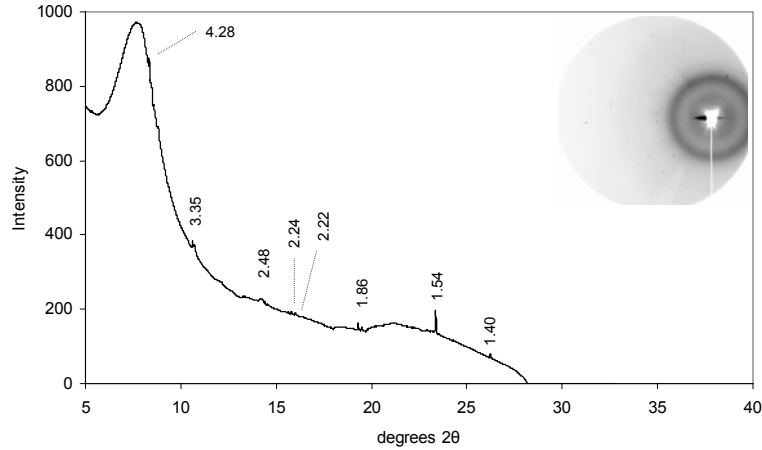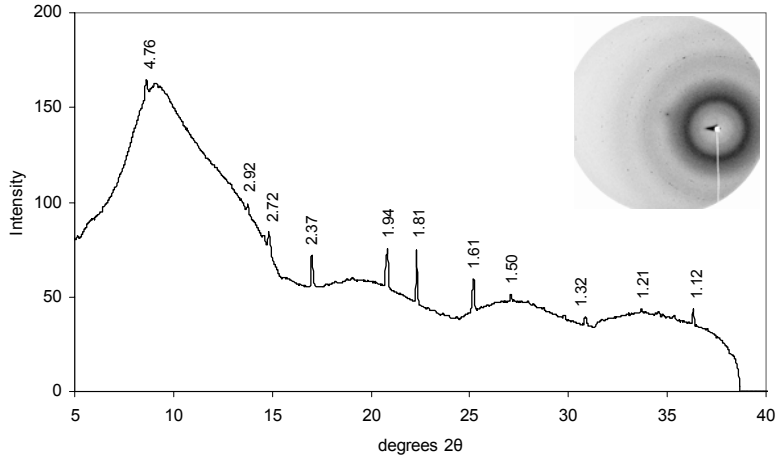
Figure A-146. Micro-XRD pattern for treatment PA 24hr point P129. Original Debye-Sherer rings are located in the top-right hand corner of the graph. The mineral species identified include sphalerite (3.12, 1.91, 1.63, 2.71, 1.24).
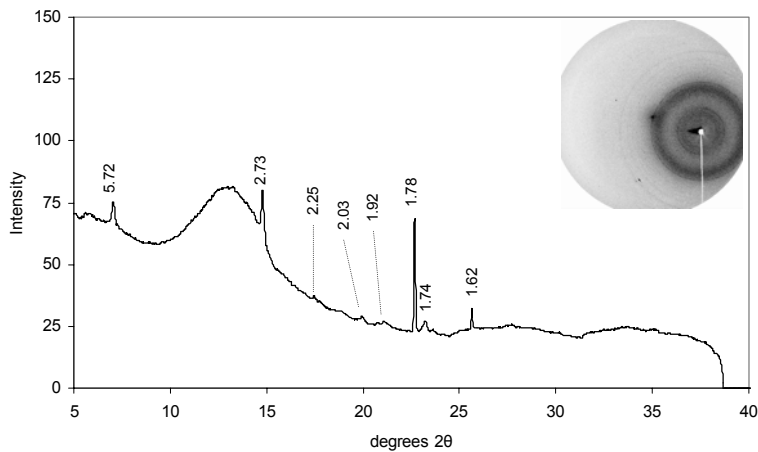
Figure A-147. Micro-XRD pattern for treatment TSP 24hr point P130. Original Debye-Sherer rings are located in the top-right hand corner of the graph. The mineral species identified include plumbogummite (2.97, 5.70, 3.50, 2.22, 2.21, 1.90, 3.44, 5.57), magnetoplumbite (2.76, 2.62, 2.93, 2.41, 1.62; 4.97, 2.88, 2.23) and galena has a major peak at 1.78.
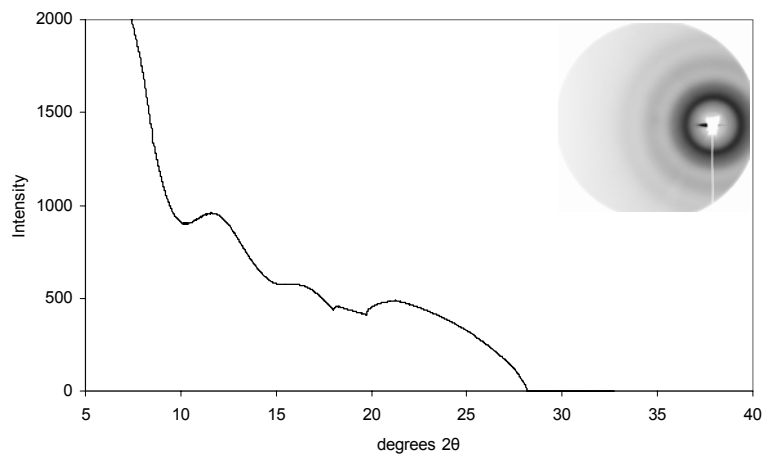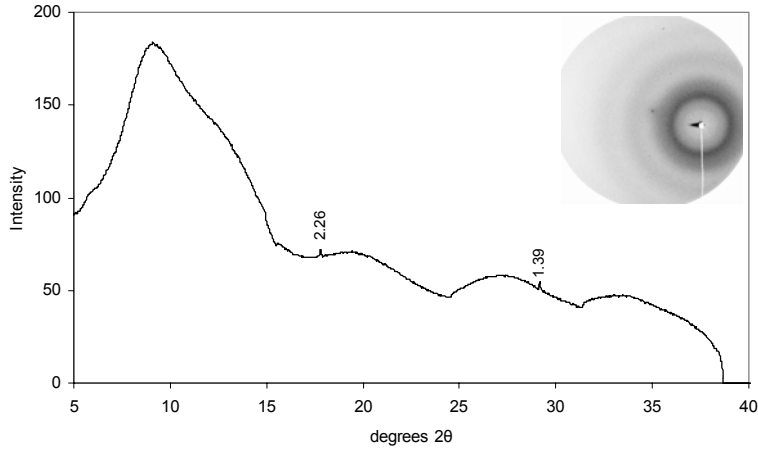
Figure A-148. Micro-XRD pattern for treatment TSP 24hr point P131. Original Debye-Sherer rings are located in the top-right hand corner of the graph. There were no mineral species that were able to be identified.
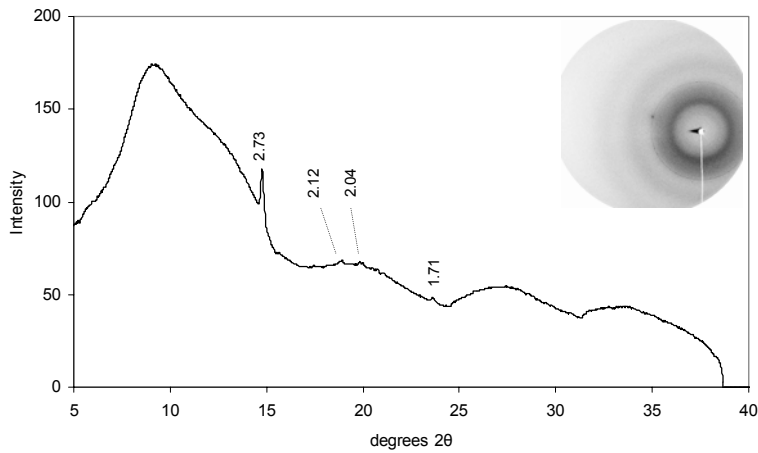
Figure A-149. Micro-XRD pattern for treatment TSP 24hr point P132. Original Debye-Sherer rings are located in the top-right hand corner of the graph. The mineral species identified include magnetoplumbite has a major peak at 2.76.
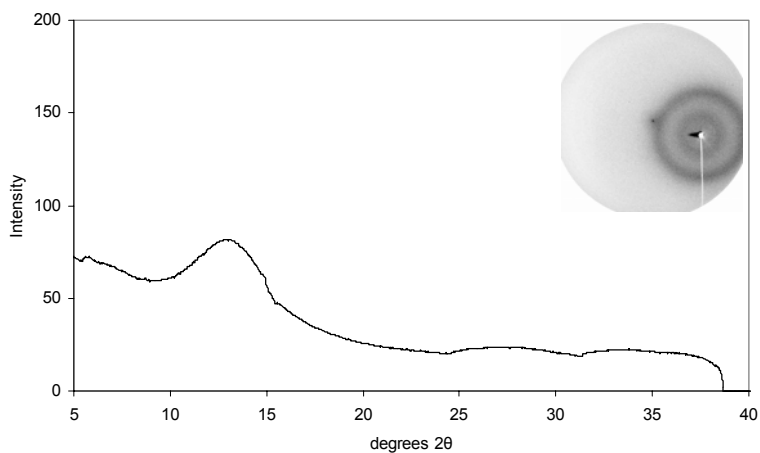
Figure A-150. Micro-XRD pattern for treatment TSP 24hr point P133. Original Debye-Sherer rings are located in the top-right hand corner of the graph. There were no mineral species that were able to be identified.
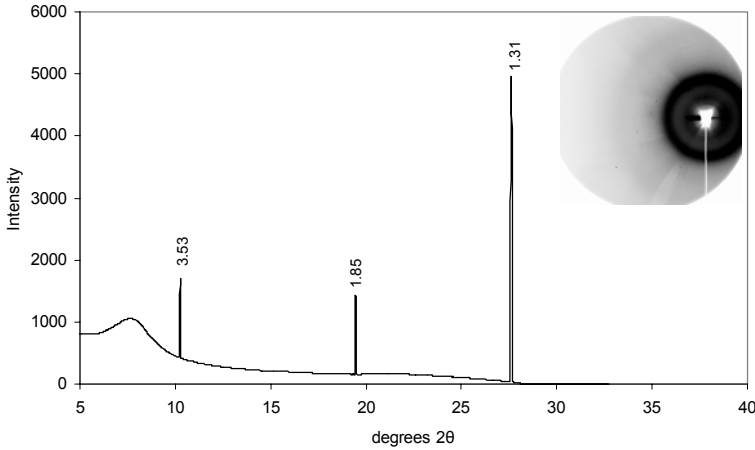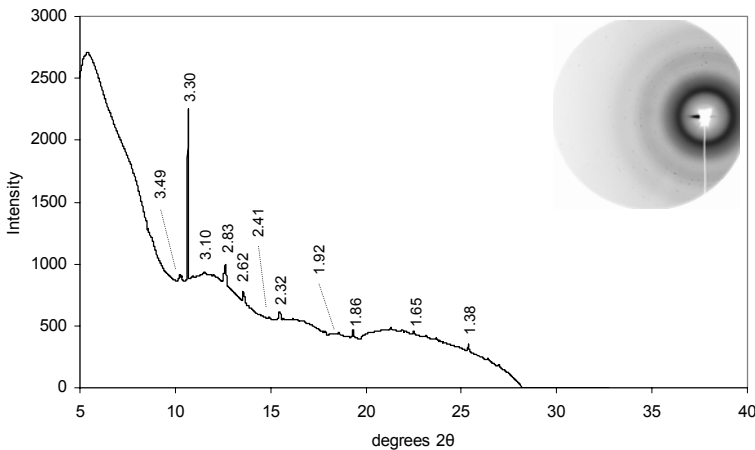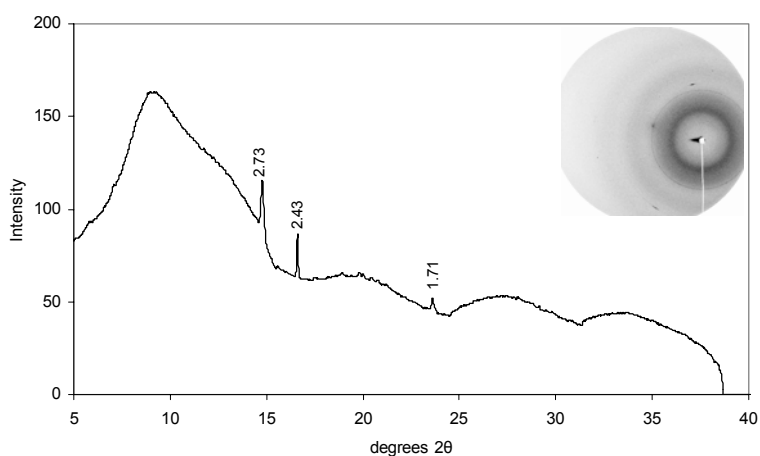

Figure A-151. Micro-XRD pattern for treatment TSP 24hr point P134. Original Debye-Sherer rings are located in the top-right hand corner of the graph. The mineral species identified include magnetoplumbite has peaks at 2.76 and 2.41 and galena has a peak at 1.71.
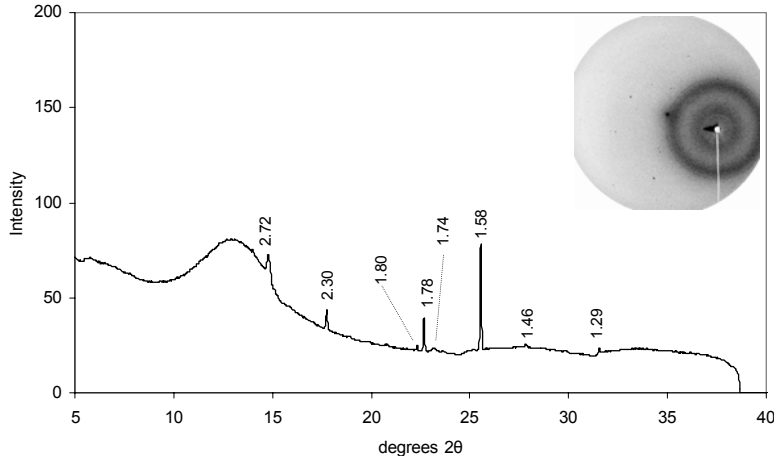
Figure A-152. Micro-XRD pattern for treatment TSP 24hr point P135. Original Debye-Sherer rings are located in the top-right hand corner of the graph. The mineral species identified include smithsonite (2.75, 3.55, 1.70, 2.33, 1.95, 2.11, 1.52, 1.49).
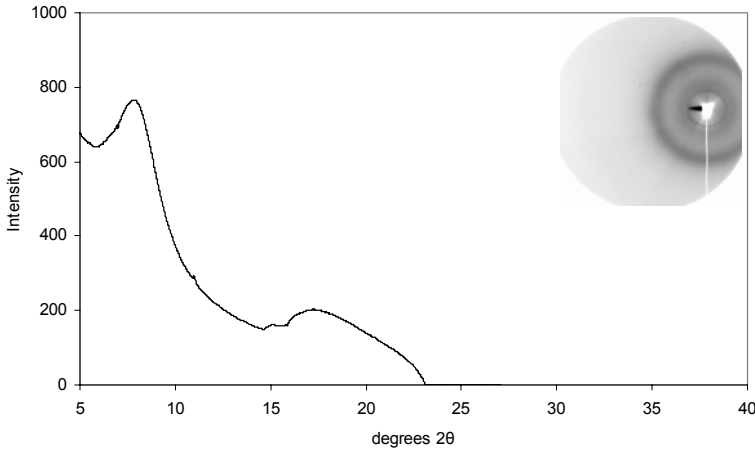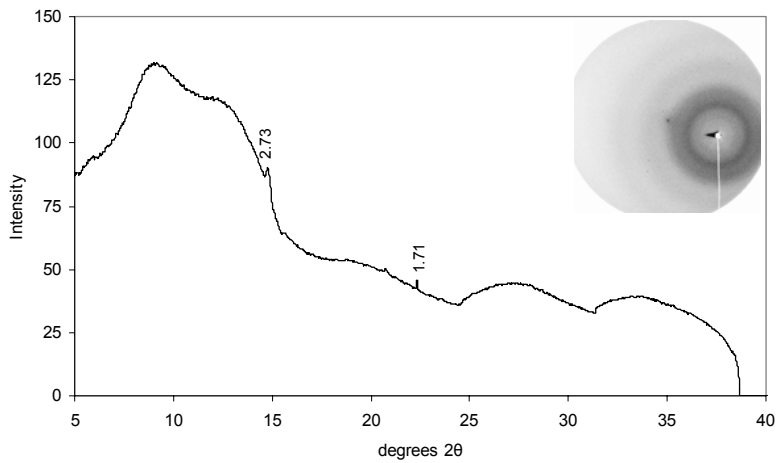

Figure A-153. Micro-XRD pattern for treatment TSP 24hr point P136. Original Debye-Sherer rings are located in the top-right hand corner of the graph. The mineral species identified include smithsonite (2.75, 3.55, 1.70, 2.33, 1.95, 2.11, 1.52, 1.49).
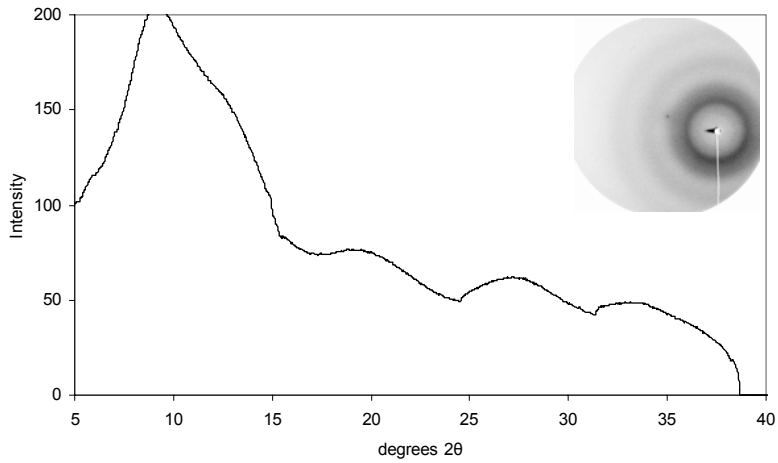
Figure A-154. Micro-XRD pattern for treatment TSP 24hr point P137. Original Debye-Sherer rings are located in the top-right hand corner of the graph. There were no mineral species that were able to be identified.
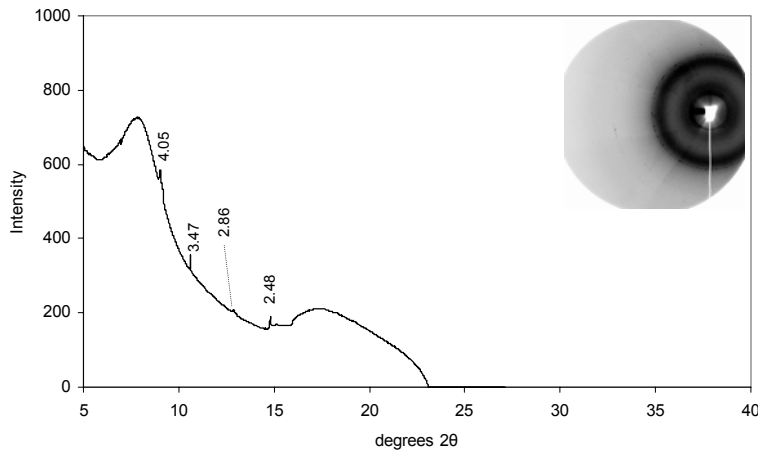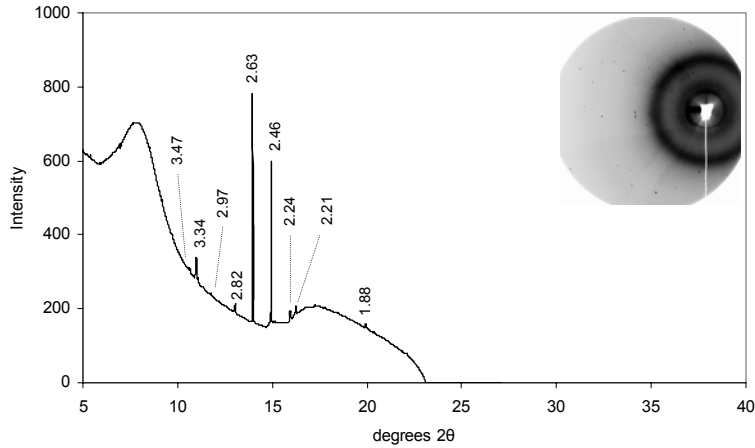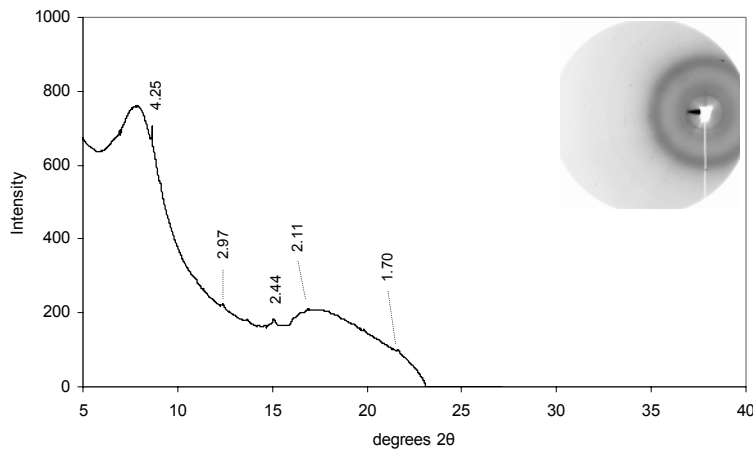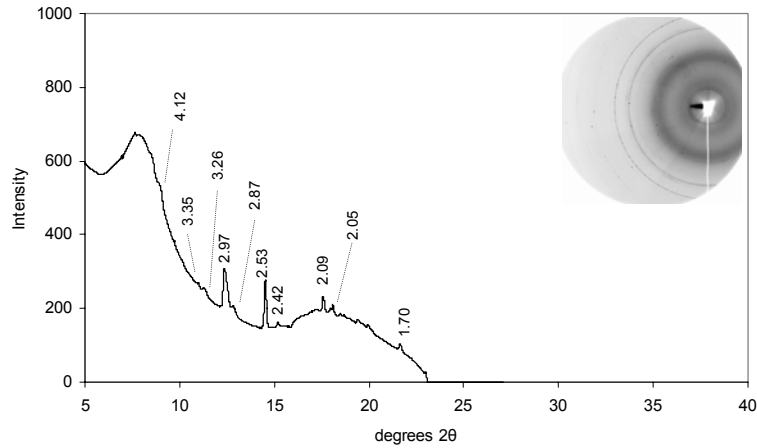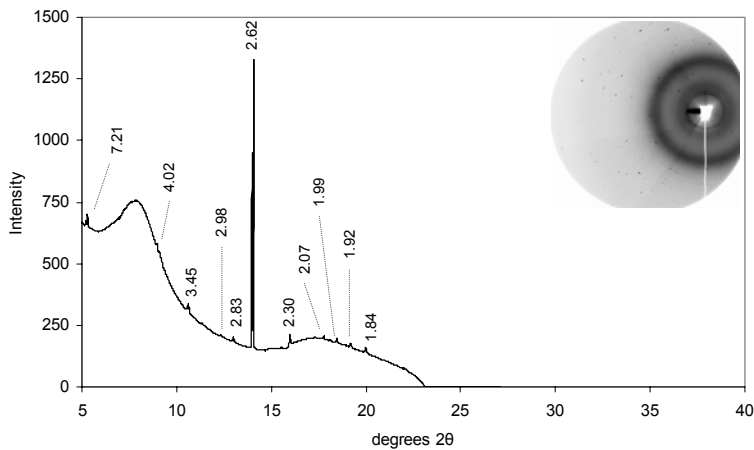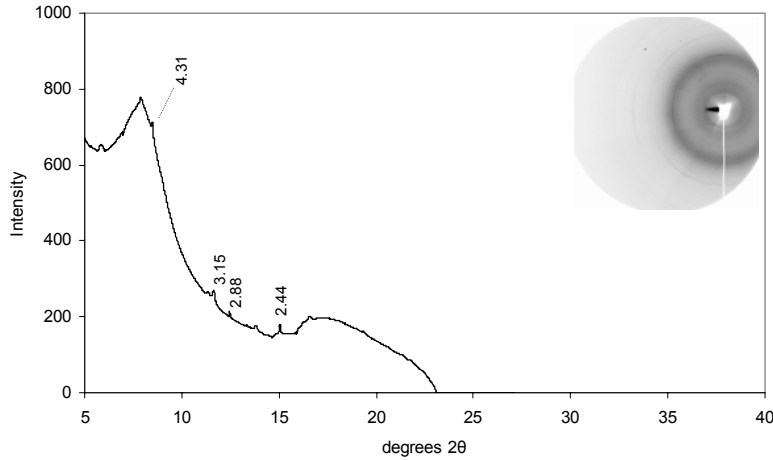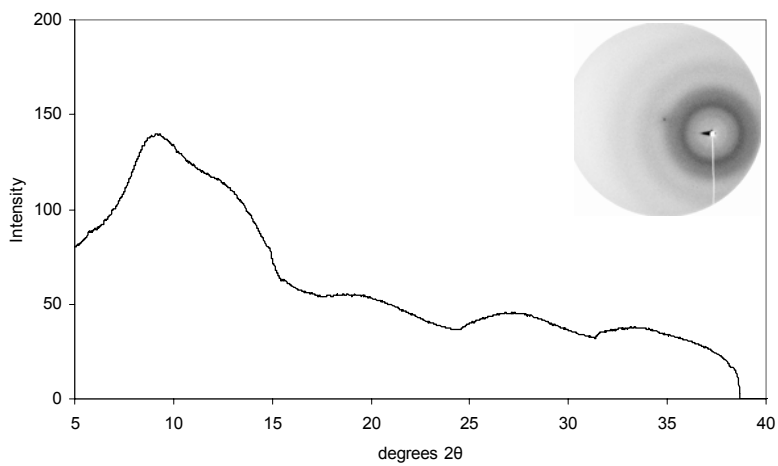

Figure A-155. Micro-XRD pattern for treatment TSP 24hr granule point P138. Original Debye-Sherer rings are located in the top-right hand corner of the graph. There were no mineral species that were able to be identified.

Appendix B - Field Research Raw Data

Table 7-1. Definition of treatments and their abbreviations. Number ID's will be used in all of the following tables for simplicity.

Treatment	Compost Rate	Lime	Bentonite	Site	Rep	Number ID
	---------------Mg ha^{-1}---------------					
C	0	0.0	0.0	1	1	1
HC	269	0.0	0.0	1	1	2
LCL	45	11.3	0.0	1	1	3
LCLB	45	11.3	2.3	1	1	4
HCL	269	11.3	0.0	1	1	5
LC	45	0.0	0.0	1	1	6
HCLB	269	11.3	13.5	1	1	7
LCLB	45	11.3	2.3	1	2	8
HC	269	0.0	0.0	1	2	9
LC	45	0.0	0.0	1	2	10
LCL	45	11.3	0.0	1	2	11
HCLB	269	11.3	13.5	1	2	12
C	0	0.0	0.0	1	2	13
HCL	269	11.3	0.0	1	2	14
HC	269	0.0	0.0	1	3	15
HCLB	269	11.3	13.5	1	3	16
HCL	269	11.3	0.0	1	3	17
C	0	0.0	0.0	1	3	18
LC	45	0.0	0.0	1	3	19
LCLB	45	11.3	2.3	1	3	20
LCL	45	11.3	0.0	1	3	21
LCL	45	11.3	0.0	2	1	22
LCLB	45	11.3	2.3	2	1	23
HCL	269	11.3	0.0	2	1	24
LC	45	0.0	0.0	2	1	25
HCLB	269	11.3	13.5	2	1	26
HC	269	0.0	0.0	2	1	27
C	0	0.0	0.0	2	1	28
HCLB	269	11.3	13.5	2	2	29
LC	45	0.0	0.0	2	2	30
C	0	0.0	0.0	2	2	31
HC	269	0.0	0.0	2	2	32
HCL	269	11.3	0.0	2	2	33
LCL	45	11.3	0.0	2	2	34
LCLB	45	11.3	2.3	2	2	35
HCLB	269	11.3	13.5	2	3	36
C	0	0.0	0.0	2	3	37
LC	45	0.0	0.0	2	3	38
LCL	45	11.3	0.0	2	3	39
HC	269	0.0	0.0	2	3	40
HCL	269	11.3	0.0	2	3	41
LCLB	45	11.3	2.3	2	3	42

Table 7-2. Microbial Biomass as determined by PLFA analysis for the 535 d after time 0 sampling.

Number ID	Gram-positive Bacteria	Gram-negative Bacteria	Actinomycetes	Fungi
	------------------------------------μmol kg^{-1}--			
1	20.82	11.35	3.69	17.17
2	58.51	36.48	3.08	24.54
3	25.78	21.13	1.66	18.60
4	10.38	6.66	0.00	6.14
5	36.44	18.99	2.57	18.24
6	18.31	20.24	2.33	14.46
7	33.48	95.62	1.22	21.81
8	20.59	14.58	1.30	12.34
9	55.70	35.56	2.57	27.75
10	35.17	20.08	2.94	15.99
11	22.20	14.41	2.46	15.17
12	32.05	20.11	1.19	15.34
13	14.63	6.59	1.82	4.85
14	31.49	21.03	1.26	16.64
15	52.09	36.29	2.62	30.89
16	36.67	29.21	3.59	20.10
17	40.30	25.02	3.22	22.29
18	22.77	14.58	2.65	12.24
19	22.07	13.69	2.24	9.83
20	17.14	11.16	1.22	10.12
21	16.64	12.81	1.45	11.89
22	23.40	12.84	1.93	10.06
23	6.69	5.51	0.00	4.51
24	37.84	23.21	1.89	15.96
25	23.36	10.18	1.92	8.10
26	47.13	55.84	2.79	18.49
27	31.15	15.51	2.75	18.67
28	13.57	11.16	2.27	3.73
29	36.92	20.60	2.85	19.96
30	23.96	11.19	1.86	8.82
31	13.80	3.72	2.44	7.97
32	47.83	23.41	3.12	19.91
33	29.03	13.93	1.75	11.92
34	19.94	89.28	1.54	8.62
35	21.02	10.96	1.46	8.24
36	40.47	20.49	2.07	15.33
37	16.28	4.50	1.61	2.20
38	21.09	10.30	1.54	6.83
39	17.45	9.28	1.17	7.35
40	38.05	20.64	2.25	14.46
41	35.34	58.74	2.24	15.74
42	12.59	7.12	0.89	6.15

Table 7-3. Microbial biomass as determined by PLFA analysis at the 711 d after time 0 sampling.

Number ID	Gram-positive Bacteria	Gram-negative Bacteria	Actinomycetes	Fungi
		μmol kg^{-1}		
1	12.09	8.30	1.85	11.20
2	46.20	27.05	2.58	17.46
3	11.15	28.01	0.91	7.83
4	6.29	7.31	0.00	6.90
5	24.14	15.37	1.26	10.45
6	6.91	6.14	0.00	7.73
7	18.80	13.93	1.30	11.92
8	10.32	8.69	0.90	10.26
9	36.50	24.65	1.79	16.69
10	8.49	5.87	0.86	4.79
11	9.94	8.18	0.00	5.83
12	24.35	14.24	1.76	10.56
13	4.48	12.89	0.00	3.29
14	19.57	27.03	1.81	9.33
15	30.64	20.58	1.52	14.95
16	31.24	21.79	1.70	15.94
17	33.79	27.27	1.91	15.65
18	14.13	9.26	1.69	11.75
19	13.57	11.84	1.49	8.26
20	10.03	8.77	0.80	6.80
21	6.45	44.09	0.00	5.64
22	13.96	11.74	1.39	8.43
23	9.70	8.51	1.11	7.57
24	39.96	24.53	2.21	17.18
25	17.43	10.41	1.20	6.96
26	34.40	25.97	2.16	13.24
27	35.37	20.24	1.53	16.34
28	15.47	7.06	2.24	7.91
29	32.29	21.89	1.86	14.05
30	17.09	10.69	1.38	6.83
31	8.95	3.49	1.14	2.73
32	46.31	44.12	2.48	17.49
33	25.02	15.48	1.51	10.53
34	14.06	7.62	1.25	8.10
35	12.69	37.68	0.82	6.52
36	37.22	21.05	2.40	12.96
37	11.11	4.39	1.20	3.85
38	21.86	13.90	1.81	9.41
39	8.84	7.61	0.00	5.49
40	33.02	21.26	1.57	15.09
41	33.83	20.98	1.91	13.53
42	8.97	8.70	0.00	5.19

Table 7-4. Mole percentages of each individual fatty acid at the 535 d after time 0 sampling.

Number ID	11:0	10:0 2OH	12:0	13:0	12:0 2OH	12:0 3OH
			----Mole %----			
1	0.0000	0.0000	0.0043	0.0000	0.0000	0.0000
2	0.0000	0.0000	0.0072	0.0021	0.0000	0.0000
3	0.0000	0.0000	0.0050	0.0000	0.0000	0.0000
4	0.0000	0.0000	0.0000	0.0000	0.0000	0.0000
5	0.0000	0.0000	0.0057	0.0000	0.0000	0.0000
6	0.0000	0.0000	0.0049	0.0000	0.0000	0.0000
7	0.0000	0.0000	0.0000	0.0000	0.0000	0.0000
8	0.0000	0.0000	0.0000	0.0000	0.0000	0.0000
9	0.0000	0.0000	0.0049	0.0000	0.0000	0.0000
10	0.0000	0.0000	0.0038	0.0000	0.0000	0.0000
11	0.0000	0.0000	0.0000	0.0000	0.0000	0.0000
12	0.0000	0.0000	0.0072	0.0000	0.0000	0.0000
13	0.0000	0.0000	0.0000	0.0000	0.0000	0.0000
14	0.0000	0.0000	0.0040	0.0000	0.0000	0.0000
15	0.0000	0.0000	0.0053	0.0000	0.0000	0.0000
16	0.0000	0.0000	0.0041	0.0000	0.0000	0.0000
17	0.0000	0.0000	0.0000	0.0000	0.0000	0.0000
18	0.0000	0.0000	0.0000	0.0000	0.0000	0.0000
19	0.0000	0.0000	0.0044	0.0000	0.0000	0.0000
20	0.0000	0.0000	0.0000	0.0000	0.0000	0.0000
21	0.0000	0.0000	0.0000	0.0000	0.0000	0.0000
22	0.0000	0.0000	0.0056	0.0000	0.0000	0.0000
23	0.0000	0.0000	0.0000	0.0000	0.0000	0.0000
24	0.0000	0.0000	0.0054	0.0000	0.0000	0.0000
25	0.0000	0.0000	0.0000	0.0000	0.0000	0.0000
26	0.0000	0.0000	0.0044	0.0000	0.0000	0.0000
27	0.0000	0.0000	0.0053	0.0000	0.0000	0.0000
28	0.0000	0.0000	0.0000	0.0000	0.0000	0.0000
29	0.0000	0.0000	0.0049	0.0000	0.0000	0.0000
30	0.0000	0.0000	0.0048	0.0000	0.0000	0.0000
31	0.0000	0.0000	0.0083	0.0000	0.0000	0.0000
32	0.0000	0.0000	0.0055	0.0000	0.0000	0.0000
33	0.0000	0.0000	0.0076	0.0000	0.0000	0.0000
34	0.0000	0.0000	0.0000	0.0000	0.0000	0.0000
35	0.0000	0.0000	0.0051	0.0000	0.0000	0.0000
36	0.0000	0.0000	0.0079	0.0000	0.0000	0.0000
37	0.0000	0.0000	0.0000	0.0000	0.0000	0.0000
38	0.0000	0.0000	0.0000	0.0000	0.0000	0.0000
39	0.0000	0.0000	0.0000	0.0000	0.0000	0.0000
40	0.0000	0.0000	0.0065	0.0000	0.0000	0.0000
41	0.0000	0.0000	0.0040	0.0000	0.0000	0.0000
42	0.0000	0.0000	0.0000	0.0000	0.0000	0.0000

Continued.

Number ID	14:0	i15:0	a15:0	15:0	14:0 2OH	14:0 3OH
				--Mole %--		
1	0.0468	0.0729	0.0558	0.0060	0.0000	0.0000
2	0.0262	0.1172	0.0804	0.0098	0.0000	0.0000
3	0.0198	0.0880	0.0874	0.0069	0.0000	0.0000
4	0.0251	0.0831	0.1103	0.0000	0.0000	0.0000
5	0.0326	0.1016	0.1278	0.0085	0.0000	0.0000
6	0.1158	0.0577	0.0611	0.0058	0.0000	0.0000
7	0.0133	0.0576	0.0535	0.0053	0.0000	0.0000
8	0.0232	0.1087	0.0842	0.0077	0.0000	0.0000
9	0.0235	0.1145	0.0806	0.0093	0.0066	0.0000
10	0.0237	0.0992	0.0773	0.0104	0.0000	0.0000
11	0.0442	0.0884	0.0876	0.0071	0.0000	0.0000
12	0.0251	0.1001	0.1143	0.0089	0.0000	0.0000
13	0.0227	0.0875	0.0755	0.0079	0.0000	0.0000
14	0.0227	0.0973	0.1039	0.0086	0.0000	0.0000
15	0.0274	0.1063	0.0799	0.0090	0.0071	0.0058
16	0.0412	0.0878	0.0701	0.0080	0.0000	0.0000
17	0.0185	0.0969	0.0913	0.0068	0.0000	0.0000
18	0.0157	0.0874	0.0578	0.0060	0.0000	0.0000
19	0.0214	0.0889	0.0750	0.0076	0.0000	0.0000
20	0.0219	0.0856	0.1032	0.0081	0.0000	0.0000
21	0.0202	0.0822	0.0932	0.0070	0.0000	0.0000
22	0.0209	0.1011	0.0824	0.0080	0.0000	0.0000
23	0.0202	0.1083	0.0830	0.0000	0.0000	0.0000
24	0.0224	0.1092	0.0964	0.0090	0.0000	0.0000
25	0.0242	0.1103	0.0933	0.0095	0.0000	0.0000
26	0.0198	0.0882	0.0765	0.0086	0.0000	0.0000
27	0.0471	0.0943	0.0823	0.0083	0.0000	0.0000
28	0.0287	0.0695	0.0575	0.0000	0.0000	0.0000
29	0.0351	0.0974	0.0872	0.0082	0.0000	0.0000
30	0.0211	0.1117	0.0869	0.0087	0.0000	0.0000
31	0.0574	0.0678	0.0748	0.0000	0.0000	0.0000
32	0.0329	0.1059	0.0994	0.0097	0.0000	0.0000
33	0.0301	0.1061	0.1041	0.0097	0.0000	0.0000
34	0.0209	0.0371	0.0411	0.0035	0.0000	0.0000
35	0.0192	0.1010	0.0975	0.0079	0.0000	0.0000
36	0.0242	0.1052	0.1020	0.0094	0.0000	0.0000
37	0.0157	0.1113	0.0952	0.0000	0.0000	0.0000
38	0.0196	0.1001	0.1000	0.0090	0.0000	0.0000
39	0.0188	0.0925	0.0980	0.0080	0.0000	0.0000
40	0.0263	0.1020	0.1000	0.0101	0.0000	0.0000
41	0.0244	0.0705	0.0688	0.0066	0.0000	0.0000
42	0.0238	0.0956	0.1006	0.0000	0.0000	0.0000

Continued.

Number ID	i16:0	16:1ω9	16:1ω11	16:0	10Me16:0	i17:0
			-Mole %-			
1	0.0344	0.0660	0.0268	0.1563	0.0267	0.0229
2	0.0453	0.0911	0.0710	0.1392	0.0313	0.0282
3	0.0286	0.0950	0.0803	0.1538	0.0250	0.0222
4	0.0313	0.0818	0.0609	0.1684	0.0283	0.0237
5	0.0379	0.0674	0.1024	0.1172	0.0282	0.0278
6	0.0280	0.1696	0.0297	0.1171	0.0164	0.0167
7	0.0209	0.4580	0.0674	0.0797	0.0164	0.0167
8	0.0296	0.0842	0.0879	0.1543	0.0261	0.0271
9	0.0432	0.0728	0.0816	0.1432	0.0344	0.0299
10	0.0432	0.0672	0.0497	0.1792	0.0341	0.0295
11	0.0282	0.0828	0.0746	0.1378	0.0284	0.0236
12	0.0345	0.0768	0.0924	0.1192	0.0271	0.0283
13	0.0577	0.0645	0.0310	0.1873	0.0383	0.0335
14	0.0390	0.0899	0.0948	0.1357	0.0308	0.0287
15	0.0401	0.0742	0.1123	0.1200	0.0289	0.0315
16	0.0319	0.1212	0.0698	0.1282	0.0399	0.0272
17	0.0365	0.0770	0.0951	0.1511	0.0291	0.0311
18	0.0416	0.0556	0.0449	0.1838	0.0290	0.0315
19	0.0461	0.0616	0.0431	0.1510	0.0277	0.0312
20	0.0317	0.0780	0.0733	0.1526	0.0288	0.0250
21	0.0301	0.1302	0.0758	0.1585	0.0233	0.0234
22	0.0561	0.0617	0.0755	0.1155	0.0339	0.0452
23	0.0510	0.0982	0.1216	0.1308	0.0392	0.0409
24	0.0480	0.0816	0.0914	0.1194	0.0324	0.0373
25	0.0596	0.0505	0.0806	0.1227	0.0313	0.0476
26	0.0410	0.2567	0.0715	0.0901	0.0328	0.0300
27	0.0487	0.0556	0.0839	0.0964	0.0228	0.0367
28	0.0533	0.2364	0.0197	0.0883	0.0349	0.0665
29	0.0422	0.0591	0.0834	0.1100	0.0376	0.0349
30	0.0614	0.0532	0.0770	0.1247	0.0313	0.0473
31	0.0494	0.0258	0.0134	0.0727	0.0329	0.0514
32	0.0495	0.0484	0.0715	0.1141	0.0411	0.0381
33	0.0485	0.0552	0.0924	0.1136	0.0291	0.0424
34	0.0167	0.6365	0.0344	0.0426	0.0112	0.0161
35	0.0472	0.0711	0.0918	0.1085	0.0320	0.0506
36	0.0454	0.0551	0.0804	0.1131	0.0350	0.0384
37	0.0820	0.0329	0.0319	0.1247	0.0447	0.0773
38	0.0567	0.0503	0.0607	0.1179	0.0358	0.0445
39	0.0448	0.0641	0.0737	0.1101	0.0363	0.0446
40	0.0541	0.0659	0.0845	0.1114	0.0312	0.0388
41	0.0345	0.3537	0.0629	0.0763	0.0215	0.0257
42	0.0410	0.0696	0.1073	0.1139	0.0261	0.0436

Continued.

Number ID	a17:0	17:1	17:0delta9,10	17:0	16:0 2OH	18:3ω6,9,12
			-------------------------------Mole %-------------------------------			
1	0.0329	0.0123	0.0161	0.0259	0.0000	0.0287
2	0.0346	0.0076	0.0300	0.0375	0.0000	0.0021
3	0.0255	0.0126	0.0267	0.0107	0.0000	0.0000
4	0.0457	0.0000	0.0230	0.0441	0.0000	0.0000
5	0.0315	0.0106	0.0262	0.0104	0.0000	0.0000
6	0.0260	0.0155	0.0164	0.0235	0.0000	0.0000
7	0.0184	0.0052	0.0157	0.0133	0.0000	0.0000
8	0.0304	0.0105	0.0279	0.0113	0.0000	0.0000
9	0.0325	0.0079	0.0309	0.0144	0.0000	0.0037
10	0.0385	0.0096	0.0308	0.0095	0.0000	0.0028
11	0.0280	0.0139	0.0241	0.0105	0.0000	0.0000
12	0.0319	0.0104	0.0267	0.0532	0.0000	0.0000
13	0.0515	0.0000	0.0272	0.0285	0.0000	0.0000
14	0.0334	0.0077	0.0270	0.0155	0.0000	0.0000
15	0.0321	0.0094	0.0308	0.0121	0.0000	0.0000
16	0.0279	0.0114	0.0236	0.0154	0.0000	0.0000
17	0.0330	0.0082	0.0264	0.0179	0.0000	0.0000
18	0.0402	0.0119	0.0255	0.0231	0.0000	0.0000
19	0.0412	0.0140	0.0310	0.0358	0.0000	0.0000
20	0.0407	0.0000	0.0244	0.0155	0.0000	0.0000
21	0.0293	0.0107	0.0210	0.0000	0.0000	0.0000
22	0.0380	0.0144	0.0300	0.0266	0.0000	0.0000
23	0.0000	0.0000	0.0354	0.0000	0.0000	0.0000
24	0.0352	0.0104	0.0327	0.0252	0.0000	0.0000
25	0.0445	0.0114	0.0344	0.0324	0.0000	0.0000
26	0.0290	0.0091	0.0253	0.0134	0.0000	0.0000
27	0.0349	0.0139	0.0245	0.0474	0.0000	0.0000
28	0.0381	0.0000	0.0234	0.0401	0.0000	0.0000
29	0.0312	0.0128	0.0315	0.0295	0.0000	0.0000
30	0.0408	0.0106	0.0360	0.0335	0.0000	0.0000
31	0.0527	0.0220	0.0180	0.0596	0.0000	0.0000
32	0.0414	0.0128	0.0324	0.0097	0.0000	0.0000
33	0.0455	0.0150	0.0290	0.0196	0.0000	0.0000
34	0.0190	0.0058	0.0113	0.0070	0.0000	0.0000
35	0.0482	0.0128	0.0286	0.0340	0.0000	0.0000
36	0.0429	0.0100	0.0316	0.0556	0.0000	0.0000
37	0.0551	0.0000	0.0253	0.0859	0.0000	0.0000
38	0.0562	0.0120	0.0355	0.0319	0.0000	0.0000
39	0.0551	0.0152	0.0313	0.0299	0.0000	0.0000
40	0.0465	0.0122	0.0320	0.0237	0.0000	0.0000
41	0.0314	0.0084	0.0200	0.0115	0.0000	0.0000
42	0.0575	0.0171	0.0286	0.0000	0.0000	0.0000

Continued.

Number ID	18:2ω9,12	18:1ω9	18:1ω9t	18:0	10Me18:0	19:0delta9,10	20:0
	---------------------------------------Mole %---------------------------------------						
1	0.1126	0.0779	0.0690	0.0413	0.0529	0.0115	0.0000
2	0.0221	0.0538	0.0674	0.0399	0.0187	0.0332	0.0041
3	0.0431	0.0901	0.1015	0.0336	0.0191	0.0194	0.0055
4	0.0455	0.0843	0.0845	0.0423	0.0000	0.0176	0.0000
5	0.0387	0.0500	0.0769	0.0434	0.0269	0.0284	0.0000
6	0.0853	0.0712	0.0601	0.0347	0.0300	0.0146	0.0000
7	0.0190	0.0377	0.0538	0.0244	0.0069	0.0166	0.0000
8	0.0371	0.0707	0.0962	0.0395	0.0206	0.0231	0.0000
9	0.0320	0.0577	0.0793	0.0416	0.0162	0.0347	0.0043
10	0.0341	0.0731	0.0766	0.0457	0.0294	0.0260	0.0067
11	0.0710	0.0729	0.0812	0.0407	0.0354	0.0194	0.0000
12	0.0199	0.0548	0.0874	0.0406	0.0130	0.0281	0.0000
13	0.0262	0.0730	0.0681	0.0536	0.0489	0.0171	0.0000
14	0.0304	0.0581	0.0798	0.0438	0.0139	0.0351	0.0000
15	0.0301	0.0566	0.0813	0.0445	0.0169	0.0345	0.0039
16	0.0314	0.0718	0.0744	0.0467	0.0309	0.0322	0.0049
17	0.0289	0.0670	0.0837	0.0415	0.0276	0.0273	0.0051
18	0.0441	0.0860	0.1110	0.0432	0.0378	0.0162	0.0078
19	0.0347	0.0759	0.1015	0.0455	0.0350	0.0202	0.0072
20	0.0379	0.0892	0.0978	0.0414	0.0242	0.0208	0.0000
21	0.0450	0.0995	0.0688	0.0376	0.0268	0.0174	0.0000
22	0.0216	0.0700	0.0867	0.0401	0.0320	0.0347	0.0000
23	0.0239	0.0719	0.0949	0.0434	0.0000	0.0372	0.0000
24	0.0147	0.0530	0.0738	0.0404	0.0189	0.0434	0.0000
25	0.0130	0.0523	0.0608	0.0495	0.0345	0.0378	0.0000
26	0.0118	0.0408	0.0517	0.0361	0.0187	0.0410	0.0035
27	0.0674	0.0588	0.0606	0.0465	0.0309	0.0339	0.0000
28	0.0440	0.0419	0.0231	0.0373	0.0642	0.0332	0.0000
29	0.0489	0.0612	0.0691	0.0439	0.0276	0.0401	0.0042
30	0.0215	0.0529	0.0634	0.0418	0.0319	0.0395	0.0000
31	0.1393	0.0783	0.0340	0.0415	0.0707	0.0300	0.0000
32	0.0377	0.0580	0.0655	0.0460	0.0262	0.0502	0.0039
33	0.0146	0.0572	0.0685	0.0485	0.0241	0.0390	0.0000
34	0.0107	0.0210	0.0267	0.0153	0.0118	0.0110	0.0000
35	0.0139	0.0529	0.0827	0.0384	0.0281	0.0285	0.0000
36	0.0136	0.0531	0.0636	0.0431	0.0199	0.0465	0.0042
37	0.0000	0.0378	0.0340	0.0444	0.0512	0.0506	0.0000
38	0.0196	0.0572	0.0800	0.0406	0.0311	0.0414	0.0000
39	0.0184	0.0756	0.0835	0.0404	0.0268	0.0329	0.0000
40	0.0118	0.0542	0.0678	0.0485	0.0234	0.0491	0.0000
41	0.0199	0.0372	0.0456	0.0316	0.0171	0.0285	0.0000
42	0.0208	0.0633	0.0938	0.0400	0.0276	0.0296	0.0000

Table 7-5. **Mole percentages of each individual fatty acid at the 711 d after time 0 sampling.**

Number ID	11:0	10:0 2OH	12:0	13:0	12:0 2OH	12:0 3OH
			----Mole %----			
1	0.0000	0.0000	0.0000	0.0000	0.0000	0.0000
2	0.0000	0.0000	0.0068	0.0000	0.0000	0.0000
3	0.0000	0.0000	0.0000	0.0000	0.0000	0.0000
4	0.0000	0.0000	0.0000	0.0000	0.0000	0.0000
5	0.0000	0.0000	0.0065	0.0000	0.0000	0.0000
6	0.0000	0.0000	0.0000	0.0000	0.0000	0.0000
7	0.0000	0.0000	0.0000	0.0000	0.0000	0.0000
8	0.0000	0.0000	0.0150	0.0000	0.0000	0.0000
9	0.0000	0.0000	0.0067	0.0000	0.0000	0.0000
10	0.0000	0.0000	0.0000	0.0000	0.0000	0.0000
11	0.0000	0.0000	0.0000	0.0000	0.0000	0.0000
12	0.0000	0.0000	0.0072	0.0000	0.0000	0.0000
13	0.0000	0.0000	0.0000	0.0000	0.0000	0.0000
14	0.0000	0.0000	0.0000	0.0000	0.0000	0.0000
15	0.0000	0.0000	0.0055	0.0000	0.0000	0.0000
16	0.0000	0.0000	0.0066	0.0000	0.0000	0.0000
17	0.0000	0.0000	0.0052	0.0000	0.0000	0.0000
18	0.0000	0.0000	0.0000	0.0000	0.0000	0.0000
19	0.0000	0.0000	0.0071	0.0000	0.0000	0.0000
20	0.0000	0.0000	0.0000	0.0000	0.0000	0.0000
21	0.0000	0.0000	0.0000	0.0000	0.0000	0.0000
22	0.0000	0.0000	0.0000	0.0000	0.0000	0.0000
23	0.0000	0.0000	0.0000	0.0000	0.0000	0.0000
24	0.0000	0.0000	0.0069	0.0000	0.0000	0.0000
25	0.0000	0.0000	0.0000	0.0000	0.0000	0.0000
26	0.0000	0.0000	0.0071	0.0000	0.0000	0.0000
27	0.0000	0.0000	0.0070	0.0000	0.0000	0.0000
28	0.0000	0.0000	0.0000	0.0000	0.0000	0.0000
29	0.0000	0.0000	0.0070	0.0000	0.0000	0.0000
30	0.0000	0.0000	0.0000	0.0000	0.0000	0.0000
31	0.0000	0.0000	0.0000	0.0000	0.0000	0.0000
32	0.0000	0.0000	0.0053	0.0000	0.0000	0.0000
33	0.0000	0.0000	0.0069	0.0000	0.0000	0.0000
34	0.0000	0.0000	0.0000	0.0000	0.0000	0.0000
35	0.0000	0.0000	0.0000	0.0000	0.0000	0.0000
36	0.0000	0.0000	0.0070	0.0000	0.0000	0.0000
37	0.0000	0.0000	0.0000	0.0000	0.0000	0.0000
38	0.0000	0.0000	0.0060	0.0000	0.0000	0.0000
39	0.0000	0.0000	0.0000	0.0000	0.0000	0.0000
40	0.0000	0.0000	0.0044	0.0000	0.0000	0.0000
41	0.0000	0.0000	0.0059	0.0000	0.0000	0.0000
42	0.0000	0.0000	0.0000	0.0000	0.0000	0.0000

Continued.

Number ID	14:0	i15:0	a15:0	15:0	14:0 2OH	14:0 3OH
				-Mole %-		
1	0.0171	0.0714	0.0388	0.0000	0.0000	0.0000
2	0.0268	0.1090	0.0926	0.0107	0.0000	0.0000
3	0.0210	0.0600	0.0516	0.0000	0.0208	0.0000
4	0.0221	0.0643	0.0589	0.0000	0.0000	0.0000
5	0.0273	0.0979	0.1320	0.0101	0.0000	0.0000
6	0.0206	0.0700	0.0566	0.0000	0.0000	0.0000
7	0.0281	0.0861	0.0852	0.0106	0.0000	0.0000
8	0.0347	0.0728	0.0598	0.0000	0.0000	0.0000
9	0.0287	0.1037	0.0863	0.0108	0.0000	0.0000
10	0.0248	0.0941	0.0742	0.0000	0.0000	0.0000
11	0.0276	0.0966	0.0889	0.0000	0.0000	0.0000
12	0.0291	0.0988	0.1021	0.0106	0.0000	0.0000
13	0.0000	0.0486	0.0343	0.0000	0.0000	0.0000
14	0.0219	0.0781	0.0748	0.0078	0.0000	0.0000
15	0.0275	0.1049	0.0883	0.0097	0.0000	0.0000
16	0.0267	0.0970	0.0861	0.0096	0.0000	0.0000
17	0.0303	0.0943	0.0896	0.0081	0.0000	0.0000
18	0.0159	0.0795	0.0471	0.0059	0.0000	0.0000
19	0.0233	0.0750	0.0598	0.0075	0.0000	0.0000
20	0.0278	0.0776	0.0854	0.0000	0.0000	0.0000
21	0.0234	0.0298	0.0299	0.0000	0.0000	0.0000
22	0.0245	0.0852	0.0588	0.0105	0.0000	0.0000
23	0.0325	0.0850	0.0628	0.0000	0.0000	0.0000
24	0.0264	0.1028	0.0908	0.0111	0.0000	0.0000
25	0.0249	0.1014	0.0783	0.0099	0.0000	0.0000
26	0.0266	0.0925	0.0908	0.0105	0.0000	0.0000
27	0.0307	0.1138	0.0863	0.0112	0.0000	0.0000
28	0.0199	0.0546	0.1121	0.0099	0.0000	0.0000
29	0.0242	0.0999	0.0892	0.0104	0.0000	0.0000
30	0.0220	0.0932	0.0685	0.0091	0.0000	0.0000
31	0.0199	0.0988	0.0527	0.0000	0.0000	0.0000
32	0.0217	0.0916	0.0781	0.0124	0.0000	0.0000
33	0.0254	0.0919	0.0873	0.0102	0.0000	0.0000
34	0.0252	0.0948	0.0778	0.0111	0.0331	0.0000
35	0.0162	0.0533	0.0444	0.0063	0.0188	0.0000
36	0.0258	0.1035	0.0966	0.0111	0.0000	0.0000
37	0.0195	0.0991	0.0558	0.0000	0.0000	0.0000
38	0.0234	0.1002	0.0730	0.0099	0.0000	0.0000
39	0.0230	0.0855	0.0721	0.0000	0.0000	0.0000
40	0.0253	0.1066	0.0816	0.0110	0.0000	0.0000
41	0.0257	0.1080	0.0843	0.0110	0.0000	0.0000
42	0.0224	0.0908	0.0707	0.0109	0.0000	0.0000

Continued.

Number ID	i16:0	16:1ω9	16:1ω11	16:0	10Me16:0	i17:0
				-----Mole %-----		
1	0.0378	0.0860	0.0292	0.2089	0.0274	0.0227
2	0.0521	0.0626	0.0642	0.1448	0.0302	0.0316
3	0.0214	0.3779	0.0365	0.1142	0.0208	0.0163
4	0.0276	0.1145	0.0426	0.1781	0.0229	0.0174
5	0.0387	0.0973	0.0681	0.1306	0.0275	0.0252
6	0.0329	0.0819	0.0359	0.2316	0.0393	0.0196
7	0.0379	0.0778	0.0678	0.1570	0.0231	0.0266
8	0.0261	0.0611	0.0391	0.1532	0.0174	0.0158
9	0.0479	0.0749	0.0653	0.1543	0.0252	0.0294
10	0.0439	0.1052	0.0405	0.1885	0.0282	0.0284
11	0.0398	0.0892	0.0568	0.1777	0.0374	0.0264
12	0.0440	0.0679	0.0667	0.1462	0.0334	0.0289
13	0.0335	0.4411	0.0179	0.1437	0.0249	0.0192
14	0.0343	0.2580	0.0556	0.1145	0.0212	0.0220
15	0.0471	0.0749	0.0636	0.1523	0.0215	0.0302
16	0.0409	0.0774	0.0603	0.1568	0.0279	0.0279
17	0.0422	0.1254	0.0657	0.1347	0.0280	0.0280
18	0.0391	0.0726	0.0334	0.2075	0.0299	0.0242
19	0.0403	0.1368	0.0300	0.1832	0.0233	0.0242
20	0.0356	0.1038	0.0527	0.1800	0.0263	0.0220
21	0.0138	0.6312	0.0192	0.0756	0.0108	0.0085
22	0.0470	0.0891	0.0626	0.1261	0.0273	0.0384
23	0.0371	0.0989	0.0832	0.1295	0.0267	0.0297
24	0.0473	0.0654	0.0668	0.1304	0.0368	0.0336
25	0.0522	0.0698	0.0584	0.1246	0.0264	0.0375
26	0.0480	0.1190	0.0712	0.1202	0.0375	0.0319
27	0.0534	0.0654	0.1028	0.1227	0.0267	0.0360
28	0.0456	0.0697	0.0186	0.1540	0.0214	0.0447
29	0.0463	0.0865	0.0860	0.1247	0.0362	0.0328
30	0.0695	0.0746	0.0661	0.1331	0.0295	0.0550
31	0.0741	0.0537	0.0246	0.1522	0.0573	0.0718
32	0.0482	0.1687	0.0612	0.1133	0.0344	0.0323
33	0.0557	0.0641	0.0664	0.1261	0.0290	0.0398
34	0.0503	0.0000	0.0811	0.1398	0.0268	0.0401
35	0.0285	0.4522	0.0360	0.0765	0.0147	0.0226
36	0.0528	0.0617	0.0608	0.1256	0.0374	0.0380
37	0.0916	0.0546	0.0313	0.1654	0.0431	0.0754
38	0.0546	0.0707	0.0589	0.1321	0.0346	0.0375
39	0.0544	0.0961	0.0612	0.1499	0.0332	0.0403
40	0.0582	0.0732	0.0863	0.1245	0.0264	0.0366
41	0.0551	0.0691	0.0704	0.1248	0.0313	0.0366
42	0.0484	0.1055	0.0644	0.1390	0.0298	0.0368

Continued.

Number ID	a17:0	17:1	17:0delta9,10	17:0	16:0 2OH	18:3ω6,9,12
			----------------------------------Mole %----------------------------------			
1	0.0256	0.0141	0.0180	0.0298	0.0000	0.0000
2	0.0362	0.0091	0.0323	0.0176	0.0000	0.0000
3	0.0127	0.0000	0.0166	0.0000	0.0000	0.0000
4	0.0119	0.0166	0.0172	0.0882	0.0000	0.0000
5	0.0271	0.0084	0.0243	0.0120	0.0000	0.0000
6	0.0150	0.0000	0.0209	0.0000	0.0000	0.0000
7	0.0273	0.0077	0.0239	0.0138	0.0000	0.0000
8	0.0096	0.0134	0.0174	0.1133	0.0000	0.0000
9	0.0305	0.0071	0.0283	0.0149	0.0000	0.0000
10	0.0258	0.0000	0.0245	0.0000	0.0000	0.0000
11	0.0219	0.0000	0.0233	0.0000	0.0000	0.0000
12	0.0286	0.0084	0.0237	0.0141	0.0000	0.0000
13	0.0164	0.0000	0.0219	0.0000	0.0000	0.0000
14	0.0231	0.0070	0.0218	0.0122	0.0000	0.0000
15	0.0316	0.0077	0.0279	0.0145	0.0000	0.0000
16	0.0301	0.0091	0.0271	0.0143	0.0000	0.0000
17	0.0285	0.0072	0.0251	0.0206	0.0000	0.0000
18	0.0289	0.0109	0.0217	0.0207	0.0000	0.0000
19	0.0272	0.0091	0.0215	0.0268	0.0000	0.0000
20	0.0219	0.0000	0.0203	0.0000	0.0000	0.0000
21	0.0083	0.0000	0.0082	0.0000	0.0000	0.0000
22	0.0206	0.0185	0.0246	0.0283	0.0000	0.0000
23	0.0172	0.0210	0.0257	0.0000	0.0000	0.0000
24	0.0290	0.0087	0.0268	0.0244	0.0000	0.0000
25	0.0244	0.0000	0.0261	0.1025	0.0000	0.0000
26	0.0291	0.0099	0.0251	0.0171	0.0000	0.0000
27	0.0338	0.0111	0.0278	0.0163	0.0000	0.0000
28	0.0262	0.0000	0.0253	0.0666	0.0000	0.0000
29	0.0288	0.0096	0.0263	0.0227	0.0000	0.0000
30	0.0261	0.0000	0.0251	0.0398	0.0000	0.0000
31	0.0172	0.0000	0.0309	0.0593	0.0000	0.0000
32	0.0305	0.0107	0.0284	0.0164	0.0000	0.0000
33	0.0345	0.0119	0.0272	0.0275	0.0000	0.0000
34	0.0229	0.0189	0.0235	0.0267	0.0000	0.0000
35	0.0130	0.0109	0.0137	0.0165	0.0000	0.0000
36	0.0337	0.0119	0.0290	0.0186	0.0000	0.0000
37	0.0268	0.0000	0.0269	0.0000	0.0000	0.0000
38	0.0290	0.0114	0.0296	0.0271	0.0000	0.0000
39	0.0232	0.0215	0.0288	0.0000	0.0000	0.0000
40	0.0337	0.0112	0.0300	0.0180	0.0000	0.0000
41	0.0328	0.0106	0.0277	0.0182	0.0000	0.0000
42	0.0211	0.0232	0.0270	0.0000	0.0000	0.0000

Continued.

Number ID	18:2ω9,12	18:1ω9	18:1ω9t	18:0	10Me18:0	19:0delta9,10	20:0
				Mole %			
1	0.09712	0.1184	0.0679	0.0400	0.0404	0.0095	0.0000
2	0.02319	0.0534	0.0795	0.0482	0.0208	0.0437	0.0045
3	0.03804	0.0651	0.0670	0.0259	0.0162	0.0178	0.0000
4	0.07153	0.1086	0.0889	0.0331	0.0000	0.0155	0.0000
5	0.03733	0.0537	0.0824	0.0443	0.0192	0.0301	0.0000
6	0.11251	0.1127	0.0878	0.0458	0.0000	0.0168	0.0000
7	0.05677	0.0705	0.0930	0.0525	0.0213	0.0332	0.0000
8	0.04925	0.1309	0.0905	0.0449	0.0192	0.0166	0.0000
9	0.03047	0.0596	0.0889	0.0479	0.0167	0.0373	0.0049
10	0.04964	0.0949	0.0769	0.0470	0.0333	0.0201	0.0000
11	0.04845	0.0773	0.1149	0.0451	0.0000	0.0286	0.0000
12	0.03223	0.0580	0.0830	0.0539	0.0262	0.0371	0.0000
13	0.05049	0.0617	0.0461	0.0402	0.0000	0.0000	0.0000
14	0.03503	0.0425	0.0733	0.0385	0.0258	0.0324	0.0000
15	0.03528	0.0672	0.0928	0.0475	0.0169	0.0331	0.0000
16	0.03769	0.0693	0.0897	0.0477	0.0178	0.0343	0.0057
17	0.02698	0.0598	0.0811	0.0419	0.0186	0.0340	0.0047
18	0.08190	0.1197	0.0774	0.0365	0.0339	0.0135	0.0000
19	0.04835	0.0926	0.0679	0.0466	0.0308	0.0185	0.0000
20	0.05785	0.0874	0.1071	0.0469	0.0232	0.0242	0.0000
21	0.02915	0.0401	0.0449	0.0192	0.0000	0.0079	0.0000
22	0.03429	0.0890	0.1184	0.0395	0.0306	0.0267	0.0000
23	0.06605	0.0786	0.1067	0.0408	0.0335	0.0251	0.0000
24	0.02810	0.0600	0.0826	0.0510	0.0199	0.0463	0.0048
25	0.01615	0.0628	0.0757	0.0514	0.0237	0.0339	0.0000
26	0.01318	0.0510	0.0725	0.0513	0.0221	0.0491	0.0045
27	0.01647	0.0498	0.0778	0.0520	0.0158	0.0383	0.0047
28	0.06170	0.1018	0.0416	0.0486	0.0516	0.0260	0.0000
29	0.01338	0.0546	0.0817	0.0490	0.0204	0.0452	0.0050
30	0.02290	0.0597	0.0934	0.0428	0.0301	0.0396	0.0000
31	0.02673	0.0787	0.0396	0.0457	0.0545	0.0423	0.0000
32	0.01719	0.0473	0.0723	0.0408	0.0178	0.0476	0.0038
33	0.02266	0.0624	0.0858	0.0578	0.0217	0.0456	0.0000
34	0.04117	0.0755	0.0994	0.0513	0.0306	0.0301	0.0000
35	0.01685	0.0440	0.0582	0.0281	0.0121	0.0173	0.0000
36	0.01837	0.0556	0.0765	0.0537	0.0250	0.0516	0.0057
37	0.04430	0.0767	0.0429	0.0501	0.0473	0.0493	0.0000
38	0.02655	0.0689	0.0866	0.0492	0.0297	0.0412	0.0000
39	0.04362	0.0868	0.1095	0.0393	0.0000	0.0316	0.0000
40	0.02152	0.0568	0.0875	0.0488	0.0171	0.0413	0.0000
41	0.02051	0.0567	0.0851	0.0531	0.0208	0.0469	0.0053
42	0.03036	0.0775	0.1256	0.0464	0.0000	0.0302	0.0000

Table 7-6. Total metal concentration as determined by 4 *M* nitric acid digest for all plots prior to amendment additions.

Number ID	Total Zn	Total Pb	Total Cd
	-------------mg kg^{-1}-------------		
1	6836	1868	28.70
2	8147	1445	38.40
3	9027	2058	42.60
4	6756	3867	31.30
5	5686	4960	16.10
6	5092	2610	15.20
7	7219	3653	23.10
8	7029	4579	31.30
9	5333	2306	25.50
10	4613	1872	24.10
11	6152	4146	25.60
12	7107	3529	29.50
13	7100	3698	26.80
14	6062	8715	18.50
15	6929	1743	26.10
16	6096	2687	26.90
17	7652	2524	32.60
18	5234	3085	23.40
19	7931	3976	29.80
20	7318	3862	43.90
21	8705	4189	32.40
22	5475	1512	47.10
23	3014	1204	20.00
24	3419	1284	21.00
25	6454	1162	43.60
26	5853	932	42.50
27	5833	747	38.90
28	7969	814	53.20
29	3458	1556	22.10
30	4439	1395	30.90
31	5678	1313	36.10
32	6814	1044	44.00
33	6883	1195	48.10
34	7271	952	50.90
35	12154	1090	89.40
36	1664	1336	11.30
37	2203	1231	14.50
38	6299	1808	44.00
39	4450	1369	31.80
40	5688	903	40.30
41	6236	1069	38.10
42	6188	1005	36.80

Table 7-7. Chemical properties of each plot at the Time 0 sampling. Table will be continued on the next several pages.

Number ID	pH	†Ca(NO$_3$)$_2$ Cd	Ca(NO$_3$)$_2$ Pb	Ca(NO$_3$)$_2$ Zn	Total Cd	Total Pb	Total Zn
				-----mg kg^{-1}-----			
1	6.56	0.46	1.60	22.38	18.90	1062.10	4108.70
2	7.83	1.80	5.66	140.20	11.00	830.70	2163.70
3	8.92	0.84	8.46	18.00	14.40	1367.50	2946.10
4	9.71	0.80	16.24	17.02	16.80	2529.50	3899.30
5	9.27	0.10	11.32	7.82	13.00	2328.10	4091.90
6	8.70	0.54	9.04	56.08	10.70	1865.90	3317.00
7	9.36	0.02	13.10	3.12	6.70	2726.30	2878.20
8	9.26	0.20	12.92	7.60	8.70	1851.20	2947.00
9	8.42	0.18	0.74	12.56	8.60	1164.00	2128.00
10	7.31	1.16	2.50	83.84	12.30	1435.30	2556.50
11	8.92	0.68	14.02	17.44	24.50	2072.40	4725.60
12	9.12	0.34	11.54	19.80	13.40	2166.10	3517.20
13	6.81	3.96	18.64	347.26	15.40	2180.40	3644.10
14	9.30	0.12	11.82	5.20	13.30	2160.90	4655.10
15	8.44	0.16	1.16	15.38	12.50	825.80	3992.50
16	9.12	0.30	5.08	13.78	10.30	1295.70	2565.50
17	9.07	0.34	2.04	22.20	12.70	966.00	2791.40
18	7.22	1.64	32.12	173.12	8.90	2464.70	2417.50
19	7.76	1.50	6.20	133.86	14.40	2293.60	3920.80
20	9.94	1.38	12.12	30.68	15.80	2074.60	3318.50
21	10.89	0.76	22.32	20.10	17.90	2636.00	4648.20
22	11.20	0.02	3.46	2.28	16.00	1080.40	1587.60
23	11.36	0.02	2.68	1.30	40.00	989.80	4935.70
24	8.97	0.06	1.38	1.70	13.10	748.10	2345.10
25	7.53	0.08	1.90	10.90	98.50	999.70	17873.20
26	8.83	0.02	1.22	1.76	21.30	638.70	3064.90
27	7.81	0.08	0.72	9.16	15.00	580.10	2559.00
28	5.83	0.36	9.02	51.20	23.50	693.70	3764.30
29	8.24	0.00	1.56	2.44	6.10	714.00	874.30
30	7.47	0.02	2.44	6.18	11.80	1026.30	2064.20
31	4.92	0.64	32.34	70.58	26.40	1114.50	4142.20
32	7.64	0.06	2.24	4.00	17.30	793.20	2557.10
33	8.93	0.04	0.86	2.08	10.60	637.10	1767.40
34	9.71	0.06	1.78	1.98	37.70	706.40	5501.80
35	9.41	0.08	1.98	2.36	9.70	568.10	1465.70
36	8.32	0.10	1.62	3.62	5.60	1235.70	877.20
37	4.92	0.48	27.48	61.30	10.00	1063.80	1568.70
38	6.75	0.10	4.36	9.84	11.60	1034.40	1993.80
39	8.20	0.06	3.40	1.80	11.90	880.80	1694.10
40	7.74	0.02	1.22	3.86	22.00	696.00	3306.70
41	8.97	0.00	1.04	3.62	7.70	609.20	1301.90
42	11.16	0.12	2.60	3.14	8.60	589.10	1429.60

† Ca(NO$_3$)$_2$: Calcium nitrate extraction for bioavailable metals

Continued.

Number ID	†Dgt Cd	Dgt Pb	Dgt Zn	Water Content	‡NH_4^+	‡NO_3^-	‡P	‡K
	----------------μg----------------			g g^{-1}	---------mg kg^{-1}---------			
1	3.0	9.5	247.0	0.09	3.5	4.7	68	96
2	1.5	16.3	123.3	0.18	6.7	64.4	517	1334
3	1.8	26.0	71.0	0.11	8.8	6.1	208	286
4	2.8	366.8	386.8	0.10	7.0	8.1	210	298
5	1.3	139.3	205.5	0.13	11.0	34.9	433	1041
6	1.8	263.0	472.8	0.35	3.2	10.2	141	197
7	0.0	103.8	94.3	0.17	8.5	134.2	510	2130
8	0.3	51.3	55.5	0.38	6.9	8.8	307	345
9	1.0	26.8	165.8	0.14	3.5	50.7	518	1461
10	2.0	16.3	182.3	0.10	2.0	13.4	232	245
11	1.3	90.5	113.5	0.09	9.6	5.0	161	340
12	1.5	144.3	243.5	0.13	9.4	26.2	388	826
13	14.0	60.0	311.3	0.08	3.1	10.8	49	87
14	0.5	154.8	177.3	0.15	9.6	30.8	482	1306
15	0.8	11.5	131.3	0.14	3.4	76.9	494	1170
16	1.5	33.0	90.0	0.15	8.8	16.7	441	719
17	1.8	10.8	90.0	0.15	10.9	57.3	493	1223
18	8.8	63.3	1266.3	0.08	3.2	8.5	61	101
19	3.3	41.5	249.0	0.10	3.0	14.3	145	363
20	2.8	47.8	65.0	0.10	5.7	8.2	170	218
21	0.3	137.3	93.0	0.08	4.1	9.0	136	329
22	0.3	0.3	6.8	0.11	8.1	39.3	300	806
23	0.3	1.0	8.8	0.12	16.6	28.7	276	575
24	0.3	4.3	18.5	0.17	8.6	134.5	672	3397
25	0.3	7.5	25.0	0.09	9.0	27.3	284	590
26	0.8	4.3	15.0	0.16	10.8	102.4	586	2474
27	0.5	4.5	54.8	0.15	7.7	160.5	625	2455
28	3.0	6.0	472.0	0.07	2.1	2.2	29	58
29	0.5	0.3	14.8	0.15	5.6	107.3	569	2189
30	0.0	2.5	17.5	0.11	14.9	59.0	402	1330
31	4.3	20.5	483.0	0.08	2.2	1.6	18	41
32	0.5	0.8	20.0	0.15	1.7	96.7	640	2635
33	0.5	3.3	12.3	0.13	13.5	164.9	650	3038
34	0.0	0.3	12.3	0.07	10.1	31.5	409	758
35	0.3	8.0	17.8	0.08	9.8	20.9	297	544
36	0.3	0.0	14.3	0.17	13.2	100.0	599	2197
37	2.8	23.3	465.3	0.08	2.1	1.5	20	41
38	0.0	9.3	20.8	0.10	9.2	28.9	307	606
39	0.3	6.0	5.5	0.09	14.6	27.1	157	482
40	0.5	0.8	29.8	0.12	9.6	239.1	806	4399
41	0.3	6.3	22.0	0.12	29.5	186.0	675	2840
42	0.5	1.0	5.5	0.10	5.3	36.4	374	755

† Dgt: Diffusive Gradients in Thin Films

‡ NH_4^+ and NO_3^- determined by KCl extraction, P determined by Mehlich-3, and K determined

by ammonium acetate extraction

Continued.

Number ID	†Ca	†Mg	†Na	Total C	Total N	C:N	Electrical Conductivity	Cation Exchange Capacity
	--------mg kg^{-1}-------			-----g g^{-1}-----			dS m^{-1}	cmol$_c$ kg^{-1}
1	294.0	38.0	7.66	4.21	0.46	9.23	0.72	10.7
2	1406.1	537.8	167.87	28.30	3.64	7.77	2.86	83.7
3	1901.4	112.7	21.25	8.88	1.08	8.22	0.76	31.0
4	1516.4	73.9	28.84	7.93	0.82	9.72	1.70	27.0
5	1636.0	334.4	133.10	14.10	1.77	7.97	5.36	49.9
6	352.5	85.6	15.51	5.36	0.56	9.59	0.91	18.3
7	2109.8	430.3	349.01	23.30	3.01	7.74	9.86	59.9
8	1935.5	153.4	33.05	8.75	1.04	8.41	1.55	29.4
9	1163.8	522.5	187.81	30.10	3.63	8.29	4.82	58.4
10	491.3	119.9	24.10	10.50	1.20	8.75	1.31	32.2
11	1271.7	60.3	12.23	4.70	0.48	9.81	1.45	26.4
12	1296.7	235.1	106.05	14.00	1.72	8.14	4.10	33.7
13	248.3	28.6	20.15	4.35	0.30	14.36	2.11	16.9
14	1832.6	396.2	148.08	17.80	2.26	7.88	3.71	44.3
15	1038.4	438.3	154.66	17.60	2.35	7.49	4.95	51.8
16	1625.6	326.1	84.87	14.10	1.75	8.06	2.58	46.0
17	1644.4	405.3	160.76	16.60	2.06	8.06	4.33	68.4
18	242.7	26.4	13.46	2.70	0.22	12.56	0.95	16.8
19	399.1	114.4	33.81	6.99	0.82	8.51	1.64	26.7
20	1597.2	69.6	23.38	5.49	0.58	9.40	2.20	24.2
21	1709.2	60.9	24.41	6.76	0.79	8.51	3.33	21.7
22	4389.4	117.5	126.10	14.30	1.39	10.29	4.69	38.1
23	2996.1	99.0	112.14	8.08	0.95	8.55	4.18	32.6
24	3669.9	690.2	602.35	40.50	5.28	7.67	11.63	95.2
25	657.7	179.2	93.87	7.81	0.96	8.10	3.92	41.4
26	3454.0	507.9	559.66	21.10	2.72	7.76	9.46	34.7
27	1484.3	661.6	433.36	26.30	3.45	7.62	12.12	33.2
28	146.0	20.6	11.96	2.81	0.25	11.15	0.26	21.6
29	2511.7	538.1	455.85	28.20	3.45	8.17	8.14	79.6
30	1150.8	380.8	236.24	19.30	2.37	8.14	6.95	51.2
31	104.7	10.0	8.16	4.57	0.34	13.32	0.31	27.0
32	1811.7	754.6	454.93	29.50	3.79	7.78	10.15	93.6
33	3303.1	595.7	525.73	30.70	4.13	7.43	12.60	66.0
34	3375.2	153.4	119.73	14.10	1.69	8.34	4.14	41.7
35	3023.1	116.3	93.29	6.74	0.79	8.58	3.20	29.0
36	2817.1	596.6	450.97	34.50	4.31	8.00	8.51	109.9
37	95.6	11.6	7.81	5.14	0.38	13.67	0.24	23.7
38	818.6	204.1	93.35	9.21	1.02	9.03	3.26	46.7
39	2594.9	105.3	83.56	10.50	1.16	9.05	3.52	31.8
40	2003.0	936.9	790.90	40.10	5.53	7.25	21.20	36.9
41	2955.6	523.4	488.32	26.20	3.38	7.75	16.07	73.2
42	3664.1	139.0	122.18	14.40	1.80	8.00	4.93	36.0

† Ammonium acetate extractable Ca, Mg, and Na

Table 7-8. Chemical properties of each plot at the 139 d after time 0 sampling. Table will be continued on the next several pages.

Number ID	pH	Ca(NO₃)₂ Cd	Ca(NO₃)₂ Pb	Ca(NO₃)₂ Zn	Total Cd	Total Pb	Total Zn
				--mg kg^{-1}--			
1	5.87	4.5	11.8	407.8	12.0	801	5210
2	7.11	0.6	5.5	16.1	14.5	550	3655
3	7.24	1.2	6.1	16.4	16.2	1377	3285
4	7.99	0.8	11.3	11.8	13.3	2069	3580
5	8.23	0.4	7.6	2.2	6.8	1436	2087
6	7.58	1.3	6.7	88.1	14.3	1560	5148
7	8.67	0.3	6.7	5.3	4.3	1426	1560
8	8.16	0.6	6.9	5.3	9.4	1523	2368
9	7.93	0.5	2.2	14.4	14.5	917	3661
10	7.16	1.8	2.6	123.9	8.2	630	1588
11	7.51	1.1	11.0	19.6	15.1	1691	3568
12	8.50	0.6	14.7	33.8	11.9	1606	3640
13	6.81	4.6	34.4	354.8	19.0	2090	5043
14	8.48	0.4	8.4	1.7	8.5	1324	3058
15	8.20	0.4	2.9	13.1	7.7	604	2845
16	8.52	0.7	8.4	5.9	6.1	918	1478
17	8.42	0.5	4.5	6.4	7.7	540	2073
18	6.77	3.3	14.9	306.0	17.9	1436	8160
19	7.15	2.2	6.8	172.2	17.2	1916	5078
20	7.66	1.7	7.7	24.2	18.1	1626	4644
21	7.93	1.1	11.0	27.4	19.4	2491	5251
22	8.09	0.3	2.9	5.2	6.2	732	939
23	7.97	0.3	3.5	4.7	3.0	600	498
24	8.10	0.3	2.7	4.4	9.2	507	1342
25	7.29	0.4	2.6	0.9	14.0	627	2090
26	8.30	0.3	2.4	5.1	9.6	412	1653
27	7.88	0.3	2.7	2.2	10.2	364	1557
28	5.05	1.2	8.8	83.6	42.5	489	6486
29	8.05	0.3	2.3	5.3	5.3	479	1245
30	6.90	0.3	3.2	0.9	5.0	675	784
31	4.70	1.5	32.0	93.2	26.4	798	4204
32	7.64	0.4	3.0	3.8	4.6	434	796
33	8.29	0.4	3.1	4.8	12.8	413	2040
34	8.23	0.4	2.1	4.4	20.1	378	3444
35	8.22	0.4	2.7	4.2	10.1	393	1553
36	8.16	0.4	3.2	4.4	6.0	613	894
37	4.61	1.2	24.3	84.2	9.1	811	1340
38	6.63	0.6	3.3	13.2	17.9	933	2660
39	8.05	0.4	3.6	5.1	8.9	657	1593
40	7.97	0.3	2.6	4.3	14.0	422	2160
41	8.33	0.3	2.4	3.8	13.6	345	1844
42	8.13	0.5	2.4	3.0	18.0	445	2160

† Ca(NO₃)₂: Calcium nitrate extraction for bioavailable metals

Continued.

Number ID	†Dgt Cd	Dgt Pb	Dgt Zn	Water Content	‡NH_4^+	‡NO_3^-	‡P	‡K
	----------------µg----------------			g g^{-1}	------------mg kg-1-----------			
1	0.55	0.8	75.2	0.06	1.5	5.6	37	39
2	0.05	0.6	1.6	0.08	1.2	30.3	1182	222
3	0.03	0.7	0.9	0.07	1.1	28.3	287	268
4	0.05	5.7	2.6	0.06	0.8	7.0	187	160
5	0.01	4.0	3.5	0.06	1.1	13.3	932	229
6	0.01	4.8	12.3	0.06	1.0	7.9	232	62
7	0.01	5.4	4.1	0.09	1.3	44.9	1607	322
8	0.00	5.5	3.3	0.07	0.9	6.7	628	231
9	0.01	1.2	1.9	0.09	1.1	19.8	1158	173
10	0.09	1.7	15.4	0.06	1.0	12.6	510	76
11	0.04	5.9	5.9	0.06	0.9	13.9	249	196
12	0.04	4.6	7.6	0.08	1.0	17.8	903	189
13	1.00	4.6	159.2	0.05	1.6	9.9	44	32
14	0.01	1.5	0.8	0.08	1.2	29.7	1231	257
15	0.05	0.1	1.1	0.06	1.1	27.3	1244	172
16	0.01	0.9	0.2	0.10	1.5	29.7	899	263
17	0.00	0.4	0.7	0.08	1.6	50.5	1331	287
18	0.48	6.4	117.4	0.05	2.2	24.5	76	54
19	0.13	4.4	21.4	0.06	1.2	13.6	309	68
20	0.28	13.6	20.9	0.06	1.1	8.3	185	193
21	0.09	9.3	12.3	0.06	1.2	10.0	355	217
22	0.04	0.3	3.2	0.08	1.5	18.6	568	535
23	0.04	0.0	3.8	0.08	2.4	17.3	286	453
24	0.05	0.0	3.3	0.08	1.8	50.2	1622	435
25	0.08	0.1	2.5	0.08	5.6	21.5	453	143
26	0.04	0.1	3.4	0.13	1.3	68.3	1695	450
27	0.05	0.1	2.8	0.09	2.8	43.2	1085	156
28	0.08	0.1	14.7	0.05	2.1	4.2	13	20
29	0.06	0.1	3.4	0.13	1.5	76.1	1596	426
30	0.06	0.7	2.6	0.07	5.1	25.3	478	134
31	0.06	0.9	16.1	0.07	3.1	4.1	15	23
32	0.05	0.1	3.4	0.12	1.5	38.6	1360	242
33	0.05	0.2	3.5	0.10	1.8	46.4	1459	330
34	0.06	0.2	2.8	0.06	2.2	33.7	550	464
35	0.03	0.0	3.5	0.06	3.1	16.7	469	494
36	0.05	0.4	3.2	0.12	1.3	107.9	1734	539
37	0.21	3.4	33.4	0.07	2.8	4.7	15	25
38	0.03	0.2	1.7	0.08	4.0	8.7	293	85
39	0.05	0.0	3.9	0.07	2.0	11.8	363	483
40	0.05	0.3	2.7	0.12	1.5	51.3	1887	254
41	0.04	0.2	3.0	0.11	2.0	86.8	1700	381
42	0.04	0.0	3.1	0.07	2.8	19.5	242	377

† Dgt: Diffusive Gradients in Thin Films

Continued.

Number ID	†Ca	Mg	Na	Total C	Total N	C:N	Electrical Conductivity
	-------mg kg^{-1}------			-----g g^{-1}-----			dS m^{-1}
1	51	48	11	4.6	0.6	7.3	0.58
2	1542	1134	164	37.0	4.6	8.0	2.40
3	260	196	10	6.9	1.1	6.5	1.24
4	143	170	6	5.8	0.5	12.2	0.66
5	450	583	13	13.6	1.7	8.0	1.21
6	127	199	14	5.5	0.7	8.2	0.93
7	1697	913	160	19.6	2.9	6.7	2.66
8	149	253	12	7.3	0.9	8.1	0.54
9	933	885	39	21.7	3.0	7.2	1.40
10	148	187	11	10.3	0.9	11.3	0.71
11	174	176	4	7.6	1.1	7.0	1.16
12	570	457	29	19.0	2.0	9.5	1.36
13	155	44	4	3.8	1.5	2.5	1.58
14	893	708	60	24.6	2.6	9.5	2.21
15	1010	961	90	13.7	1.5	9.3	1.48
16	769	656	27	31.3	3.3	9.5	1.86
17	1298	891	131	27.5	3.0	9.1	3.32
18	101	56	11	5.2	0.3	16.8	1.61
19	260	227	12	10.3	1.0	10.2	1.03
20	254	155	11	10.0	0.7	13.5	1.14
21	215	146	10	9.7	0.6	15.8	1.73
22	568	332	27	11.0	0.9	12.1	1.47
23	411	234	17	4.5	0.2	27.3	1.54
24	1576	949	159	32.1	3.5	9.1	3.85
25	589	454	54	17.7	1.7	10.2	1.93
26	2188	1050	248	32.6	3.7	8.8	3.49
27	941	661	78	25.2	2.8	9.1	2.77
28	50	35	22	3.0	0.1	25.7	0.16
29	2350	1031	277	37.2	4.2	8.9	4.03
30	642	406	64	16.5	1.7	10.0	2.36
31	48	44	11	4.1	0.1	32.4	0.18
32	1186	1062	89	36.9	4.0	9.3	2.70
33	1237	849	110	26.6	2.9	9.2	2.96
34	720	328	75	14.2	1.3	11.3	2.14
35	381	263	27	12.9	1.0	12.5	0.97
36	3014	940	422	29.3	3.2	9.3	4.07
37	82	39	35	6.1	0.2	31.9	0.97
38	394	265	32	9.7	0.8	12.1	0.12
39	416	244	24	16.0	1.2	13.6	0.80
40	2080	1405	186	37.7	4.2	8.9	3.25
41	2569	1061	251	35.3	3.9	9.0	0.92
42	428	206	41	9.4	0.7	13.6	5.19

Table 7-9. Chemical properties of each plot at the 353 d after time 0 sampling. Table will be continued on the next several pages.

Number ID	pH	Ca(NO$_3$)$_2$ Cd	Ca(NO$_3$)$_2$ Pb	Ca(NO$_3$)$_2$ Zn	Total Cd	Total Pb	Total Zn
				-----mg kg^{-1}-----			
1	6.16	2.22	0.8	305.0	15.4	879	3737
2	7.33	0.24	0.1	15.6	19.2	1051	3837
3	7.79	0.96	0.7	34.8	22.7	1431	5020
4	8.01	1.26	1.1	57.0	14.8	2027	3070
5	8.31	0	0.7	6.1	10.7	2025	3243
6	7.64	1.04	1.0	184.4	12.0	1975	3892
7	8.39	0.06	1.1	6.6	6.3	2674	2718
8	8.22	0.48	1.0	30.9	10.2	1595	2954
9	7.85	0.1	0.7	32.2	14.6	1413	4002
10	7.22	1.84	0.0	192.6	15.1	1214	3209
11	7.92	0.62	1.3	23.8	15.1	2340	3227
12	8.06	0.38	0.2	29.1	19.3	3349	4149
13	7.2	2.8	17.7	327.5	13.0	2238	3573
14	8.21	0.04	0.6	16.7	6.4	1261	2205
15	7.96	0.02	0.5	12.2	11.2	826	2956
16	7.87	0.7	0.2	74.6	17.5	1526	3982
17	8.25	0.1	0.2	7.9	18.6	1235	3841
18	7.22	1.76	6.9	269.8	11.4	2134	2979
19	7.26	2.2	0.9	269.2	17.7	2611	3868
20	7.87	2.6	0.9	134.4	17.4	1750	3406
21	7.86	1.86	1.3	129.0	25.6	3281	5205
22	7.33	0.12	1.1	1.2	8.5	1204	1145
23	7.66	0.06	1.4	0.6	14.5	1230	2184
24	8.05	0.04	1.2	0.6	13.6	851	2166
25	7.13	0.14	1.6	12.4	25.1	973	3588
26	8.19	0	1.5	0.8	28.5	605	3999
27	7.93	0.06	1.7	1.9	20.6	493	3089
28	5.09	0.5	6.9	50.7	40.0	711	5500
29	7.56	0	1.7	1.4	7.5	720	1209
30	6.52	0.1	2.2	12.1	11.6	1057	1871
31	4.8	0.52	30.7	51.2	31.3	1148	4299
32	7.36	0.06	1.7	0.9	30.4	726	3918
33	8.02	0.04	1.7	0.9	19.6	689	3084
34	7.98	0.04	1.3	1.8	25.9	665	3747
35	7.89	0.02	1.1	1.1	31.8	682	4179
36	7.45	0.04	1.2	3.7	13.4	1218	1908
37	4.46	0.64	36.0	64.8	17.3	1190	2398
38	6.18	0.22	1.3	20.1	9.4	1091	1426
39	7.32	0.04	0.9	1.0	29.6	1029	4068
40	7.7	0.02	1.9	0.9	25.5	423	3640
41	8.3	0.06	1.7	0.9	11.9	560	1951
42	8.15	0.02	1.7	1.4	15.9	639	2143

† Ca(NO$_3$)$_2$: Calcium nitrate extraction for bioavailable metals

Continued.

Number ID	†Dgt Cd	Dgt Pb	Dgt Zn	Water Content	‡NH_4^+	‡NO_3^-	‡P	‡K
	----------------µg----------------			g g^{-1}	------------mg kg-1------------			
1	0.58	0.34	55.5	0.05	1.1	2.6	91	23
2	0.18	0.04	1.6	0.12	1.4	5.8	2436	397
3	0.16	1.06	0.8	0.09	0.2	2.9	538	55
4	0.14	1.44	1.3	0.06	0.0	3.5	657	51
5	0.13	2.80	2.9	0.09	0.0	4.8	1042	214
6	0.15	2.03	6.9	0.06	0.0	1.6	376	27
7	0.04	2.74	0.1	0.10	0.0	5.7	1006	187
8	0.10	2.05	0.5	0.05	0.3	2.5	427	40
9	0.11	1.56	2.1	0.11	0.6	7.2	996	326
10	0.33	4.96	34.8	0.06	0.3	4.3	404	49
11	0.20	7.81	21.2	0.07	0.1	3.5	470	51
12	0.11	0.95	1.9	0.08	0.1	5.8	900	170
13	0.78	6.59	92.8	0.05	0.7	3.9	155	41
14	0.04	0.45	2.6	0.10	0.1	5.2	810	138
15	0.11	0.61	0.7	0.28	0.2	7.1	1081	234
16	0.16	1.61	6.0	0.09	5.0	6.6	886	157
17	0.10	0.50	0.2	0.13	0.4	6.2	1100	310
18	0.30	4.55	34.9	0.05	0.5	1.6	128	27
19	0.18	1.06	11.6	0.07	0.2	2.2	533	60
20	0.20	4.58	8.9	0.07	0.2	2.3	393	75
21	0.20	1.85	4.4	0.07	0.3	2.8	647	59
22	0.21	1.18	6.4	0.07	0.9	2.4	332	167
23	0.16	1.75	2.3	0.08	0.9	1.9	681	149
24	0.10	0.51	3.3	0.13	0.5	6.6	1034	521
25	0.10	0.40	3.0	0.07	1.8	2.5	433	201
26	0.06	0.54	3.0	0.10	0.7	7.1	1006	758
27	0.09	0.36	2.7	0.11	0.3	9.2	1217	420
28	0.24	0.66	15.7	0.05	0.6	2.2	108	17
29	0.10	0.45	3.5	0.12	0.7	9.0	1060	440
30	0.09	0.58	3.0	0.08	2.0	4.6	402	153
31	0.23	1.30	14.9	0.07	1.3	3.5	49	20
32	0.04	0.14	3.6	0.10	0.7	7.5	1052	485
33	0.11	0.14	2.9	0.09	1.0	7.2	1038	371
34	0.09	1.13	2.0	0.07	0.9	4.6	362	112
35	0.10	0.04	3.4	0.06	0.7	2.7	450	110
36	0.13	0.18	3.5	0.12	1.1	6.6	885	561
37	0.21	1.49	17.5	0.09	1.6	3.5	63	18
38	0.08	0.54	2.4	0.07	2.4	2.0	493	171
39	0.10	0.38	3.6	0.06	1.5	3.4	376	150
40	0.10	0.69	2.4	0.12	0.6	14.3	1278	519
41	0.11	0.15	3.4	0.10	0.7	8.0	1265	576
42	0.05	0.29	3.5	0.08	0.7	4.0	673	131

† Dgt: Diffusive Gradients in Thin Films

‡ NH_4^+ and NO_3^- determined by KCl extraction, P determined by Mehlich-3, and K determined

by ammonium acetate extraction

Continued.

Number ID	†Ca	Mg	Na	Total C	Total N	C:N	Electrical Conductivity
	------mg kg^{-1}-----			-----g g^{-1}-----			dS m^{-1}
1	248	23	11	3.5	0.4	9.5	0.22
2	1745	643	13	34.5	4.0	8.7	0.54
3	1305	91	34	11.3	1.2	9.6	0.27
4	1238	83	5	8.1	0.8	10.1	0.41
5	1831	412	8	19.8	2.2	9.2	0.63
6	392	74	3	4.8	0.5	10.2	0.22
7	1479	313	14	15.3	1.7	9.0	0.69
8	1306	87	11	7.7	0.7	11.3	0.31
9	1388	574	27	23.8	2.8	8.6	0.48
10	502	91	10	6.4	0.7	9.2	0.27
11	1274	93	8	9.5	0.9	10.2	0.26
12	1220	271	19	25.3	2.8	8.9	0.60
13	146	22	12	4.3	0.3	12.8	0.16
14	1000	257	14	9.1	0.9	9.9	0.55
15	1149	539	14	22.0	2.4	9.3	0.51
16	1200	278	10	15.3	1.7	9.1	0.57
17	1636	415	10	22.3	2.5	8.8	0.13
18	206	25	2	3.7	0.3	12.6	0.57
19	456	82	3	7.0	0.7	10.2	0.22
20	1092	75	3	7.7	0.8	10.1	0.36
21	1069	62	6	7.2	7.6	0.9	0.39
22	1966	97	12	8.3	7.2	1.2	0.64
23	2100	135	9	7.6	7.3	1.0	0.42
24	2733	633	18	31.2	3.4	9.2	0.80
25	784	199	12	7.5	0.7	10.1	0.60
26	2663	565	59	19.4	2.2	8.7	0.96
27	1618	651	17	26.6	3.0	8.9	0.66
28	143	20	9	2.6	0.2	11.0	0.15
29	1707	381	19	24.8	2.7	9.3	0.88
30	708	154	15	8.0	0.8	9.9	0.57
31	176	22	1	5.3	0.4	12.9	0.18
32	1641	624	17	24.1	2.7	9.0	0.64
33	1866	405	21	23.5	2.5	9.3	0.87
34	1528	101	9	6.7	0.7	10.2	0.45
35	1606	83	4	7.4	0.7	9.9	0.64
36	1927	379	28	18.0	1.7	10.5	0.96
37	152	18	4	4.8	0.4	13.1	1.26
38	577	148	10	7.1	0.7	9.8	0.75
39	1574	103	8	7.0	0.6	11.1	0.67
40	1671	701	25	27.5	3.1	8.8	0.88
41	2018	513	30	29.0	3.2	9.2	0.82
42	1846	115	22	11.8	1.2	10.1	0.43

† Ammonium acetate extractable Ca, Mg, and Na

Table 7-10. Chemical properties of each plot at the 535 d after time 0 sampling. Table will be continued on the next several pages.

Number ID	pH	Ca(NO$_3$)$_2$ Cd	Ca(NO$_3$)$_2$ Pb	Ca(NO$_3$)$_2$ Zn	Total Cd	Total Pb	Total Zn
				-----mg kg^{-1}-----			
1	6.56	5.9	6.4	279.3	21.9	2073	9102
2	7.83	0.7	0.2	27.7	11.0	922	4754
3	8.92	2.5	0.6	60.4	31.4	1801	8990
4	9.71	3.8	3.4	118.5	29.9	3836	9042
5	9.27	0.4	1.1	16.5	12.2	3199	7597
6	8.70	2.9	4.7	171.2	16.4	2715	8044
7	9.36	0.1	0.5	6.7	1.2	3282	5208
8	9.26	1.3	1.5	32.1	17.1	3773	7396
9	8.42	0.4	0.3	19.1	17.4	1632	8386
10	7.31	4.1	0.5	205.5	19.1	1586	6704
11	8.92	2.0	2.2	36.2	20.0	2790	6906
12	9.12	0.3	0.6	9.9	13.0	2657	6409
13	6.81	4.6	19.6	201.7	30.2	2987	10570
14	9.30	0.2	1.0	11.2	20.4	2589	8963
15	8.44	0.2	0.3	11.9	10.3	1222	8399
16	9.12	1.1	1.9	49.4	21.7	1903	7271
17	9.07	1.2	0.6	37.2	20.6	1478	7499
18	7.22	4.7	8.6	238.7	12.9	2485	6079
19	7.76	4.1	3.6	200.8	19.1	3006	6248
20	9.94	5.8	2.7	148.7	30.1	2716	7767
21	10.89	2.8	3.0	100.9	22.2	3144	7585
22	11.20	0.1	0.5	7.2	9.0	1480	2918
23	11.36	0.1	0.1	4.5	10.9	1272	3988
24	8.97	0.0	0.1	3.2	3.1	932	2326
25	7.53	0.2	0.1	7.0	36.5	1204	8009
26	8.83	0.0	0.1	3.9	23.6	800	6023
27	7.81	0.1	0.1	6.3	27.8	819	6993
28	5.83	1.7	12.4	89.1	29.1	832	7101
29	8.24	0.1	0.3	2.7	6.0	1135	2800
30	7.47	0.2	0.2	9.7	63.5	1337	11330
31	4.92	1.0	27.4	45.8	25.8	1285	6372
32	7.64	0.1	0.1	3.2	33.1	973	7606
33	8.93	0.1	0.3	4.8	35.8	938	7907
34	9.71	0.1	0.2	3.3	52.3	805	9477
35	9.41	0.1	0.2	3.1	89.8	1630	15423
36	8.32	0.1	0.2	9.7	7.4	1244	2396
37	4.92	1.4	30.6	57.1	16.2	1449	4842
38	6.75	0.3	0.4	11.6	8.8	1248	3079
39	8.20	0.1	0.2	3.7	25.8	903	5957
40	7.74	0.0	0.1	3.9	6.9	667	3182
41	8.97	0.1	0.2	5.6	8.4	706	3587
42	11.16	0.1	0.3	5.3	8.4	863	3377

† Ca(NO$_3$)$_2$: Calcium nitrate extraction for bioavailable metals

Continued.

Number ID	†Dgt Cd	Dgt Pb	Dgt Zn	Water Content	‡NH_4^+	‡NO_3^-	‡P	‡K
	----------------µg----------------			g g^{-1}	------------mg kg-1------------			
1	0.16	11.3	103.8	0.05	0.1	1.3	32	84
2	0.75	7.5	5.5	0.10	0.3	1.9	874	368
3	0.71	8.7	9.9	0.07	0.1	1.5	283	93
4	0.63	12.3	17.5	0.05	0.1	1.2	167	84
5	0.76	8.4	4.8	0.08	0.2	1.5	969	153
6	0.70	10.1	20.2	0.06	0.2	1.0	127	72
7	0.78	7.6	2.0	0.10	0.3	1.3	999	246
8	0.74	10.7	8.2	0.07	0.3	1.4	260	96
9	0.76	7.6	3.6	0.10	0.6	2.7	1282	351
10	0.67	8.9	21.2	0.07	0.5	1.8	370	124
11	0.69	12.1	12.6	0.06	0.1	1.5	417	107
12	0.79	6.7	7.5	0.09	0.2	1.7	1161	279
13	0.39	11.3	52.8	0.04	0.2	1.2	49	124
14	0.78	7.3	1.9	0.10	0.4	1.2	1043	203
15	0.77	7.3	3.7	0.12	0.4	1.9	1646	335
16	0.73	9.3	10.4	0.14	0.3	1.7	1926	281
17	0.75	7.6	4.5	0.11	0.3	2.0	831	246
18	0.46	10.6	54.6	0.06	0.6	1.7	56	105
19	0.63	7.5	26.7	0.06	0.5	1.6	155	121
20	0.61	11.6	21.9	0.07	0.8	1.8	186	113
21	0.79	7.3	0.9	0.06	0.3	1.2	231	91
22	0.79	6.9	0.4	0.05	0.5	2.3	359	221
23	0.78	6.8	0.5	0.05	0.4	1.7	212	190
24	0.78	7.4	0.9	0.08	0.3	3.0	1710	378
25	0.78	6.9	1.2	0.06	0.2	2.9	287	241
26	0.79	6.7	0.4	0.07	0.3	5.9	1504	711
27	0.78	6.7	1.1	0.06	0.2	2.9	1267	567
28	0.53	7.3	41.8	0.03	0.4	2.0	14	68
29	0.78	6.8	0.6	0.08	0.6	2.0	1023	527
30	0.78	7.6	1.7	0.06	0.4	1.5	165	151
31	0.66	7.6	19.1	0.05	1.1	2.1	11	69
32	0.79	6.9	1.0	0.07	0.1	4.3	1189	518
33	0.79	6.8	0.5	0.05	0.8	7.0	1062	539
34	0.78	6.8	0.8	0.04	0.1	1.8	320	264
35	0.79	6.7	0.5	0.05	0.2	5.7	335	263
36	0.78	6.7	0.7	0.09	0.7	1.7	1118	522
37	0.67	7.4	17.0	0.09	0.4	1.5	12	73
38	0.78	6.9	1.3	0.05	0.7	3.3	181	263
39	0.78	7.0	1.0	0.05	0.1	4.5	181	160
40	0.79	6.9	1.4	0.08	0.1	4.0	2154	709
41	0.78	7.0	1.7	0.06	0.1	6.6	1443	706
42	0.79	6.7	0.4	0.05	0.1	4.6	337	258

† Dgt: Diffusive Gradients in Thin Films

‡ NH_4^+ and NO_3^- determined by KCl extraction, P determined by Mehlich-3, and K determined

by ammonium acetate extraction

Continued.

Number ID	†Ca	Mg	Na	Total C	Total N	C:N	Electrical Conductivity
	-------mg kg^{-1}------			-----g g^{-1}-----			dS m^{-1}
1	340	26	6.2	4.0	0.3	13.3	0.54
2	2315	676	5.9	28.7	3.3	8.8	0.42
3	1616	93	6.3	12.4	1.2	10.5	0.30
4	1373	65	6.5	7.9	0.7	12.0	0.70
5	1729	401	6.2	17.1	1.9	9.1	0.59
6	473	68	6.5	6.6	0.5	12.0	0.23
7	2881	696	5.6	23.6	2.6	9.1	0.46
8	2177	127	6.0	14.2	1.3	10.6	0.35
9	2037	691	5.6	27.8	3.2	8.7	0.50
10	933	128	6.3	12.9	1.3	10.0	0.26
11	1916	102	5.9	11.1	1.0	11.4	0.34
12	2797	592	5.4	28.0	3.0	9.2	0.51
13	348	62	6.2	4.3	0.2	17.8	0.26
14	1932	496	4.9	22.8	2.5	9.3	0.43
15	2292	891	5.5	31.3	3.5	8.9	0.44
16	2768	736	5.5	37.4	4.0	9.3	0.48
17	2164	455	6.1	26.7	2.9	9.3	0.45
18	320	38	6.2	6.4	0.4	15.3	0.23
19	596	85	5.9	14.6	1.2	12.0	0.28
20	1688	90	5.9	13.0	1.1	12.0	0.29
21	1452	58	6.2	11.0	0.8	13.2	0.35
22	3450	168	4.9	14.0	1.2	12.1	0.61
23	2787	134	5.2	11.4	0.9	13.1	0.11
24	3561	740	5.2	35.0	3.8	9.2	0.47
25	1474	306	5.7	13.9	1.4	9.9	0.47
26	3741	824	4.2	30.9	3.4	9.1	0.74
27	2138	780	4.4	30.7	3.6	8.6	0.64
28	211	19	6.4	5.0	0.3	16.1	0.28
29	3444	654	4.9	29.5	3.1	9.5	0.63
30	1045	185	5.9	12.1	1.1	10.9	0.40
31	201	11	6.1	6.2	0.4	17.5	0.13
32	3093	1025	5.2	28.6	3.2	9.0	0.51
33	2992	691	3.0	35.4	3.7	9.5	0.91
34	2697	211	5.0	15.7	1.5	10.2	1.13
35	3774	206	4.9	16.4	1.5	10.9	0.81
36	3246	587	5.0	24.5	2.6	9.5	0.68
37	265	20	6.2	6.8	0.4	15.6	0.14
38	1211	253	5.7	9.8	0.8	11.6	0.69
39	1925	111	5.9	11.2	0.9	12.2	0.81
40	2787	1089	3.3	39.5	4.5	8.7	0.91
41	3054	773	3.0	30.2	3.3	9.2	0.88
42	4712	213	5.2	9.8	0.8	11.7	0.66

† Ammonium acetate extractable Ca, Mg, and Na

Table 7-11. Chemical properties of each plot at the 711 d after time 0 sampling. Table will be continued on the next several pages.

Number ID	pH	Ca(NO$_3$)$_2$ Cd	Ca(NO$_3$)$_2$ Pb	Ca(NO$_3$)$_2$ Zn	Total Cd	Total Pb	Total Zn
				--mg kg^{-1}--			
1	5.87	1.7	25.7	182.8	7.0	664	2500
2	7.40	0.4	1.4	32.5	13.0	766	3274
3	7.60	1.7	6.1	136.9	14.9	987	3539
4	7.48	1.8	31.8	163.0	16.2	1513	3940
5	7.75	0.3	6.2	37.6	8.9	1837	3629
6	7.56	1.0	36.7	122.2	8.0	1554	3398
7	7.85	0.2	9.3	38.4	3.5	1824	2669
8	8.02	1.0	21.7	89.4	11.6	1655	3594
9	7.76	0.5	2.8	56.8	11.7	1422	3220
10	6.93	1.7	11.1	175.8	18.0	967	3643
11	7.92	1.9	18.3	111.2	14.3	1465	3827
12	7.90	0.8	7.2	67.6	12.1	1886	3193
13	6.48	1.8	100.0	174.7	4.0	1234	1981
14	7.78	0.7	5.4	74.6	9.0	2474	3217
15	6.76	0.8	2.3	103.0	8.7	764	3143
16	7.67	1.5	4.3	224.3	20.5	1213	4656
17	7.86	1.4	2.3	116.2	18.3	997	3678
18	7.15	1.4	53.9	169.1	7.6	1412	3047
19	7.29	2.8	35.7	274.7	15.4	1788	3215
20	7.60	2.3	30.6	180.0	18.0	1497	3464
21	7.69	2.1	34.6	161.3	13.6	1391	3333
22	7.53	0.1	1.4	0.8	6.1	722	1174
23	7.23	0.1	1.1	1.6	84.4	692	7703
24	7.25	0.0	1.0	0.5	60.8	522	8849
25	7.29	0.2	1.5	9.4	30.2	733	4341
26	7.88	0.4	0.5	0.1	15.8	494	2783
27	7.65	0.3	0.3	3.1	24.4	514	3946
28	4.86	0.1	6.8	35.0	12.1	448	2345
29	7.62	0.4	0.6	0.3	5.9	720	1619
30	6.71	0.3	1.2	7.5	11.7	743	2014
31	4.46	0.1	33.8	40.4	62.2	745	7030
32	7.57	0.4	0.1	0.4	13.1	509	2253
33	7.68	0.4	0.5	0.4	28.9	532	4211
34	7.62	0.4	0.7	1.7	49.0	574	6167
35	7.29	0.3	0.6	0.7	33.5	577	4909
36	7.70	0.3	0.5	0.4	4.0	740	1068
37	4.46	0.1	12.8	27.4	25.7	639	3955
38	6.42	0.2	0.8	9.1	12.0	934	2367
39	7.89	0.3	0.6	0.9	31.9	813	5029
40	8.01	0.4	0.5	2.7	22.4	545	3584
41	8.35	0.4	0.0	1.8	12.5	514	2478
42	7.81	0.3	0.1	2.5	15.6	642	2491

† Ca(NO$_3$)$_2$: Calcium nitrate extraction for bioavailable metals

Continued.

Number ID	†Dgt Cd	Dgt Pb	Dgt Zn	Water Content	‡NH_4^+	‡NO_3^-	‡P	‡K
	--------------μg---------------			$g\ g^{-1}$	------------mg kg-1-----------			
1	0.26	12.4	110.6	0.08	1.4	2.1	38	65
2	0.76	6.3	4.5	0.17	1.0	11.7	1058	268
3	0.72	8.9	9.7	0.11	0.8	3.6	226	86
4	0.61	12.5	18.3	0.09	0.9	5.3	117	74
5	0.82	7.9	6.5	0.13	2.0	1.4	929	126
6	0.77	10.9	21.3	0.08	0.4	5.6	96	70
7	0.86	8.1	2.5	0.11	0.9	4.2	621	106
8	0.75	11.3	9.5	0.10	0.6	7.9	183	80
9	0.82	7.7	3.7	0.16	0.7	9.3	809	180
10	0.65	8.2	22.1	0.09	0.1	6.7	145	115
11	0.75	12.6	13.6	0.10	0.0	7.8	270	91
12	0.84	6.1	8.1	0.13	0.5	5.5	903	128
13	0.49	13.4	75.6	0.07	0.0	4.4	47	68
14	0.79	7.3	2.8	0.12	0.1	3.4	710	160
15	0.72	7.6	4.1	0.14	0.2	4.0	745	131
16	0.79	9.8	13.2	0.17	1.6	4.3	1202	164
17	0.86	7.1	5.6	0.16	0.5	5.4	1127	203
18	0.49	13.2	81.9	0.09	0.1	4.5	65	72
19	0.55	7.1	25.4	0.09	3.8	4.8	150	76
20	0.67	11.4	22.1	0.09	1.3	3.3	175	70
21	0.88	7.2	1.6	0.08	0.8	2.2	148	77
22	0.84	6.5	1.1	0.12	0.3	2.7	246	178
23	0.83	6.4	1.9	0.12	0.2	4.5	235	128
24	0.79	7.9	1.8	0.16	0.8	6.5	2052	390
25	0.79	6.6	2.1	0.11	0.1	3.5	350	201
26	0.77	6.9	1.1	0.16	0.2	3.5	1562	377
27	0.76	7.2	1.5	0.14	1.6	3.5	1299	273
28	0.56	8.3	51.3	0.08	3.0	3.2	93	65
29	0.85	6.7	0.9	0.18	0.5	2.8	1588	409
30	0.87	6.9	3.5	0.10	0.3	3.1	243	143
31	0.71	8.6	46.8	0.09	0.6	2.5	19	54
32	0.72	7.1	1.6	0.17	0.2	3.0	1261	417
33	0.72	6.9	0.9	0.11	0.3	3.7	1015	492
34	0.66	6.5	1.7	0.09	0.9	3.0	275	267
35	0.63	6.6	1.2	0.10	0.3	3.0	340	168
36	0.69	6.6	1.6	0.19	0.5	3.1	1311	494
37	0.74	8.4	48.7	0.05	2.2	4.1	57	75
38	0.81	7.1	2.8	0.16	1.0	4.3	278	211
39	0.84	7.3	2.3	0.11	2.7	6.1	170	152
40	0.78	6.5	1.2	0.12	0.1	3.2	1519	304
41	0.78	6.4	3.4	0.13	0.1	2.9	1656	513

† Dgt: Diffusive Gradients in Thin Films

‡ NH_4^+ and NO_3^- determined by KCl extraction, P determined by Mehlich-3, and K determined

by ammonium acetate extraction

Continued.

Number ID	†Ca	Mg	Na	Total C	Total N	C:N	Electrical Conductivity
	-------mg kg^{-1}------			-----g g^{-1}-----			dS m^{-1}
1	182	21	16.9	3.3	0.2	20.8	0.32
2	1716	300	22.7	27.9	3.1	9.0	0.27
3	1128	63	22.2	7.1	0.6	12.1	0.12
4	728	46	18.9	4.6	0.3	15.8	0.23
5	1491	200	20.6	16.8	1.8	9.4	0.38
6	277	36	14.2	3.8	0.2	18.2	0.16
7	1119	152	22.2	12.1	1.2	10.3	0.29
8	1019	58	21.7	5.5	0.4	14.9	0.12
9	1407	246	23.9	22.5	2.4	9.2	0.34
10	451	56	15.8	5.9	0.5	12.2	0.15
11	1125	67	15.9	7.9	0.5	16.2	0.12
12	1270	193	21.4	18.2	1.9	9.4	0.29
13	150	32	16.6	1.9	0.1	19.5	0.12
14	1187	169	21.1	15.5	1.5	10.1	0.28
15	1110	217	16.3	17.5	1.8	9.8	0.34
16	1510	191	23.2	24.3	2.6	9.5	0.27
17	1547	227	20.3	21.1	2.3	9.4	0.29
18	257	38	14.0	4.7	0.2	24.2	0.10
19	300	41	18.4	5.2	0.3	19.3	0.15
20	519	41	17.5	6.6	0.5	14.4	0.16
21	535	36	20.1	7.0	0.3	21.0	0.13
22	2247	100	28.9	10.2	0.7	15.1	0.23
23	1978	94	19.0	9.1	0.7	13.0	0.22
24	2864	306	27.3	31.0	3.3	9.3	0.47
25	1301	181	23.6	10.2	0.9	11.1	0.34
26	2759	298	22.1	30.2	3.1	9.6	0.51
27	1803	297	19.9	29.1	3.2	9.2	0.33
28	288	41	20.1	3.5	0.1	33.1	0.15
29	2868	298	28.9	26.8	2.8	9.6	0.35
30	1041	141	22.9	8.1	0.6	12.6	0.28
31	175	27	19.3	3.8	0.1	41.6	0.10
32	1934	321	26.7	32.5	3.6	9.1	0.50
33	2119	292	33.0	25.6	2.7	9.5	0.58
34	2837	175	28.1	13.2	1.2	11.5	0.36
35	2087	121	20.5	9.3	0.8	12.1	0.25
36	2966	294	26.3	28.3	3.1	9.3	0.45
37	357	54	20.4	3.6	0.2	23.9	0.20
38	1041	154	24.8	9.3	0.8	11.3	0.46
39	1674	77	24.0	8.1	0.6	13.9	0.47
40	1785	295	22.0	23.2	2.7	8.8	0.35
41	2269	309	30.4	32.9	3.7	8.9	0.46
42	2147	108	20.2	7.6	0.6	12.3	0.24

† Ammonium acetate extractable Ca, Mg, and Na

Table 7-12. Chemical properties of each plot at the 841 d after time 0 sampling. Table will be continued on the next several pages.

Number ID	pH	Ca(NO₃)₂ Cd	Ca(NO₃)₂ Pb	Ca(NO₃)₂ Zn	Total Cd	Total Pb	Total Zn
				-------mg kg^{-1}-------			
1	5.58	2.1	27.8	195.2	10.8	770	2492
2	7.03	0.6	2.1	35.4	15.5	742	4449
3	7.22	1.5	5.5	140.2	11.1	1060	3848
4	7.11	1.4	35.4	171.0	18.6	1746	4997
5	7.36	0.2	5.2	33.4	11.0	1590	2959
6	7.18	0.9	35.9	119.9	7.2	1670	3387
7	7.46	0.4	8.7	40.4	9.4	2002	1935
8	7.62	1.1	20.6	92.7	15.3	1558	4558
9	7.37	0.4	3.9	66.2	8.8	1237	3792
10	6.58	1.9	14.2	182.5	21.0	991	3630
11	7.52	1.8	15.8	105.7	17.3	1610	5201
12	7.51	0.5	8.4	74.6	10.5	1802	3471
13	6.16	1.9	95.3	193.0	7.7	1198	2513
14	7.39	1.0	5.0	72.1	9.3	2662	2623
15	6.42	1.0	2.8	111.0	10.0	816	3133
16	7.29	1.1	6.7	240.2	29.2	1292	3375
17	7.47	1.6	2.5	118.7	16.7	908	4665
18	6.79	1.8	54.6	164.2	5.5	1675	3588
19	6.93	3.0	42.1	290.0	14.9	1633	3204
20	7.22	2.2	28.7	181.8	13.0	1586	4707
21	7.31	1.9	33.0	154.4	19.2	1508	3624
22	7.15	0.1	1.7	1.0	8.0	754	1489
23	6.87	0.1	1.5	2.5	75.6	715	6281
24	6.89	0.2	1.4	0.8	66.3	466	8818
25	6.93	0.4	1.5	15.0	29.7	782	3146
26	7.49	0.2	1.0	0.2	18.6	556	3530
27	7.27	0.2	0.6	4.5	28.1	495	4648
28	4.62	0.1	7.6	42.9	7.7	547	2337
29	7.24	0.3	0.8	0.9	4.0	734	2200
30	6.37	0.1	1.0	9.1	19.2	785	2190
31	4.24	0.2	29.8	49.0	69.7	891	8916
32	7.19	0.6	0.2	0.1	10.0	595	1837
33	7.30	0.5	0.5	0.5	21.1	500	4196
34	7.24	0.5	1.0	2.2	53.6	647	4469
35	6.93	0.2	1.1	0.4	45.2	615	6226
36	7.32	0.1	0.7	1.1	9.9	718	1258
37	4.24	0.1	17.9	31.6	17.0	656	3941
38	6.10	0.3	0.9	8.7	6.6	998	3217
39	7.50	0.3	1.1	0.4	27.1	873	5468
40	7.61	0.3	1.0	2.2	22.0	604	4546
41	7.93	0.5	0.3	3.1	16.9	486	2020
42	7.42	0.2	0.1	1.6	22.3	705	2482

† Ca(NO₃)₂: Calcium nitrate extraction for bioavailable metals

Continued.

Number ID	†Dgt Cd	Dgt Pb	Dgt Zn	‡NH_4^+	‡NO_3^-	‡P	‡K
	----------------μg----------------				--------mg kg-1-----------		
1	0.31	14.1	105.3	1.1	2.5	53	50
2	0.69	7.7	3.9	1.4	13.0	1213	196
3	0.70	6.4	12.1	0.9	4.5	308	79
4	0.65	13.2	17.4	1.0	4.1	267	65
5	0.88	8.5	5.2	1.4	0.7	861	105
6	0.75	11.9	25.3	0.6	6.7	194	67
7	0.92	7.7	3.9	0.7	4.9	949	46
8	0.71	12.1	15.4	0.7	7.4	361	67
9	0.84	6.4	2.1	1.0	10.0	953	92
10	0.62	6.8	27.0	0.5	6.2	332	107
11	0.83	11.1	12.7	0.2	8.6	313	77
12	0.81	6.0	10.0	0.1	4.1	851	59
13	0.44	15.3	94.7	0.4	4.8	69	37
14	0.86	7.7	4.7	0.2	3.0	855	126
15	0.73	6.8	4.5	0.6	3.5	1042	51
16	0.82	10.7	16.1	1.8	4.9	1071	96
17	0.79	6.8	7.0	0.7	4.1	976	168
18	0.52	14.0	97.9	0.1	4.9	77	50
19	0.57	8.7	27.2	2.9	4.0	258	48
20	0.77	14.2	30.3	1.7	4.6	222	44
21	0.83	6.8	2.4	1.1	1.8	303	65
22	0.90	7.6	2.6	0.6	4.1	361	144
23	0.78	6.5	3.8	0.2	3.2	338	87
24	0.72	8.9	2.2	0.7	7.0	1418	401
25	0.77	5.8	2.7	0.3	3.9	361	168
26	0.84	6.7	0.9	0.3	5.0	1271	200
27	0.81	7.8	2.6	1.1	4.4	1099	131
28	0.63	9.7	55.0	3.5	3.0	51	62
29	0.72	4.8	1.6	0.9	3.0	1167	317
30	0.85	7.7	4.4	0.8	4.2	338	135
31	0.67	10.1	63.7	0.9	3.7	23	42
32	0.65	8.9	3.3	0.4	3.4	1100	336
33	0.75	9.0	1.5	0.1	3.6	1045	449
34	0.67	7.3	2.8	0.2	4.0	383	271
35	0.58	6.4	0.8	0.3	3.2	378	107
36	0.77	7.8	1.5	0.9	2.9	1129	467
37	0.70	9.7	52.0	2.3	4.0	33	77
38	0.91	6.5	4.1	1.3	3.2	310	170
39	0.80	7.1	3.8	2.4	7.7	249	145
40	0.71	6.6	1.6	0.1	3.6	1529	131
41	0.82	6.9	5.9	0.4	3.4	1348	373
42	0.64	7.3	1.2	0.8	2.7	367	97

† Dgt: Diffusive Gradients in Thin Films

‡ NH_4^+ and NO_3^- determined by KCl extraction, P determined by Mehlich-3, and K determined by ammonium acetate extraction

Continued.

Number ID	†Ca	Mg	Na	Total C	Total N	C:N	Electrical Conductivity
	-------mg kg^{-1}------			-----g g^{-1}-----			dS m^{-1}
1	146	17	9.3	3.2	0.1	23.7	0.27
2	1273	133	17.5	27.1	2.9	9.2	0.24
3	787	43	15.6	6.0	0.3	20.9	0.11
4	386	32	11.0	4.2	0.3	16.3	0.22
5	1286	150	13.6	16.5	1.7	9.7	0.32
6	163	25	6.2	3.7	0.2	21.0	0.15
7	895	114	17.5	10.3	1.1	9.2	0.24
8	713	41	15.8	4.4	0.3	13.9	0.10
9	972	197	20.5	18.2	2.1	8.8	0.33
10	315	40	7.9	5.4	0.4	12.2	0.12
11	1013	60	8.6	7.2	0.4	16.9	0.12
12	889	154	17.0	16.2	1.7	9.6	0.29
13	120	21	8.9	1.8	0.1	20.1	0.11
14	730	110	18.3	13.8	1.3	10.2	0.26
15	888	162	9.8	16.6	1.6	10.1	0.32
16	1057	153	19.5	23.3	2.3	10.0	0.26
17	1237	204	13.4	19.8	2.1	9.6	0.26
18	206	32	6.3	4.5	0.2	25.2	0.08
19	210	39	11.5	4.9	0.2	20.1	0.14
20	467	38	10.4	6.1	0.4	14.9	0.15
21	197	26	13.0	6.4	0.3	22.8	0.11
22	1464	71	34.0	9.9	0.7	15.1	0.20
23	1404	70	14.0	7.3	0.6	12.9	0.19
24	2304	211	29.0	27.5	2.9	9.4	0.41
25	1148	130	19.5	9.2	0.8	11.4	0.32
26	2035	224	23.4	28.7	2.9	9.9	0.47
27	1521	249	18.1	27.6	2.8	10.0	0.32
28	201	37	12.6	2.5	0.1	26.6	0.14
29	2388	238	34.5	24.3	2.5	9.8	0.29
30	936	108	17.9	5.5	0.6	8.8	0.24
31	152	24	12.1	3.4	0.1	37.4	0.09
32	1210	241	27.4	30.2	3.2	9.4	0.46
33	1501	225	72.2	18.5	2.2	8.6	0.53
34	2553	144	31.5	11.1	0.9	12.1	0.32
35	1669	94	17.3	5.3	0.7	8.1	0.24
36	2710	203	27.8	27.1	2.6	10.4	0.41
37	250	39	13.5	3.5	0.1	26.3	0.19
38	895	139	21.7	8.9	0.8	11.6	0.43
39	1456	53	19.5	7.1	0.5	13.6	0.42
40	1143	266	28.9	22.0	2.4	9.2	0.31
41	1686	216	60.6	31.3	3.0	10.6	0.41
42	1717	87	15.8	5.9	0.6	10.6	0.22

† Ammonium acetate extractable Ca, Mg, and Na

Table 7-13. Microbial activity measurements taken at Time 0 sampling. Table is continued on the next page.

Number ID	Arylsulfatase mg p-nitrophenol kg^{-1}	Acid Phosphatase mg p-nitrophenol kg^{-1}	Alkaline Phosphatase mg p-nitrophenol kg^{-1}
1	8	308	103
2	125	1552	2545
3	6	283	337
4	18	160	147
5	151	220	1709
6	44	208	770
7	70	1070	3075
8	17	313	506
9	130	704	2218
10	13	403	1074
11	12	250	195
12	141	528	970
13	10	246	340
14	94	579	1901
15	95	523	1195
16	98	631	1593
17	119	613	1518
18	15	124	396
19	74	423	815
20	14	122	510
21	8	196	713
22	2	1195	440
23	20	156	326
24	25	3050	2956
25	84	87	398
26	205	1892	2901
27	204	844	2392
28	5	343	458
29	81	2380	3184
30	37	117	1531
31	6	659	175
32	133	2824	2634
33	61	799	1904
34	5	177	910
35	9	650	534
36	147	1663	2425
37	12	396	418
38	56	120	1471
39	15	99	787
40	106	1566	2656
41	102	694	1622
42	3	307	243

Continued.

Number ID	β-Glucosidase mg p-nitrophenol kg^{-1}	d-aminase mg NH$_4^+$ kg^{-1}	Nitrification mg N-NO$_3^-$ kg^{-1} d^{-1}	MBM C* mg C kg^{-1} soil	MBM N* mg N kg^{-1} soil
1	192	0.99	0.08	332	9
2	598	2.50	0.55	900	142
3	174	2.00	0.43	451	36
4	80	0.35	0.19	337	38
5	187	1.13	0.13	426	58
6	219	0.97	0.65	495	21
7	95	2.74	0.08	466	154
8	190	2.48	0.29	108	38
9	459	3.10	0.34	469	78
10	256	1.01	0.21	450	26
11	138	1.15	0.39	351	31
12	242	2.21	0.25	343	70
13	26	0.82	0.48	319	23
14	234	3.14	0.44	399	76
15	376	3.03	0.47	557	61
16	78	2.11	0.58	111	31
17	288	2.69	0.36	542	112
18	86	1.54	0.15	159	15
19	152	1.68	0.16	313	32
20	92	1.61	0.18	283	26
21	40	2.00	0.32	112	25
22	71	2.99	0.25	282	86
23	3	2.45	0.72	171	85
24	474	3.33	0.23	761	179
25	136	2.67	0.90	438	65
26	246	5.29	0.40	723	158
27	331	4.03	0.14	613	248
28	13	1.01	1.05	400	9
29	361	5.66	0.36	228	89
30	190	1.41	0.05	168	105
31	34	1.38	0.60	280	14
32	395	6.04	0.45	714	127
33	169	3.87	0.35	561	249
34	20	1.52	0.38	341^{-1}	66
35	47	1.08	0.15	331	51
36	313	5.67	1.23	536	91
37	51	0.89	0.08	354	4
38	140	0.97	0.07	335	48
39	26	1.67	0.18	418	73
40	311	7.00	0.69	740	423
41	106	4.69	1.26	498	285
42	140	1.54	0.24	60	85

Table 7-14. Microbial activity measurements taken at 139 d after time 0 sampling. Table is continued on the next page.

Number ID	Arylsulfatase mg p-nitrophenol kg^{-1}	Acid Phosphatase mg p-nitrophenol kg^{-1}	Alkaline Phosphatase mg p-nitrophenol kg^{-1}
1	26	42	296
2	139	1253	2781
3	51	457	385
4	37	171	276
5	80	188	806
6	20	273	867
7	271	721	1381
8	64	837	296
9	137	200	2125
10	50	365	755
11	34	406	392
12	94	501	778
13	5	298	394
14	155	490	1189
15	159	509	1930
16	103	310	1446
17	116	484	1568
18	5	64	438
19	27	345	649
20	6	76	505
21	17	366	367
22	104	1424	525
23	75	461	1069
24	226	1265	1429
25	28	263	831
26	293	1327	2975
27	134	1168	2238
28	0	74	39
29	328	1844	3280
30	53	408	650
31	15	98	110
32	279	1513	3152
33	170	677	1998
34	54	346	221
35	41	272	215
36	267	2053	2790
37	3	57	257
38	47	355	663
39	66	465	712
40	228	985	2408
41	336	1609	2229
42	46	284	295

Continued.

Number ID	β-Glucosidase mg p-nitrophenol kg^{-1}	d-aminase mg NH$_4^+$ kg^{-1}	Nitrification mg N-NO$_3^-$ kg^{-1} d^{-1}	MBM C* mg C kg^{-1} soil	MBM N* mg N kg^{-1} soil
1	182	1.2	0.03	199	11
2	607	3.3	0.41	460	45
3	196	2.2	0.36	93	55
4	71	0.4	0.09	255	8
5	251	1.1	0.18	254	21
6	221	1.3	0.11	221	22
7	372	3.7	0.60	86	67
8	133	2.6	0.14	434	6
9	958	3.8	0.26	101	15
10	309	1.8	0.16	347	11
11	129	1.5	0.20	202	21
12	285	2.7	0.26	206	28
13	155	0.9	0.16	67	9
14	177	4.1	0.39	79	18
15	391	3.0	0.33	284	41
16	268	6.0	0.48	251	45
17	262	3.5	0.46	170	89
18	275	1.8	0.33	59	27
19	125	2.0	0.14	156	20
20	44	1.9	0.13	88	13
21	47	2.0	0.13	100	17
22	96	3.5	0.31	107	10
23	40	3.1	0.21	190	20
24	292	5.3	0.56	378	63
25	186	3.5	0.21	233	43
26	440	9.6	0.91	214	101
27	430	6.3	0.35	292	68
28	36	1.5	0.08	71	2
29	478	11.1	0.81	211	60
30	163	1.7	0.30	109	44
31	62	2.1	0.03	64	9
32	584	9.3	0.48	516	114
33	174	5.9	0.36	151	93
34	110	1.6	0.33	105	59
35	51	1.3	0.13	177	42
36	448	7.9	1.40	256	152
37	52	1.5	0.06	77	4
38	161	1.8	0.06	217	12
39	81	1.9	0.15	135	24
40	509	9.3	0.50	261	93
41	310	8.5	1.11	141	144
42	177	1.9	0.18	161	41

Table 7-15. Microbial activity measurements taken at 353 d after time 0 sampling. Table is continued on the next page.

Number ID	Arylsulfatase mg p-nitrophenol kg^{-1}	Acid Phosphatase mg p-nitrophenol kg^{-1}	Alkaline Phosphatase mg p-nitrophenol kg^{-1}
1	29	196	58
2	306	753	2596
3	57	331	218
4	55	15	326
5	119	322	1363
6	6	56	400
7	158	453	671
8	14	42	171
9	284	936	2143
10	76	397	488
11	78	96	115
12	155	561	887
13	4	22	747
14	175	862	1254
15	254	728	2005
16	107	434	846
17	190	679	2500
18	13	118	277
19	45	118	1062
20	149	276	1163
21	59	148	528
22	58	527	857
23	86	689	934
24	232	980	3322
25	167	326	807
26	260	1280	2262
27	267	896	2663
28	10	817	234
29	251	1090	3043
30	67	486	795
31	10	701	163
32	283	1046	2911
33	229	491	2424
34	91	467	1226
35	164	157	549
36	294	993	1940
37	115	1413	264
38	137	248	531
39	85	604	903
40	174	1359	2767
41	289	1238	2252
42	129	734	1215

Continued.

Number ID	β-Glucosidase mg p-nitrophenol kg^{-1}	d-aminase mg NH$_4^+$ kg^{-1}	Nitrification mg N-NO$_3^-$ kg^{-1} d^{-1}	MBM C* mg C kg^{-1} soil	MBM N* mg N kg^{-1} soil
1	386	0.1	0.30	28	3.7
2	796	16.0	0.96	348	22.1
3	128	5.4	0.21	131	5.5
4	45	0.2	0.06	85	8.5
5	172	11.5	0.21	133	16.0
6	78	2.0	0.05	87	0.5
7	137	9.6	0.21	116	21.0
8	61	1.9	0.15	97	3.2
9	645	11.9	0.48	88	29.8
10	268	3.4	0.26	136	12.8
11	72	4.0	0.10	47	8.6
12	262	2.9	0.35	149	21.3
13	50	7.4	0.05	70	10.5
14	149	8.9	0.33	160	18.4
15	612	16.2	0.39	233	36.2
16	252	3.9	0.63	79	25.9
17	369	9.5	0.47	51	24.7
18	199	0.3	0.24	38	1.0
19	112	7.6	0.26	123	1.6
20	80	9.0	0.21	37	2.2
21	28	8.3	0.04	37	4.8
22	66	5.2	0.32	181	2.7
23	102	7.5	0.27	59	1.1
24	456	21.0	0.58	284	26.9
25	196	8.3	0.51	191	3.2
26	388	15.0	0.80	360	29.0
27	478	14.5	0.76	266	41.1
28	66	0.2	0.00	112	1.6
29	517	14.2	0.56	111	40.5
30	133	12.2	0.54	78	14.7
31	1	1.5	0.01	73	8.6
32	656	19.8	0.33	98	31.2
33	258	12.9	0.53	263	29.0
34	88	7.2	0.28	145	14.5
35	68	5.0	0.24	76	4.3
36	240	6.3	0.51	249	26.7
37	6	1.1	0.05	87	8.8
38	146	3.0	0.26	275	0.5
39	81	6.5	0.23	159	8.0
40	523	14.6	0.88	280	70.2
41	404	6.0	0.98	175	34.0
42	83	10.0	0.08	129	11.4

Table 7-16. Microbial activity measurements taken at 535 d after time 0 sampling. Table is continued on the next page.

Number ID	Arylsulfatase mg p-nitrophenol kg^{-1}	Acid Phosphatase mg p-nitrophenol kg^{-1}	Alkaline Phosphatase mg p-nitrophenol kg^{-1}
1	55	219	225
2	278	1568	2424
3	70	372	308
4	32	504	628
5	79	835	1891
6	33	577	115
7	160	1182	2081
8	80	589	3207
9	195	1289	2843
10	91	835	566
11	92	536	2309
12	144	1553	1937
13	40	392	367
14	214	1128	1922
15	233	1381	2543
16	263	1610	2174
17	201	905	2314
18	47	189	84
19	64	734	595
20	42	659	685
21	76	646	308
22	60	302	1108
23	75	274	3341
24	241	813	630
25	133	628	185
26	232	679	568
27	124	1095	2185
28	7	9	359
29	129	894	1700
30	77	424	717
31	26	11	381
32	200	1357	1987
33	158	644	1985
34	124	391	1377
35	44	241	3129
36	147	585	2527
37	5	103	152
38	77	538	658
39	72	582	1203
40	280	1478	1012
41	192	771	1751
42	2	328	619

Continued.

Number ID	β-Glucosidase mg p-nitrophenol kg^{-1}	d-aminase mg NH$_4^+$ kg^{-1}	Nitrification mg N-NO$_3^-$ kg^{-1} d^{-1}	MBM C* mg C kg^{-1} soil	MBM N* mg N kg^{-1} soil
1	250	1.6	0.25	85	37
2	847	3.9	1.01	630	219
3	223	3.6	0.43	349	62
4	109	3.4	0.13	254	22
5	256	3.5	0.52	287	81
6	151	3.4	0.14	205	16
7	274	2.6	0.68	321	79
8	152	1.6	0.25	290	49
9	741	4.3	0.69	529	198
10	327	2.8	0.33	145	82
11	130	3.1	0.27	274	50
12	419	3.4	0.45	276	107
13	138	3.4	0.07	84	21
14	242	3.4	0.53	400	103
15	595	2.6	0.69	565	241
16	421	1.6	0.63	359	121
17	470	4.1	0.95	433	128
18	241	3.7	0.25	110	42
19	170	3.8	0.26	241	43
20	192	2.6	0.18	80	35
21	99	3.0	0.17	209	83
22	139	3.6	0.36	185	40
23	188	2.9	0.21	254	34
24	518	3.1	0.67	248	156
25	293	2.1	0.33	249	61
26	460	1.7	0.72	365	124
27	605	1.8	0.52	387	101
28	166	1.6	0.02	72	10
29	518	1.6	0.54	196	92
30	261	1.7	0.44	251	57
31	99	1.7	0.05	80	9
32	717	1.7	0.66	484	186
33	319	2.1	0.60	256	111
34	117	1.5	0.42	200	66
35	150	1.6	0.33	392	68
36	356	1.5	0.49	293	107
37	71	1.6	0.03	113	7
38	279	1.6	0.43	241	61
39	199	1.5	0.25	380	89
40	651	1.8	0.98	442	215
41	442	1.8	0.65	339	106
42	158	1.7	0.18	252	49

Table 7-17. Microbial activity measurements taken at 711 d after time 0 sampling. Table is continued on the next page.

Number ID	Arylsulfatase mg p-nitrophenol kg^{-1}	Acid Phosphatase mg p-nitrophenol kg^{-1}	Alkaline Phosphatase mg p-nitrophenol kg^{-1}
1	40	255	253
2	220	1801	2216
3	77	433	460
4	3	671	152
5	37	531	906
6	9	242	620
7	37	498	1001
8	27	60	463
9	220	1535	2096
10	91	486	731
11	9	366	549
12	52	398	1049
13	2	193	240
14	66	384	800
15	140	1736	1690
16	97	394	1396
17	99	880	1497
18	36	382	369
19	18	308	624
20	29	275	86
21	5	149	163
22	56	361	1457
23	99	386	801
24	182	1306	2331
25	84	466	739
26	145	1051	2190
27	160	788	2039
28	42	402	31
29	163	1050	2213
30	109	508	664
31	1	677	117
32	201	1173	2262
33	139	887	1964
34	50	329	728
35	36	321	605
36	165	1123	2232
37	37	804	142
38	7	402	735
39	98	590	665
40	188	1097	2103
41	147	977	2051
42	47	296	634

Continued.

Number ID	β-Glucosidase mg p-nitrophenol kg^{-1}	d-aminase mg NH$_4^+$ kg^{-1}	Nitrification mg N-NO$_3^-$ kg^{-1} d^{-1}	MBM C* mg C kg^{-1} soil	MBM N* mg N kg^{-1} soil
1	100	1.8	0.02	78	64
2	438	3.3	0.25	331	214
3	104	2.6	0.12	144	36
4	60	2.2	0.02	121	20
5	100	2.4	0.13	138	69
6	147	2.6	0.11	122	17
7	151	2.7	0.09	161	53
8	65	2.7	0.07	130	29
9	379	3.6	0.28	325	191
10	201	3.4	0.08	154	61
11	79	3.2	0.11	143	35
12	177	3.5	0.07	179	66
13	61	1.9	0.01	116	13
14	122	3.6	0.11	166	39
15	334	3.9	0.28	212	110
16	282	2.9	0.11	234	85
17	336	3.8	0.13	210	105
18	81	1.1	0.03	173	48
19	108	3.2	0.10	136	30
20	51	1.8	0.08	98	11
21	38	2.2	0.14	52	15
22	147	3.6	0.07	176	64
23	91	3.2	0.07	145	55
24	321	3.3	0.10	251	151
25	124	3.4	0.03	157	89
26	304	3.8	0.15	181	141
27	329	2.5	0.23	262	136
28	124	1.5	0.05	132	58
29	317	3.7	0.18	284	141
30	125	3.2	0.03	190	82
31	110	1.7	0.04	83	11
32	445	3.9	0.21	296	186
33	216	3.1	0.09	230	127
34	60	2.2	0.10	155	31
35	126	2.8	0.14	168	49
36	539	3.8	0.10	241	120
37	81	1.5	0.06	127	16
38	38	3.1	0.05	208	82
39	146	0.7	0.11	160	46
40	273	3.5	0.28	255	168
41	267	3.6	0.09	257	167
42	76	2.9	0.05	134	33

Table 7-18. Plant biomass measurements for the 535 d sampling at sites A and B. Refer to Table 7-1 for number ID.

Number ID	Pigweed Biomass	Switchgrass Biomass	Foxtail Biomass	Tufted Hairgrass Biomass
	g m^{-2}	g m^{-2}	g m^{-2}	g m^{-2}
1	29.7	0.0	0.0	0.0
2	38.3	73.1	0.0	19.1
3	20.1	2.6	0.0	16.1
4	6.0	9.3	0.0	2.3
5	62.6	20.2	0.0	33.7
6	17.8	6.3	0.0	2.6
7	36.0	22.6	0.0	0.0
8	27.2	5.1	0.0	0.0
9	47.6	9.8	0.0	17.5
10	45.2	1.7	0.0	34.7
11	47.6	8.0	0.0	9.9
12	21.0	57.2	0.0	22.7
13	13.7	0.0	0.0	18.6
14	169.5	6.7	0.0	41.2
15	91.7	5.6	0.0	60.3
16	75.1	3.2	0.0	47.7
17	38.5	15.9	0.0	63.4
18	25.5	0.0	0.0	7.4
19	10.9	0.0	0.0	33.5
20	0.0	2.1	0.0	59.4
21	0.0	2.5	0.0	16.4
22	0.0	21.0	23.5	0.0
23	0.0	25.5	46.6	0.0
24	0.0	29.6	52.4	0.0
25	0.0	20.6	3.9	0.0
26	0.0	92.1	52.4	0.0
27	0.0	73.3	48.8	0.0
28	0.0	0.0	0.0	0.0
29	0.0	72.8	31.7	0.0
30	0.0	13.3	31.7	0.0
31	0.0	0.0	0.0	0.0
32	0.0	47.1	42.5	0.0
33	0.0	109.9	54.2	0.0
34	0.0	16.1	31.9	0.0
35	0.0	9.4	5.2	0.0
36	0.0	62.0	56.5	0.0
37	0.0	0.0	0.0	0.0
38	0.0	23.6	62.3	0.0
39	0.0	16.8	8.6	0.0
40	0.0	41.9	65.4	0.0
41	0.0	72.5	71.9	0.0
42	0.0	14.9	35.5	0.0

Table 7-19. Pigweed nutrient content at 535 d. Continued on the next page.

Pigweed Cd	Pigweed Pb	Pigweed Zn	Pigweed Fe	Pigweed Ca
mg kg^{-1}	mg kg^{-1}	mg kg^{-1}	g kg^{-1}	g kg^{-1}
48.9	51.8	2570	0.1	13.6
12.8	34.5	1769	0.2	13.2
24.3	72.8	1569	0.1	17.4
12.1	129.1	1687	0.1	12.2
6.5	76.8	1315	0.1	10.2
17.3	84.3	2247	0.1	10.1
4.8	90.4	1621	0.1	12.2
11.2	58.3	1676	0.1	14.2
12.4	30.7	1616	0.0	9.3
15.1	33.1	1823	0.0	13.1
10.0	81.3	1344	0.1	13.3
8.4	101.2	1513	0.1	14.3
45.4	146.7	2530	0.1	9.8
5.2	48.3	1479	0.0	9.1
17.9	25.6	2268	0.1	7.7
12.0	38.0	1743	0.1	14.0
11.5	30.9	1585	0.1	10.3
22.2	88.2	2245	0.1	12.1
30.4	123.4	2400	0.1	12.0
0.0	0.0	0.0	0.0	0.0
0.0	0.0	0.0	0.0	0.0
0.0	0.0	0.0	0.0	0.0
0.0	0.0	0.0	0.0	0.0
0.0	0.0	0.0	0.0	0.0
0.0	0.0	0.0	0.0	0.0
0.0	0.0	0.0	0.0	0.0
0.0	0.0	0.0	0.0	0.0
0.0	0.0	0.0	0.0	0.0
0.0	0.0	0.0	0.0	0.0
0.0	0.0	0.0	0.0	0.0
0.0	0.0	0.0	0.0	0.0
0.0	0.0	0.0	0.0	0.0
0.0	0.0	0.0	0.0	0.0
0.0	0.0	0.0	0.0	0.0
0.0	0.0	0.0	0.0	0.0
0.0	0.0	0.0	0.0	0.0
0.0	0.0	0.0	0.0	0.0
0.0	0.0	0.0	0.0	0.0
0.0	0.0	0.0	0.0	0.0
0.0	0.0	0.0	0.0	0.0
0.0	0.0	0.0	0.0	0.0
0.0	0.0	0.0	0.0	0.0

Continued.

Pigweed K	Pigweed P	Pigweed Mg	Pigweed N
g kg^{-1}	g kg^{-1}	g kg^{-1}	g kg^{-1}
3.1	7.4	2.3	12.9
2.3	4.7	5.8	13.1
2.5	3.7	4.1	8.7
3.2	2.7	4.8	13.7
3.0	3.4	6.2	11.4
3.0	5.7	5.4	12.2
2.9	5.2	6.1	3.4
3.0	4.5	4.2	9.4
2.9	5.6	5.5	11.7
2.7	5.6	4.0	2.9
2.6	2.8	4.8	9.1
1.9	3.7	5.1	6.5
3.2	3.3	4.1	7.2
3.3	5.9	6.1	6.3
3.3	4.4	4.9	12.1
3.2	9.0	6.7	12.6
2.5	4.4	4.9	9.9
3.0	6.4	4.8	14.2
2.6	6.7	4.3	14.8
0.0	0.0	0.0	0.0
0.0	0.0	0.0	0.0
0.0	0.0	0.0	0.0
0.0	0.0	0.0	0.0
0.0	0.0	0.0	0.0
0.0	0.0	0.0	0.0
0.0	0.0	0.0	0.0
0.0	0.0	0.0	0.0
0.0	0.0	0.0	0.0
0.0	0.0	0.0	0.0
0.0	0.0	0.0	0.0
0.0	0.0	0.0	0.0
0.0	0.0	0.0	0.0
0.0	0.0	0.0	0.0
0.0	0.0	0.0	0.0
0.0	0.0	0.0	0.0
0.0	0.0	0.0	0.0
0.0	0.0	0.0	0.0
0.0	0.0	0.0	0.0
0.0	0.0	0.0	0.0
0.0	0.0	0.0	0.0
0.0	0.0	0.0	0.0
0.0	0.0	0.0	0.0
0.0	0.0	0.0	0.0

Table 7-20. Tufted Hairgrass nutrient content at 535 d. Continued on the next page.

Tufted Haigrass Cd	Tufted Haigrass Pb	Tufted Haigrass Zn	Tufted Haigrass Fe	Tufted Haigrass Ca
mg kg^{-1}	mg kg^{-1}	mg kg^{-1}	g kg^{-1}	g kg^{-1}
0.0	0.0	0.0	0.0	0.0
6.6	73.3	1222	0.8	8.0
1.4	96.2	445	0.8	6.1
1.2	158.7	501	0.7	6.7
3.8	201.4	1028	1.0	7.9
3.6	107.1	751	0.5	6.5
0.0	0.0	0.0	0.0	0.0
0.0	0.0	0.0	0.0	0.0
4.7	62.0	897	0.6	5.3
3.4	77.8	882	0.6	7.1
3.7	127.7	508	0.4	7.2
5.5	127.3	901	0.6	7.2
2.9	188.5	1181	0.3	4.0
7.0	352.9	1379	1.1	4.9
1.9	80.7	884	0.7	7.4
1.4	65.0	574	0.5	5.9
3.1	59.1	821	0.5	6.2
4.2	151.5	1268	0.5	6.7
4.1	188.6	1163	0.9	7.0
1.3	114.9	606	0.5	6.5
2.1	253.7	1146	0.5	8.2
0.0	0.0	0.0	0.0	0.0
0.0	0.0	0.0	0.0	0.0
0.0	0.0	0.0	0.0	0.0
0.0	0.0	0.0	0.0	0.0
0.0	0.0	0.0	0.0	0.0
0.0	0.0	0.0	0.0	0.0
0.0	0.0	0.0	0.0	0.0
0.0	0.0	0.0	0.0	0.0
0.0	0.0	0.0	0.0	0.0
0.0	0.0	0.0	0.0	0.0
0.0	0.0	0.0	0.0	0.0
0.0	0.0	0.0	0.0	0.0
0.0	0.0	0.0	0.0	0.0
0.0	0.0	0.0	0.0	0.0
0.0	0.0	0.0	0.0	0.0
0.0	0.0	0.0	0.0	0.0
0.0	0.0	0.0	0.0	0.0
0.0	0.0	0.0	0.0	0.0
0.0	0.0	0.0	0.0	0.0
0.0	0.0	0.0	0.0	0.0
0.0	0.0	0.0	0.0	0.0

Continued.

Tufted Haigrass K	Tufted Haigrass P	Tufted Haigrass Mg	Tufted Haigrass N
g kg^{-1}	g kg^{-1}	g kg^{-1}	g kg^{-1}
0.0	0.0	0.0	0.0
0.5	2.0	3.1	8.0
0.9	1.7	1.8	5.4
0.9	0.8	2.1	5.1
0.7	1.7	3.1	6.9
0.6	1.9	2.3	6.7
0.0	0.0	0.0	0.0
0.0	0.0	0.0	0.0
0.6	1.4	2.4	3.9
1.4	3.8	2.1	7.3
0.8	1.7	2.0	6.1
0.3	1.2	1.9	4.2
0.9	0.8	1.1	5.0
0.2	0.8	1.4	4.8
0.4	1.9	2.8	7.7
1.0	2.8	2.3	5.7
1.4	4.0	3.0	8.2
1.4	3.8	2.3	10.1
1.1	2.4	2.0	6.2
0.8	0.8	1.6	3.6
1.2	1.8	2.1	6.8
0.0	0.0	0.0	0.0
0.0	0.0	0.0	0.0
0.0	0.0	0.0	0.0
0.0	0.0	0.0	0.0
0.0	0.0	0.0	0.0
0.0	0.0	0.0	0.0
0.0	0.0	0.0	0.0
0.0	0.0	0.0	0.0
0.0	0.0	0.0	0.0
0.0	0.0	0.0	0.0
0.0	0.0	0.0	0.0
0.0	0.0	0.0	0.0
0.0	0.0	0.0	0.0
0.0	0.0	0.0	0.0
0.0	0.0	0.0	0.0
0.0	0.0	0.0	0.0
0.0	0.0	0.0	0.0
0.0	0.0	0.0	0.0
0.0	0.0	0.0	0.0
0.0	0.0	0.0	0.0

Table 7-21. Switchgrass nutrient content at 535 d. Continued on the next page.

Switchgrass Cd	Switchgrass Pb	Switchgrass Zn	Switchgrass Fe	Switchgrass Ca
mg kg^{-1}	mg kg^{-1}	mg kg^{-1}	g kg^{-1}	g kg^{-1}
0.0	0.0	0.0	0.0	0.0
1.2	22.4	600	0.1	8.1
2.8	78.3	463	0.3	10.7
3.2	154.8	457	0.4	12.6
1.9	108.5	724	0.1	5.8
1.6	71.7	507	0.1	10.0
0.5	76.5	653	0.1	8.5
1.9	100.2	415	0.2	11.4
2.2	37.8	713	0.2	7.4
2.1	43.8	603	0.2	9.3
2.1	117.7	392	0.3	10.9
1.0	51.5	399	0.0	0.0
0.0	0.0	0.0	0.1	7.7
0.5	82.6	414	0.2	9.2
0.8	40.6	604	0.1	7.4
4.8	75.2	885	0.3	8.2
2.2	37.5	612	0.1	8.1
0.0	0.0	0.0	0.0	0.0
0.0	0.0	0.0	0.0	0.0
6.4	164.3	808	0.5	12.0
4.6	243.6	708	0.3	12.6
1.2	41.3	53	0.2	8.8
1.8	66.7	456	1.1	14.9
0.4	34.0	268	0.2	7.6
0.8	48.0	347	0.4	9.0
2.0	26.0	164	0.2	6.5
0.1	23.8	231	0.1	5.9
0.0	0.0	0.0	0.0	0.0
0.1	35.3	198	0.2	7.5
0.2	48.7	192	0.3	7.8
0.0	0.0	0.0	0.0	0.0
0.4	41.0	263	0.4	7.7
0.3	29.8	100	0.2	7.2
0.0	23.6	79	0.2	8.8
4.8	47.0	955	0.6	9.3
0.8	61.6	414	0.6	7.7
0.0	0.0	0.0	0.0	0.0
1.3	47.9	259	0.2	8.1
0.2	42.6	122	0.4	11.7
0.2	34.8	164	0.1	5.0
0.1	20.2	261	0.2	6.3
1.3	24.1	248	0.2	10.8

Continued.

Switchgrass K	Switchgrass P	Switchgrass Mg	Switchgrass N
g kg^{-1}	g kg^{-1}	g kg^{-1}	g kg^{-1}
0.0	0.0	0.0	0.0
1.2	5.4	3.5	8.7
0.6	1.4	2.6	6.1
0.5	0.6	2.0	5.5
0.4	1.0	2.1	4.7
0.7	1.8	3.6	4.3
0.9	5.0	4.1	7.7
0.4	0.8	2.0	4.9
1.0	4.8	3.7	7.4
0.5	1.7	2.0	2.2
0.6	1.1	2.1	5.6
0.0	0.0	0.0	4.8
0.8	2.9	3.8	0.0
0.5	1.1	2.8	4.0
0.5	2.8	3.1	7.4
0.4	1.3	2.2	4.6
0.8	2.3	3.2	5.8
0.0	0.0	0.0	0.0
0.0	0.0	0.0	0.0
0.4	1.1	1.8	3.9
0.3	0.8	1.7	6.5
0.5	0.7	1.8	4.4
1.3	1.8	4.7	7.6
1.0	1.4	2.9	5.8
0.8	1.1	2.7	5.5
0.9	1.4	2.3	4.4
0.8	2.3	3.1	4.5
0.0	0.0	0.0	0.0
1.0	1.5	2.8	5.2
0.8	1.2	2.3	5.5
0.0	0.0	0.0	0.0
0.9	2.6	3.7	7.5
0.8	1.0	2.5	4.8
0.5	0.4	1.6	4.4
1.2	1.9	2.6	5.9
0.8	1.6	2.4	5.7
0.0	0.0	0.0	0.0
0.8	1.5	2.7	4.8
0.9	0.6	2.1	4.0
0.7	1.4	2.5	4.9
0.6	0.6	2.2	4.9
0.6	1.3	1.4	5.8

Table 7-22. Yellow Foxtail nutrient content at 535 d.

Foxtail Cd mg kg^{-1}	Foxtail Pb mg kg^{-1}	Foxtail Zn mg kg^{-1}	Foxtail Fe g kg^{-1}	Foxtail Ca g kg^{-1}	Foxtail K g kg^{-1}	Foxtail P g kg^{-1}	Foxtail Mg g kg^{-1}	Foxtail N g kg^{-1}
0.0	0.0	0.0	0.0	0.0	0.0	0.0	0.0	0.0
0.0	0.0	0.0	0.0	0.0	0.0	0.0	0.0	0.0
0.0	0.0	0.0	0.0	0.0	0.0	0.0	0.0	0.0
0.0	0.0	0.0	0.0	0.0	0.0	0.0	0.0	0.0
0.0	0.0	0.0	0.0	0.0	0.0	0.0	0.0	0.0
0.0	0.0	0.0	0.0	0.0	0.0	0.0	0.0	0.0
0.0	0.0	0.0	0.0	0.0	0.0	0.0	0.0	0.0
0.0	0.0	0.0	0.0	0.0	0.0	0.0	0.0	0.0
0.0	0.0	0.0	0.0	0.0	0.0	0.0	0.0	0.0
0.0	0.0	0.0	0.0	0.0	0.0	0.0	0.0	0.0
0.0	0.0	0.0	0.0	0.0	0.0	0.0	0.0	0.0
0.0	0.0	0.0	0.0	0.0	0.0	0.0	0.0	0.0
0.0	0.0	0.0	0.0	0.0	0.0	0.0	0.0	0.0
0.0	0.0	0.0	0.0	0.0	0.0	0.0	0.0	0.0
0.0	0.0	0.0	0.0	0.0	0.0	0.0	0.0	0.0
0.0	0.0	0.0	0.0	0.0	0.0	0.0	0.0	0.0
0.0	0.0	0.0	0.0	0.0	0.0	0.0	0.0	0.0
0.0	0.0	0.0	0.0	0.0	0.0	0.0	0.0	0.0
0.0	0.0	0.0	0.0	0.0	0.0	0.0	0.0	0.0
0.0	0.0	0.0	0.0	0.0	0.0	0.0	0.0	0.0
0.0	0.0	0.0	0.0	0.0	0.0	0.0	0.0	0.0
0.0	0.0	0.0	0.0	0.0	0.0	0.0	0.0	0.0
3.1	38.1	303	0.2	11.2	1.2	1.4	3.6	9.1
7.5	34.1	400	0.2	8.3	1.5	1.4	3.6	6.3
2.4	42.3	899	1.1	6.8	2.3	2.5	3.6	9.0
5.2	50.9	1044	0.6	6.9	0.3	1.6	1.4	6.3
2.4	29.6	536	0.5	7.2	1.6	1.6	3.1	5.7
1.8	42.9	572	0.6	7.2	1.2	1.2	2.7	6.2
0.0	0.0	0.0	0.0	0.0	0.0	0.0	0.0	0.0
0.9	25.7	533	0.4	5.3	1.9	2.7	3.5	6.0
6.2	33.7	546	0.2	5.8	1.1	1.9	2.8	4.9
0.0	0.0	0.0	0.0	0.0	0.0	0.0	0.0	0.0
0.8	34.6	525	0.6	6.8	2.0	2.1	4.0	5.5
0.2	20.4	215	0.1	5.6	2.3	3.0	3.5	6.1
5.3	21.9	802	0.1	8.6	1.4	1.2	3.7	4.3
0.2	23.0	97	3.3	7.5	2.1	2.3	3.4	4.4
2.2	45.8	619	0.4	6.9	1.6	1.6	2.9	5.7
0.0	0.0	0.0	0.0	0.0	0.0	0.0	0.0	0.0
4.3	35.7	445	0.3	7.7	1.3	2.0	3.2	4.5
7.2	32.3	735	0.4	9.5	0.8	1.1	2.7	9.2
7.2	34.0	802	0.5	6.3	2.0	2.9	3.5	9.5
1.9	22.9	551	0.4	7.2	2.7	2.6	4.6	9.5
9.0	22.3	1656	1.0	8.7	0.8	0.8	1.8	8.1

Table 7-23. Plant biomass measurements for the 841 d sampling at sites A and B. Refer to Table 7-1 for number ID.

Number ID	Pigweed Biomass	Switchgrass Biomass	Marestail Biomass	Tufted Hairgrass Biomass
	g m^{-2}	g m^{-2}	g m^{-2}	g m^{-2}
1	7.0	0.0	0.0	0.0
2	0.0	98.8	0.0	18.2
3	20.4	1.7	0.0	0.0
4	14.8	0.0	0.0	0.0
5	22.7	76.4	0.0	4.8
6	1.5	0.0	0.0	11.8
7	127.9	60.6	0.0	0.0
8	6.9	8.4	0.0	0.0
9	8.7	51.0	0.0	0.0
10	16.2	0.0	0.0	11.5
11	9.1	13.9	0.0	0.0
12	5.9	84.7	0.0	7.1
13	0.0	0.0	0.0	0.0
14	31.8	54.1	0.0	22.1
15	13.7	35.6	0.0	0.0
16	16.7	8.3	0.0	11.3
17	22.9	56.3	0.0	8.0
18	10.3	0.0	0.0	0.0
19	10.9	0.0	0.0	0.0
20	13.2	0.0	0.0	5.7
21	18.4	0.0	0.0	5.6
22	0.0	34.8	10.7	0.0
23	0.0	23.7	15.1	0.0
24	0.0	51.5	31.9	0.0
25	0.0	5.1	12.7	0.0
26	0.0	173.9	2.8	0.0
27	0.0	71.9	25.1	0.0
28	0.0	0.0	0.0	0.0
29	0.0	132.9	99.5	0.0
30	0.0	37.7	7.1	0.0
31	0.0	0.0	0.0	0.0
32	0.0	84.6	96.0	0.0
33	0.0	122.7	76.7	0.0
34	0.0	36.3	0.0	0.0
35	0.0	0.0	12.3	0.0
36	0.0	202.7	56.8	0.0
37	0.0	0.0	0.0	0.0
38	0.0	45.7	4.5	0.0
39	0.0	25.1	8.9	0.0
40	0.0	56.5	39.2	0.0
41	0.0	86.1	19.5	0.0
42	0.0	10.6	0.0	0.0

Table 7-24. Smooth Pigweed metal and nutrient content at 841 d. Continued on the next page.

Pigweed Cd	Pigweed Pb	Pigweed Zn	Pigweed Fe
mg kg^{-1}	mg kg^{-1}	mg kg^{-1}	g kg^{-1}
49.6	38.5	5684	0.03
0.0	0.0	0.0	0.00
14.7	150.7	1268	0.24
11.2	99.3	1850	0.06
5.8	144.4	1424	0.17
9.0	64.9	1774	0.07
1.6	23.9	1322	0.06
15.1	174.6	2987	0.05
9.7	51.0	1507	0.06
14.7	29.0	2131	0.03
7.9	64.8	1084	0.04
9.7	65.8	1762	0.04
0.0	0.0	0.0	0.00
6.5	43.4	1586	0.04
20.9	10.4	3939	0.03
9.9	14.9	2099	0.03
11.0	47.9	1902	0.03
17.9	60.3	3325	0.03
16.8	48.9	2883	0.03
19.7	97.5	2672	0.07
16.7	127.8	2779	0.03
0.0	0.0	0.0	0.00
0.0	0.0	0.0	0.00
0.0	0.0	0.0	0.00
0.0	0.0	0.0	0.00
0.0	0.0	0.0	0.00
0.0	0.0	0.0	0.00
0.0	0.0	0.0	0.00
0.0	0.0	0.0	0.00
0.0	0.0	0.0	0.00
0.0	0.0	0.0	0.00
0.0	0.0	0.0	0.00
0.0	0.0	0.0	0.00
0.0	0.0	0.0	0.00
0.0	0.0	0.0	0.00
0.0	0.0	0.0	0.00
0.0	0.0	0.0	0.00
0.0	0.0	0.0	0.00
0.0	0.0	0.0	0.00
0.0	0.0	0.0	0.00
0.0	0.0	0.0	0.00
0.0	0.0	0.0	0.00

Continued.

Pigweed Ca	Pigweed K	Pigweed P	Pigweed Mg
g kg^{-1}	g kg^{-1}	g kg^{-1}	g kg^{-1}
9.1	2.8	5.9	1.8
0.0	0.0	0.0	0.0
11.1	1.6	2.4	2.3
11.0	2.8	3.2	3.9
15.2	0.8	2.4	4.1
7.6	2.7	4.4	4.4
12.4	1.2	2.9	7.6
11.2	2.5	4.1	3.2
7.9	1.4	2.6	3.0
9.8	2.2	4.0	2.7
9.5	2.2	3.2	3.0
8.3	2.0	3.4	3.6
0.0	0.0	0.0	0.0
9.8	2.0	3.4	4.0
6.6	2.6	3.9	2.9
8.2	2.8	5.6	4.2
8.6	2.3	4.6	4.9
7.0	3.1	7.0	3.6
8.5	2.9	6.2	3.1
9.1	2.8	4.3	3.9
9.4	2.5	3.4	2.6
0.0	0.0	0.0	0.0
0.0	0.0	0.0	0.0
0.0	0.0	0.0	0.0
0.0	0.0	0.0	0.0
0.0	0.0	0.0	0.0
0.0	0.0	0.0	0.0
0.0	0.0	0.0	0.0
0.0	0.0	0.0	0.0
0.0	0.0	0.0	0.0
0.0	0.0	0.0	0.0
0.0	0.0	0.0	0.0
0.0	0.0	0.0	0.0
0.0	0.0	0.0	0.0
0.0	0.0	0.0	0.0
0.0	0.0	0.0	0.0
0.0	0.0	0.0	0.0
0.0	0.0	0.0	0.0
0.0	0.0	0.0	0.0
0.0	0.0	0.0	0.0
0.0	0.0	0.0	0.0
0.0	0.0	0.0	0.0

Table 7-25. Tufted Hairgrass metal and nutrient content for the 841 d sampling. Continued on the next page.

Tufted Haigrass Cd	Tufted Haigrass Pb	Tufted Haigrass Zn	Tufted Haigrass Fe
mg kg^{-1}	mg kg^{-1}	mg kg^{-1}	g kg^{-1}
0.0	0.0	0.0	0.0
0.8	7.3	487	0.0
0.0	0.0	0.0	0.0
0.0	0.0	0.0	0.0
1.8	28.8	563	0.0
0.2	43.5	320	0.1
0.0	0.0	0.0	0.0
0.0	0.0	0.0	0.0
0.0	0.0	0.0	0.0
1.5	20.0	433	0.0
0.0	0.0	0.0	0.0
3.8	35.0	609	0.0
0.0	0.0	0.0	0.0
1.1	2.6	244	0.0
0.0	0.0	0.0	0.0
4.1	26.0	929	0.0
2.1	42.8	680	0.1
0.0	0.0	0.0	0.0
0.0	0.0	0.0	0.0
11.8	141.7	1181	0.1
1.5	82.0	600	0.1
0.0	0.0	0.0	0.0
0.0	0.0	0.0	0.0
0.0	0.0	0.0	0.0
0.0	0.0	0.0	0.0
0.0	0.0	0.0	0.0
0.0	0.0	0.0	0.0
0.0	0.0	0.0	0.0
0.0	0.0	0.0	0.0
0.0	0.0	0.0	0.0
0.0	0.0	0.0	0.0
0.0	0.0	0.0	0.0
0.0	0.0	0.0	0.0
0.0	0.0	0.0	0.0
0.0	0.0	0.0	0.0
0.0	0.0	0.0	0.0
0.0	0.0	0.0	0.0
0.0	0.0	0.0	0.0
0.0	0.0	0.0	0.0
0.0	0.0	0.0	0.0
0.0	0.0	0.0	0.0
0.0	0.0	0.0	0.0

Continued.

Tufted Haigrass Ca	Tufted Haigrass K	Tufted Haigrass P	Tufted Haigrass Mg
g kg^{-1}	g kg^{-1}	g kg^{-1}	g kg^{-1}
0.0	0.0	0.0	0.0
3.1	1.1	3.2	2.1
0.0	0.0	0.0	0.0
0.0	0.0	0.0	0.0
9.5	0.9	1.5	3.4
3.8	0.8	1.8	2.0
0.0	0.0	0.0	0.0
0.0	0.0	0.0	0.0
0.0	0.0	0.0	0.0
4.9	1.0	2.8	1.6
0.0	0.0	0.0	0.0
4.6	1.4	4.7	3.4
0.0	0.0	0.0	0.0
0.0	0.0	0.0	0.0
0.0	0.0	0.0	0.0
4.7	1.5	4.1	2.9
4.4	1.3	3.6	2.5
0.0	0.0	0.0	0.0
0.0	0.0	0.0	0.0
7.0	1.3	2.2	1.9
3.3	1.2	2.4	1.6
0.0	0.0	0.0	0.0
0.0	0.0	0.0	0.0
0.0	0.0	0.0	0.0
0.0	0.0	0.0	0.0
0.0	0.0	0.0	0.0
0.0	0.0	0.0	0.0
0.0	0.0	0.0	0.0
0.0	0.0	0.0	0.0
0.0	0.0	0.0	0.0
0.0	0.0	0.0	0.0
0.0	0.0	0.0	0.0
0.0	0.0	0.0	0.0
0.0	0.0	0.0	0.0
0.0	0.0	0.0	0.0
0.0	0.0	0.0	0.0
0.0	0.0	0.0	0.0
0.0	0.0	0.0	0.0
0.0	0.0	0.0	0.0
0.0	0.0	0.0	0.0
0.0	0.0	0.0	0.0

Table 7-26. Switchgrass metal and nutrient content at the 841 d sampling. Continued on the next page.

Switchgrass Cd	Switchgrass Pb	Switchgrass Zn	Switchgrass Fe
mg kg^{-1}	mg kg^{-1}	mg kg^{-1}	g kg^{-1}
0.0	0.0	0.0	0.0
1.1	2.4	295	0.1
0.2	18.3	245	0.0
0.0	0.0	0.0	0.0
0.5	61.0	358	0.0
0.0	0.0	0.0	0.0
0.6	20.9	355	0.0
1.9	62.8	428	0.0
1.7	9.8	298	0.0
0.0	0.0	0.0	0.0
0.1	46.9	174	0.0
0.2	29.2	288	0.0
0.0	0.0	0.0	0.0
0.0	20.9	392	0.0
0.4	11.5	431	0.0
0.5	12.0	481	0.0
0.7	18.9	414	0.0
0.0	0.0	0.0	0.0
0.0	0.0	0.0	0.0
0.0	0.0	0.0	0.0
0.0	0.0	0.0	0.0
0.8	20.0	134	0.0
0.1	24.9	185	0.2
0.6	8.9	213	0.0
0.3	15.1	179	0.0
0.5	9.2	174	0.0
0.5	9.9	171	0.0
0.0	0.0	0.0	0.0
0.8	10.8	92	0.0
0.8	22.2	124	0.1
0.0	0.0	0.0	0.0
0.5	11.5	169	0.1
0.1	11.9	102	0.1
1.1	10.3	215	0.2
0.0	0.0	0.0	0.0
0.3	19.8	176	0.1
0.0	0.0	0.0	0.0
0.9	40.2	344	0.1
0.1	24.3	133	0.1
0.4	13.4	272	0.1
0.2	10.5	186	0.1
0.6	12.6	176	0.1

Continued.

Switchgrass Ca	Switchgrass K	Switchgrass P	Switchgrass Mg
g kg^{-1}	g kg^{-1}	g kg^{-1}	g kg^{-1}
0.0	0.0	0.0	0.0
2.9	0.7	2.9	1.8
4.2	0.4	1.6	1.8
0.0	0.0	0.0	0.0
5.7	0.5	2.2	2.5
0.0	0.0	0.0	0.0
3.4	0.5	2.4	2.3
5.8	0.7	1.9	1.8
3.7	0.7	3.1	2.5
0.0	0.0	0.0	0.0
4.5	0.5	1.7	1.7
5.6	0.5	2.7	2.9
0.0	0.0	0.0	0.0
4.0	0.8	3.2	3.0
3.5	0.7	3.6	2.9
4.7	0.7	3.0	2.5
4.8	0.7	2.7	2.0
0.0	0.0	0.0	0.0
0.0	0.0	0.0	0.0
0.0	0.0	0.0	0.0
0.0	0.0	0.0	0.0
4.8	0.5	1.3	1.7
5.2	0.4	0.8	1.3
3.9	0.4	1.8	2.3
3.5	0.4	1.4	1.7
3.4	0.4	1.6	2.0
2.9	0.4	1.3	2.0
0.0	0.0	0.0	0.0
3.4	0.3	1.2	1.8
2.9	0.4	0.8	1.5
0.0	0.0	0.0	0.0
2.8	0.4	1.6	2.1
3.3	0.3	0.8	1.4
5.4	0.5	0.9	1.6
0.0	0.0	0.0	0.0
3.6	0.3	1.1	1.8
0.0	0.0	0.0	0.0
4.2	0.5	1.9	2.0
4.4	0.4	0.5	1.1
4.3	0.4	0.9	2.2
4.1	0.4	0.7	1.6
5.5	0.5	0.8	1.1

Table 7-27. Marestail metal and nutrient content at the 841 d sampling. Continued on the next page.

Marestail Cd	Marestail Pb	Marestail Zn	Marestial Fe
mg kg^{-1}	mg kg^{-1}	mg kg^{-1}	g kg^{-1}
0.0	0.0	0.0	0.0
0.0	0.0	0.0	0.0
0.0	0.0	0.0	0.0
0.0	0.0	0.0	0.0
0.0	0.0	0.0	0.0
0.0	0.0	0.0	0.0
0.0	0.0	0.0	0.0
0.0	0.0	0.0	0.0
0.0	0.0	0.0	0.0
0.0	0.0	0.0	0.0
0.0	0.0	0.0	0.0
0.0	0.0	0.0	0.0
0.0	0.0	0.0	0.0
0.0	0.0	0.0	0.0
0.0	0.0	0.0	0.0
0.0	0.0	0.0	0.0
0.0	0.0	0.0	0.0
0.0	0.0	0.0	0.0
0.0	0.0	0.0	0.0
0.0	0.0	0.0	0.0
0.0	0.0	0.0	0.0
0.0	0.0	0.0	0.0
5.5	11.4	309	0.1
3.4	5.3	380	0.1
6.9	10.2	397	0.1
3.3	3.3	355	0.1
3.6	4.6	427	0.1
0.0	0.0	0.0	0.0
2.6	2.0	166	0.0
0.0	0.0	0.0	0.0
0.0	0.0	0.0	0.0
2.8	1.7	371	0.1
2.5	2.7	316	0.1
0.0	0.0	0.0	0.0
4.1	3.9	247	0.1
7.3	6.4	310	0.1
0.0	0.0	0.0	0.0
1.2	14.1	351	0.1
0.0	0.0	0.0	0.0
2.2	3.1	285	0.1
3.6	2.2	269	0.1
0.0	0.0	0.0	0.0

Continued.

Marestail Ca	Marestail K	Marestail P	Marestail Mg
g kg^{-1}	g kg^{-1}	g kg^{-1}	g kg^{-1}
0.0	0.0	0.0	0.0
0.0	0.0	0.0	0.0
0.0	0.0	0.0	0.0
0.0	0.0	0.0	0.0
0.0	0.0	0.0	0.0
0.0	0.0	0.0	0.0
0.0	0.0	0.0	0.0
0.0	0.0	0.0	0.0
0.0	0.0	0.0	0.0
0.0	0.0	0.0	0.0
0.0	0.0	0.0	0.0
0.0	0.0	0.0	0.0
0.0	0.0	0.0	0.0
0.0	0.0	0.0	0.0
0.0	0.0	0.0	0.0
0.0	0.0	0.0	0.0
0.0	0.0	0.0	0.0
0.0	0.0	0.0	0.0
0.0	0.0	0.0	0.0
0.0	0.0	0.0	0.0
0.0	0.0	0.0	0.0
0.0	0.0	0.0	0.0
0.0	0.0	0.0	0.0
12.0	1.2	1.2	1.5
11.1	1.5	2.8	3.6
8.9	1.2	2.9	2.1
10.6	1.3	2.2	3.4
8.7	1.3	2.3	3.7
0.0	0.0	0.0	0.0
10.9	1.3	2.2	3.0
0.0	0.0	0.0	0.0
0.0	0.0	0.0	0.0
8.6	1.2	3.7	4.4
9.6	1.4	2.0	3.0
0.0	0.0	0.0	0.0
11.7	1.6	1.6	1.4
13.0	1.2	1.8	2.7
0.0	0.0	0.0	0.0
5.1	0.8	1.9	2.1
0.0	0.0	0.0	0.0
9.6	1.1	1.7	3.6
8.5	1.3	1.6	2.5
0.0	0.0	0.0	0.0